WASM: Minerals, Energy and Chemical Engineering

Investigating the Performance of Hard Rock Pillars with Different Width to Height Ratios and the Effects of Inclination, a Discontinuity and Blasting

Jessu Kashi Vishwanath

This thesis is presented for the Degree of

Doctor of Philosophy

of

Curtin University

December 2018

DECLARATION

To the best of my knowledge and belief this thesis contains no material previously published by any other person except where due acknowledgement has been made.

This thesis contains no material which has been accepted for the award of any other degree or diploma in any other university.

Signed: Kashi Vishwanath

Date: December 2018

Abstract

Pillars are an important part of most underground mines. Pillars are typically left in between stopes to maintain stability. The design and stability of the pillars are the two most complicated and inter-related challenges in ground control (rock mechanics) studies. Inadequately sized pillars can lead to local pillar failure that can even result in chain pillar failure that can lead to catastrophic collapse. Oversized pillars lead to the excess ore left leading to economic loss. Therefore, appropriate pillar design is essential for the effective operation of the mines. This also involves monitoring the pillars to ensure they are performing as predicted by the mine.

Pillar design depends on the failure mechanisms of the pillars. The factors influencing the failure mechanisms of the pillars include pillar inclinations, presence of discontinuity, blast damage, roof/floor conditions and water conditions. Empirical, analytical approaches that have been conducted for pillar design do not differentiate these factors in designing the pillars. Numerical modelling is a platform that can be used to understand the failure mechanisms of the pillars under these factors if calibrated. Laboratory tests and numerical modelling was conducted to understand the failure mechanisms and to determine the pillars strength under these circumstances. Therefore, pillar design was divided into three phases namely inclination effects, discontinuity effects, blast damage effects. Lastly, observational validation process was conducted through strain monitoring of the pillar design.

In the first phase, reduction factors were determined for two different rock types which were found to be consistent throughout all the width to height ratios of the pillars for each inclination. With numerical modelling, the reduction factors were determined for each inclination and a relationship between the reduction factors and pillar inclination was determined. This relationship can be used in the empirical approach to account for the

pillar inclinations. In the second phase, dip and direction of the discontinuities were determined to be the most important factors. It was determined that a discontinuity with largest cutting angle in the pillar between the two open sides of the pillar lead to the sliding failure. The discontinuity angle in the failure path of the inclined pillar should be avoided as they lead to the lowest strength even in larger width to height ratio pillars. Charts were developed to account for discontinuity effect on pillar design in normal and inclined loading condition. In the third phase, the disturbance factor and the blast damage thickness were determined to be the most important parameters in defining the strength of the pillars. The pillar height was also determined as the parameter that influences the blast effect on the pillars. The tables were created to determine the strength of the pillars under different conditions of disturbance factor and blast damage thickness.

The observational validation process was developed using strain monitoring. A ratio of elastic strain to failure strain was determined for different width to height ratio. A relationship was developed between the strain ratio and the width to height ratio which can be used to monitor the condition of the pillars. It was determined that if the in-situ strain on the instruments was higher than the failure strain determined by the equation then the pillar is unstable, and the information can be used for the better design of the next set of pillars.

A design flowchart with sub-sections has been created to utilize these findings efficiently into designing the pillar and carrying out the monitoring studies. The monitoring studies would provide a feedback in quantitative terms to optimize the next set of pillars provided the ground conditions remain relatively similar. Pillar designs include the inclinations, discontinuity orientations and the blast effects to consider to effectively create an optimized and safe pillar system.

Acknowledgements

First, I would like to sincerely thank Dr. A.J.S. (Sam) Spearing for giving me this priceless opportunity to pursue a PhD study at WASM. He has always been very supportive and provided me with great guidance and motivation until the end of my studies. I would also like to thank Dr. Roger Thompson, chairperson and Dr. Mostafa Sharifzadeh, co-supervisor.

Lastly, I would like to thank my parents, sister and future wife for their unconditional caring, love and motivation.

Author's peer reviewed papers

Papers published or accepted for publication:

Jessu, K.V., Spearing, A.J.S. (2019) Performance of Inclined Pillar with a major discontinuity. *International Journal of Mining Science and Technology*. Vol. 29(3), 437-443

Jessu, K.V., Spearing, A.J.S. (2018) Effect of Dip of Pillar Strength. *Journal of South African Institute of Mining and Metallurgy.* Vol. 118, 765-776

Jessu, K.V., Spearing, A.J.S., Sharifzadeh M. (2018) A Parametric Study of Blast Damage on Hard Rock Pillars. *Energies*, 11(7), 1901.

Jessu, K.V., Kostecki, T.R., Spearing, A.J.S., Esterhuizen G.S. (2018) Effect of Discontinuity Dip Direction on Hard Rock Pillar Strength. *SME Transactions*. Vol. 344, pp. 25-30

Jessu, K.V., Spearing, A.J.S., Sharifzadeh M. (2018). Laboratory and Numerical Investigation on Strength Performance of Inclined Pillars. Energies. 11(11), 3229

Jessu, K.V., Spearing, A.J.S., (2019). Direct Strain Evaluation Method for Laboratory Based Pillar Performance. Journal of Rock Mechanics and Geotechnical Engineering. (Accepted. Yet to Publish)

Table of Contents

TABLE OF FIGURES

TABLE OF TABLES

Chapter 1

Introduction

1.1.Introduction

In underground mines, the main objective is to extract as much of the orebody as possible both safely and economically. In practice, this is constrained by geology, the stress tensor and the rock mass properties in which mining is being carried out. To maintain the macro stability of the stopes, the common practice is to leave the rock pillars that may be later removed during secondary mining. Coates (1981) defined the pillars as "the in-situ rock between two or more underground openings."

Pillars left in the underground mines can have simple to complex geometries depending on the geology and grade distribution of the orebody and its surroundings, the orientation of the orebody and the presence of geological features. The mining method and the use of the pillars are also important factors for their geometry and stability. Pillars are basically classified into regional support pillars and local support pillars depending on the purpose of the pillars. The regional support pillars are typically:

1) Barrier Pillars

   In the room and pillar mining method, the barrier pillars act as the regional support to stabilize the panel and minimize the surface subsidence and separate one panel from the other.

2) Crown Pillars

   In steeply dipping orebodies, the near surface rock above the uppermost stope which provides regional support to the surface structures.

3) Shaft Pillars

   Large pillars are left around the shaft to ensure the stability of the shaft and the immediate infrastructure, and prevent surface subsidence and damage to the surface structures

The local support pillars according to the orebody orientations:

1) Flat lying orebodies
    a. Square/ Rectangular/ Irregular Pillars

In flat lying or gentle dipping orebodies, the room and pillar mining is adopted. Where the pillars act as the primary support in between the rooms and drifts.

2) Steeply dipping orebodies
    a. Sill Pillar

       In steeply dipping orebodies, the cut and fill mining, open stope mining and similar mining methods use the sill pillar. They are horizontal pillars supporting the stopes of the two different horizons.

    b. Rib Pillar

       Rib pillars act as the local support pillar between the stopes at the same mining horizon.

In this thesis, local support pillars only will be considered for the study of the failure mechanisms of the pillars, evaluation of the strength of the pillars and monitoring techniques for the pillars.

Pillars that are under-designed can lead to abrupt failure that can ultimately lead to a progressive pillar run and hence, the catastrophic pillar failure which can cause a whole stope or even a mine to collapse. A major incident of catastrophic pillar failure was observed in South Africa in Coalbrook Coal Mine on 21st January 1960 where 437 workers lost their lives when pillars within an area of 324 hectares collapsed (Salaman and Munro, 1967). In another room and pillar metal mine, failure of central four pillars in the mine triggered a chain failure of the pillars effecting 100 pillars at Magmont Mine, Missouri (Dismuke et al., 1994; Zipf 2000). The pillars that are over-designed lead to excess ore left in the mine that affects the production of the mine ultimately resulting in an economic loss for the deposit. Therefore, it is essential to understand the pillar performance and design the pillars safely and cost effectively.

The Coalbrook disaster triggered the formation of Coal Mine Research Controlling Council (CMRCC) in South Africa to study the pillar behavior in the coal mines and to design the pillars in a safe manner. Salamon and Munro (1967) conducted studies on the

125 pillars with 27 collapsed pillars and delivered a power function to estimate the strength of the coal pillars. It was concluded that the pillar strength evaluated was done through empirical methods and it should not be used beyond the boundaries of the database. Hedley and Grant (1972) adopted the coal formula to evaluate the strength of the pillars in Canadian Uranium Mines. The pillar studies were then conducted by many researchers to evaluate the strength empirically and this is discussed in Chapter 2 in detail. The two major empirical approaches that are widely used in the hard rock mining industry are the Hedley and Grant (1972) and Lunder and Pakalnis (1997).

Empirical approaches do not differentiate between the different failures mechanisms in the pillars. This is the significant drawback as the strength of the pillar depends on its failure mechanism. For example, the failure behavior of a rock sample under uniaxial compressive test is a shear plane passing through the center of the pillar while a rock sample with inclined discontinuity under uniaxial compression is sliding along the discontinuity. Failure mechanism in the pillars is similar to that of the rock sample (Esterhuizen, 2006). Therefore, the pillar failure mechanisms need to be also considered when designing the pillars. The empirical approaches are still helpful but may need to be modified considering the different factors that influence the failure mechanism of the pillars.

The factors that influence the failure mechanism of the pillars can be classified as:

- The orientation of the orebody and the stress tensor
- How the stresses change during subsequent mining operations
- Presence of geological structures
- Blast damage of the Pillar Skin
- Roof/ Floor conditions
- Water

In this thesis, pillar performance will consider the failure mechanisms.

1.2.Objective of the Thesis

The main objectives of this thesis are given as follows:

1) Empirical approaches seldom consider the effect of the inclinations on the hard rock pillar strength and the change of failure mode. The strength of the inclined pillars is less than the normally loaded pillars, therefore, adjustment is a required in the empirical approach to account for the inclination. Laboratory tests were conducted to understand the effects of inclination effects on the sample. Numerical simulations were conducted for large scale pillars and calibrated to the horizontal performance of pillars using the empirical approach.
2) Discontinuities in pillars play a major role in determining the strength of the pillar. To investigate the effect of the discontinuity orientation and the dip as well as in the dip directions with the help of the numerical approach to develop the designs of the pillar orientation according to the discontinuity orientation. The calibration of the numerical model was performed with the discontinuities orientated towards the pillar face and calibrated to the empirical and numerical approach. The numerical modelling was extended to inclined pillars to understand the failure mechanisms in the presence of discontinuities. The performance of the inclined pillars was evaluated, and an approach was developed to take the discontinuities into account.
3) Blasting causes the degradation of the pillar skin. To determine the effect of this skin degradation on the pillar strength a blast factor is needed to alter the properties of the skin in the numerical models. Calibration was performed through the strength performance of the horizontal pillars. An approach was developed to considering the blasting in terms of blast factor and blast thickness to design the pillar.
4) Monitoring of the pillars is essential to understand the condition of the pillar. Of importance is whether the pillars are as stable, unstable or failed, and this changes over time. Currently, the practice of monitoring the pillars is through visual

inspection and by estimating the fracture length developed in the pillars. Both the methods are qualitative and may vary according to the properties of the rock type. Therefore, a quantitative method has been developed for pillar monitoring based on strain analysis. Laboratory tests were conducted to understand the axial strains developed on the samples with different geometries.

In addition, an approach was developed to use these theories according to the geology of the orebody, orebody orientations, and natural occurring discontinuities and the blasting effects.

1.3.Outline of the Thesis

The chapters of this thesis have attempted to discuss the pillar designs and the failure mechanisms of the pillars by first reviewing the published literature in the form of empirical approaches, analytical methods and numerical techniques and current practices. The drawbacks of the approaches were identified and the parameters effecting the pillar failure behavior were taken as the key parameter to conduct this study.

The structure adopt in this thesis aids the future researchers and the industry professionals to understand the different failure mechanisms and evaluate the strength of the pillar according to the conditions of the pillars in the mine. It also provides with a potential monitoring system for pillars.

1.3.1. Chapter 2: State of the Art for Pillar Design

Chapter 2 provides an overview of the current pillar design methodology. The pillar failure modes are discussed which were based on the visual observations and the fracture length developed on the pillars (Prichard and Hedley, 1993; Lunder, 1994; Brady and Brown, 2006; Esterhuizen; 2006; Roberts et al., 2007; Styles et al., 2010). The concepts such as:

- Empirical approaches (Hedley and Grant, 1972; Potvin et al., 1989; Lunder and Pakalnis, 1997; Esterhuizen et al., 2008)
- Analytical methods (Zhou et al., 2011; Wattimena, 2014; Tomory et al., 2014; Zhou et al., 2015)

- Numerical techniques (Hedley et al., 1984; Martin and Maybee, 2000; Esterhuizen et al., 2006; Dolinar and Esterhuizen, 2007; Suorineni et al., 2011 and 2014; Elmo and stead, 2014; Napa Garcia and Navarro Torres, 2017)

are reviewed and their strength and shortcomings are discussed in detail.

1.3.2. Chapter 3: Laboratory and Numerical Investigation on Strength Performance of Inclined Pillars

K.V. Jessu, A.J.S. Spearing, M. Sharifzadeh (2018) "Laboratory and Numerical Investigation on Strength Performance of Inclined Pillars", Energies, 11(11), 3229

Inclined pillars undergo oblique loading which is a combination of compressive as well as shear loading in the underground mines which is not considered in designing the pillars. Gypsum molds and sandstone were tested in the laboratory with four different geometries and three different inclinations. The strength of the inclined samples was evaluated and the reduction in strength of the inclined samples with respect to the horizontal samples were explained failure mechanism of the inclined samples. Reduction factors were introduced to account for inclination effects for the samples. The laboratory samples provide the basis to establish the strength of the in-situ pillars. For large scale pillars, numerical models were simulated and calibrated to an empirical approach. An equation was developed to access the strength reduction factor at any inclination that can be incorporated in the empirical approach.

1.3.3. Chapter 4: Effect of dip on Pillar Strength

K.V. Jessu, A.J.S. Spearing (2018). Effect of dip on Pillar Strength. South African Institute of Mining and Metallurgy. Vol. 118, 756-765

Studies on inclined pillars have been conducted in the form of case studies (Hedley et al., 1984; Whyatt and Varley, 2008) where a single pillar was evaluated for its strength and its failure mechanism. Therefore, to evaluate the strength and the failure process of the inclined hard rock pillars at any given geometry, FLAC^{3D} (Itasca, 2018), a three-dimensional finite difference code used for resolving geotechnical problems was used.

Square as well as rectangular pillars were simulated at four different inclinations with four different geometries. The constitutive model and the properties were adopted from Esterhuizen et al., (2006) and Dolinar and Esterhuizen (2007) and the horizontal pillar strength was calibrated to the theoretical results given by Lunder and Pakalnis (1997). The failure mechanism of the pillars was discussed in detail to understand the dominant failure mechanisms of the pillars at a given geometry and inclination. The failure mechanisms would help in understanding the brittle failure mechanism in inclined pillars that lead to rock burst conditions.

1.3.4. Chapter 5: Effect of Discontinuity Dip Direction on Hard Rock Pillar Strength

K.V. Jessu, T.R. Kostecki, A.J.S. Spearing, G. Esterhuizen (2019). Effect of Discontinuity Dip Direction on Hard Rock Pillar Strength. SME Transactions. (Accepted, yet to be published)

Discontinuities play a major role in determining the strength of the sample as well as the pillars. The effect of discontinuity has been studied in cylindrical samples (Jaeger and Cook, 1994) where the orientation of the discontinuity in the strike direction is not considerable. Esterhuizen (2006) conducted studies on discontinuities in the direction of the pillar face while the strike direction of the discontinuities was not considered. As the discontinuities can occur in any strike direction, FLAC^{3D} (Itasca, 2018) was used to develop simulation that account for the discontinuities in strike direction. The properties and the constitutive models were maintained the same as the previous chapter and the discontinuity were introduced in the pillars in the form of Discrete Fracture Network (DFN). Only one major discontinuity was taken into consideration as the effect of multiple discontinuities can be evaluated with a help of equation given by Esterhuizen (2008). The performance of the pillars with three different discontinuity dips orientated towards the pillar face were evaluated which were calibrated to that of the numerical results of the Esterhuizen (2006). The numerical simulations were then carried out to understand the

effect of discontinuity at three different dip directions. This would help engineers in understanding the interactions of pillar orientations vis a vis a major discontinuity.

1.3.5. Chapter 6: Performance of Inclined Pillar with Major Discontinuity

K.V. Jessu, A.J.S. Spearing (2018) Performance of Inclined Pillar with Major Discontinuity. International Journal of Mining Science and Technology. https://doi.org/10.1016/j.ijmst.2018.09.006

Studies on discontinuities has been conducted only on horizontal pillars (Madden, 1995; Esterhuizen, 2006; Elmo and Stead, 2010) while the discontinuity effects on the inclined pillars has not been considered. Numerical modelling with the discontinuities were extended to the inclined pillars. Four different inclined pillars were used to determine the effect of the discontinuities on the pillars strength. For every pillar geometry, thirty-six different discontinuities were simulated at every 10° inclination was evaluated. It was expressed in the form of the polar coordinates form where the radius was defined by the strength of the pillar and the theta defined by the angle of the inclination of the discontinuity. The failure process was discussed according to the discontinuity and an approach was developed to evaluate the discontinuities effecting the inclined pillars according to its orientations. The dip directions of the discontinuities were also evaluated in the inclined pillars and the discussion were generated to design the pillar according to the discontinuities.

1.3.6. Chapter 7: A Parametric Study of Blast Damage on Hard Rock Pillar Strength

Jessu, K.V.; Spearing, A.J.S.; Sharifzadeh, M. A (2018). Parametric Study of Blast Damage on Hard Rock Pillar Strength. Energies, 11, 1901

Drilling and blasting is the most common method employed to develop hard rock excavations. A major challenge in this method is that it causes damage to the skin of the excavation due to the blast that can decrease the strength of the pillars (Bahrani et al., 2010). Pillars were simulated in FLAC^{3D} as the previous chapters and the skin of the

pillars was modelled with the help of the blast factor developed by Hoek et al., 2002. The properties of the skin were reduced according to the blast damage factor and four different damage factors were selected to carry out the parametric studies. The blast thickness is also an important factor that was considered in the models to evaluate the strength of the pillars. As the zone thickness is significant in determining the effect of blasting on the pillars, zone thickness equivalent to the least damage thickness was adopted. The blast damage was evaluated at different pillar heights to show the difference of blasting according to the volume of the pillars. Inclined pillars were also evaluated under blast damage. Tables were proposed to use for different blast damage factors and blast thickness which can be implemented in the underground mines for safe design of the pillars.

1.3.7. Chapter 8: Direct Strain Evaluation method for laboratory-based pillar performance

K.V. Jessu, A.J.S. Spearing. Direct Strain Evaluation for Laboratory-based Pillar Performance. Journal of Rock Mechanics and Geotechnical Engineering (Accepted. Yet to be published.)

The condition of the pillar is currently determined with the help of visual inspection or the length of the fracture relative to the pillar height (Lunder, 1994; Roberts, 2007) while there is no quantitative measuring tool to determine the condition of the pillars. Strain developed on the pillars can be used as a measure to understand the condition of the pillars. Sakurai (1981) developed direct strain evaluation method to determine the stability of the tunnels based on the laboratory samples and then co-related it to the in-situ tests. Idris et al., (2015) and Napa Garcia and Navarro Torres (2017) extended this method to pillars with the help of numerical modeling while the constitutive model used was Hoek and Brown which overestimates the pillar strength. Therefore, the direct strain evaluation technique was extended to the pillars in this thesis that was carried out with the help of laboratory tests with different geometries and different rock specimens. Sandstone and molded gypsum samples were used for testing in the laboratory. The strain analysis of the samples was carried out where the elastic strain and the failure strain were analyzed for

each of the samples. The ratio was generated between the failure strain and the elastic strain that was then related to the size of the sample. A relationship defining the strain ratio and the geometry of the sample was established. An approach was defined to use this relationship to monitor and design the pillars in an underground mine.

1.3.8. Chapter 9: Conclusions

The three main aspects of the failure mechanisms in the hard rock pillars were evaluated and proposed in the form of pillar design equations, tables and charts. Chapter 9 details the use of the results from the thesis in a single design chart. The proposed approach shows the step-by-step procedure to use these theories according to the orientation of the orebody, the geological effects and the blasting effects for the practical use in the underground mines.

Engineers need to have the basic knowledge about the uniaxial compressive strength, pillar orientation, discontinuity orientation and the expected blast damage. These parameters can then be used as an input in the design chart for the effective design of the pillars. For progressive optimization of the pillars and to determine the condition of the pillars, the direct strain evaluation technique can be implemented. This will effectively optimize the geometries of the mine pillars and increase the stability and safe workings of the personnel.

The limitations of the research work are also discussed and the future work that can deal with these limitations were detailed.

References

Bahrani, N. Suorineni, F. T., and Kaiser, P. K. (2010). Stability Analysis of Rib Pillars in Mechanized and Drill and Blast Excavations Using Numerical Modeling. In Proceedings of the MEMO'2010, Sudbury, ON, Canada, 24–27 October 2010.

Brady, B. H. G., Brown, E. T. (2007). Rock mechanics for underground mining. Chapman & Hall, UK.

Coates, D. F., Gyenge, M. (1981). Incremental design in rock mechanics. Monograph, vol. 880. Ottawa: Canadian Government Publishing Centre.

Dismuke, S. R., Forsyth, W. W. and Stewart, S. B. V. (1994). The Evolution of Mining Strategy Following the Collapse of the Window Area at the Magmont Mine, Missouri. Proceedings of the CIM Annual General Meeting, District 6, Metal Mining; pp 3-8.

Dolinar, D. R. and Esterhuizen, G. S. (2007). Evaluation of the effects of length on strength of slender pillars in limestone mines using numerical modelling. *Proceedings of the 26th International Conference on Ground Control in Mining*. Morgantown, WV: West Virginia University, pp. 304–313.

Elmo, D. and Stead, D. (2010). An integrated numerical modelling–discrete fracture network approach applied to the characterisation of rock mass strength of naturally fractured pillars. Rock Mechanics and Rock Engineering, 43(1):3–19

Esterhuizen, G. S. (2006). An evaluation of the strength of slender pillars. *Transactions of Society for Mining, Metallurgy, and Exploration, Inc.*; Vol. 320. Littleton, CO: Society for Mining, Metallurgy, and Exploration, Inc., pp. 69–76.

Esterhuizen, G. S., Dolinar, D. R. and Ellenberger, J. L. (2008). Pillar strength and design methodology for stone mines. *Proceedings of the 27th International Conference on Ground Control in Mining.* Morgantown, WV: West Virginia University, pp. 241–253.

Hedley, D. G. F. and Grant F. (1972). Stope and pillar design for the Elliot Lake uranium mines. *Canadian Institute of Mining and Metallurgy Bulletin*; Vol. 65, pp. 37-44.

Hedley, D. G. F., Roxburgh, J. W. and Muppalaneni, S. N. (1984). A case history of rock bursts at Elliot Lake. *Proceedings of Second International Conference on Stability in Underground Mining*, (ed. C. O. Brawner), 210–234, New York, American Institute of Mining, Metallurgical and Petroleum Engineers Inc.

Hoek, E., Carranza Toress, C. and Corkum B. (2002). Hoek-Brown failure criterion – 2002 edition, Proc. 5th. North American Rock Mechanics Symposium and 17th Tunneling

Association of Canada Conference. ATM TAC 2002. University of Toronto, University of Toronto, pp. 267-271.

Idris M. A., Sainag, D. and Nordlund, E. (2015). Stochastic assessment of pillar stability at Laisvall mine using artificial neural network, *Tunneling and Underground Space Technology*, Vol. 49, pp. 307–319.

Itasca Consulting Group (2016). Fast Lagrangian Analysis of Continua in 3Dimensions, Minneapolis, Minnesota, USA.

Jaeger, J. C., and Cook N. G.W. (1979). Fundamentals of Rock Mechanics, 3rd Ed. New York: Chapman and Hall.

Lunder, P. J. and Pakalnis R. (1997) Determining the strength of hard rock mine pillars. *Bulletin of Canadian Institute of Mining and Metallurgy*; Vol. 90, pp. 51-55.

Madden, B. J., Canbulat, I., Jack, B. W. and Prohaska, G. D. (1995). A reassessment of Coal Pillar Design Procedures. Safety in Mines Research Advisory Committee, COL 021, December 1995, pp 1-148

Martin, C. D. and Maybee W. G. (2000). The strength of hard-rock pillars. International Journal of Rock Mechanics and Mining Sciences 37:1239–1246

Napa-García, G. F. and Navarro Torres, V.F. (2017). Applicability of failure strain for the stability evaluation of square pillars in room and pillar mining, in M Hudyma & Y Potvin (eds), *Proceedings of the First International Conference on Underground Mining Technology*, Australian Centre for Geomechanics, Perth, pp. 557-565.

Potvin, Y., Hudyma, M.R. and Miller, H. (1989). Design guidelines for open stope support. Bull Can Min Metall, 82, 53-62.

Pritchard, C. J. and Hedley, D. G. F. (1993). Progressive pillar failure and rock bursting at Denison Mine. *Rock bursts and Seismicity in Mines*. Young (ed.). Baikema, Rotterdam.

Roberts, D.P., Tolfree, D. and McIntire, H. (2007). Using confinement as a means to estimate pillar strength in a room and pillar mine. 1st Canada-US Rock Mechanics Symposium, Vancouver, 1455-1462.

Salamon, M. D. G. and Munro A. H. (1967). A study of the strength of coal pillars. J. South Afr. Inst. Min. Metallurgy 68:55-67.

Sakurai, S. (1981) Direct strain evaluation technique in construction of underground opening. *Proceedings of the 22nd US Symposium on Rock Mechanics*, American Rock Mechanics Association, Alexandria, pp. 278–282.

Styles, T. D., Zhang, Y., Stead, D., Elmo, D., Roberts, D. and Yanske, T. (2010). A photogrammetric approach to brittle fracture characterization in mine pillars. 44th US Rock Mechanics Symposium, Salt Lake City, 1475-1482.

Suorineni, F. T., Mgumbwa, J. J., Kaiser, P. K. and Thibodeau, D. (2011). Mining of orebodies under shear loading Part 1 – case histories, *Mining Technology (Trans. Inst. Min. Metall. A)*, 120(3), 138–147.

Suorineni, F. T., Mgumbwa, J. J., Kaiser, P. K. and Thibodeau, D. (2014). Mining of orebodies under shear loading Part 2 – failure modes and mechanisms, *Mining Technology* (Trans. Inst. Min. Metall. A), 123(4),240–249.

Wattimena R. K. (2014). Predicting the stability of hard rock pillars using multinomial logistic regression. Int J Rock Mech Min Sci 71:33–40

Whyatt, J. and Varley, F. (2008). Catastrophic failures of underground evaporite mines. In *Proceedings of twenty-seventh International Conference on Ground Control in Mining*. 113–122, Morgantown, ICGCM.

Zipf, R. K. (2001) Toward pillar design to prevent collapse in room-and-pillar mines. 108th Annual Exhibit and Meeting, Society for Mining, Metallurgy and Exploration, Denver.

Zhou, J., Li, X. B., Shi, X. Z., Wei, W. and Wu B. B. (2011) Predicting pillar stability for underground mine using Fisher discriminant analysis and SVM methods. Trans Nonferrous Metals Soc China 21(12):2734–2743

Zhou, J., Li, X., Mitri, H. S. (2015) Comparative performance of six supervised learning methods for the development of models of hard rock pillar stability prediction. Nat Hazards 79:291–316

Chapter 2

State of the Art of Pillar Design

2.1. Introduction

In hard rock underground mines, pillars are often left between the openings (stopes) to maintain the macro stability of the openings. They need to be adequately designed to avoid sudden failure, maintain stability but also not be over-designed such that safety is assured and extraction and profit are maximized. Depending on the nature of the ore body and hence the mining method selected, the pillars can have varying complexity.

Flat lying tabular ore bodies generally use room (bord) and pillars mining operations where the checkerboard pillars are left for the local internal support and the barrier pillars for the regional support. Depending on the high economic value of the deposit, a drift and fill with pillar extraction could rather be considered. When the orebodies have a significant dip, ribs pillars are frequently used for the local support and sill pillars to divide the orebody into multiple mining horizons. Crown pillars can be typically used to prevent collapse to surface. This thesis mainly deals with the pillars that are used for the local (internal) stope support.

A systematic literature review has been conducted and is presented in a manner as follows:

1. Pillar failure modes which includes the stress induced failures, structure-controlled failures and the pillar rating systems
2. Empirical approaches that consider the width to height ratio, minimum principal stress, length to width ratio and discontinuity orientation.
3. Analytical approaches which include statistical distributions, probabilistic methods, and machine learning methods or the hybrid methods (a combination of all the above methods).
4. Numerical approaches for pillar designs including the boundary element methods, finite element and difference methods, discrete element methods and hybrid numerical models to determine the strength and potential failure modes of the pillars.

2.2. Pillar failure modes

Several factors influence the failure modes in hard rock pillars: these include rock type and properties, local and regional geological structures, pillar slenderness and in situ stress conditions (Brady and Brown, 2007). Structure-controlled and stress-controlled type of failure modes can describe the hard rock pillar failures. Structure controlled are where pillar failure caused due to unstable rock block sliding along the discontinuities in a low in situ stress environment as shown in Figure 2.1 and at greater depths with higher in situ stress, stress controlled tensile fractures running parallel to maximum principal stress causes the failure (Hoek et., 1995).

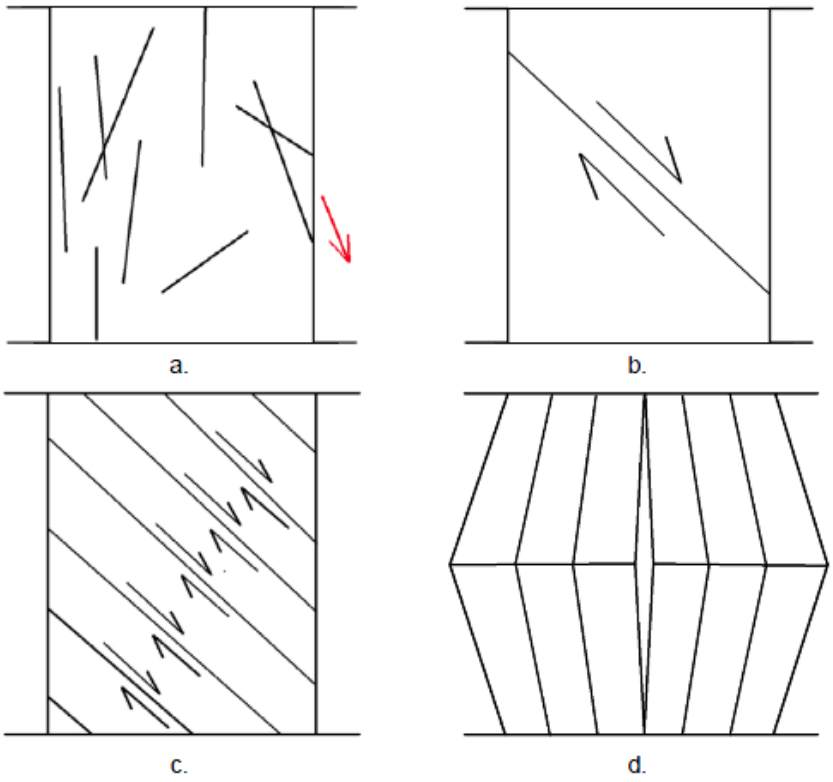

Figure 2.1: Structure controlled failures a) rock block sliding b) through going shear failure c) transgressive shear failure and d) buckling failure (Brady and Brown, 2007)

Pritchard and Hedley (1993) first classified the pillars of the Denison mine based on the stress induced progressive failure into five categories as shown in Figure 2.2. The progressive failure mechanism is based on the large pillar. The minor spalling of the walls was represented as the Stage 1 followed by major spalling as Stage II which is caused due to the low confinement on the outer skin of the pillar and high tangential stress leading to cracks and slab formation parallel to the direction of the major principal stress in the pillars. With the increase in spalling, outer skin of the pillar is lost and pillar stress is

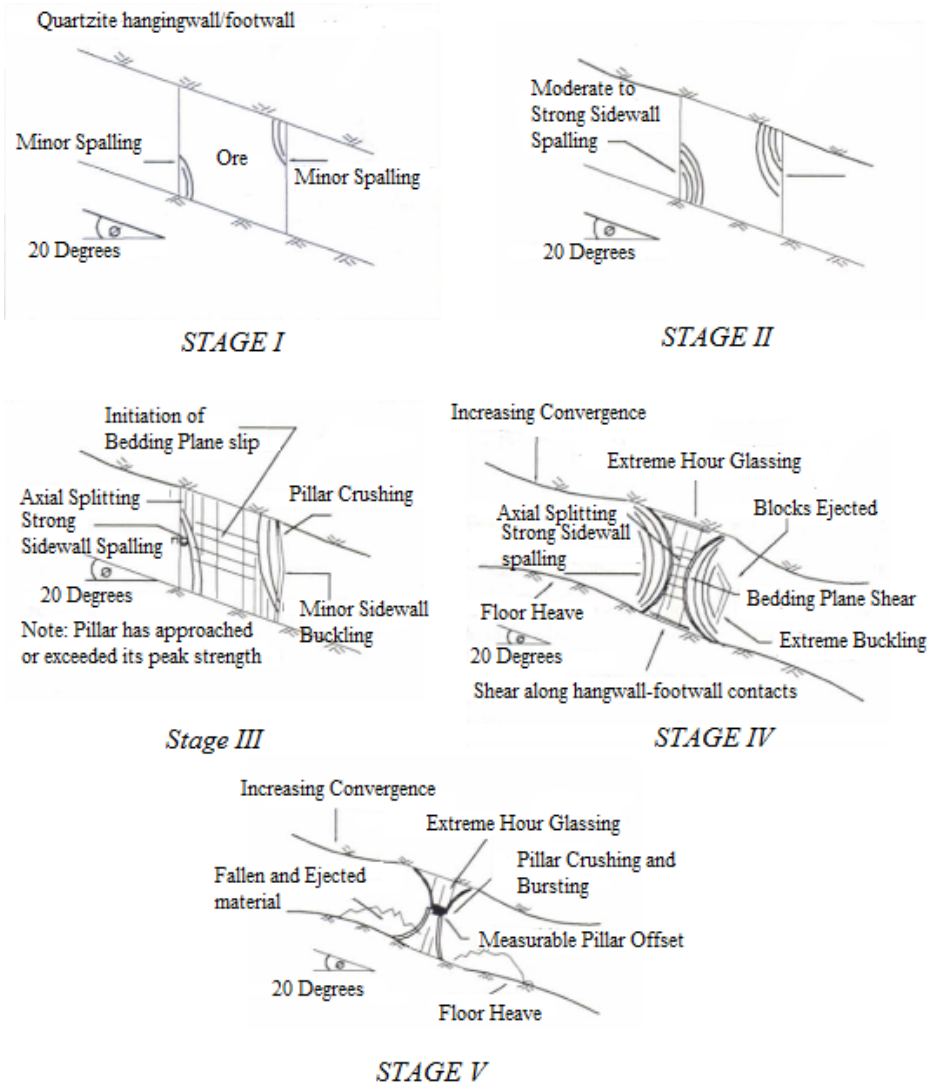

Figure 2.2: Pillar failure classification stages by Pritchard and Hedley (1993)

redistributed to the intact rock as shown in Stage III. The further loss in confinement to the pillar core leads to the damage of the newly exposed walls (Stage IV) ultimately leading to the failure of the pillar (Stage V).

Lunder (1994) classified the pillars into five classes depending on the fractures observed on the pillars from the underground mines of Westmin Resouces Ltd. When the pillar showed no signs of stress induced fracturing on the outer skin of the pillar, it was classified as the Class I. As the corners of the pillars started developing fractures, the pillars were classified as Class II pillars. Pillars were classified as Class III when the fractures observed on the outer skin of the pillar had a length less than or equal to half the pillar height and apertures (opening) of less than 5mm. When the fractures coalesced and the length of the fractured were greater than the half the pillar height with aperture greater than 5mm, it was classified as the Class IV pillars. Finally, the disintegrated pillars with blocks falling apart with fractures passing through the pillar core and the aperture higher than 10mm are classified as Class V pillars.

Fang and Harrison (2002) simulated rock pillar failures by developing a local degradation model. It consists of degradation index that classifies the rock fracture at microscopic level into two components namely brittle and ductile. The brittle component reduces the local material elasticity and strength, whilst the ductile component results to plastic deformation. The failure process of width to height ratio of 2.0 was simulated to the corresponding stress strain curve of the pillar as shown in Figure 2.3 and 2.4.

Stage (a) shows the fracture initiation followed by spalling caused by coalescence of the fractures in Stage (b). In stage (c), the shear fractures emanate from the one of the pillar ends and grow towards the other end in an inclined fashion to the center of the pillar in stage (d). Development of shear to the center of the pillar from both sides was determined as the peak strength stage (e) and the stage (f) was caused by the extension of the shear fractures (Figure 2.4). The modelling was performed for the hard rock pillars while it was calibrated to the coal pillar.

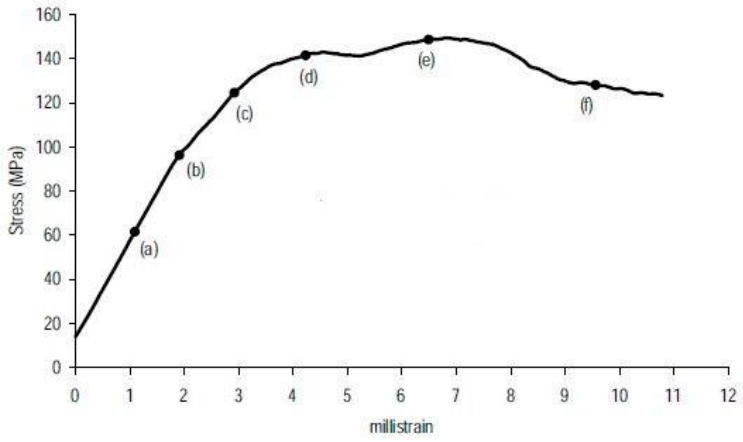

Figure 2.3: Stress-strain curve showing the behavior of W/H ratio of 2.0 (Fang and Harrison, 2002)

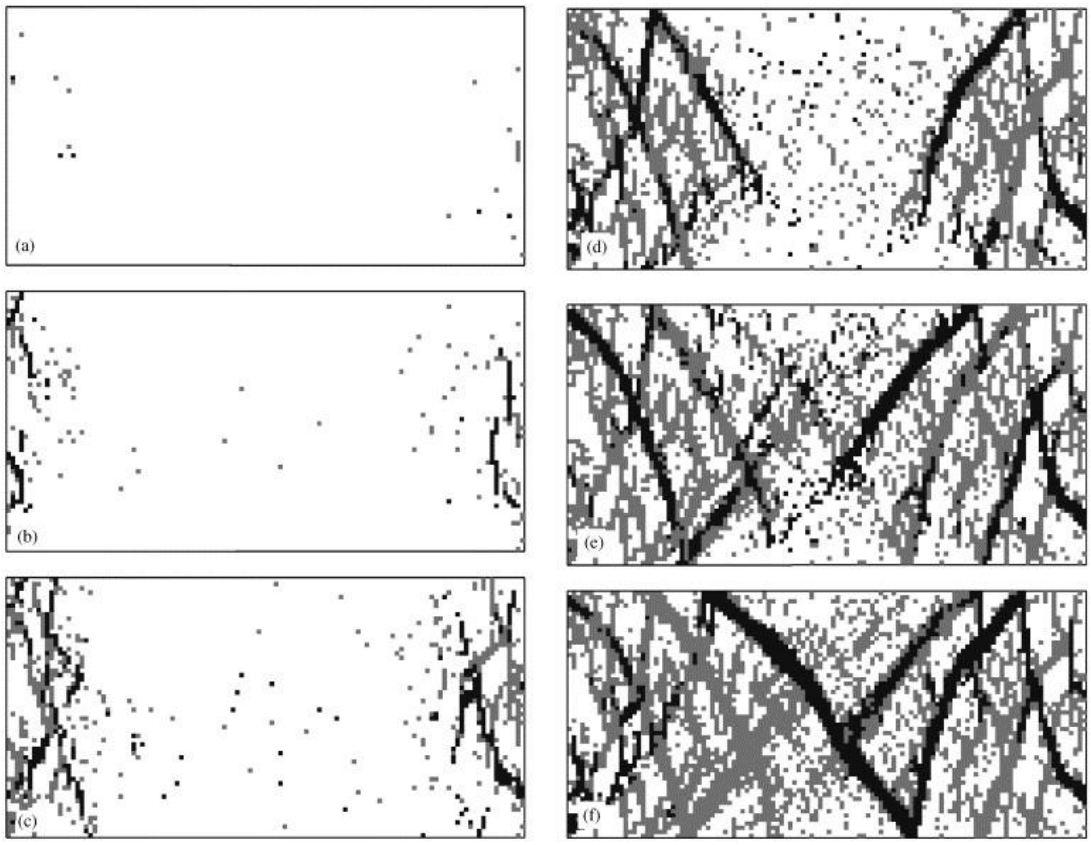

Figure 2.4: Pillar failure stages of W/H ratio of 2.0 using the FLAC2D with local degradation model (Fang and Harrison, 2002)

Esterhuizen et al. (2006) conducted pillar studies in the limestone mines in the United States and developed pillar stress rating similar to that of the Lunder (1994) and geological rating system that describes the effect of the geological structures such as the joints and the faults on the pillar strength by visual inspection. They were classified as none, minor, moderate, severe and very severe according to the block fallout after blasting as shown in Figure 2.5. None representing the joint block fallout less than 0.3m and that between 0.3-1m was classified as minor. Moderate represented the pillar effected with block fallout of about 1-3m and higher than 3m were recognized as severe. When the pillar was bisected with a through-going structure with more than 35° dip angle, where the strength depends on the discontinuity strength, it was classified as very severe.

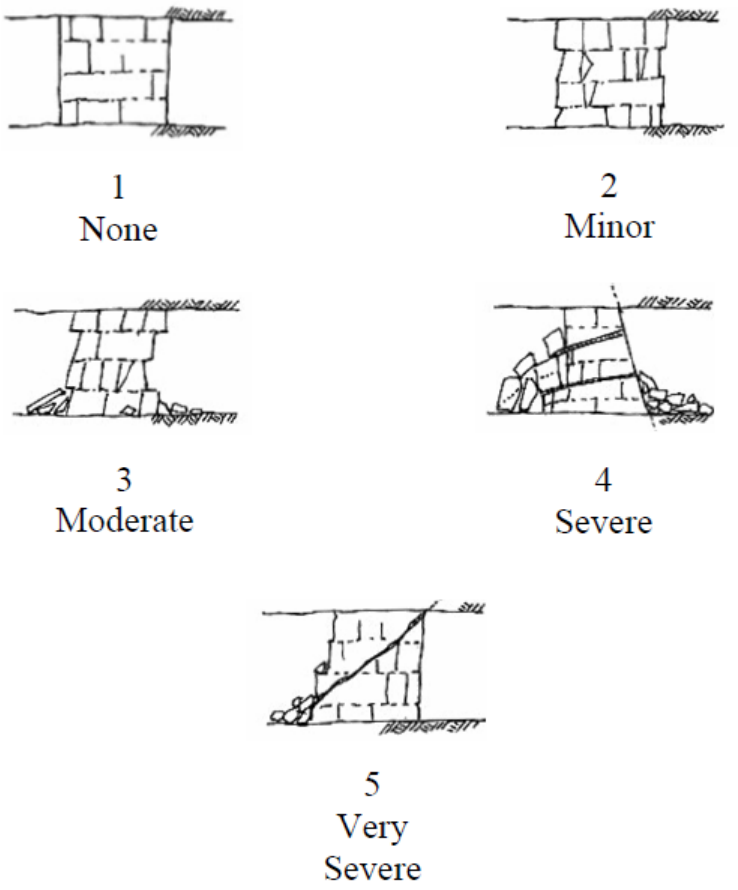

Figure 2.5: Geological rating system of pillar failure after Esterhuizen et al. (2006)

Roberts et al. (2007) described the progressive stress-induced pillar failure through a 6-stage pillar rating system starting from an intact pillar at stage one to failed pillar at stage six as shown in Figure 2.6. First stage was described as the intact pillar where it shows no indication of the stress induced fracturing. Second stage defined when the minor spalling was observed on the pillar face where the fractures are relatively small when compared to the pillar height. The substantial spalling with feathery slabs on the pillar face was denoted as the third stage where the fractures were estimated up to half the pillar height.

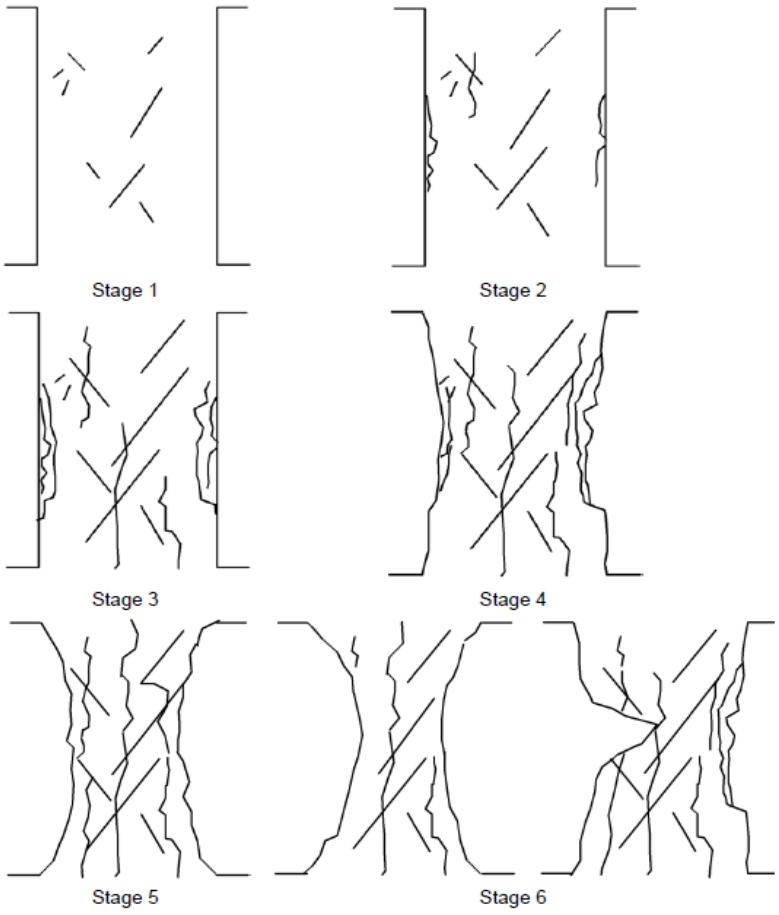

Figure 2.6: Pillar failure rating system; Stage 1: Intact pillar; Stage 2: Minor spalling; Stage 3: Substantial spalling; Stage 4: Formation of hour glass shape; Stage 5: Well-developed hour glass shape; Stage 6: Failed pillar - Two different ways (Roberts et al., 2007)

Fourth stage was the early development of the hour glass formation with large slabs on the pillar face and fractures greater than the half of the pillar height. Fifth stage comprised of well-developed hour glass formation with large open fractures cutting through the core and massive spalling on the pillar face. Failed pillar in the sixth stage was classified as extreme hour glass formation or fall out of major blocks from the pillar which carries minimal residual load carrying capacity. These stages were used as the primary reference for the numerical models.

Hard rock pillar damage characterization was conducted with the help of close range digital photogrammetry by Styles et al. (2010) as shown in Figure 2.7. Total station survey combined with the photogrammetric models were used to develop layout of the pillar face and the surface are of the pillar. An artificial plane, a meter inside the pillar face is taken to develop the cross-sectional area of the face to understand the hourglass formation. It is an efficient way to classify the pillar without direct access to the area.

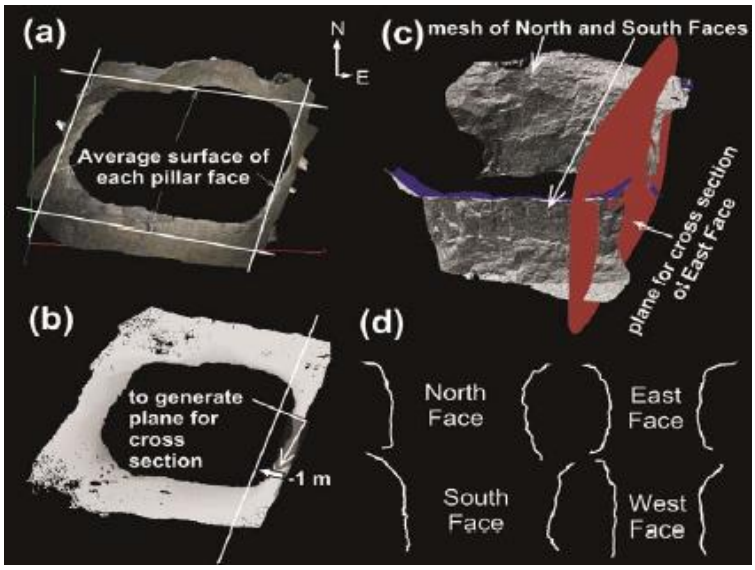

Figure 2.7: Pillar failure characterization with the help of close range digital photogrammetry a) average surface area of the pillar b) cross-sectional plane c) perpendicular cross-sectional plane d) generated pillar independent face profiles (Styles et al., 2010)

2.3. Empirical Approaches for Pillar Design

Numerous pillar studies have been conducted in the last few decades and most common being the empirical approaches that are the result of the back analysis from stable and failed pillars. One of the earliest hard rock empirically based pillar strength study was conducted by Bunting (1911) where the thirteen anthracite prisms were tested in laboratory with specimen sizes between 5 cm and 10 cm. It was demonstrated that the strength of the pillar has a relation to their lateral dimension and height that is given as:

$$\sigma_p = 700 + 300\,\frac{b}{h} \quad (psi) \tag{2.1}$$

Where σ_p is the crushing strength per unit area (psi), b is the least lateral dimension (inch) and h is the height of the prism (inch). The acceptable safety factor was taken as 2.5 that was considered in the equation derived by Bunting. Equation (2.1) was extended to evaluate the behavior of the pillars where 8 pillars were analyzed including one failed pillar.

Obert and Duvall (1946) conducted extensive studies on different rock types and with width to height ratios of half to 3 and determined a relationship between the strength of the specimen and the width to height (W/H) ratio that is given as:

$$\sigma_p = \sigma_0 \left(0.778 + 0.222\,\frac{W}{H}\right) \tag{2.2}$$

where σ_0 is the compressive strength of the rock specimen with W/H ratio of 1.

Pillar research was given a great importance after the Coalbrook pillar disaster after which the Salaman and Munro (1967) investigated 125 coal pillars to establish a relationship between the strength of the coal pillars and the shape of the pillars that is given as:

$$\sigma_p = K\frac{W^{0.44}}{H^{0.66}} \tag{2.3}$$

where K is the constant depending on the strength of the coal which is given 7.17.

Hedley and Grant (1972) investigated 28 granite pillars based on stable, partially failed and failed pillars and expressed the strength of the pillars as:

$$\sigma_p = K \frac{W^{0.5}}{H^{0.75}} \tag{2.4}$$

Where σ_p is the pillar strength, K is the unit strength of the rock, w and h are the width and height of the pillar respectively. Most of the early pillar studies (Potvin et al., 1989; Sjoberg, 1992) were conducted in Canada, where all the data sets were evaluated and have updated throughout the years.

Wagner (1980) considered blast damage effect on coal pillars with drill and blast method in the Salaman and Munro database. It was considered that 0.3 m of the pillar is affected by blasting. To develop the pillars with continuous miners where there is no blast damage, an equation was derived to quantify the benefit of using the continuous miner:

$$\sigma_{pd} = \sigma_p * \left(1 + \frac{\Delta W}{W}\right)^{2.46} \tag{2.5}$$

where the σ_{pd} is the pillar strength without blast damage, σ_p is the pillar strength from Salaman and Munro formula, ΔW is the damaged pillar width and W is the nominal pillar width. To take the effective width into consideration for the rectangular pillars, an equivalent width theory was derived by Wagner (1980):

$$w_{eff} = \frac{4A}{P} \tag{2.6}$$

Where W_{eff} is the effective width, A is the area of the pillar and P is the perimeter of the pillar.

Martin and Maybee (2000) listed out all the empirical approaches to determine the strength of the pillar with different rock types as shown in Table 2.1. Coal pillar studies were extensively conducted which are also represented in Table 2.1.

Table 2.1. Empirical Approaches to determine pillar strength (Martin and Maybee, 2000).

Empirical Approaches (MPa)	UCS Rock Strength (MPa)	Rock Type	No. of Pillars considered	References
$133\frac{W^{0.5}}{H^{0.75}}$	230	Quartzites	28	Hedley and Grant, 1972
$65\frac{W^{0.46}}{H^{0.66}}$	94	Metasediments	57	Kimmelmann et al., 1984
$35.4(0.778 + 0.222\frac{W}{H})$	100	Limestone	14	Krauland and Soder et al., 1987
$0.42\sigma_c\frac{W}{H}$	–	Canadian Shield	23	Potvin et al., 1989
$74(0.778 + 0.222\frac{W}{H}$	240	Limestone	9	Sjoberg, 1992
$0.42\sigma_c(0.68 + 0.52k)$	–	Hard Rocks	178	Lunder and Pakalnis, 1997
$k(\frac{\sqrt{W}}{H})$	-	Coal	-	Holland and Gaddy, 1964
$6.2(0.64 + 0.36\frac{W}{H})$	-	Coal	66	Bieniawski, 1975
$6.2(0.64 + 0.54\frac{W}{H} - 0.18\frac{W^2}{LH})$		Coal		Mark and Chase, 1997

Lunder (1994) developed a back-analysis approach with 178 case histories from Canadian mines. This approach also included the confinement effect that is important for the pillars over width to height ratio of 1. Major part of these pillars includes the rib and sill pillars. Three regions were proposed in which the factor of safety (FOS) less than 1 is classified as failed, while the region between FOS of 1 and 1.4 was labelled as unstable and FOS greater than 1.4 as stable pillars. It is the most commonly used empirical pillar approach that is used to design the pillars and is given as:

$$\sigma_p = K * UCS * (C1 + C2 * \kappa) \tag{2.7}$$

where σ_p is the ultimate strength of the pillar (MPa), K is the pillar size factor, UCS is the uniaxial compressive strength of the intact rock (MPa), C1 and C2 are the empirical rock mass constants and κ is the friction term which is calculate as:

$$\kappa = \tan\left[cos^{-1}\left(\frac{1 - C_{pav}}{1 + C_{pav}}\right)\right] \tag{2.8}$$

$$C_{pav} = Coeff * \left[Log\left(\frac{W}{H} + 0.75\right)\right]^{1.4(W/H)} \tag{2.9}$$

where C_{pav}, the average pillar confinement and the Coeff is the coefficient of pillar confinement.

Iannacchione (1999) conducted studies on stone pillars in limestone mines where it was concluded that the small pillars with width to height ratios of less than 1.2 have low strength and are mainly affected by the discontinuities present in the rock mass and the pillars with width to height ratio of greater than 1.5 would have higher strength. The largest discontinuity angle that effects the strength of the pillars was found to be 45° + ϕ/2 where ϕ is the friction angle of the discontinuity.

Esterhuizen et al., (2008) developed an empirical approach based on numerical modelling which also addressed the discontinuities in the pillar. It is also noteworthy that a constant of 0.65 was used to degrade the uniaxial compressive strength (UCS) of the limestone that

implies that the pillar strength is only applicable to the limestone mines. They proposed the pillar strength (S) can be calculated using:

$$S = 0.65 * UCS * LDF * \frac{w^{0.30}}{h^{0.59}} \quad (2.10)$$

where UCS is the Uniaxial Compressive Strength of the intact rock (MPa), w and h are the width and height of the pillar respectively and the LDF is the Large Discontinuity Factor which is given as:

$$LDF = 1 - DDF * FF \quad (2.11)$$

where DDF is the Discontinuity Dip Factor and FF is the Frequency Factor. This provides an estimate on average impact of large discontinuities on pillar strength.

Esterhuizen (2008) modified the Wagner (1992) equivalent width method to estimate the benefit of the length on the pillar strength and is calculated as follows:

$$w_e = w + \left(\frac{4A}{C} - w\right) * LBR \quad (2.12)$$

where w_e is the equivalent width of the pillars, w is the width of the pillar, A is the pillar plan area and C is the circumference of the pillar and LBR is the Length Benefit Ratio which increase from zero to one as the pillar width to height ratio increases from 0.5 to 1.4.

Elmo and Stead (2010) on the basis of the numerical modelling developed a graphical approach that relates the pillar strength with the fracture intensity. It shows that the strength of the pillar is inversely proportional to the fracture intensity. It was also concluded that there is a relationship between the fracture intensity, fracture length, UCS, fracture toughness and width to height ratio. The strength variation is higher in the slender pillars and as the size of the pillar increases, the

Da Silva (2013) conducted studies on uniaxial compressive stress tests using prismatic and cylindrical specimens and defined a relationship between strength and width to height

ratio. Three rock types were tested namely manganese, basalt and limestone and three different relationships were generated. The shape effect was then integrated with the size effect conducted by Ayres da Silva (2014) in designing the pillars at large scale in manganese mine.

Walls and Mpunzi (2017) conducted hard rock pillar studies in a room and pillar mine where Hedley and Grant approach was used to design the pillars. The 'K' factor was modified for two different scenarios in the mine depending on the clay filled structures and the uncertainties in the rock mass conditions.

2.3.1. Tributary Area Theory

The empirical approach is generally based on the tributary area theory that is a simple and effective way to estimate the stress on the pillars (Salaman and Munro, 1967; Hedley and Grant, 1972). The pillar vertical stress (P_s) can be calculated with the help of the overburden stress and the extraction ratio (r) which is given as:

$$P_s = \gamma g h \left(\frac{1}{1-r}\right) \tag{2.13}$$

where γ is the density of the rock, g is the gravity and h is the overburden height.

If the pillar width and length are given by w_p and l_p and the room spans are given by w_r and l_r as shown in Figure 2.8, then the tributary area of the pillar is estimated as:

$$A = \left(w_p + w_r\right)\left(l_p + l_r\right) \tag{2.14}$$

The extraction ratio can be estimated as:

$$r = 1 - \frac{w_p * l_p}{\left(w_p + w_r\right)\left(l_p + l_r\right)} \tag{2.15}$$

Safety factors are implemented to design any geotechnical structure to account for uncertainties in the rock properties. Safety factor (FS) in the underground pillars is implemented in the form of:

$$FS = \frac{\sigma_p}{P_s} \tag{2.16}$$

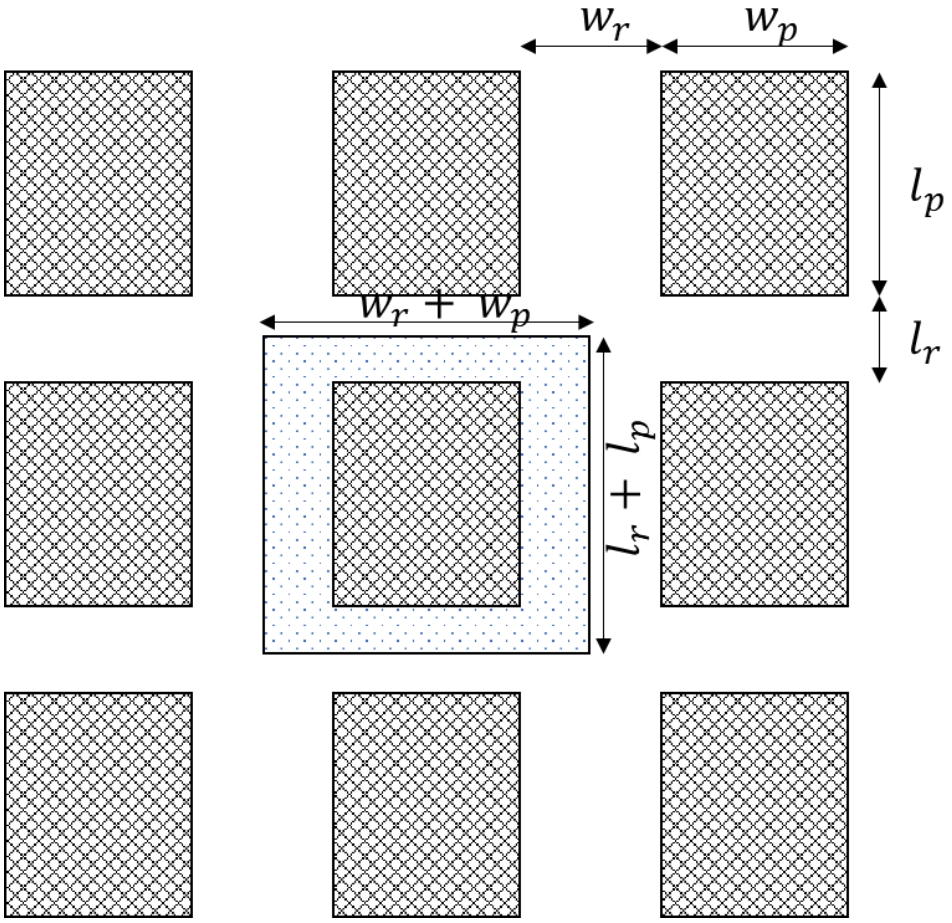

Figure 2.8: Tributary area theory

2.3.2. Safety Factors for Pillar Design

If pillar stress is greater than the pillar strength, then the pillar fails as it cannot sustain the load on it, therefore, the pillars with safety factor of less than 1 should be obviously avoided, unless yield pillars are required (i.e. pillars in post failure by design). The safety factor of pillar should be greater than 1 to keep the pillars stable. Factor of safety of 2.5 was implemented in the anthracite pillars by Bunting (1911) and as the research continued towards better understanding of the pillar strength and the pillar failure behavior, the safety factors were lowered to 1.4-1.6 (Hedley and Grant, 1967; Lunder and Pakalnis,

1997). Safety factors were also obtained with the help of quantitative analysis of the factors effecting the pillars and the probabilistic studies (Ghasemi et al., 2010a; 2010b; Song and Yang, 2018)

The empirical approaches are dependent on the site-specific factors that should be included as caveats with the formula developed. This could include the ranges of the rock mass types and properties; the depth and the geology. Potential uncertainties therefore prevail if adopted with mining systems outside the conditions of the database. Even though the empirical approaches provide the user with reasonable estimates of the pillar strengths in the complex in situ conditions, the deformation characteristics in the pillar failure process are seldom considered.

The pillar strength depends on the failure characteristics similar to the specimens in the laboratory where if specimen subjected to uniaxial compressive loading will lead to shear failure passing through the center of the pillar while the specimen with lower width to height ratio will lead to spalling at the edges with higher strength. The specimen with discontinuities slide along the discontinuities leading to lower strength of the specimen. Therefore, the empirical studies should be modified to consider the failure mechanism of the pillars.

2.4. Analytical Approaches for Pillar Design

Apart from the empirical approaches, numerous analytical approaches were conducted in the last decade with the help of statistics, probabilistic methods, and artificial intelligence methods or the hybrid methods that is the combination of the methods.

One of the earliest statistical studies to estimate the hard rock pillar strength was conducted by Esterhuizen (1993) and concluded that the pillar strength can be related to variability in the rock mass properties and mining factors. Griffiths et al., (2002) conducted studies on underground pillar stability with the help of probabilistic methods. It was concluded that with the help of Monte-Carlo simulations, a direct relationship can be established between the factor of safety and probability of failure. Cauvin et al., (2009)

conducted the pillars studies of the abandoned room and pillar mines in France with the help of statistical distribution and probabilistic functions to determine the uncertainties of the input parameters on the pillar strength. It was concluded that the uncertainties in the shape determination and the back analysis are two main problems that can impact the strength of the pillar.

Zhou et al., (2011) conducted studies on the pillar stability with the help of the Support Vector Machine (SVM) method and Fisher discriminant analysis technique which are statistical techniques by using width and height of the pillar, width to height ratio of the pillar, uniaxial compressive strength of the intact rock and pillar stress. It was concluded that uniaxial compressive strength and the height of the pillar are the most important parameters followed by the pillar stress, width and width to height ratio. It was also concluded that SVM methods were better than the Fisher discriminant analysis technique in determining the pillar stability for underground mines.

Wattimena (2014) and Tomory et al., (2014) applied a logistic regression method to predict the probability of the pillar stability with the help of log linear regression based on categorical empirical data. Idris et al., (2015) conducted stochastic assessment of the pillar stability using Artificial Neural Network (ANN). It was concluded that the factor of safety is not an adequate parameter to establish the stability of the pillars with the uncertainties in rock mass material properties. It was determined that the probability of failure and the reliability assessment are the two main parameters for pillar stability.

Zhou et al., (2015) compared six supervised learning methods to assess the pillar stability in hard rock mines. The six supervised learning methods were: linear discriminant analysis, multinomial logistic regression, multilayer perceptron neural networks, support vector machine (SVM), random forest (RF), and gradient boosting machine. These methods were applied on 251 pillar cases from various mines with six parameters. It was concluded that the database was represented by SVM and RF learning methods in a realistic manner.

The use of analytical studies has become more and more common in the last decade in these areas. These methods can be adopted to understand the risk reassessment and the probability of failure for the pillar stability. However, there is a need to understand the failure mechanism of the pillars to develop the risk assessments around those pillars. Therefore. These equations should be used with caution and should not be directly implemented in the field.

2.5. Numerical Approach for Pillar Design

Numerical approaches can be subdivided into continuum, discrete and hybrid models. The continuum models include Boundary Element Method (BEM), Finite Element Method (FEM) and Finite Difference Method (FDM). Discrete methods comprise of Discrete Element Method (DEM) and Discrete Fracture Networks (DFN) and the hybrid models are the combination of continuum and discrete methods. The use of the methods depends on the scale of the model and fractures. Continuum modelling is preferred for massive or highly deteriorated rock mass. It can also be used for the rocks having few fractures and with no significant effects of fracture opening and complete block detachment. Discrete elements are applicable to model large number of fractures and the large-scale displacement of the block movement is important to understand (Jing and Hudson, 2002)

2.5.1. Boundary Element Method

Boundary Element Method (BEM) for rock mass modelling is useful in reducing the computational time as it includes simple mesh generation and input data preparation when compared to other continuum methods. It can also be used to simulate the fracturing process in rocks, however limited to fracturing in homogenous and linear elastic bodies (Jing and Hudson, 2002).

There are three methods in BEM's applicable for rock mass modelling which include direct method, indirect method and displacement discontinuity method. The Direct Method involves solving of the stresses and displacements directly from the specific boundary conditions. The Indirect Methods comprises of calculating the stresses at boundaries at the start followed by calculating displacements with the help of separate

relations. The Displacement Discontinuity Method is suitable for simulating the fracture growth and is applied to rock fracture problems.

Hedley et al., (1984) conducted stress analysis on two pillars with same extraction ratio. One pillar was strike pillar where it was undergoing normal loading condition and other was at 20° inclination where it was undergoing oblique loading condition as shown in Figure 2.9. The stress analysis showed that at same stress, the strike pillar was stable with a factor of safety of 1.2 while in the dip pillar, the failure extended from one side of the pillar to the opposite side of the pillar. Therefore, the dip pillars caused the domino pillar burst effect in the Quirke Mine.

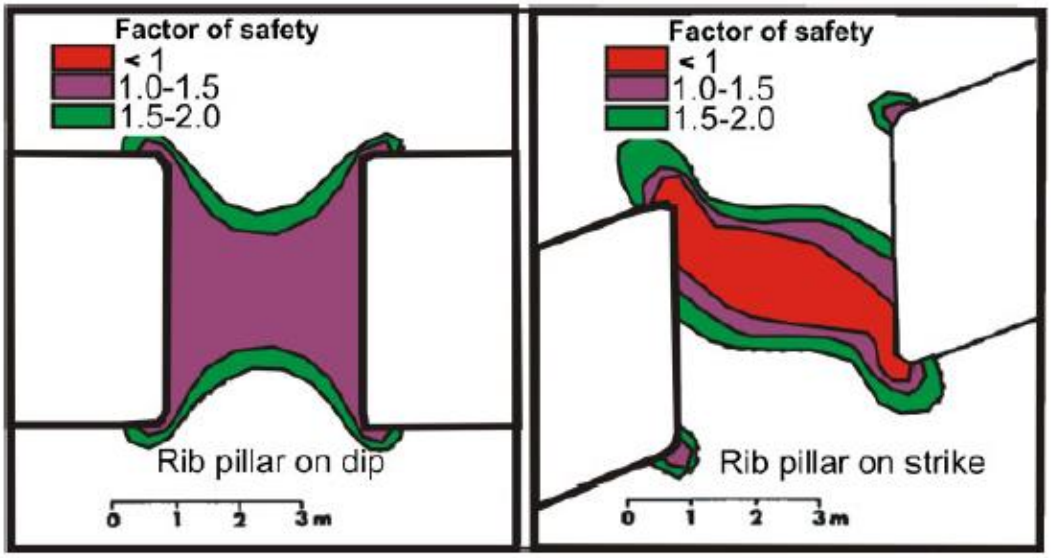

Figure 2.9: Pillar under a) normal loading b) oblique loading (Hedley et al., 1984)

Maybee (2000) used Examine2D (Rocscience, 1999), a two-dimensional indirect method and Map3D (Wiles, 2009), a three-dimensional DDM code to simulate the hard rock pillars and determine the stress on the pillars to compare it with the tributary area theory. It was concluded that the 13 pillars in a row is required in a two-dimensional plane to provide an accurate representation of the stresses in a room and pillar mine.

In Doe Run Mine, for the pillar stability analysis, a DDM code NFOLD (Golder Associates, 2001) is been used (Lane et al., 1999). In the NFOLD models, the ore body is characterized as an infinite elastic material with the excavations represented with elastic, nonlinear with post peak properties. Roberts (2007) conducted studies on NFOLD by modelling the Doe Run mine pillars and linked it to the pillar rating system as shown in the Figure 2.4. The central elements of the pillar are provided with higher strength to reflect the lateral confinement effect that was derived from the Lunder's average pillar confinement formula.

Kaiser et al., 2010 conducted studies on deep hard rock underground pillars with Examine2D (Figure 2.10) and concluded that the pillars exceeding the width to height ratio of 1.5 to 2.0 may have higher strength than the strength evaluated by the empirical methods. In the squat pillars, the core of the pillar is confined such that the rock mass may exhibit higher strength and it is not as affected by the failure of spalling propagation from the walls.

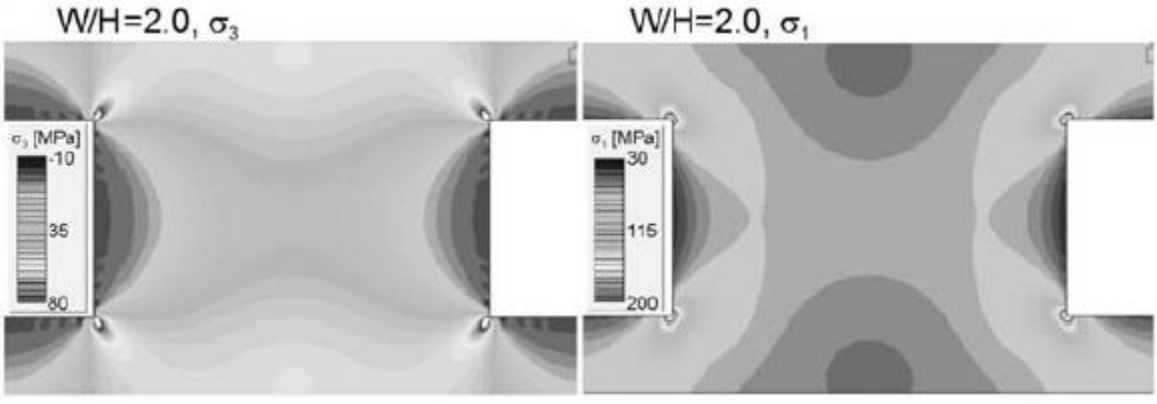

Figure 2.10: σ3 and σ1 contours in Examine2D of pillar with W/H ratio of 2.0 (Kaiser, 2010)

Rahjoo et al., 2016 conducted studies on effects of intermediate principle stress on the strength of highly brittle rock masses and characterized it as critical entity for evaluating the location and depth of pillar spalling. They proposed extensional strain criterion to

establish the pillar strength in massive hard rocks. This strain theory is different than the Strain Evaluation theory developed by Sakurai (1981).

2.5.2. Finite Element/Difference Method (FEM/FDM)

The general principle of Finite Element Method is to divide the area of the problem into smaller divisions called finite elements and conduct the local approximation inside each finite element followed by performing the finite element assembly to find the solution of the global matrix equation. It was the first numerical method which was able to account for material heterogeneities, non-linearity, complex geometries and boundary conditions (Jing and Hudson, 2002).

The basic technique of the Finite Difference Method is to discretize the governing partial differential equations by substituting the partial derivatives with differences defined over a certain interval in the coordinate direction (Jing and Hudson, 2002). There are three different schemes in FDM that include explicit or forward, implicit or backward and the central difference method.

Hoek and Brown (1980) conducted studies on rock pillar with the help of FEM and characterized the stresses developed on the pillars. They concluded that at the mid height of the pillar displays uniform stress distribution for the slender pillars. The stress observed at the center of the pillar is approximately equal to the uniaxial compressive strength which can is given as: maximum principal stress (σ_1) is equal to average external stress and the minimum principal stress is equal to zero.

Tang and Kaiser (1998) developed FEM code RFPA (Rock Failure Process Analysis) and conducted rib pillar failure studies to simulate the damage accumulation and seismic energy release. They showed the interdependence of stress, strain, acoustic or seismic emissions and seismic energy release. It was also concluded that the pillar load bearing capacity reduces drastically with weak hanging or footwall that leads to seismicity occurring at much lower stress levels than expected.

Maybee and Martin (2000) conducted pillar studies with Phase2D (Rocscience, 2018), finite element method software. They used the brittle Hoek Brown parameters to evaluate the strength of the hard rock pillars. It was concluded that the traditional Hoek Brown parameters overestimated the rock mass strength for pillars with higher W/H ratios. Figure 2.11 shows the failed pillar with the mesh in Phase2D.

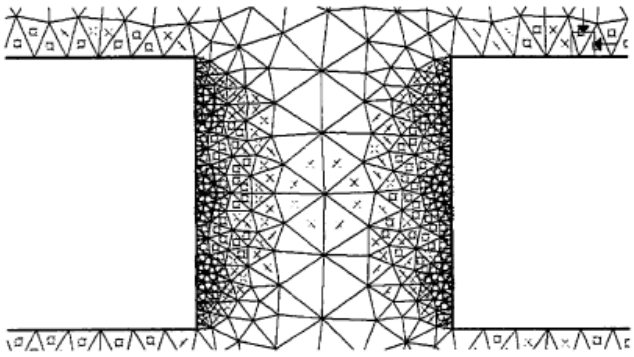

Figure 2.11: Phase 2D model showing pillar failure (Martin and Maybee, 2000)

Feng et al., (2006) developed Elasto-Plastic Cellular Automation (EPCA) code to simulate the non-linear fracturing of rocks under uniaxial compression and understand the fracturing process, stress-strain curves, acoustic emissions and compressive strength of 2D heterogeneous rock specimens. The factors that were investigated were homogeneity, softening coefficients, specimen sizes and height/width ratios, the spatial distribution of the material parameters and yield criteria and residual strength coefficient. It was concluded that the EPCA code could reproduce realistic failure phenomena observed in laboratory based uniaxial compression tests. Except the yield criteria and residual strength, all the other factors influence the failure modes of the rock samples. Homogeneity, softening coefficients and height/width values have distinct influence on stress-strain curves.

Esterhuizen et al. (2006) conducted numerical studies with FLAC3D (Itasca, 2005) on stone pillars in limestone mines and concluded that the hard rock pillar failure is in brittle fashion at width to height ratio less than 1 as the failure passes through the center of the

pillar (Figure 2.12). For width to height ratio over 1 would lead to spalling on the sides (brittle failure) followed by shear failure as shown in the Figure 2.12. Hard rock pillar with discontinuity was also simulated to understand the effect of geological structure on the hard rock pillar and it was determined that it behaves similar to that of the rock sample with a fracture plane.

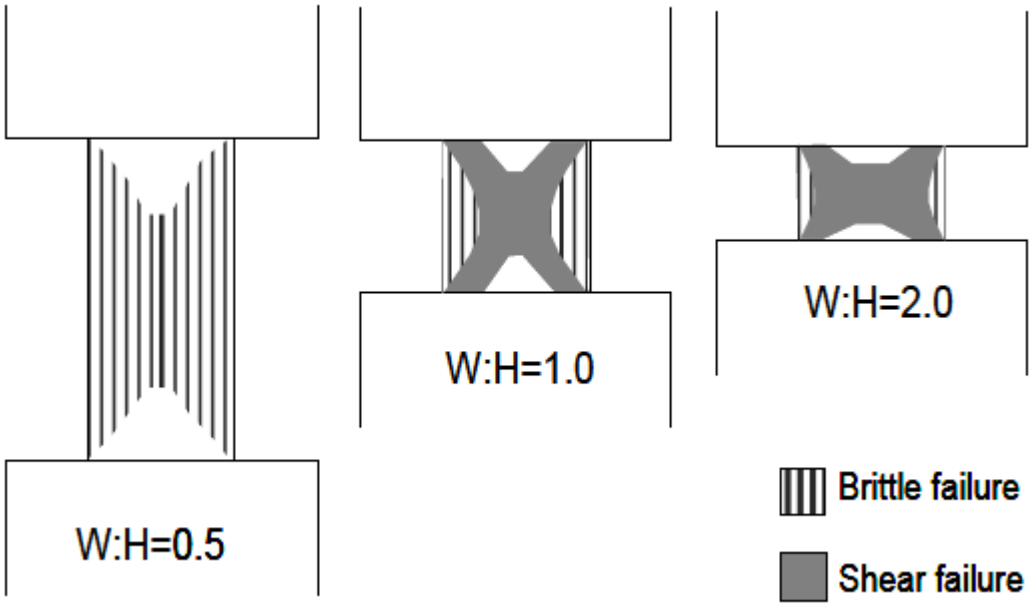

Figure 2.12: Failure modes in slender and squat pillars (Esterhuizen et al., 2006)

Dolinar and Esterhuizen (2007) simulate rectangular pillars with FLAC3D to understand the increase in strength of the pillars with increasing length. It was concluded that the length had very little effect on the slender pillars and for the squat pillars, the strength increases distinctly with length. The discontinuity facing the long axis of the pillar had higher strength rather than discontinuity facing short axis of the pillar.

Baharani et al., 2010 conducted finite element analysis on pillars considering the blasting effect where a hypothetical case study was performed. It was concluded that the slender pillars are prone to strain bursting and the strength of the wider pillars is affected due to

drill and blast methods. It was also shown that the yielding of the pillar side walls is higher due to blast damage.

Suorineni et al., (2011) described as the orebodies subjected to oblique loading conditions which is a combination of compressive and shear loads are more characteristic to cause rock bursts. Suorineni et al., (2014) conducted studies on pillars with Phase2D under oblique loading conditions. It was concluded that rock bursts can also be caused due to the orientation of the major far-field principal stresses relative to pillar strike or dip. Stress distribution in the pillar when the far-field principal stresses are oriented at an angle to the pillar as shown in Figure 2.13.

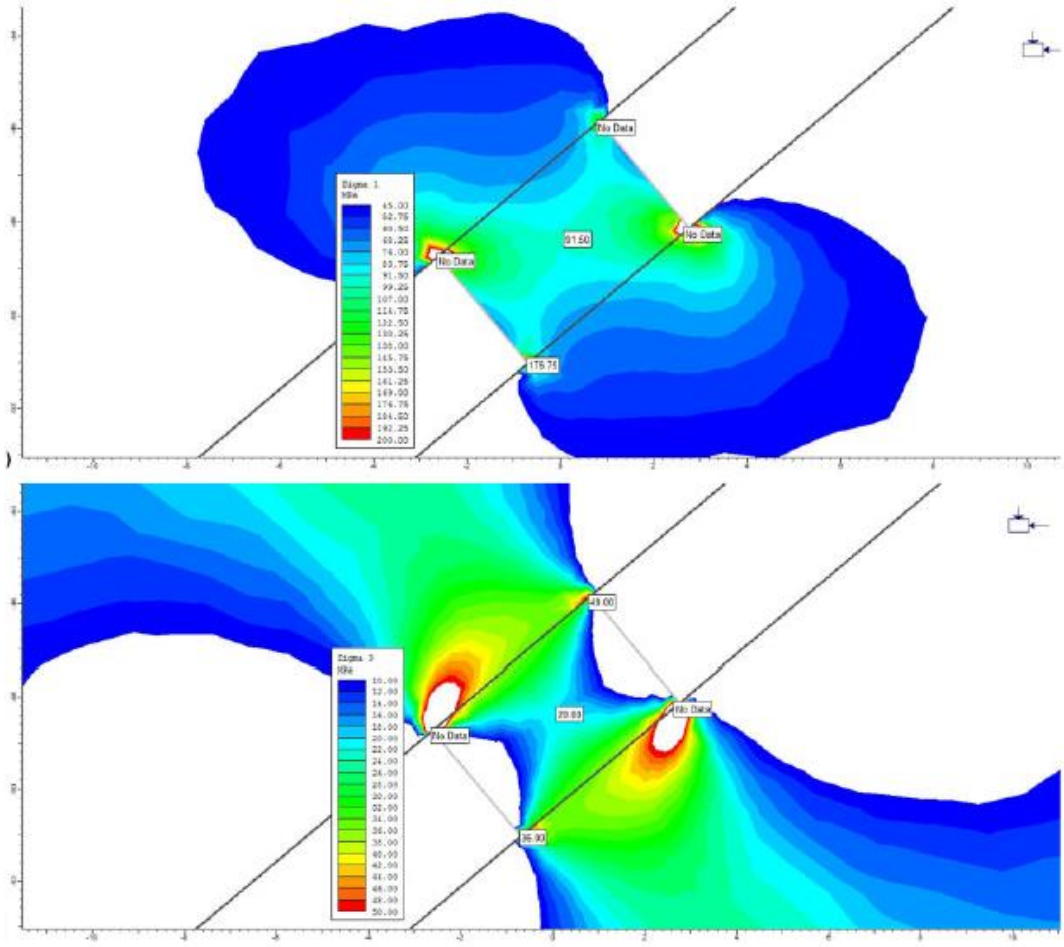

Figure 2.13: Stress distribution in a pillar oriented at an angle to the major farfield principal stress (Suorineni et al., 2014)

Ma et al., (2016) conducted studies on failure modes of mine pillars under shear loading with RFPA2D. It was concluded that there is a variation in the strength of the mine pillars and the corresponding failure modes with the dip and width to height of the pillars. The pillar stress concentration first appears at four corners with increasing dip angles leading to micro cracking and then coalesce at the center of the pillar.

Vakili (2017) proposed an improved unified constitutive model in Flac3D based on Hoek and Brown criterion for peak properties and followed by cohesion and friction softening at low confinements and cohesion softening and friction hardening at higher confinements. This constitutive model is similar to the ubiquitous strain softening/hardening model used by Esterhuizen (2006) and Lorig and Cabrera (2014) to simulate the pillars. It was concluded that the model shows comparable results to that of the Lunder and Pakalnis (1997). The constitutive model was specifically made to model only pillars while it had limitations that it cannot include anisotropy and the effect of intermediate to large scale discontinuities.

Idris et al., (2015) adopted Direct Strain Evaluation technique developed by Sakurai (1981) to develop the probability of failure and reliability assessment for pillars with each mining step with the help of numerical modelling.

Direct Strain evaluation technique (Figure 2.14) describes that the failures strain (ε_f) is different from the critical strain (ε_c) which can be related with a help of a factor (R_f). The corelation was defined as:

$$\varepsilon_f = \frac{\varepsilon_c}{1 - R_f} \tag{2.17}$$

where R_f was found to lie in between 0.05 and 0.8. Sakurai (1981) derived the factor with the help of specimens under uniaxial compression loading in the laboratory. Sakurai (1999) introduced a factor to establish a critical strain for the rock mass to that of the laboratory based critical strain.

Napa Garcia and Navarro Torres (2017) conducted numerical studies on pillars with help of FLAC3D (Itasca, 2017) using Hoek and Brown constitutive model by varying width to height ratios, Geological Strength Index (GSI), uniaxial compressive strength. Direct Strain evaluation method was adopted, and it was determined that the relation could established between the ratio of failure strain to critical strain and width to height ratio of the pillars. The numerical models were not calibrated to the empirical database and it is important to note that the Hoek-Brown constitutive model was determined by Maybee and Martin as the conservative model at higher width to height ratio.

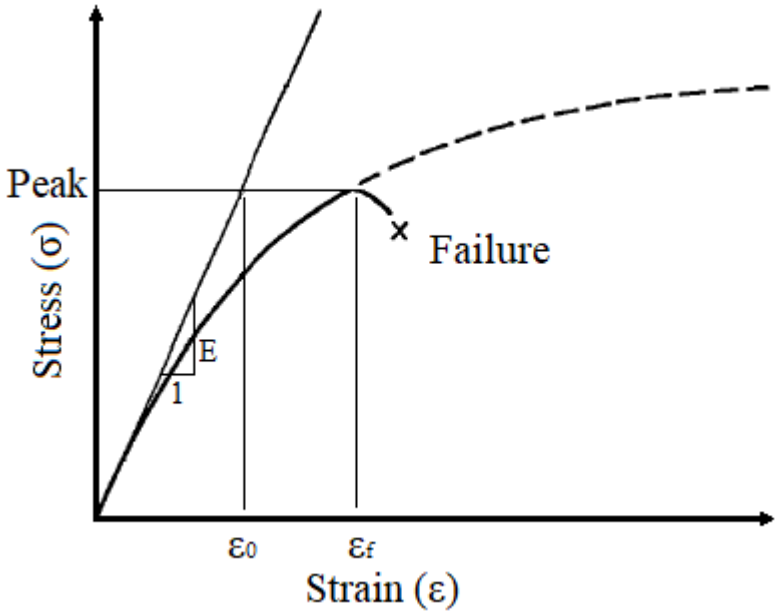

Figure 2.14: Sakurai's (1981) illustration of critical strain and failure strain

2.5.3. Discrete Methods

Discrete element modelling is an assemblage of the rigid or deformable blocks/particles and calculating the contact forces by continuously updating the entire deformation process to represent an appropriate constitutive model. It is mainly based on equations of motion of rigid or deformable bodies using implicit and explicit formulations (Jing and Hudson, 2002). The computer codes that are most used in DEM are UDEC, 3DEC (Itasca, 2002) which are two dimensional and three-dimensional models while PFC (Itasca, 2002) which deals with the granular modelling.

Esterhuizen et al. (2008) conducted pillar studies with UDEC computer code on limestone mines with discontinuities dipping at different angles. It was concluded that the discontinuities effect the strength of the slender pillars and it has little effect on squat pillars. An equation was derived with the help of these numerical studies that estimates the strength of the pillars in the presence of discontinuities. The pillar strength was also severely affected in the presence of weak clay filled or softened bedding bands.

Zhang (2014) adopted a Synthetic Rock Mass (SRM) approach to characterize the strength and failure mechanisms of the jointed rock pillars as shown in the Figure 2.15. It was also concluded that the fracture length, fracture intensity and fracture orientation are the three significant parameters effecting the strength of the pillar. It was also concluded that at constant fracture intensity, the fracture length has an inverse relation to that of the pillar strength. It was also noteworthy that at constant fracture intensity, with different fracture orientations, the fracture initiation stress remained same showing that the fracture initiation stress can be used as the measure for the degraded UCS strength for the empirical pillar strength approaches.

Muaka et al., (2017) investigated the pillar failure mechanisms transacted with the clay structures in the ore body, roof and floor. The joints in the rock mass were modelled in the form of discrete fracture networks in the two-dimensional discrete element approach software UDEC. It concluded that the strain softening region is dependent on loading velocity, tessellation size, damping magnitude, therefore, the modelling is less robust, and calibration and validation is the key. The pillar failure mechanisms were determined to be satisfactory when compared to the underground pillar failure mechanism.

2.5.4. Hybrid Methods

Elmo and Stead (2010) constructed a series of ELFEN (Rockfield, 2007) two-dimensional pillar models incorporating joints and concluded that the inclined joints dipping at higher than the friction angle of the joint favor shear sliding failure while the vertical joints and the joints sipping below the joint friction angle displayed splitting failure. It was also described that the lower joint stiffness lead to more realistic pillar mechanical response

which include discrete block displacement, lateral spalling and pillar core fracturing. Figure 2.16 shows the progressive failure of the pillars with fractures and the stress strain curves of the pillar.

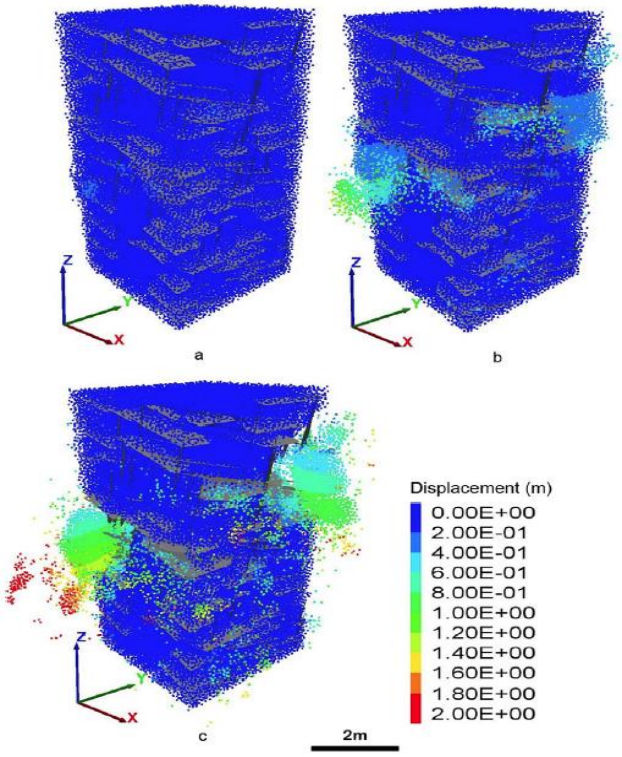

Figure 2.15: PFC model showing joints and progressive failure in rock pillars (Zhang, 2014)

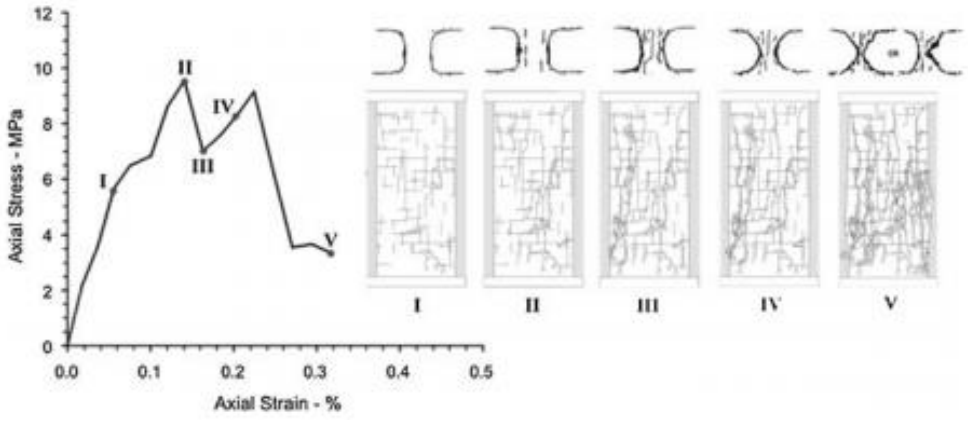

Figure 2.16: Progressive failure in ELFEN model with stress strain graph (Elmo and Stead, 2010)

Fakhimi et al., (2015) conducted studies on the sandstone samples in the laboratory and determined that the axial splitting failure behavior can be the major cause of the strain burst conditions in the pillars. Hybrid discrete finite element model was used to develop the laboratory test setup and was shown that the pillar width, pillar length, and the uniaxial compressive strength are the major contributing factors for violent failure of the pillars. It was concluded that the W/H ratios of less than 1 are prone to violent outburst as shown in Figure 2.17.

Figure 2.17: Strain burst of the specimen in the hybrid model (Fakhimi et al., 2015)

2.6. Summary

In this chapter, a systematic literature review was conducted on the hard rock pillars that included the failure modes of the pillars, empirical approaches, analytical approaches, and numerical approaches which include boundary element methods, finite element/difference methods, discrete element methods and hybrid methods.

Stress controlled pillar failures were studied which showed that the brittle failure along the outer skin of the pillars followed by shear failure leading to hourglass formation and then complete failure of the pillars. The structure-controlled pillar failures showed the failure of the pillars through shear along the joints and sliding of the blocks formed by the joints.

Empirical approaches where designed with the help of stable and unstable cases while some where formed with the help of numerical studies. Analytical approaches are being developed exponentially from the last decade and currently there are several mathematical models that represent the stability of the pillars.

Numerical approaches have been developed to understand the stress distribution in the pillars, observing the stress strain curves of the pillars and pillar failure modes assumed as continuum and in the presence of fractures.

From the literature review, it was found that the strength of the pillars is defined by the failure mechanism of the pillars. The failure mechanism was found to be mainly dependent on:

- Orientation of the orebody

Case studies have been conducted on inclined pillars that showed that the inclined pillars have lower strength than the normal pillars and the failure mechanism differs from the normal loading pillars. The case studies are only limited to the study of few selected pillars. There is no generalized relation defining the strength of the pillars at different inclination and their respective failure mechanism of the pillars.

- Presence of Discontinuities

One of the main factor that defined the failure mechanism of the pillar was found to be existence of the discontinuities in the pillars. The studies on the discontinuities in the pillar are mainly conducted on horizontal pillars while the effect of discontinuities on inclined pillars has not been conducted.

- Blasting effect

Blasting causes fractures on the pillar skin that reduces strength of the pillars. To account for the blast effect on coal pillars, a thin width of 0.3 m was taken as the blast zone in coal pillars to evaluate the strength of the coal pillars. The strength of the hard rock pillars can be evaluated with different blast zone thickness and with the help of the blast damage factor, a parametric study can be conducted.

Monitoring of the pillars has been conducted with the help visual inspection or with the help of the fractures developed on the pillars. It would be difficult to evaluate the fractures developed on the pillars, if the shotcrete is sprayed or the mesh is attached to the pillar.

Monitoring in the tunnels has been established with the help of Direct Strain Evaluation Technique developed by Sakurai (1981) which can be extended to evaluate the strength of the pillars.

References

Ayres da Silva, L. A., Ayres da Silva, A. L. M. and Sansone, E. C. (2013). The shape effect and rock mass structural control for mine pillar design. In: EUROCK 2013, Wroclaw. *EUROCK 2013: Rock Mechanics for Resources, Energy and Environment*. Croydon: CRC Press/Balkema, p. 563–67.

Ayres da Silva, L. A. and Ayres da Silva, A. L. M. (2014). The interaction between the scale effect and the shape effect in the mine pillar design. Rock Engineering and Rock Mechanics. pp: 683-687

Bahrani, N., Suorineni, F. T. and Kaiser, P. K. (2010). Stability Analysis of Rib Pillars in Mechanized and Drill and Blast Excavations Using Numerical Modeling. In Proceedings of the MEMO'2010, Sudbury, ON, Canada, 24–27 October 2010.

Bieniawski, Z. T. and Van H. W. L. (1975). The significance of *in situ* tests on large rock specimens. International Journal of Rock Mechanics and Mining Science Geomechanics Abstract 12(4):101-113.

Brady, B. H. G. and Brown, E. T. (2007). Rock mechanics for underground mining. Chapman & Hall, UK.

Bunting, D. (1911). Chamber-pillars in deep anthracite mines. Transactions of the AIME, p. *739–748*.

Cauvin, M., Verde, T., Salmon, R. (2009) Modeling uncertainties in mining pillar stability analysis. Risk Anal 29(10):1371–1380

Coates, D.F., Gyenge, M. (1981) Incremental design in rock mechanics. Monograph, vol. 880. Ottawa: Canadian Government Publishing Centre.

Dismuke, S. R., Forsyth, W. W. and Stewart, S. B. V. (1994) The Evolution of Mining Strategy Following the Collapse of the Window Area at the Magmont Mine, Missouri. Proceedings of the CIM Annual General Meeting, District 6, Metal Mining; pp 3-8.

Dolinar, D. R. and Esterhuizen, G. S. (2007). Evaluation of the effects of length on strength of slender pillars in limestone mines using numerical modelling. *Proceedings of the 26th International Conference on Ground Control in Mining*. Morgantown, WV: West Virginia University, pp. 304–313.

Elmo, D. and Stead, D. (2010). An integrated numerical modelling–discrete fracture network approach applied to the characterisation of rock mass strength of naturally fractured pillars. Rock Mechanics and Rock Engineering 43(1):3–19

Esterhuizen, G. S. (1993) Variability considerations in hard rock pillar design. In: Proceedings of the SANGORM symposium: rock engineering problems related to hard rock mining at shallow to intermediate depth, Rustenburg, South Africa

Esterhuizen, G.S. (2006). An evaluation of the strength of slender pillars. *Transactions of Society for Mining, Metallurgy, and Exploration, Inc.*; Vol. 320. Littleton, CO: Society for Mining, Metallurgy, and Exploration, Inc., pp. 69–76.

Esterhuizen, G. S., Iannacchione, A. T., Ellenberger, J. L. and Dolinar, D. R. (2006). Pillar stability issues based on a survey of pillar performance in underground limestone mines. *Proceedings of the 25th International Conference on Ground Control in Mining.* Morgantown, WV: West Virginia University, pp. 354-361

Esterhuizen, G. S., Dolinar, D. R. and Ellenberger, J. L. (2008). Pillar strength and design methodology for stone mines. *Proceedings of the 27th International Conference on Ground Control in Mining.* Morgantown, WV: West Virginia University, pp. 241–253.

Esterhuizen, G. S., Dolinar, D. R. and Ellenberger, J. L. (2011). Pillar strength in underground stone mines in the United States. International Journal of Rock Mechanics and Mining Sciences, 48, 42-50.

Fakhimi, A. and Hemami, B. (2015). Axial splitting of rocks under uniaxial compression. *International Journal of Rock Mechanics and Mining Sciences*, *79*, 124-134.

Fang, Z. and Harrison, J. P. (2002). Development of a local degradation approach to the modelling of brittle fracture in heterogeneous rocks. International Journal of Rock Mechanics and Mining Sciences, 39, 443-457.

Feng, X. T., Pan, P. Z. and Zhou, H. (2006). Simulation of the rock micro fracturing process under uniaxial compression using an elasto-plastic cellular automaton. International Journal of Rock Mechanics and Mining Sciences, 43, 1091-1108.

Ghasemi, E., Shahriar, K. and Sharifzadeh, M. (2010). A new method for risk assessment of pillar recovery operation. Safety Science. 48 (10), pp. 1304-1312

Ghasemi, E., Shahriar, K., Sharifzadeh, M. and Hashemolhosseini (2010). Quantifying the uncertainty of pillar safety factor by Monte Carlo Simulation – a case study. Arch. Min. Sci., Vol. 55 (3), pp. 583-595

Griffiths, D. V., Fenton, G. A. and Lemons, C. B. (2002). Probabilistic analysis of underground pillar stability. Int J Numer Anal Meth Geomech 26(8):775–791

Hedley, D. G. F. and Grant F. (1972) Stope and pillar design for the Elliot Lake uranium mines. *Canadian Institute of Mining and Metallurgy Bulletin*; Vol. 65, pp. 37-44.

Hedley, D. G. F., Roxburgh, J. W. and Muppalaneni, S. N. (1984). A case history of rock bursts at Elliot Lake. *Proceedings of Second International Conference on Stability in Underground Mining*, (ed. C. O. Brawner), 210–234, New York, American Institute of Mining, Metallurgical and Petroleum Engineers Inc.

Hoek, E., Carranza Toress, C. and Corkum, B. (2002). Hoek-Brown failure criterion – 2002 edition, Proc. 5th. North American Rock Mechanics Symposium and 17th Tunneling Association of Canada Conference. ATM TAC 2002. University of Toronto, University of Toronto, pp. 267-271.

Hoek, E., Kaiser, P. K. and Bawden, W. F. (1995). Support of underground excavations in hard rock. Rotterdam: balkema publ.

Hoek, E. and Brown, E. T. (1980). Underground excavation in Rock. The Institution of Mining and Metallurgy, London.

Holland, C. T. and Gaddy, F. L. (1964). The strength of coal in mine pillars, Proc 6th US Symp. on Rock Mechanics (University of Missouri, Rolla, MO) pp. 450-466.

Idris, M. A., Sainag, D. and Nordlund, E. (2015) Stochastic assessment of pillar stability at Laisvall mine using artificial neural network, *Tunneling and Underground Space Technology*, vol. 49, pp. 307–319.

lannacchione, A. T. (1999). Analysis of pillar design practices and techniques for U.S. limestone mines. *Trans. Instn. Min. Metall.* (sect. A: Min. lndustry, 108, September-December pp. A 152-A 160.

Itasca Consulting Group (2018). Fast Lagrangian Analysis of Continua in 3Dimensions, Minneapolis, Minnesota, USA.

Jaeger, J. C. and Cook N. G. W. (1979). Fundamentals of Rock Mechanics, 3rd Ed. NewYork: Chapman and Hall.

Jing, L. and Hudson, J. A. (2002). Numerical methods in rock mechanics. International Journal of Rock Mechanics and Mining Sciences, 39, 409-427.

Kaiser, P. K., Kim, B., Bewick, R. P. and Valley, B. (2010). Rock strength and depth and implications for pillar design. 5th International Seminar on Deep and High Stress Mining, Santiago, Chile, 463-476.

Kimmelmann, M. R., Hyde, B. and Madgwick, R. J. (1984). The use of computer applications at BCL Limited in planning pillar extraction and design of mining layouts. Proceedings of ISRM symposium: design and performance of underground excavations, London, 53-63.

Krauland, N. and Soder, P. E. (1987). Determining pillar strength from pillar failure observations. Eng Min J, 8, 34-40.

Lane, W. L., Yanske, T. R., Clark, L. M. and Roberts, D. P. (2001). Pillar extraction and rock mechanics at the Doe Run Company in Missouri 1991 to 2000. Underground mining methods-engineering fundamentals and international case studies, Society for mining, Metallurgy, and Exploration, 95-103.

Lorig, L. J., and Cabrera, A. (2013). Pillar Strength Estimates for Foliated and Inclined Pillars in Schistose Material. *Proceedings of 3rd International FLAC/DEM Symposium*, Hangzhou, China, October 2013. Paper: 01-01, H. Zhu et al., Eds. Minneapolis: Itasca International Inc.

Lunder, P. J. (1994). Hard Rock Pillar Strength Estimation an Applied Approach. (Thesis). Vancouver (BC): University of British Columbia.

Lunder, P. J. and Pakalnis, R. (1997) Determining the strength of hard rock mine pillars. *Bulletin of Canadian Institute of Mining and Metallurgy*; Vol. 90, pp. 51-55.

Ma, T., Wang, L., Suroineni, F. T. and Tang, C. (2016) Numerical Analysis on Failure Modes and Mechanisms of Mine Pillars under Shear Loading. Hindawi Publishing Corporation, Shock and Vibration, Volume 2016, 1-14.

Madden, B. J., Canbulat, I., Jack, B. W. and Prohaska, G. D. (1995). A reassessment of Coal Pillar Design Procedures. Safety in Mines Research Advisory Committee, COL 021, December 1995, pp 1-148

Martin, C. D. and Maybee, W. G. (2000) The strength of hard-rock pillars. International Journal of Rock Mechanics and Mining Sciences 37:1239–1246

Mark, C. and Chase, F. E. (1997). Analysis of retreat mining pillar stability, Proceedings: New technology for ground control in retreat mining, IC 9446, NIOSH. pp. 1-34.

Muaka, J. J. M., Duma, S., Mushangwe, P., Gardner, L., Chindedza, T., Walls, J. and Joughin, W.C. (2017). Modelling hard rock jointed pillars using a distinct element and

discrete fracture network approach considering the effect of a clay-filled shear structure. Deep Mining 2017, Perth, Australia. pp. 311-328

Napa-García, G. F., Navarro Torres, V. F. (2017) Applicability of failure strain for the stability evaluation of square pillars in room and pillar mining, in M Hudyma & Y Potvin (eds), *Proceedings of the First International Conference on Underground Mining Technology*, Australian Centre for Geomechanics, Perth, pp. 557-565.

Obert, L., Duvall, W. I. (1967). Rock Mechanics and the Design of Structures in Rock, John Wiley & Sons Inc. New York pp. 542-545.

Potvin, Y., Hudyma, M. R. and Miller, H. (1989). Design guidelines for open stope support. Bull Can Min Metall, 82, 53-62.

Pritchard, C. J. and Hedley, D. G. F. (1993). Progressive pillar failure and rockbursting at Denison Mine. *Rockbursts and Seismicity in Mines*. Young (ed.). Baikema, Rotterdam.

Rahjoo, M., Roo, K. S., Ebarhardt, E. (2016). Stress-induced spalling analysis of extraction level pillars using a 3-D extensional strain failure criterion. American Rock Mechanics Association. 16-763

Roberts, D. P., Tolfree, D. and McIntire, H. (2007). Using confinement as a means to estimate pillar strength in a room and pillar mine. 1st Canada-US Rock Mechanics Symposium, Vancouver, 1455-1462.

Rocsience (1999). Finite element analysis for excavations and slopes [Online]. University of Toronto.

Salamon, M. D. G. and Munro, A. H. (1967). A study of the strength of coal pillars. J. South Afr. Inst. Min. Metallurgy 68:55-67.

Sakurai, S. (1981). Direct strain evaluation technique in construction of underground opening. *Proceedings of the 22nd US Symposium on Rock Mechanics*, American Rock Mechanics Association, Alexandria, pp. 278–282.

Sakurai, S. (1999). Interpretation of field measurements in tunneling practice. *Proceedings of the 9th ISRM Congress*, International Society for Rock Mechanics, Lisbon, pp. 1517–1523

Sjoberg, J. (1992). Failure modes and pillar behaviour in the Zinkgruvan mine. 33rd US Rock Mechanics Symposium, Sante Fe, 491-500.

Song, G. and Yang, S. (2018). Probability and reliability analysis of pillar stability in South Africa. International Journal of Mining Science and Technology. 28 (4) pp. 715-719

Styles, T. D, Zhang, Y., Stead, D., Elmo, D., Roberts, D. and Yanske, T. (2010). A photogrammetric approach to brittle fracture characterization in mine pillars. 44th US Rock Mechanics Symposium, Salt Lake City, 1475-1482.

Suorineni, F. T., Mgumbwa, J. J., Kaiser, P. K. and Thibodeau, D. (2011). Mining of orebodies under shear loading Part 1 – case histories, *Mining Technology (Trans. Inst. Min. Metall. A)*, 120(3), 138–147.

Suorineni, F. T., Mgumbwa, J. J., Kaiser, P. K. and Thibodeau, D. (2014). Mining of orebodies under shear loading Part 2 – failure modes and mechanisms, *Mining Technology* (Trans. Inst. Min. Metall. A), 123(4),240–249.

Tang, C. A. and Kaiser, P. K. (1998). Numerical simulation of damage accumulation and seismic energy release during brittle rock failure - Part I: fundamentals. International Journal of Rock Mechanics and Mining Sciences, 35, 113-121.

Tomory, A. M., Carvalho, J., Kowalczyk, M., and Tomory, B. (2014). Logistic Regression in Hard Rock Pillar Design. American Rock Mechanics Association. 7044

Vakili, A. (2016) An improved unified constitutive model for rock material and guidelines for its application in numerical modelling. Computers and Geotechnics. 80 pp. 261-282

Wagner, H. (1980). Pillar Design in Coal Mines. J. South Afr. Inst. Min. Metallurgy pp. 37-45.

Walls, J. and Mpunzi, P. (2017). The interaction between the scale effect and the shape effect in the mine pillar design. AfriRock 2017 Rock Mechanics for Africa, Cape Town, 2-7 October. pp. 847-860

Wattimena, R. K. (2014). Predicting the stability of hard rock pillars using multinomial logistic regression. Int J Rock Mech Min Sci 71:33–40

Whyatt, J. and Varley, F. (2008). Catastrophic failures of underground evaporite mines. In *Proceedings of twenty-seventh International Conference on Ground Control in Mining*. 113–122, Morgantown, ICGCM.

Zipf, R. K. (2001). Toward pillar design to prevent collapse in room-and-pillar mines. 108th Annual Exhibit and Meeting, Society for Mining, Metallurgy and Exploration, Denver.

Zhang, Y. (2014). Modelling Hard Rock Pillars Using a Synthetic Rock Mass Approach. PhD Dissertation. Simon Fraser University.

Zhou, J., Li, X. B., Shi, X. Z., Wei, W., Wu, B. B. (2011). Predicting pillar stability for underground mine using Fisher discriminant analysis and SVM methods. Trans Nonferrous Metals Soc China 21(12):2734–2743

Zhou, J., Li, X. and Mitri, H. S. (2015). Comparative performance of six supervised learning methods for the development of models of hard rock pillar stability prediction. Nat Hazards (2015) 79:291–316

Chapter 3

Laboratory and Numerical Investigation on Strength Performance of Inclined Pillars

This chapter has been accepted and published in Energies as:

Jessu, K.V., Spearing, A.J.S., Sharifzadeh M., (2018) Laboratory and Numerical Investigation on Strength Performance of Inclined Pillars. Energies. 11(11), 3229

Abstract

Pillars play a critical role in an underground mine, as an inadequate pillar design could lead to pillar failure which may result in catastrophic damage while an over-designed pillar would lead to ore loss causing economic loss. Pillar design is dictated by the inclination of the ore body. Depending on the orientation of the pillars, loading can be axial (compression) in horizontal pillars and oblique (compression as well as shear loading) in inclined pillars. Empirical and numerical approaches are the two most commonly used methods for pillar design. Current empirical approaches are mainly based on horizontal pillars and inclination of the pillars in the dataset are not taken into consideration. Laboratory and numerical studies were conducted with different width to height ratios and at different inclinations to understand the reduction in strength due to inclined loading and to observe the failure mechanism. The specimen strength reduces consistently over all the width to height ratios at a given inclination. The strength reduction factor for Gypsum were found to be 0.78 and 0.56 and for sandstone were 0.71 and 0.43 at 10° and 20° inclinations respectively. The strength reduction factors from numerical models were found to be 0.94 for 10° inclination, 0.87 for 20° inclination, 0.78 for 30° inclination and 0.67 for 40° inclination and a fitting equation was proposed for strength reduction factor with respect to inclination. The achieved results could be used at preliminary design stages and can be verified during the real mining practice.

3.1. Introduction

Pillars are the primary support systems in underground mines and are typically left between the openings to maintain their stability. The design and stability of the pillars are the two most complicated challenges in the ground control studies. Unfeasible and incompetent direct loading tests on the pillars in the underground mines lead to adopt empirical based designs and back analysis. The empirical design theories are predominantly based on the stable, unstable and failure of the pillars which does not consider the different failure mechanisms of the pillars. The factors that influence different failure mechanisms in the pillars are:

- Orientation of the orebody (Inclined pillars)
- Presence of geological structures
- Blast damage
- Weak floor or roof

This chapter mainly focuses on the inclined pillars in orebodies with different orientations.

Following the catastrophic pillar collapse at the Coal Brook colliery on January 21, 1960, pillar stability and pillar design optimization was more thoroughly investigated to obtain more reliable design approaches. One of the first empirical approaches was developed by Salaman and Munro (1967). This empirical approach was later modified and applied for the Canadian Uranium mines by Hedley and Grant (1972) similarly based on stable, unstable and failed pillars to develop a relationship between the pillar strength and the geometric parameters of the pillar.

$$\sigma_p = k\,\frac{W^a}{H^b} \tag{3.1}$$

Where σ_p is the strength of the pillar (MPa), k is the unit strength of the rock sample (MPa), W is the width of the pillar and H is the height of the pillar with constants a and b given as 0.5 and 0.75 respectively.

One of the commonly used empirical approach is the confinement formula to determine the strength of the hard rock pillars developed by Lunder and Pakalnis (1997) based on the 178 pillars which was given as:

$$\sigma_p = K * UCS * (C1 + C2 * \kappa) \tag{3.2}$$

Where σ_p is the ultimate strength of the pillar (MPa), K is the pillar size factor, UCS is the uniaxial compressive strength of the intact rock (MPa), C1 and C2 are the empirical rock mass constants and κ is the friction term which is calculated as:

$$\kappa = \tan\left[cos^{-1}\left(\frac{1 - C_{pav}}{1 + C_{pav}}\right)\right] \quad (3.3)$$

$$C_{pav} = Coeff * \left[Log\left(\frac{W}{H} + 0.75\right)\right]^{1.4(W/H)} \quad (3.4)$$

Where, C_{pav} is the average pillar confinement and Coeff is the coefficient of pillar confinement.

Few other researchers developed similar empirical relationships between the pillar strength and geometry of the pillar (Kimmelmann, et al, 1984; Krauland and Soder et al., 1987; Potvin et al., 1989; Sjoberg, 1992).

Numerical tools were used by researchers to understand the failure mechanism and to evaluate the strength of the hard rock pillars. Elastic brittle plastic constitutive model in finite element and boundary element modelling packages was developed to evaluate the strength of the pillars (Martin and Maybee, 2000). The slender pillars in the limestone room and pillars with the help of numerical modelling were classified as the pillars with highly variable strength as it depends on the structures which had little impact on higher width-to-height (W/H) ratio pillars (Esterhuizen et al., 2006 and 2008). Failure mechanisms in the slender pillars were described as brittle failure where the failure plane is passing through the centre of the pillar while in larger pillars, the failure mechanism was described to be spalling followed by shear failure. Elmo and Stead (2010) and Zhang (2017) conducted studies on the joint spacing, joint length and joint orientation to develop an understanding between the area/volumetric fracture intensity and the strength of the pillars. These studies have all been based on the normal loading of the pillars where it causes compression loads on the pillars (Figure 3.1a).

Inclined pillars undergo oblique loading, which is combination of compressive and shear stresses as shown in the Figure 3.1b. Hedley et al., (1984) conducted stress analysis studies

on two pillars with one along 45° dip and other with normal loading with same extraction ratio. It was concluded that the failure in the dip pillar extended from one corner to another corner while the normal pillar was stable which resulted in domino pillar bursting in Quirke mine. Progressive failure of the 20° inclined pillars was described by Pritchard and Hedley (1993) at Denison mine. It was described by spalling at the two sides of the pillars followed by the hour glass fracture formation in an inclined fashion which ultimately lead to a complete failure in larger width to height ratios. Case studies conducted on the inclined pillars and associated excavation which undergo oblique loading were described to be at higher risk of failure when compared to the pillars with normal loading (Kvapil et al., 1989; Whyatt and Varley, 2008). The case studies were only based on one pillar and the failure mechanism of that specific pillar while the strength of the pillar was not evaluated to take into consideration to develop the pillars in inclined fashion.

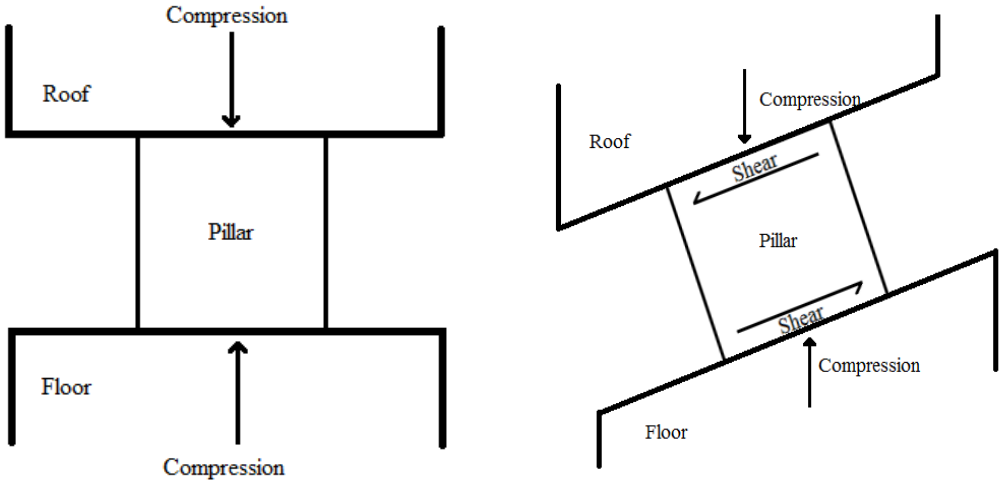

a) b)

Figure 3.1 a) Normal loading and b) Oblique loading on the pillars

Two-dimensional finite-element numerical studies were conducted to evaluate the strength of the hard rock pillars at different orientations of the far field principal stresses and was concluded that the strength of the pillars with higher W/H ratio were highly affected by the orientation of the pillars (Suorineni et al., 2011; Suorineni et al., 2014).

Jessu and Spearing (2018) conducted similar numerical studies to that of Suorineni (2014) but with finite difference code in a three-dimensional model to evaluate the strength and the failure mechanisms of the pillars at different inclinations. It was concluded that as the inclination increases, the pillars with higher W/H ratios are significantly lower in strength when compared to horizontal pillars. The study also described that the brittle failure mechanism is the dominant failure mechanism in the inclined pillars where failure starts from one corner of the pillar to another corner of the pillar. All the studies conducted were through numerical modelling studies, no laboratory testing was conducted to show the effectiveness of numerical modelling results.

This chapter deals with the laboratory testing of the specimen under inclined loading and evaluating the reduction in the strength when compared to specimen tested under normal loading. The failure mechanisms will be evaluated at the laboratory scale and it will be related to the cause of strength reduction. The results of the numerical modelling of the pillars presented by Jessu and Spearing (2018) were further evaluated to present the strength reduction factors.

3.2. Materials and Test methods

Moulded Gypsum and Sandstone core specimen were tested under uniaxial and oblique loading conditions. These were selected by the authors as the moulded gypsum was extensively used by many researchers (Bobet and Einstein, 1998; Wong and Einstein, 2009) as a representative of brittle rock and both moulded gypsum and sandstone have lower strength which is best suitable for the currently developed testing methodology.

Gypsum specimen were prepared by mixing the gypsum powder to the water with a mass ratio of 100:35. The PVC tubes of 50mm inner diameter were used to cast the specimens. The PVC tubes were cut perpendicular to the tube length to cast the normal specimens while for inclined specimens, the PVC tubes were cut at angle on the both ends. After pouring the mixture into the moulds, it was stirred to remove the bubbles in the mixture and then placed in the oven at a temperature of 40° C until the mass of the specimen

reaches a constant value which was attained in three days. All the specimens were created in a single batch for consistency. The surface of the normal sample was made smooth and parallel according to the ISRM standards with the help of the grinder, while for the inclined specimens, the surfaces were polished with sandpaper of coarse grit #60 and then with fine grit #200. Gypsum specimens with three different inclinations and four different width to height ratios were prepared as shown in Figure 3.2a and 3.2b. Five specimens were tested for every test, therefore, a total of 60 gypsum specimens were tested.

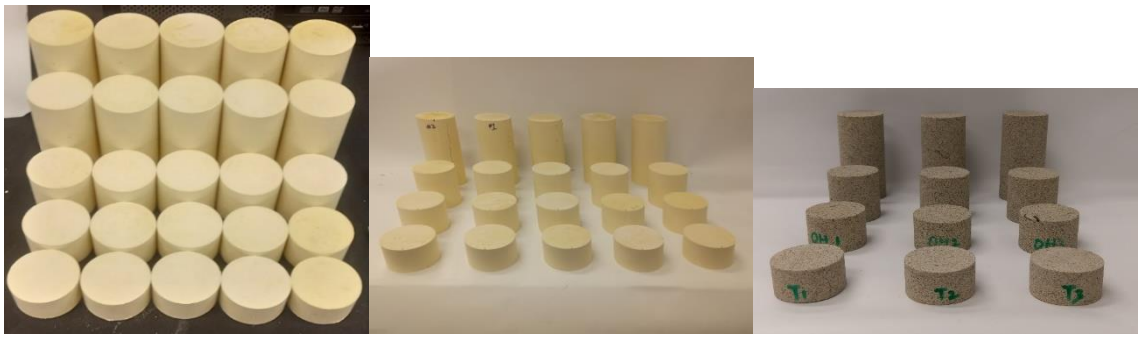

a) b) c)

Figure 3.2: a) 0° gypsum specimens b) 10° inclined gypsum specimens c) sandstone specimen

The sandstone core of 42 mm diameter was used to conduct the test. The sandstone specimens were cut at different lengths to produce different width to height ratios (Figure 3.2c). The sample ends were prepared to be parallel and straight as specified in the ISRM standards with the help of the grinder. The specimens were then loaded with inclined platens at different width to height ratios.

Uniaxial Compression Testing Machine (Figure 3.3a), which was controlled by a servo computer program GCTS CATS 1.8 software was used to test the gypsum and sandstone specimens in normal and inclined fashion. Straight platens were used for uniaxial compression testing of the normal specimens while for the inclined testing, platens were manufactured at 10° and 20° angles. The inclined platens were fixed to the frame of the

testing machine and then the inclined testing of the sandstones specimens was done as shown in Figure 3.3b.

a) b)

Figure 3.3: a) Uniaxial compressive testing machine b) modified platens for inclined pillar testing

As the Gypsum specimens were casted in the inclined fashion, they were placed directly at the centre of the straight platens and a load of 0.2 kN was applied such that the sample does not slip or tumble down the platen. For sandstone specimens, as they cannot be prepared (cut) with inclined ends, the straight specimens were placed on inclined platens in such a manner that the centre of the sample coincides with centre point of the frame as shown in Figure 3.3b. After placing it on the lower platen, a load of 0.2 kN was applied to hold the sample in position.

The machine records load and displacement data automatically at a rate of 600 samples/ minute. Displacement type loading rate was adopted with a fixed loading rate of 0.12 mm/min, which was in accordance with the ISRM standards as the gypsum and sandstone specimens with L/D ratio of 2.5 reached their peak strength in the range of 5 to 10 minutes. The testing materials, and the loading conditions are specified in Table 3.1.

Table 3.1: Test design for laboratory specimens.

Test No.	Rock Type	Diameter	W/H Ratio	Inclination	No. of tests
1	Gypsum	50	0.4	0	5
2			0.5		5
3			1.0		5
4			1.5		5
5			2.0		5
6		50	0.5	10	5
7			1.0		5
8			1.5		5
9			2.0		5
10		50	0.5	20	5
11			1.0		5
12			1.5		5
13			2.0		5
14	Sandstone	42	0.4	0	3
15			0.5		3
16			1.0		3
17			1.5		3
18			2.0		3
19		42	1.0	10	3
20			1.5		3
21			2.0		3
22		42	0.5	20	3
23			1.0		3
24			1.5		3
25			2.0		3

Each test was conducted three or five times and the results were presented in the form of the averages. Therefore, to verify if the average results are representative of the observed results, a statistical Pearson's Chi-Square test was conducted for all the strength values, elastic modulus and the equations proposed.

Pearson's Chi-Square test (1900) is a statistical test to determine if the observed values are significantly different from the expected value. Two hypotheses are made where null hypothesis assumes there is no significant difference between the observed values and the expected value while the alterative hypothesis suggests there is a significant difference. The test is conducted with the help of the formula:

$$\chi^2 = \frac{[O - E]^2}{E} \tag{3.5}$$

Where $\chi^2$is the chi-square goodness of fit test, O is the observed value and E is the expected value. Degrees of freedom are determined with the help of the constraints which is defined by one less than the number of the observed values. The Chi-square and degrees of freedom are evaluated, and the probability is determined with the help of the tables. If the probability is observed to be less than the significance level which is generally taken as 0.05 or 0.1, then the null hypothesis is rejected. This shows that the expected value is significantly different when compared to the observed value.

Chi-Square goodness of fit is used in this chapter to determine if the average values are representative of the observed values. The chi-square values and the degrees of freedom are for all the tests conducted. The probability or the p-value is determined to show the non-significant difference between the observed values and the average values.

3.3. Results

3.3.1. Material properties of the two different rock types:

Initially, the uniaxial compressive strength and elastic modulus of the moulded gypsum and the sandstone were determined by preparing the specimens of length to diameter ratio of 2.5 as per the ISRM standards. The gypsum moulds and the sandstone specimens had a diameter of 50 mm and 42 mm, and lengths of about 125 mm and 105 mm respectively. Five specimens were tested for moulded gypsum and three specimens for sandstone for consistency. The stress strain graphs of the gypsum and the sandstone specimens are shown in Figure 3.4a and 3.5a. The failure modes were found to be axially splitting in the gypsum samples and single shear plane failure in the sandstone samples as shown in Figure 3.4b and 3.5b.

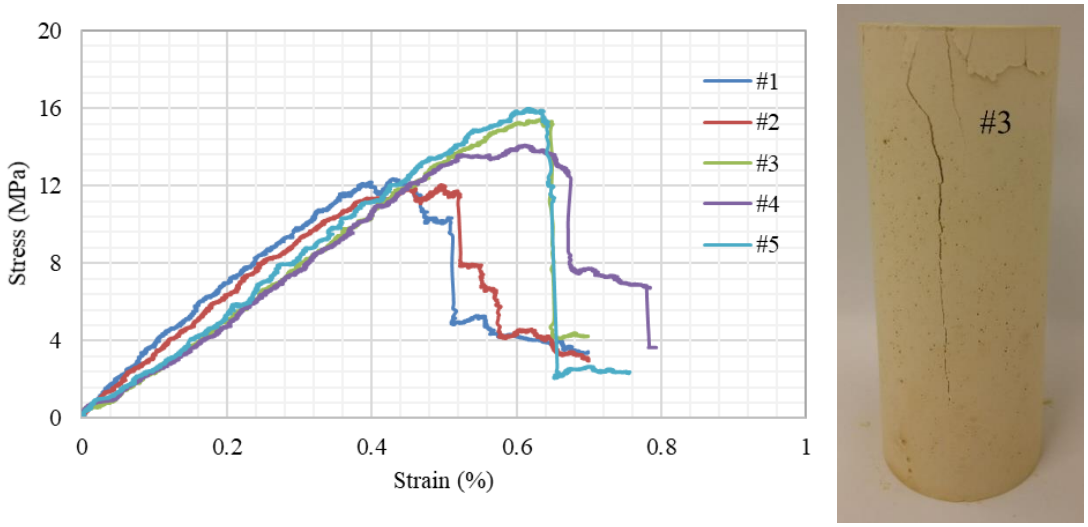

a) b)

Figure 3.4: a) Stress-strain behaviour of the moulded gypsum under UCS test. b) Axial splitting failure mechanism of the moulded Gypsum under UCS test.

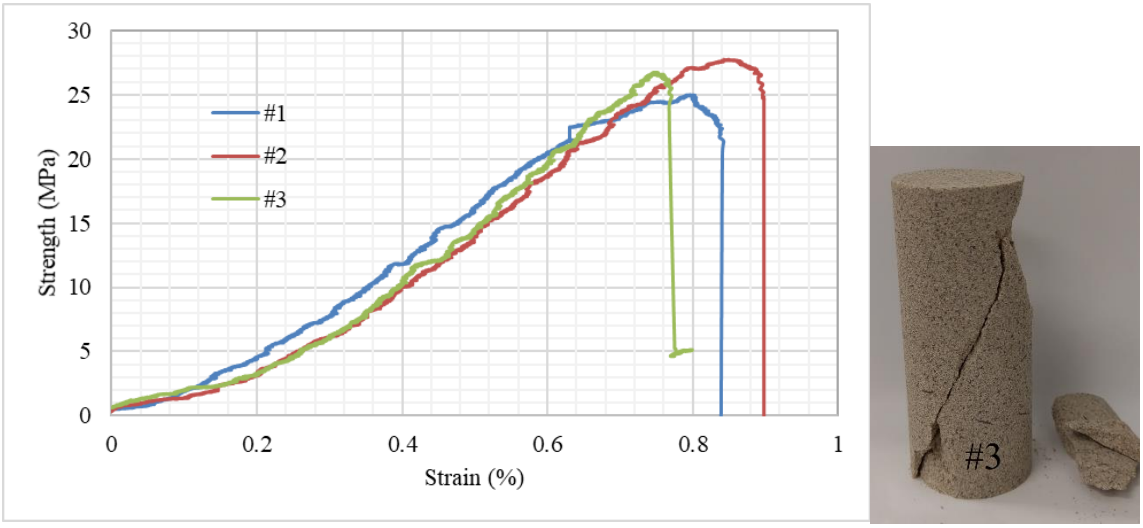

a) b)

Figure 3.5: a) Stress-strain behaviour of the sandstone under UCS test b) Shear failure mechanism of the sandstone under UCS test

The average uniaxial strength and the average elastic modulus of the Moulded Gypsum and Sandstone with their standard deviations are shown in Table 3.2. The standard deviations are less than 10% for uniaxial compressive strength and elastic modulus for both the specimens. Goodness of fit statistical test (Chi square test) was conducted on the specimens to understand if the average strength and average elastic modulus is appropriately representing the sample strength and elastic modulus. The P-value greater than 0.05 in the goodness of fit test suggests that the difference between the sample strength and the average strength is not significant. Therefore, the average strength and the average elastic modulus are representative of the strength and the elastic modulus of all the specimens.

Table 3.2: Statistical analysis of the moulded gypsum and sandstone specimens.

Parameters\Rock Type	Moulded Gypsum	Sandstone
Average Strength (MPa)	13.9	26.9
Standard Deviation (MPa)	±1.8	±0.2
Goodness of Fit test (p-value)	0.9234	0.9287
Average Elastic Modulus	2.8	3.8
Standard Deviation (GPa)	±0.2	±0.2
Goodness of Fit test (p-value)	0.9499	0.8521

3.3.2. Strength of Gypsum and Sandstone specimens at different inclinations:

Moulded gypsum and sandstone was tested with four different width-to-height ratios of 0.5, 1.0, 1.5 and 2.0. The heights of the specimens were varied to attain the width to height ratio. Specimens with inclination of 0°, 10° and 20° were tested to evaluate their strength and understand the failure mechanism at different width to height ratios.

Figure 3.6 shows the strength of the specimens at different inclinations which show less than 10% standard deviation in all the specimens. It can be observed that the strength of the specimens positively corresponds to width to height ratio and the rate of increase

decreases with inclination. It can be observed that the strength reduction due to inclination is higher in specimens with larger W/H ratios than the smaller W/H ratios.

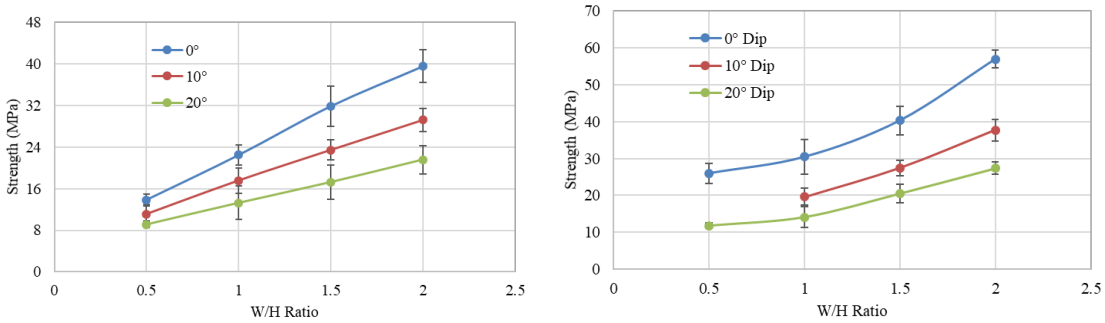

a) b)

Figure 3.6: Strength variation of the a) moulded gypsum specimens b) sandstone specimen with respect to W/H ratio at different inclinations.

3.3.3. Failure Mechanism of Gypsum Specimen at different inclinations:

The failure mechanisms of the gypsum specimens in the normal loading conditions are shown in the Figure 3.7. The axial splitting failure was dominant in the specimens with W/H ratio of 0.5 which also passes through the centre of the sample. The sample strength reaches the peak and drops down rapidly due to the failure of the sample from the centre of the pillar. In larger specimens where W/H ratio is greater than 1.0, the failure was observed to be spalling on the sides which causes reduction in size of the specimens to form hour glass formation. Therefore, this is similar to the failure mechanism observed in the underground mine pillars where slender pillars are observed to fail through the centre of the pillar and the larger pillars through the gradually spalling on the sides and then hourglass formation leading to complete failure (Roberts, 2007).

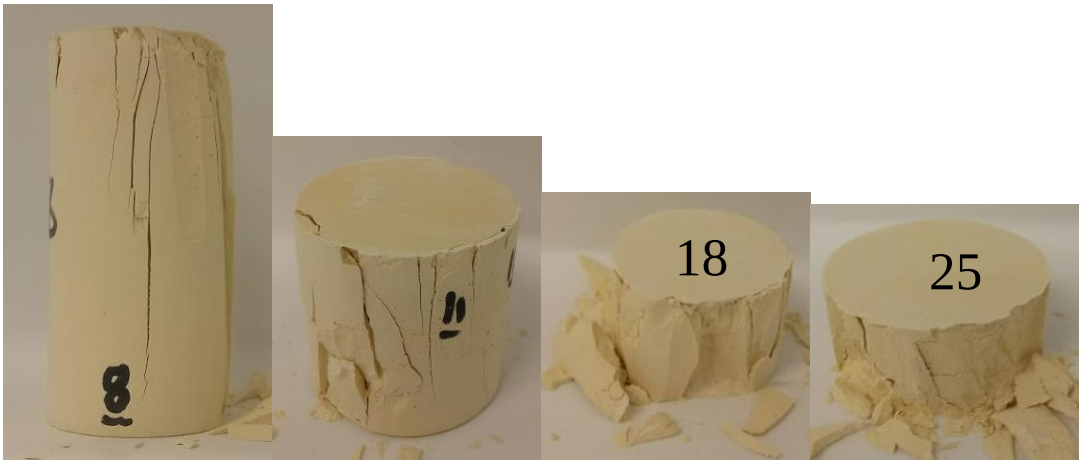

a) b) c) d)

Figure 3.7: Failure mechanism of the gypsum specimens under normal loading conditions a) W/H ratio of 0.5 b) W/H ratio of 1.0 c) W/H ratio of 1.5 d) W/H ratio of 2.0.

The failure mechanisms of the 10° specimens are shown in Figure 3.8. The failure of the sample with W/H ratio of 0.5 was observed to be axial splitting which is similar to that of the failure of the sample in normal loading condition. The failure was observed to be passing through the centre of the sample (Figure 3.8a) and the strength dropped rapidly as it reached the peak. In larger specimens, the failure is mainly concentrated on the skin of the specimens and particularly at two corners as shown in the Figure 3.8b, 3.8c and 3.8d. Comparing 3.8b and 3.8d, the area effected due to the failure to total area of sample is higher in W/H ratio of 1.0 and it decreases with increase in W/H ratio. This shows that the load bearing surface is higher in W/H ratio of 2.0, therefore, the strength of the specimen increases with increase in W/H ratio.

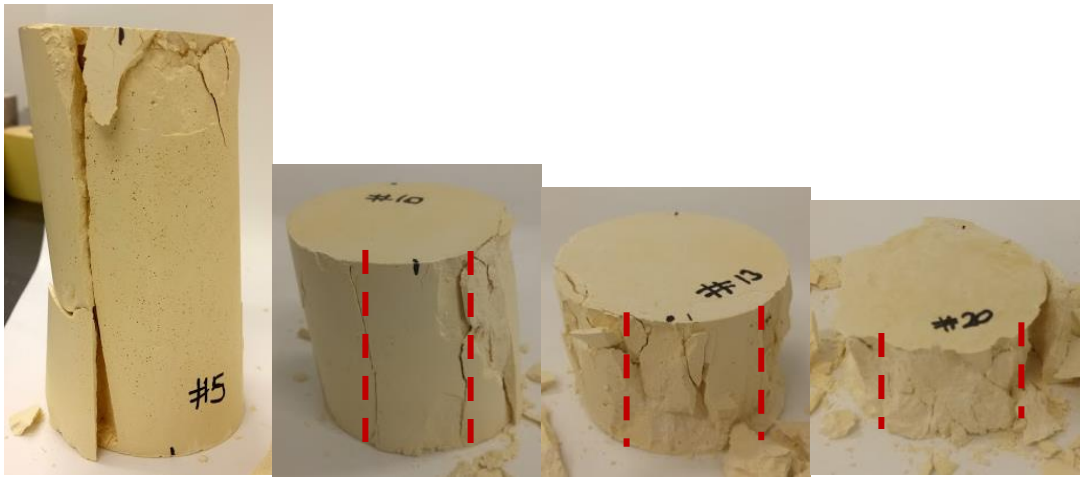

a) b) c) d)

Figure 3.8: Failure mechanism of the 10° inclined specimen with a) W/H ratio of 0.5 b) W/H ratio of 1.0 c) W/H ratio of 1.5 d) W/H the ratio of 2.0

The failure of the 20° inclined specimens (Figure 3.9) is similar to that of the 10° inclined specimens where the failure of the W/H ratio of 0.5 is due to axial splitting and passes through the centre of the sample (Figure 3.9a). In larger specimens, the stress concentrations are higher at the two corners and breakage is mainly observed in these two corners as shown in Figure 3.9b, 3.9c and 3.9d.

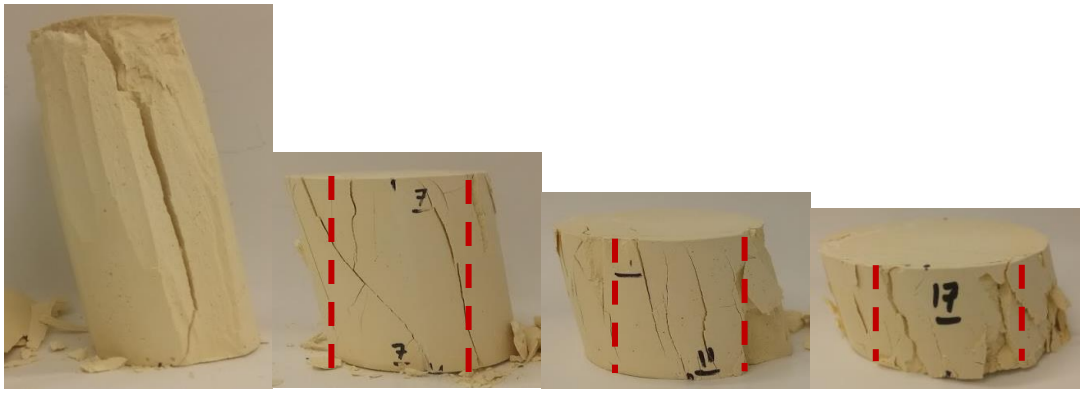

a) b) c) d)

Figure 3.9: Failure mechanisms of the 20° inclined gypsum specimens with a) W/H ratio of 0.5 b) W/H ratio of 1.0 c) W/H ratio of 1.5 d) W/H ratio of 2.0

3.4. Numerical Modelling

FLAC^{3D}, a geotechnical finite difference modelling package was used to simulate the pillars as shown in Figure 3.10. Three-dimensional co-ordinate system was used where horizontal plane is represented in the x and y- directions and the vertical plane is represented in z- direction. For the inclined pillars, inclination was measured from the x-direction as shown in Figure 3.10b. The model consists of main floor, main roof and pillar with a height of 4 m considering the Lunder and Pakalnis (1997) database. The width of the pillars was varied to achieve the width to height ratio of the pillars. Extraction ratio is kept constant for all the vertical pillars at 75% and for the inclined pillars, the boundaries were established far enough to avoid boundary effects on the performance of the inclined pillar and its failure behaviour. The thickness of the roof and the floor was maintained at three times the pillar height in all the models to avoid the boundary effects.

Boundary conditions such as fixed supports were placed at the bottom of the floor which restricts the displacement and velocity in both parallel and normal directions. Roller supports were placed on the sides with which the velocity and displacement is restricted in normal direction. The loading was applied in the form of uniform velocity on the top of the roof until the pillar has entirely failed and the residual strength reaches 50% of peak strength as recommended by Lorig and Cabrera (2013).

Bilinear strain hardening/ softening ubiquitous joint constitutive model was applied to simulate the pillars which is based on the Mohr Coulomb strength criterion and strain softening/ hardening as a function of the deviatoric plastic strain (Itasca, 2018). Elastic criterion was applied to simulate the roof and floor to ensure that the roof and floor were stronger than the pillar and the failure is only induced in the pillar. The model properties are summarized in Table 3.3 and 3.4 (Dolinar and Esterhuizen, 2007).

The critical parameter in defining the strain softening properties is the model element size. The element size used was 0.25 m * 0.25 m * 0.25 m throughout the model and the cohesion softening was carried out to calibrate the horizontal pillar results to that of the Lunder and Pakalnis (1997). The horizontal pillars were simulated at four different width

to height ratios of 0.5, 1.0, 1.5 and 2.0. The numerical model results were found to be in the range of 2% of the theoretical results as shown in the Figure 3.11a.

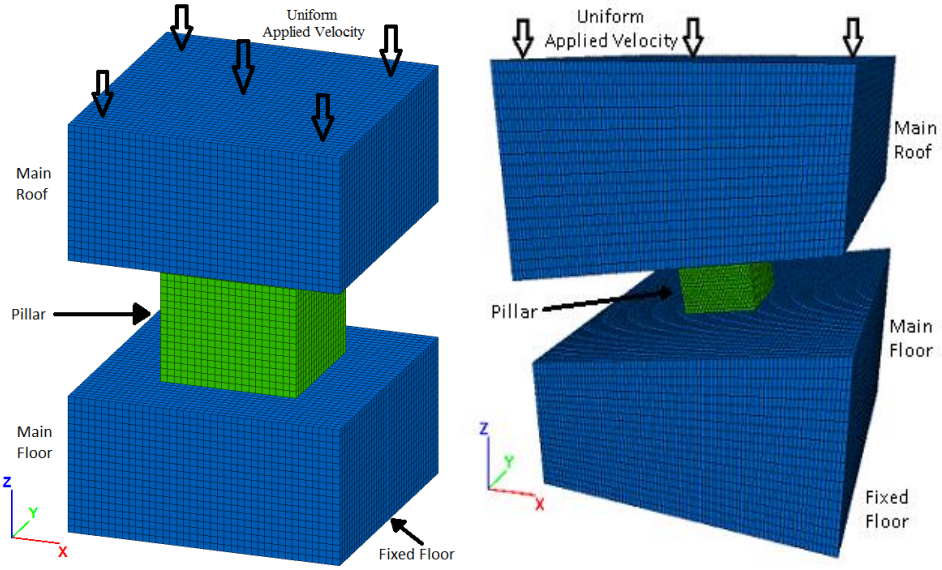

a) b)

Figure 3.10: Numerical models of a) normal loading b) inclined loading (Jessu and Spearing, 2018)

Table 3.3: Model Properties (Dolinar and Esterhuizen, 2007)

Rock Mass Properties	Numerical Value
Bulk Modulus	40,000 MPa
Shear Modulus	24,000 MPa
Intact Rock Strength (UCS)	150 MPa
Cohesion (Brittle)	25 MPa
Friction (Brittle)	0°
Cohesion (Mohr-Coulomb)	8.1 MPa
Friction (Mohr-Coulomb)	47.6°
Tensile strength	2.7 MPa
Dilation angle	30 °

Table 3.4. Joint Properties (Dolinar and Esterhuizen, 2007)

Joint Properties	Numerical Value
Joint Cohesion	1 MPa
Joint Friction	42°
Joint Tension	0.4 MPa
Joint Dilation	0°

Jessu and Spearing (2018) simulated pillars at five different inclinations of 0°, 10°, 20°, 30° and 40° with four different width to height ratios. It was concluded that the pillar strength increases with increase in width to height ratio at all the inclination of the pillars as shown in Figure 11. The results presented in Jessu and Spearing (2018) for numerical modelling of horizontal and inclined pillars have been analysed further to determine the strength reduction factors.

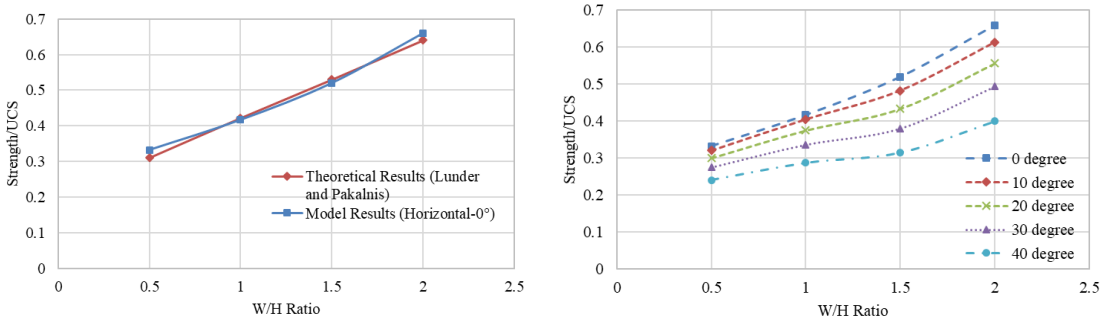

a) b)

Figure 3.11: a) Calibration chart for numerical models to that of theoretical models. b) Pillar strength-W/H ratios in normal and inclined loading conditions (Jessu and Spearing, 2018).

3.5. Discussion

3.5.1. Evaluating Strength Reduction Factors with Laboratory and Numerical Methods

As the strength of the inclined specimens were found to be less than the horizontal specimens, the ratio of the strength of the inclined specimens to strength of the horizontal specimens were determined.

3.5.1.1. Strength Reduction factors for Gypsum specimens and Sandstone specimens

It was found that at a specific inclination the percentage reduction in the strength of the specimens for all the width to height ratios was similar as shown in Figure 3.12. At 10° inclination, the strength of the gypsum specimens was found to be about 76 – 79% of the normal specimens and at 20° inclination, about 54 – 59% of the normal specimens. In sandstone specimen, it was found that the strength of the 10° specimens are 67 – 72% of the normal specimens while the strength of the 20° specimens is about 42 – 47% of the normal specimens. Therefore, a reduction factor can be developed to determine the strength of inclined specimens with respect to the strength of normal specimens.

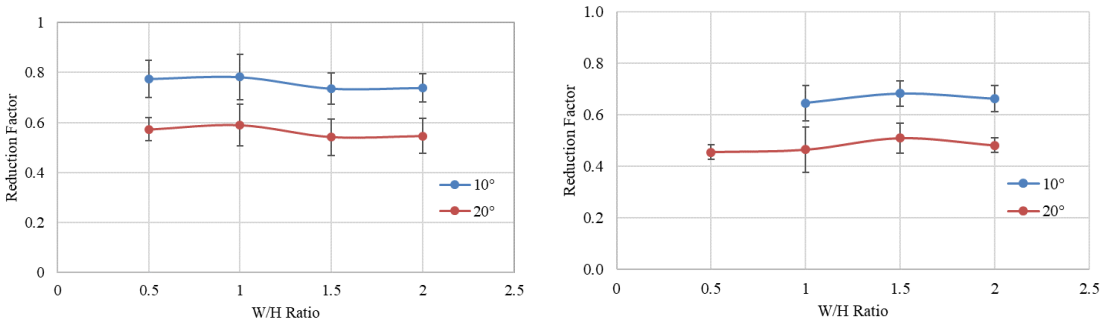

a) b)

Figure 3.12: Strength reduction factor for two different inclinations for a) gypsum specimens b) sandstone specimens.

The average reduction factor was determined for 10° and 20° inclined gypsum specimens as 78% and 56% while for the 10° and 20° inclined sandstone specimens as 71% and 43% as shown in Table 3.5. The goodness of fit test was conducted to determine if these factors are representative for all the specimens. The p-value was evaluated (Table 3.5) and found to be greater than 0.05, which shows that the difference between the reduction factor for individual specimens and the average reduction factor is not significant. Therefore, the average reduction factor can be adopted to consider the effect of inclination on the specimens across all the width to height ratios.

Table 3.5: Average strength reduction factors and Goodness of fit test results for Gypsum Specimens

Specimen	Parameter	10° Inclined Specimens	20° Inclined Specimens
Gypsum	Strength Reduction Factor	0.78	0.56
	Goodness of Fit test	$P(\chi^2 \geq 15.63, 19) = 0.6811$	$P(\chi^2 \geq 11.97, 19) = 0.8867$
Sandstone	Strength Reduction Factor	0.71	0.43
	Goodness of Fit test	$P(\chi^2 \geq 3.69, 8) = 0.8836$	$P(\chi^2 \geq 6.64, 11) = 0.8273$

3.5.1.2. Strength Reduction factors for numerically simulated pillars

In the laboratory-based results of Gypsum as well as Sandstone, the strength of the inclined specimens to the strength of the normal specimens at all the W/H ratios were consistent. The laboratory results show that the strength reduction factors can be used to predict the strength of the inclined specimens at width to height ratio. The laboratory test results are the basis for understanding the strength of the large-scale pillars (Ayres Da Silva, 2013 and 2014). Therefore, as the strength reduction factors are consistent throughout all the W/H ratios for a specific inclination in the laboratory specimens, the strength reduction factors should be consistent throughout all the W/H ratios in the large-scale pillars.

The strength reduction factors were evaluated by comparing the strength of the inclined pillars to that of the normal pillars as shown in the Figure 3.13a. The strength reduction factors were found be slightly higher at the smaller W/H ratios than at larger W/H ratios. For 10° inclined pillars, the reduction factor ranged from 0.92 – 0.97. Similarly, for 20°, 30° and 40°, the range of the strength reduction factors were found to be in between 0.83 – 0.90, 0.73 – 0.83, 0.61 – 0.72 respectively.

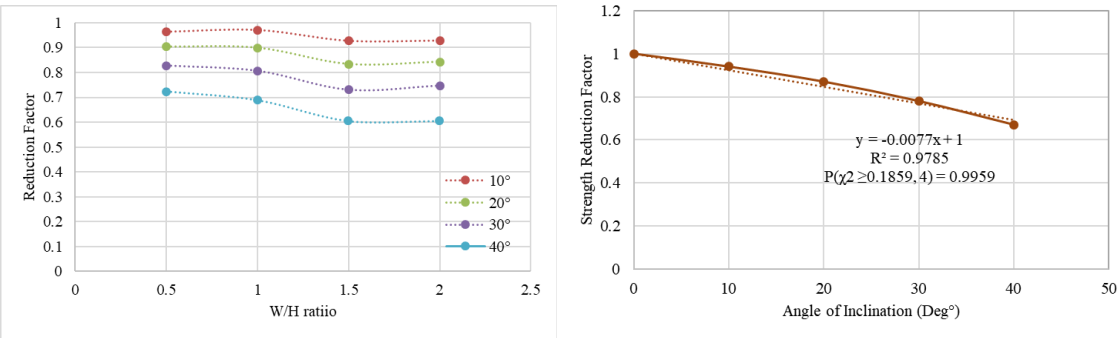

a) b)

Figure 3.13: a) Reduction factors for the numerically simulated inclined pillars b) average strength reduction factor vs pillar inclination

The average of these strength reduction factors was evaluated and are shown in the Table 3.6. Goodness of fit test was conducted to understand if the average can be used as the representative throughout all the pillar width to height ratios for an inclination of the pillar. The p-value from the chi-square test (Table 3.6) were found be higher than 0.05 which effectively explains that difference between the average reduction factor and the individual reduction factor is not significant. Therefore, the average strength reduction factors can be utilized to represent throughout all the width to height ratios.

Table 3.6: Strength reduction factors for pillars with numerical modelling

	10° Inclined Pillar	20° Inclined Pillar	30° Inclined Pillar	40° Inclined Pillar
Strength Reduction Factor	0.94	0.87	0.78	0.67
Goodness of Fit test	P ($\chi^2 \geq 0.16, 3$) = 0.9837	P ($\chi^2 \geq 0.47, 3$) = 0.9254	P ($\chi^2 \geq 0.82, 3$) = 0.8443	P ($\chi^2 \geq 1.61, 3$) = 0.6562

Inclined laboratory test results are compared to the numerical test results at 10° and 20° inclinations as shown in Table 3.7. In sandstone, it was found that it had higher reduction in strength when compared to Gypsum which can be attributed to the scale of

the samples (i.e. Diameter of Gypsum samples is higher than the Sandstone samples). Similarly, as the numerically simulated pillars are very large when compared to the laboratory samples, the reduction in strength of the pillars is less as shown in Table 3.7.

Table 3.7: Strength Reduction factors for laboratory and Numerical models

Specimen	Diameter	10° Inclined Specimens	20° Inclined Specimens
Sandstone	42 mm	0.71	0.43
Gypsum	50 mm	0.78	0.56
Numerical Model	Large	0.94	0.87

For large scale pillars, the numerical models were simulated and calibrated to Lunder and Pakalnis (1997). It was found that the strength reduction factors were consistent throughout all the width to height ratio for any inclination. To account for inclination in the empirical approach developed by Lunder and Pakalnis (1997), relationship between inclination and the reduction factor was developed.

The linear relationship was developed between the average strength reduction factors (RF) and inclination of the pillar (θ) as shown in Figure 3.13b. The equation can be written as:

$$RF = 1 - 0.0077(\theta) \qquad R^2 = 0.9785 \qquad (6)$$

3.5.2. Failure mechanism of the inclined specimens and pillars:

The failure mechanism in the inclined specimens is different to that of the horizontal specimens as shown in Figures 3.7, 3.8 and 3.9. In the inclined specimens, the failure is mainly concentrated at the two corners of the specimens towards the sample dip. To understand the strength loss in the inclined specimens, a theoretical method was developed based on areal or volumetric failure of the specimens/pillars.

In Figure 3.14, the red dotted lines show the breakage of the skin of the specimens and the shaded area show the effected corners. In 10° inclined specimens, area of the corners

effected is less than that of the 20° inclined specimens. In a two-dimensional space, the area effected can be estimated by rectangle and triangle area which is mainly dependant on the angle of inclination (θ) and the height of the sample (H).

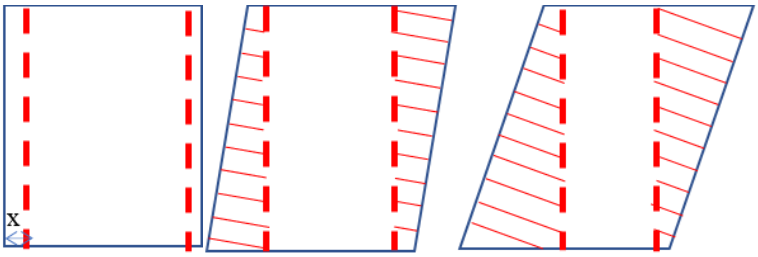

a) b) c)

Figure 14: Effected area a) in normal sample b) 10° inclined sample c) 20° inclined sample

For normal condition, if x is the effected skin width then the area effected (A_N) can be given as area of rectangle such as:

$$A_N = 2 * x * H \tag{3.6}$$

For inclined conditions, the area effected (A_θ) can be estimated with area of rectangle and triangle such as:

$$A_\theta = 2 * x * H + 2 * 0.5 * H^2 * \tan\theta \tag{3.7}$$

The ratio between the affected area in inclined loading condition and the normal loading condition is dependent on the angle of inclination (θ) which is given as:

$$\frac{A_\theta}{A_N} = 1 + \left(\frac{0.5 * H}{x}\right) * \tan\theta \tag{3.8}$$

$$\frac{A_\theta - A_N}{A_N} = K * \tan\theta \tag{3.9}$$

Where $(0.5 * H/x)$ is dependent on the sample with normal loading condition is represented as a constant 'K'. Therefore, the ratio is directly proportional to the angle of inclination of the pillar ($\tan\theta$).

Strength loss in the inclined specimens when compared to the normal specimens were determined in gypsum and sandstone specimen as shown in Table 3.8. The proportionality constant was determined between the strength loss and the angle of inclination of the sample. The proportionality constant was found to be similar across both the inclinations. Therefore, strength loss is also directly proportional to the inclination of the sample. As the strength loss and the ratio of the failure area are both directly proportional to the inclination of the sample, it can be concluded that the failure of the corners of the inclined specimens leads to the loss of strength when compared to the normal specimens.

Table 3.8: Comparison of strength loss to inclination of the Gypsum specimens.

Specimen	Parameter	10° Inclined Specimens	20° Inclined Specimens
Gypsum	Strength Reduction Factor	0.78	0.56
	Strength loss (%)	22%	44%
	$Tan(\theta)$	Tan 10° = 0.176	Tan 20° = 0.363
	Proportionality Constant = Strength loss/Tan (θ)	125	121
Sandstone	Strength Reduction Factor	0.71	0.43
	Strength loss (%)	29%	57%
	$Tan(\theta)$	Tan 10° = 0.176	Tan 20° = 0.363
	Proportionality Constant = Strength loss/Tan (θ)	164	157

Similar to the laboratory tests, the loss of strength was evaluated for all the numerically simulated inclined pillars which were found to be approximately 34 – 39 times the

inclination of the pillar as shown in Table 3.9. This indicates that the strength loss is directly proportional to inclination of the pillar and therefore, can be attributed to the failure of the corners of the pillars.

As the failure in the numerical models can be interpreted, volumetric analysis of the elastic and yielded zones was carried out to develop a relationship between the strength loss and the volume effected in inclined pillars to the volume effected in horizontal pillars. The failure in the horizontal and inclined pillars at the peak strength of W/H ratio 1.0 is shown in Figure 3.15. The skin width effected was determined between 1 – 1.25 m for W/H ratio of 1.0 in both horizontal and inclined pillars. The volume was estimated for the yielded zones in the horizontal pillar and inclined pillar and the ratio was determined for all the inclined pillars as shown in Table 3.9. It was found that the volumetric ratio of the failure region of the inclined pillars (Table 3.9) was twice the strength loss across all the inclinations. Therefore, the strength loss in the inclined pillars can be attributed mainly to the failure of the corners.

Table 3.9: Strength reduction factors for pillars with numerical modelling

	10° Inclined Pillar	20° Inclined Pillar	30° Inclined Pillar	40° Inclined Pillar
Strength Reduction Factor	0.94	0.87	0.78	0.67
Strength loss (%)	6%	13%	22%	33%
$Tan(\theta)$	Tan 10° = 0.176	Tan 20° = 0.363	Tan 30° = 0.577	Tan 40° = 0.839
Proportionality Constant	34	35	38	39
$\frac{V_\theta - V_N}{V_N}$	0.12	0.24	0.38	0.55

3.5.3. Example of the use of Strength Reduction Factors for Inclined Pillar design

Let's assume the pillar stress was 55 MPa with an extraction ratio of 0.75. If the safety factor used to design the pillars is taken as 1.4, then the design of the pillar should be such that it has a strength of 77 MPa. Let's take the uniaxial compressive strength of the rock is about 150 MPa, then with the help of the Lunder and Pakalnis (1997), the width to height ratio needed to design a horizontal pillar having 77 MPa was found to be 1.5.

For 20° inclination, maintaining all the conditions same, if the pillar with W/H ratio of 1.5 is designed, the safety factor reduces by a factor 0.87 as the actual strength of the 20° inclined pillar is 0.94 times the horizontal pillar. Therefore, the safety factor for 20° inclined pillar turns out to be 1.2 which could be considered as a reasonably good design. If the safety factors are to be maintained at 1.4, the W/H ratio needed to design a 20° inclined pillar can be evaluated by including the 0.87 as the reduction factor in the Lunder and Pakalnis (1997) approach and was calculated to be 1.9. Therefore, the strength reduction factors can be better used to design the inclined pillars with reasonably good safety factors.

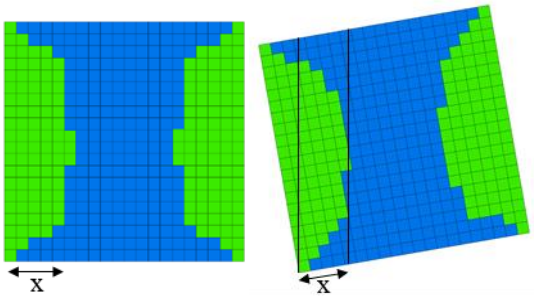

a) b)

Figure 3.15: Yielded zones of a) Horizontal pillar b) Inclined pillar (Jessu and Spearing, 2018)

Note: Blue represent Elastic Zones and Green Represent yielded zones

3.6. Conclusions

Based on the laboratory and numerical results, the following conclusions are drawn:

- Strength reduction factors of 0.78 and 0.56 for 10° and 20° inclined gypsum and 0.71 and 0.43 for 10° and 20° sandstone specimens are consistent throughout all the width to height ratios at a specific sample inclination. Therefore, average strength reduction factors can be utilized for designing the inclined pillars with respect to the horizontal pillars.
- Horizontal pillars were calibrated to the Lunder and Pakalnis (1997) database. Average strength reduction factors obtained from numerical modelling are 0.94 for 10° inclination, 0.87 for 20° inclination, 0.78 for 30° inclination and 0.67 for 40° inclination. These reductions factors can be used in the empirical approach (Equation 3.2) to evaluate the strength of the inclined pillars.
- With the numerical modelling, an equation is proposed for strength reduction factors with respect to the inclinations.
- Reduction factors will lead to better design of inclined pillars with adequate safety factors.
- In larger pillars, the failure at the corners of the inclined pillars leads to the excessive loss of strength when compared to the horizontal pillars.

Reference:

Ayres da Silva, L. A and Ayres da Silva, A. L. M. (2014). The interaction between the scale effect and the shape effect in the mine pillar design. Rock Engineering and Rock Mechanics, pp: 683-687.

Ayres da Silva, L. A., Ayres da Silva, A. L. M. and Sansone, E. C. (2013). The shape effect and rock mass structural control for mine pillar design. In: EUROCK 2013, Wroclaw. *EUROCK 2013: Rock Mechanics for Resources, Energy and Environment*. Croydon: CRC Press/Balkema, p. 563–67.

Bobet, A. and Einstein, H. H. (1998). Fracture coalescence in rock-type materials under uniaxial and biaxial compression. Int. J. Rock Mech. Min. Sci., 35, pp. 863-888

Dolinar, D. R. and Esterhuizen, G. S. (2007). Evaluation of the effects of length on strength of slender pillars in limestone mines using numerical modelling. *Proceedings of the 26th International Conference on Ground Control in Mining*. Morgantown, WV, USA, July 2007: West Virginia University, pp. 304–313.

Elmo, D. and Stead, D. (2010) An integrated numerical modelling–discrete fracture network approach applied to the characterisation of rock mass strength of naturally fractured pillars. Rock Mechanics and Rock Engineering 43(1):3–19

Esterhuizen, G. S. (2006). An evaluation of the strength of slender pillars. *Transactions of Society for Mining, Metallurgy, and Exploration, Inc.* Vol. 320. Littleton, CO: Society for Mining, Metallurgy, and Exploration, Inc., pp. 69–76.

Esterhuizen, G. S., Dolinar, D. R. and Ellenberger, J. L. (2008). Pillar strength and design methodology for stone mines. *Proceedings of the 27th International Conference on Ground Control in Mining.* Morgantown, WV: West Virginia University, pp. 241–253.

Hedley, D. G. F. and Grant, F. (1972). Stope-and-pillar design for the Elliot Lake Uranium Mines. Bulletin of Canadian Institute of Mining and Metallurgy 65:37–44.

Hedley, D. G. F., Roxburgh, J. W. and Muppalaneni, S. N. (1984). A case history of rock bursts at Elliot Lake. *Proceedings of Second International Conference on Stability in Underground Mining*, (ed. C. O. Brawner), 210–234, New York, American Institute of Mining, Metallurgical and Petroleum Engineers Inc.

Itasca Consulting Group, (2018). Fast Lagrangian Analysis of Continua in 3Dimensions, Minneapolis, Minnesota, USA

Jessu, K. V. and Spearing, A. J. S, (2018). Effect of Dip on Pillar Strength. South African Institute of Mining and Metallurgy, 118, 765-776.

Kimmelmann, M. R., Hyde, B., and Madgwick, R. J. (1984). The use of computer applications at BCL Limited in planning pillar extraction and design of mining layouts. Proceedings of ISRM symposium: design and performance of underground excavations, London, 53-63.

Krauland, N. and Soder, P. E. (1987). Determining pillar strength from pillar failure observations. Eng Min J, 8, 34-40.

Kvapil, R. L., Beaza, J. R. and Flores, G. (1989). Block caving at EI Teniente mine, Chile, *Institute of Mining and Metallurgy (Transactions of Institute of Mining and Metallurgy A)*, 98(6), A43–A56.

Lorig, L. J. and Cabrera, A. (2013). Pillar Strength Estimates for Foliated and Inclined Pillars in Schistose Material. In *Proceedings of 3rd International FLAC/DEM Symposium*, Hangzhou, China, October 2013. Paper: 01-01, H. Zhu et al., Eds. Minneapolis: Itasca International Inc. 2013

Lunder, P. J. and Pakalnis, R. (1997). Determination of the strength of hard rock mine pillars. Bulletin for Canadian Institute of Mining and Metallurgy 90(1013):51–55

Martin, C. D. and Maybee, W. G. (2000). The strength of hard-rock pillars. International Journal of Rock Mechanics and Mining Sciences 37:1239–1246

Potvin, Y., Hudyma, M. and Miller, H. D. S. (1989). Rib pillar design in open stope mining. Bulletin for Canadian Institute of Mining and Metallurgy 82(927):31–36.

Pearson, K. (1900). On the criterion that a given system of deviations from the probable in the case of a correlated system of variable is such that it can be reasonably supposed to have arisen from random sampling. *Philosophical Magazine*. Series 5. 50: 157– 175. doi:10.1080/14786440009463897.

Pritchard, C. J. and Hedley, D. G. F. (1993). Progressive pillar failure and rockbursting at Denison Mine. *Rockbursts and Seismicity in Mines*. Young (ed.). Baikema, Rotterdam.

Roberts, D. P., Tolfree, D., McIntire, H. (2007). Using confinement as a means to estimate pillar strength in a room and pillar mine. 1st Canada-US Rock Mechanics Symposium, Vancouver, 1455-1462.

Salamon, M. D. G. and Munro, A. H. (1967). A study of the strength of coal pillars. J. S. Afr. Inst. Min. Metall. September 1967.

Sjoberg, J. S. (1992) Failure modes and pillar behaviour in the Zinkgruvan mine. In: Tillerson JA, Wawersik WR (eds) Proceedings of the 33rd U.S. rock mechanics symposium. A.A. Balkema, Sante Fe. Rotterdam, pp 491–500

Suorineni, F. T., Mgumbwa, J. J., Kaiser, P. K. and Thibodeau, D. (2011). Mining of orebodies under shear loading Part 1 – case histories, *Mining Technology (Trans. Inst. Min. Metall. A),* 120(3), 138–147.

Suorineni, F. T., Mgumbwa, J. J., Kaiser, P. K. and Thibodeau, D. (2014). Mining of orebodies under shear loading Part 2 – failure modes and mechanisms, *Mining Technology* (Trans. Inst. Min. Metall. A), 123(4),240–249.

Wong, L. and Einstein, H. (2009). Crack Coalescence in Moulded Gypsum and Carrara Marble: Part 2—Microscopic Observations and Interpretation. Rock Mechanics and Rock Engineering. 42. 513-545. 10.1007/s00603-008-0003-3.

Whyatt, J. and Varley, F. (2008). Catastrophic failures of underground evaporite mines. In *Proceedings of twenty-seventh International Conference on Ground Control in Mining*. 113–122, Morgantown, ICGCM.

Zhang, Y. (2014). Modelling Hard Rock Pillars Using a Synthetic Rock Mass Approach. PhD dissertation. Simon Fraser University, Canada.

Chapter 4

Effect of Dip on Pillar Strength

This chapter has been published in SAIMM as:

Jessu, K.V., Spearing, A.J.S. (2018) Effect of Dip of Pillar Strength. *Journal of South African Institute of Mining and Metallurgy*. Vol. 118, 765-776

Abstract

Pillars are commonly left in underground mining either for secondary extraction after the primary stopes have been filled or to maintain the overall macro-stability of the mine during its useful life by supporting the overburden. The dip, dimensions and geological features of an orebody determine the mining method used. If pillars are used, the orientation of pillars can vary from horizontal to vertical and anything in-between. The pillars left in underground mines can be loaded axially or obliquely (axial and shear components) depending on their orientation and that of the field stresses. Empirically established methods or numerical modelling are used to design mine pillars. Studies on square and rectangular pillars under normal and oblique loading were also conducted. The strength of the horizontal pillars was calibrated to the Lunder and Pakalnis pillar strength while the strength of the inclined pillars is obtained in reference to the horizontal pillar performance. The failure modes are described for inclined pillars at different width to height ratio where brittle failure was determined to be the dominant failure in the inclined pillars. The rectangular pillars are only beneficial when the length is increased along the dip at higher inclinations and with W/H ratios greater than 1.5.

4.1. Introduction

In hard rock underground mines, pillars are typically left between the openings (stopes) to maintain the stability of the openings. They are usually rib pillars (vertical or near vertical) or crown/sill pillars (horizontal and near horizontal) They need to be adequately designed to avoid sudden failure, maintain stability and not be over-designed such that rock related safety is maintained and, extraction and profit are maximized. Depending on the nature of the ore body and the mining method, the pillars can have varying complexity. Flat lying tabular ore bodies generally use room and pillars or drift and fill mining operations where the pillars are left for the local macro-roof support and larger barrier pillars for the regional support. When the orebodies have a significant dip, ribs pillars are frequently used for the local support, sill pillars to divide the orebody into multiple mining horizons. Crown pillars can be used to prevent collapse to surface for example. This chapter will be mainly dealing with the pillars that are used for the local roof stope support.

Pillar stability is essential for the efficient working of the underground mining activities. Unless designed to be yield pillars, the under designed pillars can cause failure of that pillar and in addition, it may lead to a domino effect causing instability of the whole excavation. On the contrary, the overdesigned pillars may lead to unnecessary ore loss and can become uneconomical to mine.

4.1.1. Normal Loading on Square and Rectangular Pillars:

Studies have been conducted on the pillar size, shape and stability in normal loading conditions for many years. Hedley and Grant (1972) conducted studies on pillar stability in hard rock (granite) room and pillar mines and derived an empirical relation between the strength of the pillars to their width to height ratio. Lunder and Pakalnis (1998) considered the role of confinement in determining the strength of hard rock pillars. Martin and Maybee (2000) led numerical modelling studies using elastic-brittle-plastic to determine the strength of the pillars and concluded that the dip pillars have comparatively less strength than the horizontal pillars. Esterhuizen (2008) concluded that for the room and pillar limestone deposits, the slender pillars have variable strength depending on the structures while the geological features have little impact on the squat pillars.

Rectangular pillars are proven to be effective in maximizing the strength of the pillars as suggested by several researchers (Wagner, 1992; Mark and Chase, 1997; Galvin et al., 1999; Dolinar and Esterhuizen, 2007). The geological structures have less impact over the rectangular pillars when oriented with longer axis of the pillar (Dolinar and Esterhuizen, 2007). Little research has been undertaken to date on the inclined rectangular pillars.

4.1.2. Oblique Loading on Pillars:

Pillars dipping at an angle are subjected to oblique loading which is a combination of the compressive and shear stresses as shown in Figure 4.1. Pritchard and Hedley (1993) classified the pillars based on the progressive failure into five categories at Denison Mine. This was conducted in an ore body dipping at 20° showing the hour glass fracture formation which ultimately leads to the critical cross section area of the pillar core and ultimate failure.

Suorineni et al., 2011 has highlighted that both pillars and excavations under oblique loading mechanism are at elevated risks of failure. This was supported by the case studies reported by Kvapil et al. (1989), Hedley et al. (1994), and Whyatt and Varley (2008). Suroineni et al., 2014 conducted studies to determine the failure modes of the pillars to different orientation of far field principal stresses with the help of two-dimensional numerical modelling and concluded that the pillars are mainly affected by orientation of the far field principal stresses, width-to-height ratio and maximum to minimum principal stress ratio.

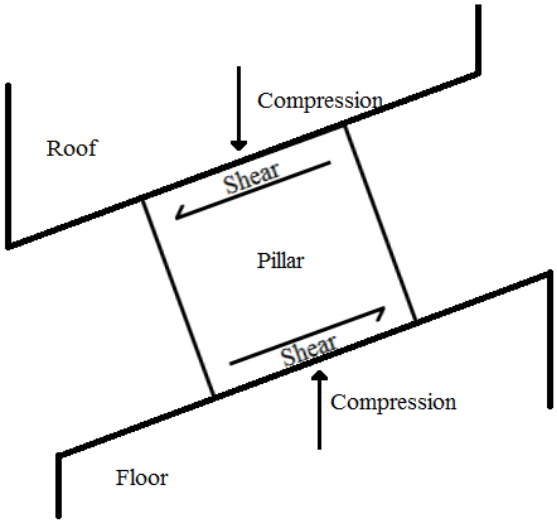

Figure 4.1: Oblique loading on the pillar at an inclination

This chapter will discuss about the failure modes of the pillars at different pillar inclinations and determine the strength of the inclined square and the rectangular pillars at different width to height ratios.

4.2. Modelling Approach

Numerical modelling is a platform that provides a valuable insight into the potential failure modes of the pillar if the input parameters are carefully selected and calibration possible. FLAC^{3D} (Itasca, 2016), a finite difference numerical modelling package was used to simulate the horizontal and inclined pillars as the models can be calibrated to the realistic failure methodology of the hard rock pillars (Esterhuizen, 2006). A three-

dimensional model was constructed to study the individual horizontal and inclined pillars as shown in Figure 4.2.

The coordinate system used in the horizontal plane is represented by x and y axis and the vertical plane by the z axis. Main roof, pillar and the main floor are the main components of the model as shown in Figure 4.2. The height of the pillar is kept constant and the pillar width is varied to simulate the different width to height ratios. The extraction ratio of the horizontal pillar model was kept constant at 75% and the boundaries of the inclined pillars were far enough from the to avoid its influence the pillar system behavior.

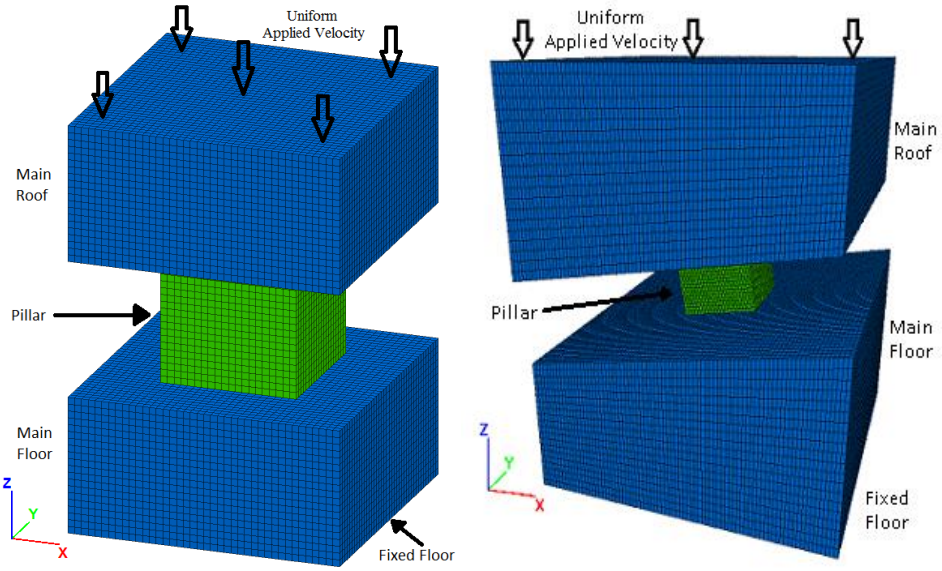

a) b)

Figure 4.2: FLAC^{3D} model a) horizontal pillar b) 10° inclined pillar

The floor was fixed such that the displacements and the velocities are restricted in normal and parallel directions. Side boundaries were incorporated with rollers such that the displacements and the velocities are restricted only in the normal direction. A uniform velocity was applied on top of the main roof to simulate the compression loading in the horizontal model and oblique loading in the inclined pillar models (Lorig and Cabrera, 2013).

To simulate the pillar to be of a mine depth 300m, the pillar was subjected to a vertical stress of about 8.1MPa and the vertical to horizontal stress ratio was maintained at 1:1. The model was run to equilibrium under elastic conditions and was converted to bilinear conditions after reaching the equilibrium which is representative of the rock mass behavior as elastic before the excavation and as brittle and plastic after the excavation (Esterhuizen, 2006). The pillar models were then subjected to the uniform velocity till the complete failure of the pillar. The stress strain curves were developed to obtain the strength of the pillars with the help of a FISH function (FISH is script in FLAC3D to derive user defined variable and functions).

The properties are very critical in numerical modelling to ensure the model is realistic. The performance of the pillars is best represented by the brittle Hoek-Brown criterion (Martin et al., 1999; Kaiser et al., 2000; Esterhuizen et al., 2006). The brittle Hoek Brown damage initiation criterion is established on the development of the brittle cracks which generally occurs at 0.3 to 0.5 times the uniaxial compressive strength and then is followed by the shear failure of the pillars. The uniaxial compressive strength of the rocks was taken to be 150 MPa, therefore the rock mass compressive strength was estimated to be about 50 MPa. Therefore, a bilinear strength envelope was used in which strength is independent of friction at low confinement and is equal to one third of the uniaxial compressive strength followed by friction hardening at the higher confinement (Kaiser, 2000).

Sub ubiquitous model, an inbuilt FLAC^{3D} program designed to simulate the bilinear rock strength based on Mohr Coulomb failure criterion and strain softening as a function of deviatoric plastic strain (Itasca, 2016). The rock properties and joint properties of the model were derived with the help of the Uniaxial Compression Strength and the Rock Mass Rating (RMR) of 70 which were obtained by Dolinar and Esterhuizen (2007). The model properties are shown in the Table 4.1 and 4.2.

Table 4.1: Model Properties (Dolinar and Esterhuizen, 2007)

Rock Mass Properties	Numerical Value
Bulk Modulus	40,000 MPa
Shear Modulus	24,000 MPa
Intact Rock Strength (UCS)	150 MPa
Cohesion (Brittle)	25 MPa
Friction (Brittle)	0°
Cohesion (Mohr-Coulomb)	8.1 MPa
Friction (Mohr-Coulomb)	47.6°
Tension	2.7 MPa
Dilation	30 °

Table 4.2. Joint Properties (Dolinar and Esterhuizen, 2007)

Joint Properties	Numerical Value
Joint Cohesion	1 MPa
Joint Friction	42°
Joint Tension	0.4 MPa
Joint Dilation	0°

Strain softening performance is dependent on the model element size which is determined by using the same element size throughout all the models and calibrating the numerical model results to that of the theoretical results (Itasca, 2016). The model element size was kept at 0.5m * 0.5m * 0.5m for all the models and the cohesion softening was performed to calibrate the model results with the Lunder and Pakalnis (1994) results.

4.2.1. Model Calibration:

The models were generated at different width to height ratios of 0.5, 1.0, 1.5 and 2.0. The model strength of the pillars was then compared to the theoretical results from Lunder and Pakalnis (1994) as shown in Figure 4.3. The difference between the model results and the theoretical results is less than 2%.

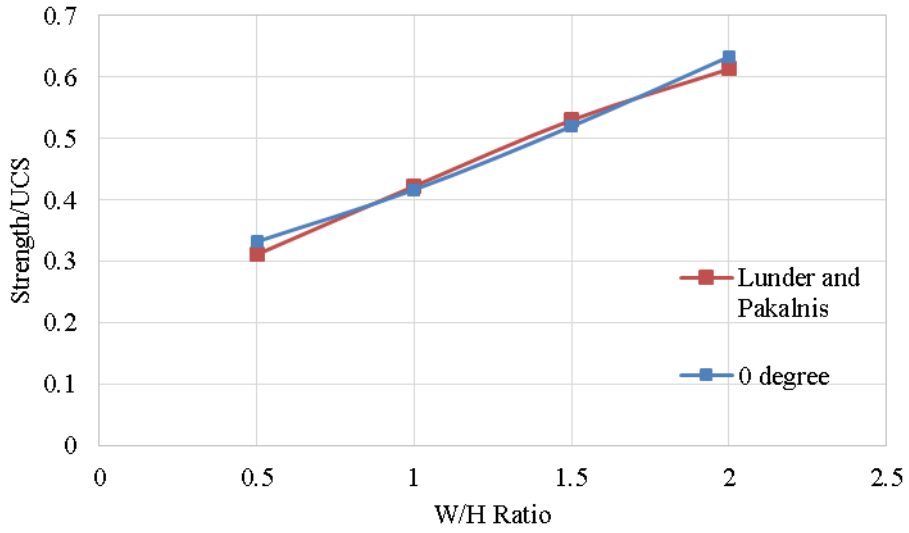

Figure 4.3: Model calibration chart

4.3. Results and Discussion:

4.3.1. Effects on strength of inclined pillar undergoing oblique loading:

The inclined pillars experience oblique loading which is a combination of compressive load and shear load. To evaluate the strength of the inclined pillars, the models were simulated with different pillar inclinations of 0°, 10°, 20°, 30° and 40° at varying width to height ratios and the results are shown in Figure 4.4. The pillar strength decreases with increasing pillar inclinations which is similar to the results presented by Suroineni et al., (2014). At lower W/H ratios, the pillar strength decreases slightly with the increase in pillar inclinations. At higher W/H ratios, as the pillar inclination increases, the strength of the pillar is drastically reduced when compared to the pillar under pure compression.

4.3.2. Failure Modes of Inclined Pillars:

The pillar failure mechanism was studied to understand the load shedding after failure of the pillars. Failure modes were derived from the model results. To understand the pillar failure modes, a section at the center of the pillar in the direction of y-axis (Figure 4.5) has been extracted and the yielded zones have been presented for all the pillar inclinations at different stages of loading. The failure modes of the horizontal and the inclined pillars

will be presented at the width to height ratios of 0.5 and 1.0. The horizontal pillar undergoes only compressive loading while the inclined pillars undergo oblique loading which is a combination of compressive and shear loads.

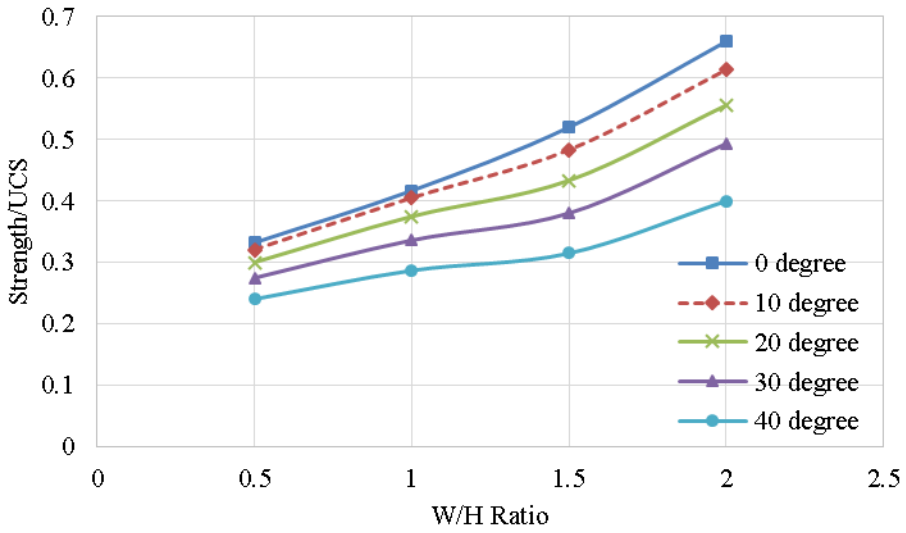

Figure 4.4: Effect on strength of inclined pillars undergoing oblique loading

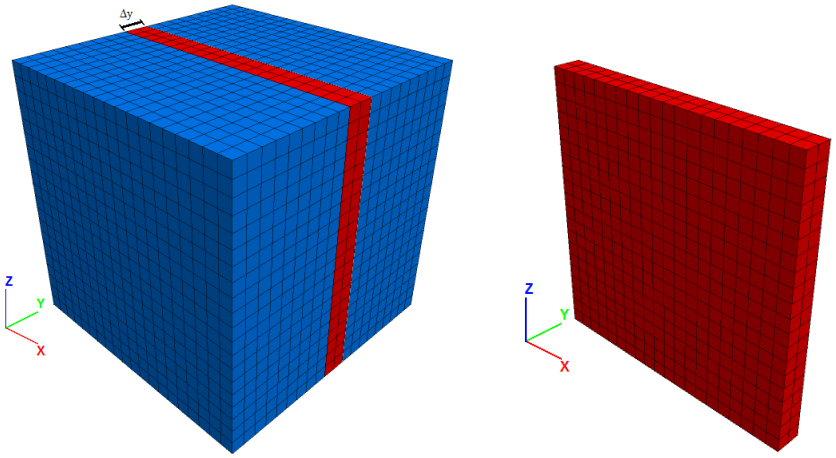

a) b)

Figure 4.5: a) Pillar with section Δy b) section Δy

4.3.2.1. Pillar failure modes in W/H ratio of 0.5

Stress strain graphs of the pillar with W/H ratio of 0.5 at different inclinations are presented in Figure 4.6. At W/H ratio of 0.5, the pillars fail by brittle spalling. It is mainly due to the absence of sufficient confinement in the pillars to mobilize the frictional component of the rock strength (Esterhuizen, 2006). The progressive failure of the pillars has been shown in five stages which are indicated in Figure 4.6. The progressive failures of the horizontal and inclined pillars are shown in Figure 4.7. Stage 1 of the pillar describes about the pillar before loading. The elastic zones are highlighted in blue and the yielded zones are represented in green.

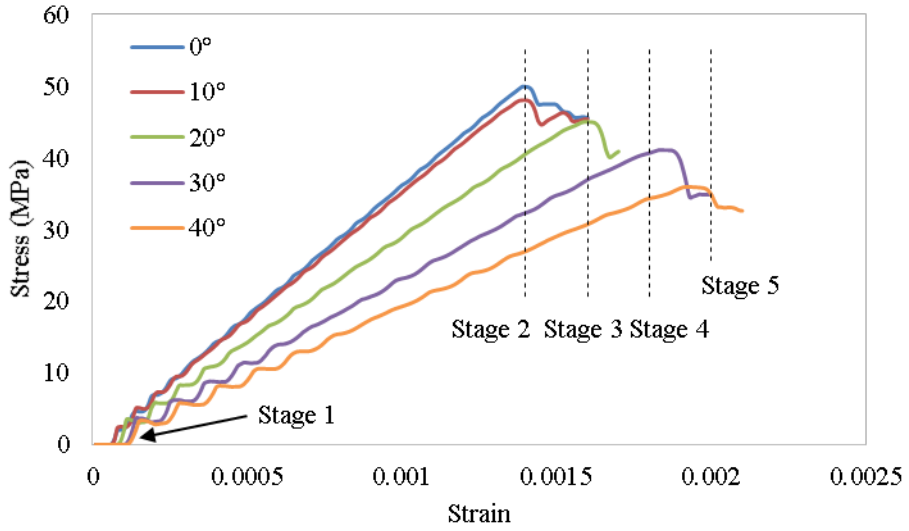

Figure 4.6: Stress-strain charts of pillars at different inclinations with W/H ratio of 0.5

Horizontal pillars (0° Pillar) fail as the average pillar stress approaches the brittle rock strength. The brittle rock strength (50MPa) which is one third of the uniaxial compressive strength (150MPa) can be observed in the graph as the strength of the horizontal pillar. The brittle failure commences at the outer skin of the pillar and then progresses towards the core of pillar at the peak stress. *Stage 2*, where the pillar is at its peak stress, the core has been yielded leading to total failure of the pillar as shown in Figure 4.7a. *Stage 3* shows the post peak stage of the pillar stress showing that pillar has totally yielded

(Esterhuizen, 2006). Final Stages (*Stage 4* and *Stage 5*) are represented as totally yielded meaning the whole pillar is yielded (all zones are green).

In inclined pillars, the *Stage 1* shows the pillar before loading (Figure 4.7). The *Stage 2* shows the initiation of the yielding on the outer skin of the pillars in the opposite corners of the pillar inclination. The *Stage 2* of 10° pillar inclination shows the yielding extending towards the center of the pillar similar to that of the formation of shear plane (Figure 4.7b). As the yielding occurs at the center of the pillar before the total yielding of the outer skin, the strength of the pillar is reduced when compared to that of the horizontal pillars.

The *Stage 3* of the inclined pillars show that at lower pillar inclination, the yielding extends from the outer skin to the pillar towards it center (Figure 4.7b and 4.7c). While at higher pillar inclinations, the yielding is developed only at the two corners of the pillars in the direction of pillar inclination (Figure 4.7d and 4.7e). From *Stage 3*, it can be concluded that the higher the inclination of the pillar, it can sustain higher axial strain to attain the peak strength which may be due to the pillar slide at roof and floor contacts. It can also be observed that with the increase in pillar inclination the yielding distance between the two corners of the pillars decreases attributing to the strength reduction.

The *Stage 4* of the lower inclination pillars (10° and 20° dip pillars) show the post peak phase of the pillar (Figure 4.7b and 4.7c) while for the 30° pillar, the yielding of the pillar has extended from the outer skin to the center of the pillar as shown in Figure 4.7d. It can be observed that the 30° pillar at *Stage 4* is at its peak strength when the yield is approaching the center of the pillar (Figure 4.6). Therefore, it can be concluded that the loss of core causes the pillar strength reduction with the increase in the pillar inclination. The *Stage 4* of the 40° pillar shows the yielding at the outer skin of the pillar as shown in Figure 4.7e.

At *Stage 5*, the pillars other than at 40° inclination are in the post peak phase (Figure 4.7b, 4.7c and 4.7d). The yielding in the 40° pillar at *Stage 5* extends towards the center which is the point of peak strength in the pillar (Figure 4.7e). It can be observed that for the

inclined pillars there is a rapid increase in yielding of the pillar in the last stage. For example, the yielding in the *Stage 4* of the 40° pillar is limited to outer skin while in the *Stage 5*, the yielding has reached the center of the pillar.

Therefore, it can be summarized that the failure along a single plane in a brittle fashion is the dominant pillar failure mechanism at all inclinations with W/H ratio of 0.5. The failure commences at the two pillar corners and coalesce towards the center of the pillar which results in the peak strength of the pillar. At higher inclinations, the pillar can sustain higher axial strains while the pillar strength is reduced. While it is well-known that the yielding of the outer skin of the pillar is an indication for the pillar to be at its peak strength in horizontal pillars (Esterhuizen, 2006); however, for the inclined pillars the yielding at the outer skin may not be clear indication to reach to that conclusion.

It should also be noted that as the pillar core is yielded even before the complete yielding of the pillar's outer skin, it can be concluded that the failure can be a violent failure such as pillar burst. Rapid increase in the yielding of the inclined pillars from the outer skin to the pillar to the center of the pillar which is also a factor towards the violent failure of the pillar at inclinations.

4.3.2.2. Pillar failure mechanism in W/H ratio of 1.0

Stress strain graphs of the pillars with different inclinations at W/H ratios of 1.0 are shown in Figure 4.8. The failure modes of the pillars at W/H ratio is important as failure of the horizontal pillar failure occurs with brittle failure at the outer skin of the pillar followed by shear failure. The transition from brittle failure to shear failure is also observed in Figure 4.8 where the stress strain line of the horizontal pillar changes its slope to reach the peak stress. The progressive failure of the pillars is shown in four stages as shown in Figure 4.8. The horizontal and inclined pillar with zero initial load have been shown in the *Stage 1* of Figure 4.9.

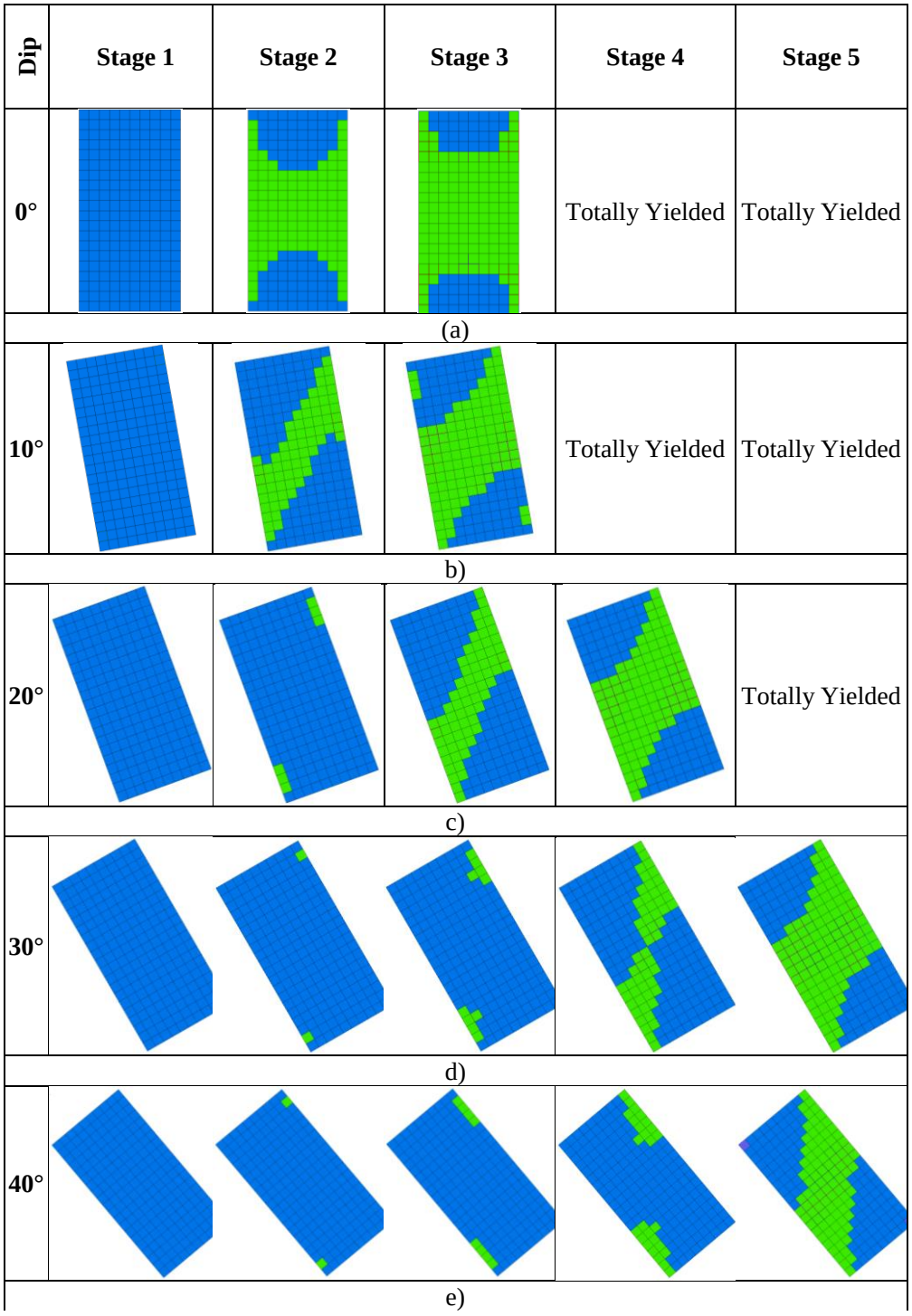

Figure 4.7: Failure modes of the pillars with W/H ratio of 0.5 at different stages in a) horizontal pillar b) 10° inclination c) 20° inclination d) 30° inclination e) 40° inclination (Note: Blue zones represent elastic and Green zones represent yielded/plastic)

Stage 1 shows elastic zones throughout the pillar as they are at zero load. The *Stage 2* of the Horizontal pillar (0° Pillar) shows that the yielding commences at the four corners of the pillar by brittle failure as shown in Figure 4.9a. As the pillar load increases, the brittle failure increases followed by the shear failure. The *Stage 3* and *Stage 4* shows the complete brittle failure at the outer skin of the pillar and the shear failure starting to develop behind the brittle failure zones. The pillar stress can decrease before the core of the pillar has been yielded by shear failure which is similar to the results of the compression tests on small coal pillars reported by Wagner (1974).

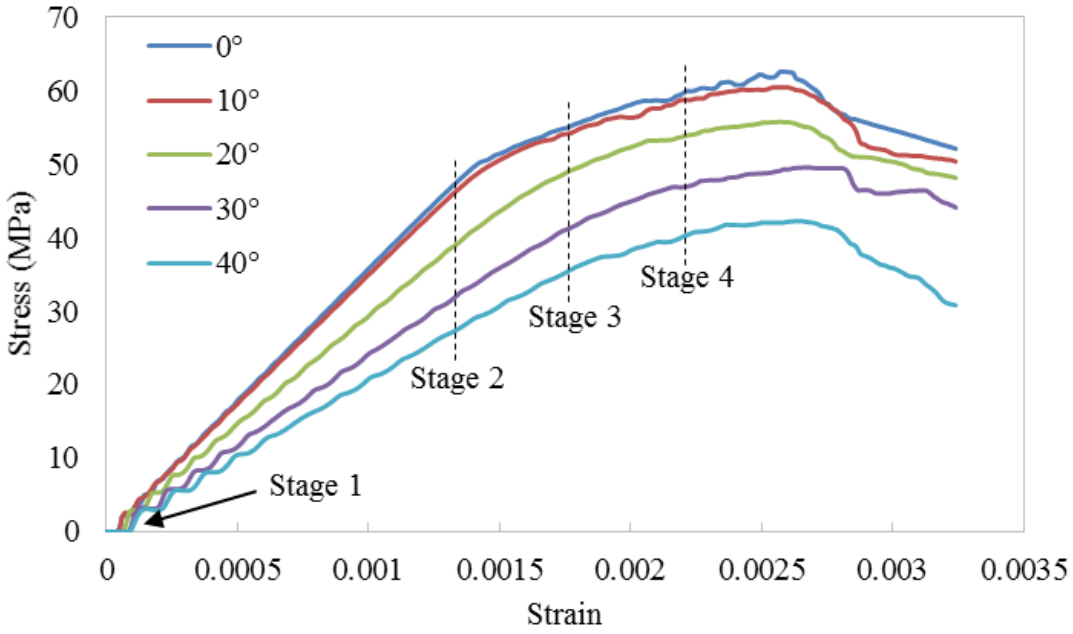

Figure 4.8: Stress-strain graph of horizontal and inclined pillar with W/H ratio of 1.0

The *Stage 1* of the inclined pillars show the pillars before loading (Figure 4.9). The *Stage 2* shows that the stress on the pillar is accumulated at the two opposite corners of the pillar in the direction of inclination due to the brittle failure (Figure 4.9). The *Stage 3* of the 10° pillar shows the complete yielding of the outer skin of the pillar due to brittle failure which can be attributed to "Inclined Hourglass" formation (Figure 4.9b) while for the 20° pillar, the brittle failure extends from the two corners of the pillars to insides of the pillar (Figure

4.9c). The pillars at 30° and 40° inclination indicates the brittle failure extending towards the center of the pillar from the outer skin of the pillars (Stage 3 of Figure 4.9c and 4.9d). Therefore, the higher inclination pillars can sustain more axial strain to attain the peak strength which may be due to the sliding of the pillars at roof and floor contacts.

Higher percentage of zones in the inclined pillars of 10° and 20° are yielded due to the brittle failure when compared to the horizontal pillar (*Stage 3* of Figure 4.9b; and *Stage 4* of Figure 4.9c) which shows the "Inclined Slender Hourglass" formation with the increase in pillar inclination. Due to brittle failure, the depth of yielded zones has also increased in the inclined pillars. As the load increases, the shear failure commences behind the brittle failure due to which the outer skin of the pillar is completely encompassed into brittle failure. The area for shear failure decreases with the increase in inclination of the pillar leading to lower strength of the inclined pillars.

At higher pillar inclination of 30° and 40°, the brittle failure extends towards the center of the pillar leading to core loss (*Stage 4* of Figure 4.9c and 4.9d) which is found to be the peak stress of the pillar. Due to this loss of confinement in the inclined pillars, the shear failure is absent in the 30° and 40° inclined pillars leading to lower strength of the pillars. It can also be observed that there is a rapid increase in the yielding at Stage 4 of 30° and 40° pillar which shows that the pillars at W/H ratio of 1.0 can also cause violent outburst at higher inclinations.

Therefore, it can be summarized that the pillars with W/H ratio of 1.0 at lower inclination lead to "Inclined Hourglass" formation which becomes slender with the increase in the inclination. At higher inclination, the dominant failure mode is brittle failure which extends towards the center of the pillar leading to the violent outburst as the core is yielded even before the outer skin of the pillar. The rapid yielding of the higher inclination pillars due to the brittle failure may also be a basis to the violent outburst.

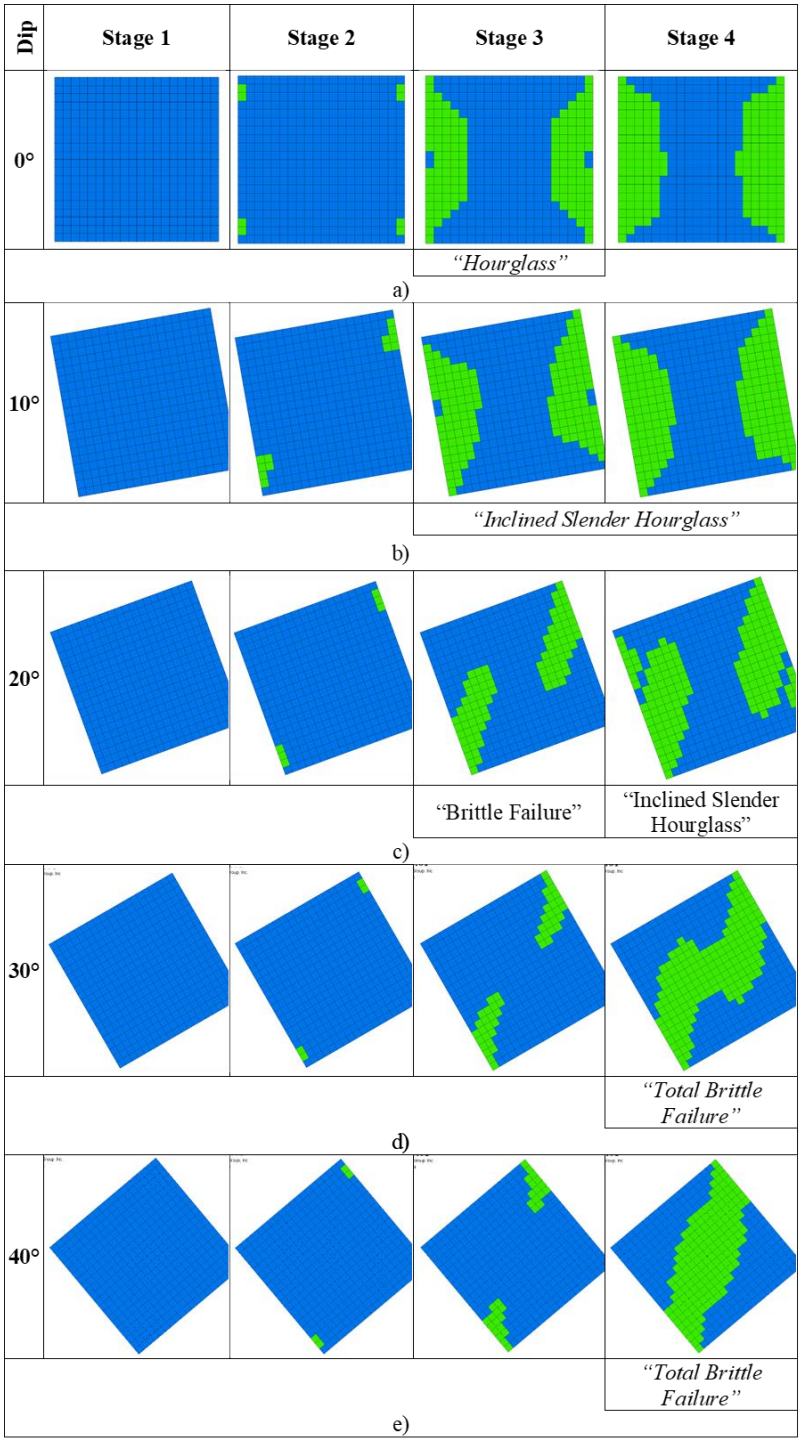

Figure 4.9: Failure mechanism of the pillars with W/H ratio of 1.0 at different stages in a) horizontal pillar b) 10° inclination c) 20° inclination d) 30° inclination e) 40° inclination (Note: Blue zones represent elastic and Green zones represent plastic)

The pillar failure mechanism of 20° inclined models simulate similar behavior observed in the Dension mine classified by Pritchard and Hedley (1993). The minor spalling at the ends of the pillars can be observed in the models (Stage 3 of Figure 4.9c) as well as in the Figure 4.10 which then progresses towards the strong sidewall spalling which resembles the Stage 4 of Figure 4.9d. Therefore, it can be concluded that the pillar failure mechanisms at other inclinations would show similar failure mechanism in the in situ as shown in the Figure 4.9 and 4.11.

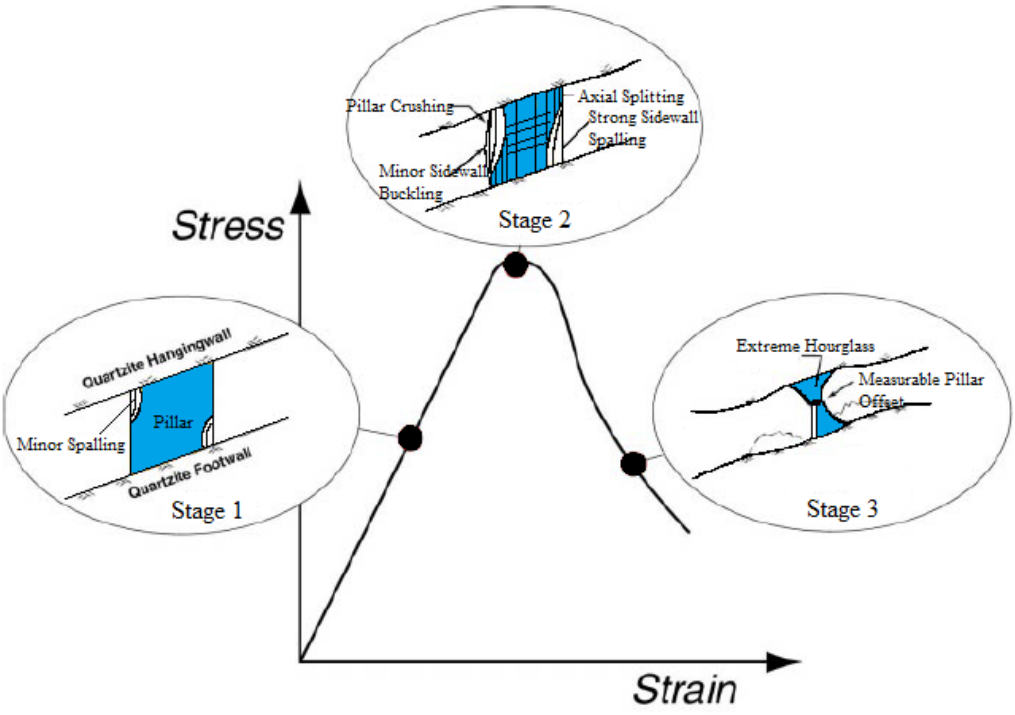

Figure 4.10: progressive pillar failure mechanism observed in Dension mine with 20° dip pillars (Pritchard and Hedley, 1993).

4.3.2.3. Pillar failure mechanism in pillars with W/H ratio more than 1

The transformation was observed from complete brittle failure at W/H ratio of 0.5 to partial brittle failure in addition with shear failure at W/H ratio of 1.0. The transformation was observed for 0°, 10° and 20° pillars while for the 30° and 40° inclined pillars it was observed to be total brittle failure. A similar transformation will be observed at higher inclinations with increase in W/H ratio. Therefore, it can be concluded that the at higher

W/H ratios, the failure mode of the pillars will be partial brittle failure in combination with shear failure as classified in Figure 4.11.

The *"Inclined Hourglass"* formation in the inclined pillars which becomes slender with increase in inclination can be attributed to the decrease in the strength of the inclined pillars at W/H ratio of 1.0. It can be concluded that similar behavior will be observed at higher W/H ratios.

4.3.3. Rectangular Pillars

Models were simulated to understand the effects of inclination on the rectangular pillars. The inclined rectangular pillars can be classified into dip and strike pillars. For the strike pillars, the length of the pillar was increased perpendicular to the direction of inclination (Figure 4.12a) while for the dip pillars, the length of the pillar was increased perpendicular to the direction of the inclination (Figure 4.12b). The three width-to-height ratios of 0.5, 1.0 and 1.5 and length to width ratios of 1.0, 2.0 and 3.0 at varying pillar inclinations were simulated to obtain the strength of the rectangular pillar.

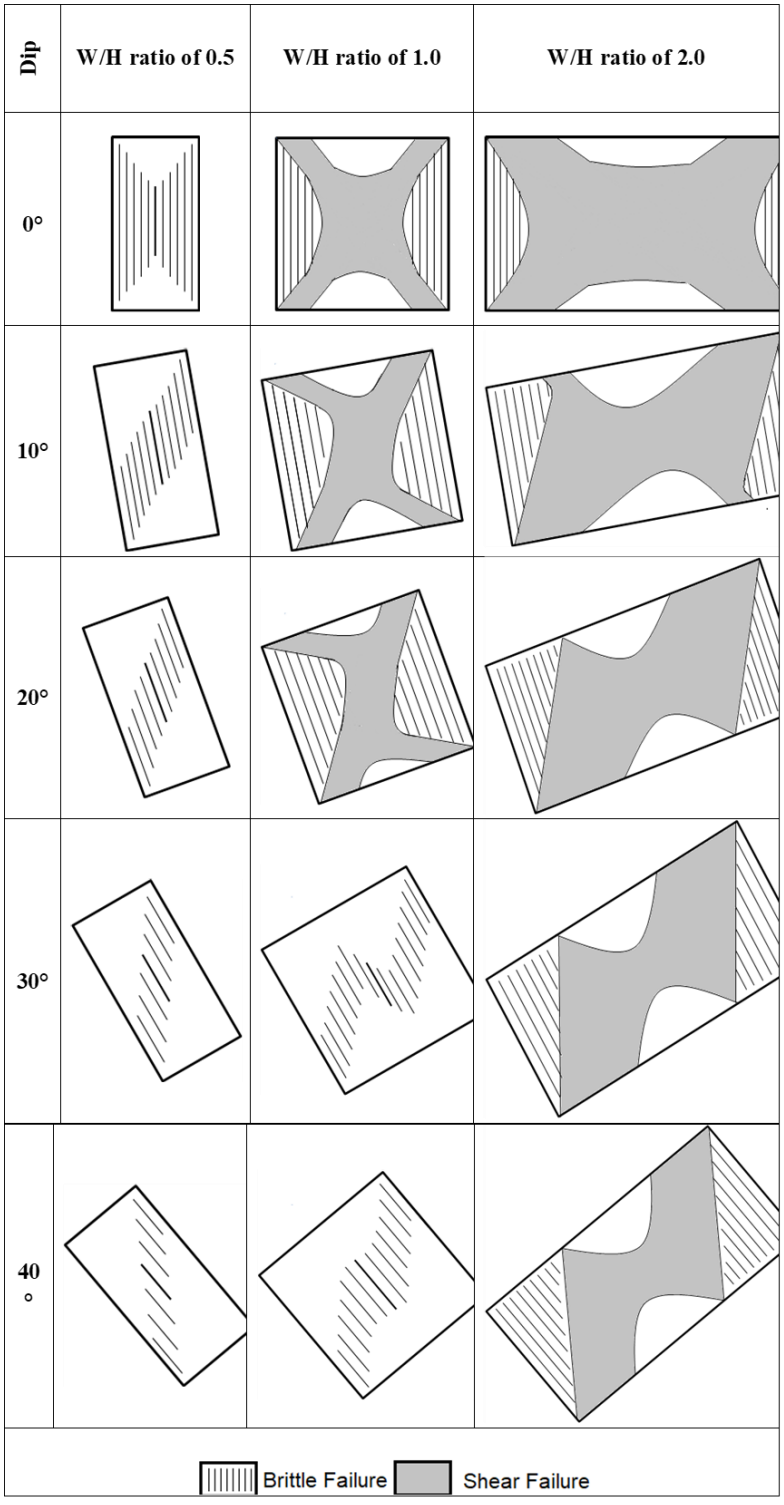

Figure 4.11: Pillar failure classification with brittle and shear failure at different inclinations

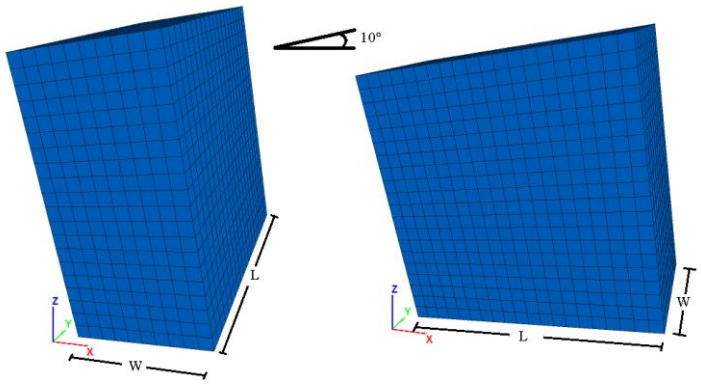

Figure 4.12: Model of 10° inclined rectangular pillar with W/H ratio of 0.5 and L/W ratio of 2.0 along a) strike and b) dip

For the horizontal pillars, the rectangularity in dip is equal to the strike. The pillars with W/H ratios of 0.5 with varying L/W ratio have similar strengths as the failure mechanism is dominated by brittle failure. At W/H ratio of 1.0 and 1.5, the pillar strength increases with increase in L/W ratio as shown in Figure 4.13. It is due to the fact that at higher W/H ratios, the shear failure is the dominant and with the increase in length, a large shear failure area is formed which results in the increase of the pillar strength. It can be concluded that the pillars have higher strength with increasing L/W ratio at higher W/H ratios. The model results were similar to the results of Dolinar and Esterhuizen (2007).

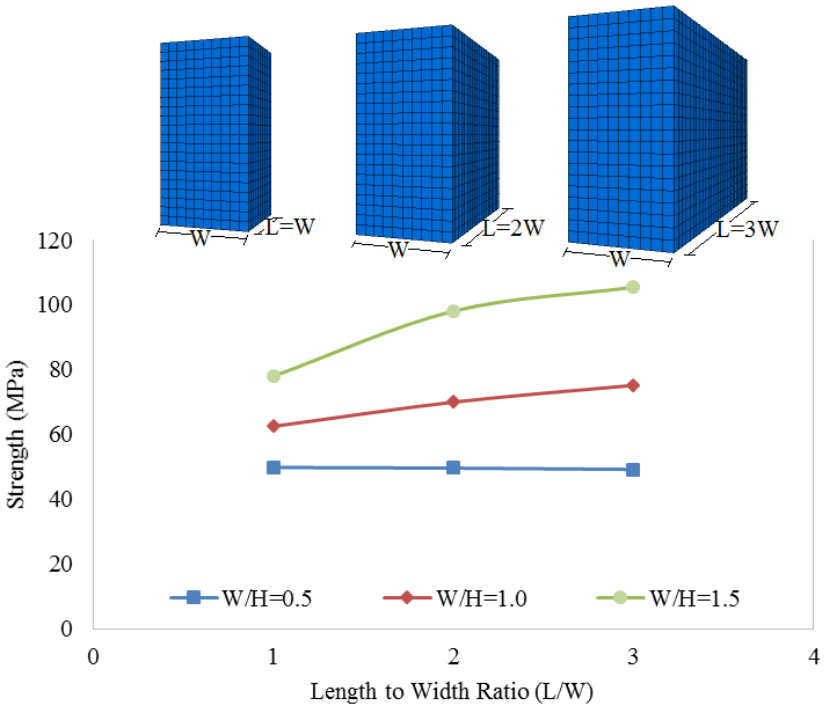

Figure 4.13: Results of the horizontal rectangular pillar at different W/H ratios

The rectangular pillars at 10°, 20°, 30° and 40° along the strike and dip were simulated to determine the strength of the pillars. Fifteen models each for different inclinations were modelled: Three models with W/H ratio of 0.5, 1.0 and 1.5 and L/W ratio of 1.0 to represent the square pillars, six models each with W/H ratio of 0.5, 1.0 and 1.5 and L/W ratio of 2.0 and 3.0 along strike and dip.

At 10° inclination, the strength of the pillar increases with increase in length of the pillars at higher width-to-height ratio and remains same at W/H ratio of 0.5. The pillars with lower W/H ratios show no difference in strength with the dip and strike pillars (Figure 4.14) similar to that of the horizontal pillars (Figure 4.13). While at higher W/H ratio of 1.5, the dip pillars represent 7% higher strength when compared to strike pillars as shown in Figure 4.14.

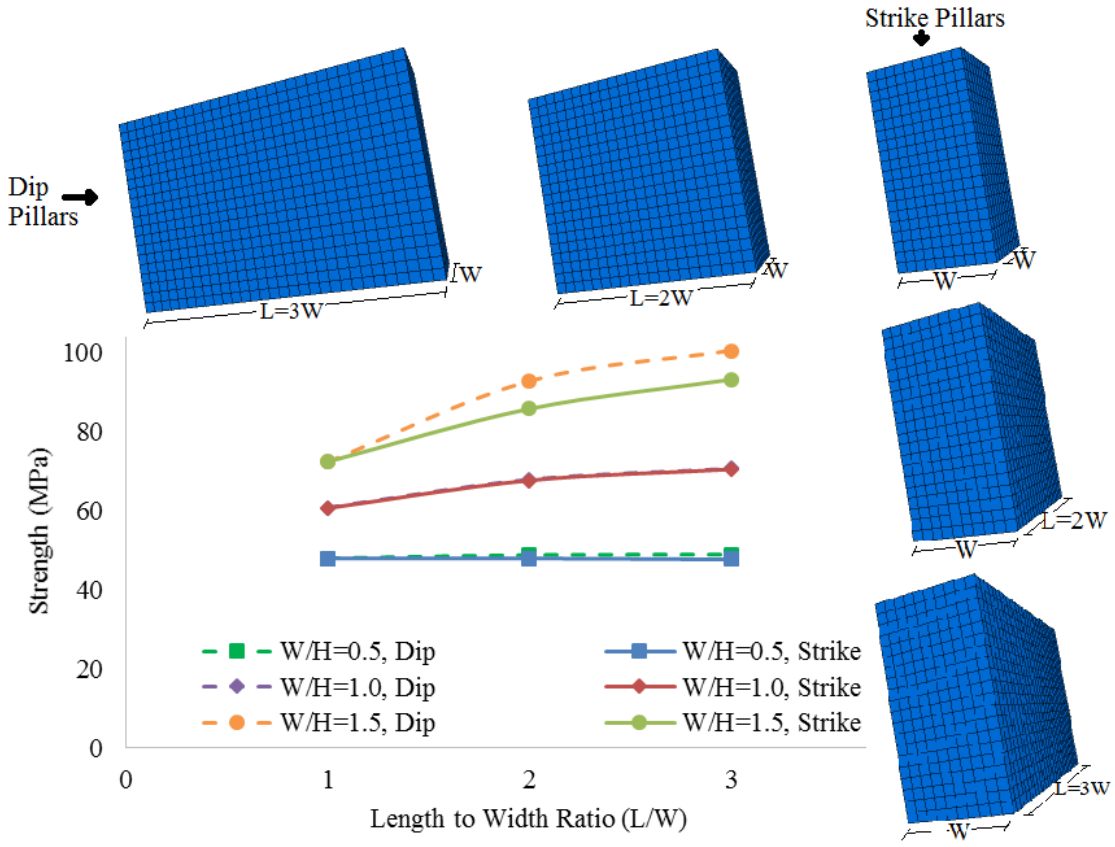

Figure 4.14: Results of 10° inclined rectangular pillars with length extended along dip and strike.

At 20° and 30° inclinations, the strength of the pillars increases with increases in length along dip at any W/H ratio. It can also be observed that strength of the rectangular pillars with length extended along strike show minimal to no increase in strength when compared to square pillars (Figure 4.15 and 4.16). At W/H ratio of 1.5, the strength of the dip rectangular pillars has 14% and 20% more strength than the strike rectangular pillars at 20° and 30° inclinations respectively. Therefore, it can be concluded that the rectangular are only beneficial when the longer axis is along dip with W/H ratio greater than or equal to 1.5.

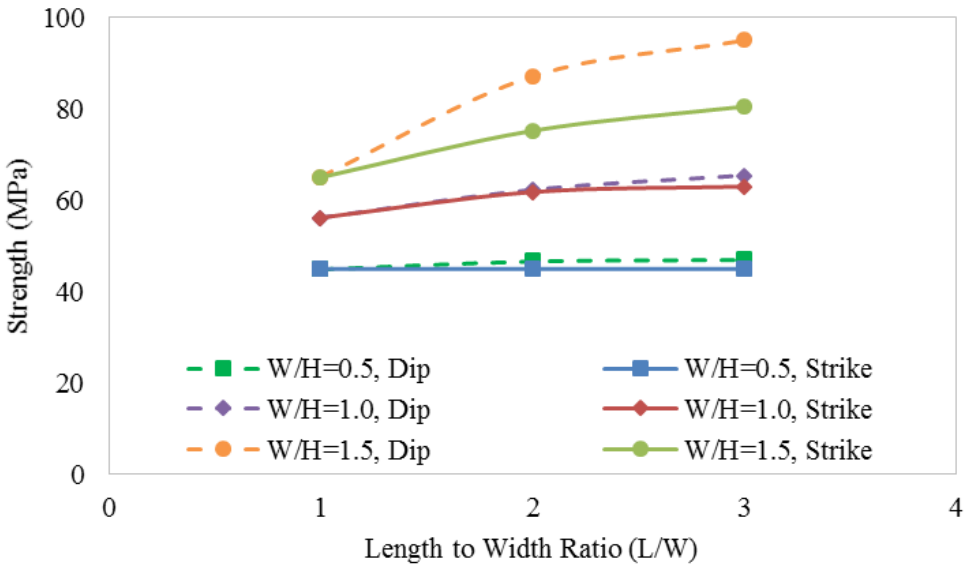

Figure 4.15: Results of 20° inclined rectangular pillars with length extended along dip and strike.

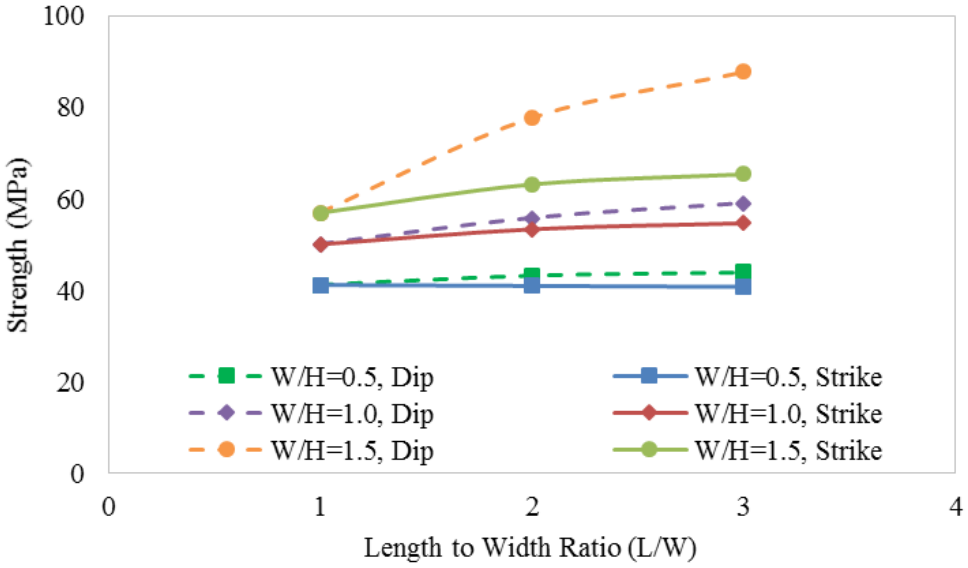

Figure 4.16: Results of 30° inclined rectangular pillars with length extended along dip and strike.

At 40° inclination, it can be observed that the strike pillars show no increase in the strength of pillars with the extension of the length at any W/H ratio (Figure 4.17). This means that

the square pillar with W/h ratio of 1.5 and the rectangular pillar with W/H ratio of 1.5 and L/W ratio of 3 along the strike has equal strength. This can be used for determining the strength of the Sill pillars.

Sill pillars are inclined and considered to be infinite in length and modelled in two-dimensional framework. The simple approximation for the strength of the sill pillars can be made by calculating the strength of the square pillar at that inclination and W/H ratio. This holds true as the length is not contributing towards the increase in strength of the pillar.

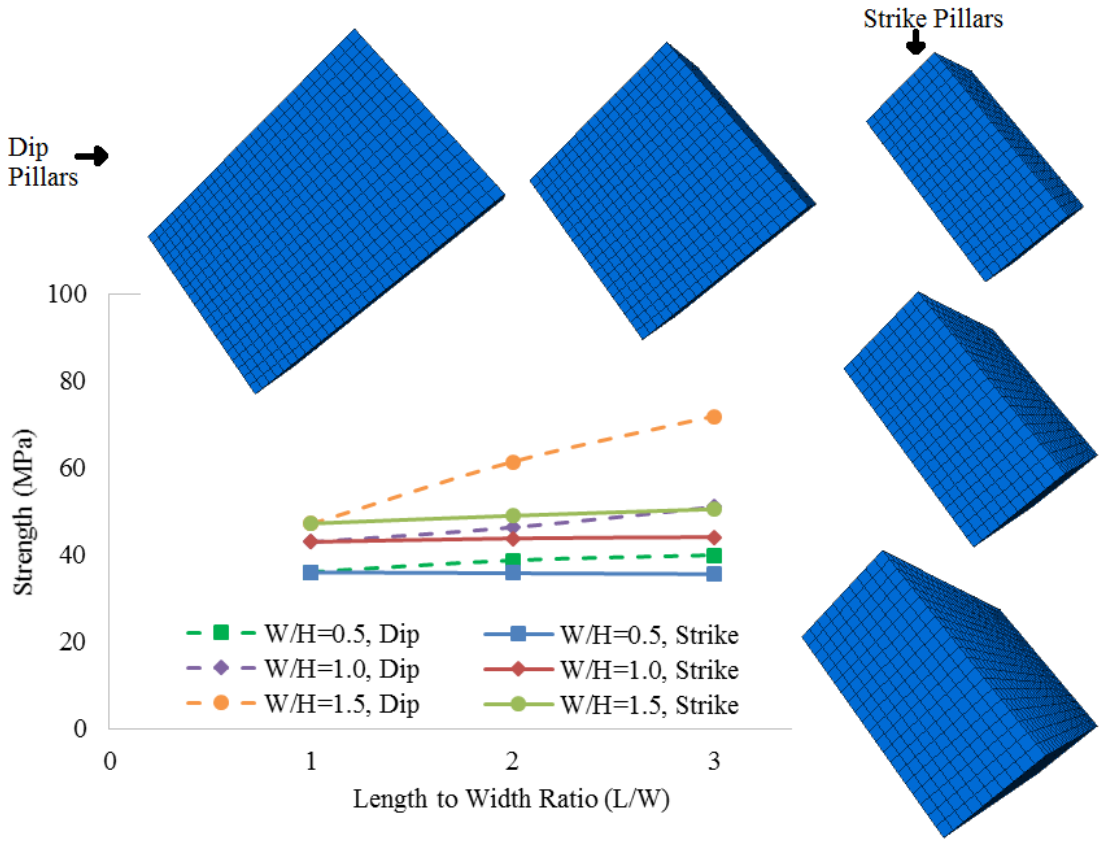

d)

Figure 4.17: Results of 40° inclined rectangular pillars with length extended along dip and strike

4.4. Conclusions:

Based on the modelling undertaken, the effects of dip on the pillar strength are concluded as follows:

- The pillar strength is relatively low at higher inclinations when compared to horizontal pillars. Therefore, higher safety factors are required while designing the inclined pillars with the traditional approaches.
- Brittle failure is the dominant failure mechanism in the inclined pillars. The initiation of the pillar deformation is sluggish, while the rapid yielding occurs when it reaches its peak stress.
- The violent outburst can be expected in the inclined pillars due to the core loss even before the deformation in the outer skin of the pillar and due to the rapid deformation near its peak stress.
- The rectangular pillars are only beneficial when the length of the pillars is increased along the dip at higher inclinations and with W/H ratios greater than 1.5.
- The strength of the sill pillars can be approximately measured with the help of the square pillars as the inclined pillars with increased length in the strike direction show minimal to no increase in strength when compared to square pillar.

References:

Dolinar, D. R. and Esterhuizen, G. S. (2007). Evaluation of the effects of length on strength of slender pillars in limestone mines using numerical modelling. *Proceedings of the 26th International Conference on Ground Control in Mining*. Morgantown, WV: West Virginia University, pp. 304–313.

Esterhuizen, G. S. (2006). An evaluation of the strength of slender pillars. *Transactions of Society for Mining, Metallurgy, and Exploration, Inc.* Vol. 320. Littleton, CO: Society for Mining, Metallurgy, and Exploration, Inc., pp. 69–76.

Esterhuizen, G. S., Dolinar, D. R. and Ellenberger, J. L. (2008). Pillar strength and design methodology for stone mines. *Proceedings of the 27th International Conference on Ground Control in Mining.* Morgantown, WV: West Virginia University, pp. 241–253.

Galvin, J. M., Hebblewhite, B. K. and Salamon, M. D. G. (1999). University of New South Wales coal pillar strength determinations for Australian and South African mining conditions. *Proceedings of the Second International Workshop on Coal Pillar Mechanics and Design*. Pittsburgh, PA: U.S. Publication No. 99-114, IC 9448, pp. 63– 71.

Hedley, D. G. F., Roxburgh, J. W. and Muppalaneni, S. N. (1984). A case history of rock bursts at Elliot Lake. *Proceedings of Second International Conference on Stability in Underground Mining*, (ed. C. O. Brawner), 210–234, New York, American Institute of Mining, Metallurgical and Petroleum Engineers Inc.

Hedley, D. G. F. and Grant, F. (1972). Stope and pillar design for the Elliot lake uranium mines. *Canadian Institute of Mining and Metallurgy Bulletin.* Vol. 65, pp. 37-44.

Itasca Consulting Group, (2016). Fast Lagrangian Analysis of Continua in 3Dimensions, Minneapolis, Minnesota, USA.

Kaiser, P. K., Diederichs, M. S., Martin, C. D., Sharp, J. and Steiner, W. (2000). Underground works in hard rock tunneling and mining. *Proceedings of GeoEng2000*, 841–926, Melbourne, ICMS.

Kaiser, P. K., Kim, B., Bewick, R. P. and Valley, B. (2011). Rock mass strength at depth and implications for pillar design, *Mining Technology (Transactions of Institute of Mining and Metallurgy-A)*, 120(3), 170–179.

Kvapil, R. L., Beaza, J. R. and Flores, G. (1989). Block caving at EI Teniente mine, Chile, *Institute of Mining and Metallurgy (Transactions of Institute of Mining and Metallurgy A)*, 98(6), A43–A56.

Lorig, L. J. and Cabrera, A. (2013). Pillar Strength Estimates for Foliated and Inclined Pillars in Schistose Material. *Proceedings of 3rd International FLAC/DEM Symposium*,

Hangzhou, China, October 2013. Paper: 01-01, H. Zhu et al., Eds. Minneapolis: Itasca International Inc. 2013

Lunder, P.J. and Pakalnis, R., (1997). Determining the strength of hard rock mine pillars. *Bulletin of Canadian Institute of Mining and Metallurgy.* Vol. 90, pp. 51-55.

Mark, C. and Chase, F.E. (1997). Analysis of retreat mining pillar stability (ARMPS). *Paper presented at the seminar on new technology for ground control in retreat mining*. Pittsburgh, US Bureau of Mines. Pp. 17-34

Martin, C. D., Kaiser, P. K. and McCreath, D. R. (1999). Hoek–Brown parameters for predicting the depth of brittle failure around tunnels. *Canadian Geotechnical Journal*. 36(1), 136–151.

Martin, C. D. and Maybee, W. G. (2000). The strength of hard rock pillars. *International Journal of Rock Mechanics and Mining Sciences.* Vol. 37, pp. 1239-1246.

Pritchard, C. J. and Hedley, D. G. F. (1993). Progressive pillar failure and rockbursting at Denison Mine. *Rockbursts and Seismicity in Mines*. Young (ed.). Baikema, Rotterdam.

Suorineni, F. T., Mgumbwa, J. J., Kaiser, P. K. and Thibodeau, D. (2011). Mining of orebodies under shear loading Part 1 – case histories, *Mining Technology (Trans. Inst. Min. Metall. A)*, 120(3), 138–147.

Suorineni, F. T., Mgumbwa, J. J., Kaiser, P. K. and Thibodeau, D. (2014). Mining of orebodies under shear loading Part 2 – failure modes and mechanisms, *Mining Technology* (Trans. Inst. Min. Metall. A), 123(4),240–249.

Wagner, H. (1974). Determination of the complete load-deformation characteristics of coal pillars. In *3rd Congress, International Society of Rock Mechanics.* Denver, Colorado, VII, Part B, pp. 1067-1081.

Wagner, H. (1992). Pillar design in South African collieries. In *Workshop on Coal Pillar Mechanics and Design*, U.S. Bureau of Mines, IC 9315, pp. 283-301.

Whyatt, J. and Varley, F. (2008). Catastrophic failures of underground evaporite mines. In *Proceedings of twenty-seventh International Conference on Ground Control in Mining*. 113–122, Morgantown, ICGCM.

Chapter 5

Effect of Discontinuity Dip Direction on Hard Rock Pillar Strength

This chapter has been accepted and yet to publish in SME Transactions as:

Jessu, K.V., Kostecki, T.R., Spearing, A.J.S., Esterhuizen G.S. (2018) Effect of Discontinuity Dip Direction on Hard Rock Pillar Strength. *SME Transactions*. Vol. 344, pp. 25-30.

Abstract:

Discontinuities are geologic occurrences in rock and when present within a pillar, reduce the strength of the pillar. Empirical formulas that are commonly used to determine the pillar strength do not explicitly take into account the presence of discontinuities and thus can overestimate the pillar strength. The effect of discontinuities on the strength of pillars have been investigated using numerical models, but in these models the discontinuity strike was parallel with the pillar faces. In this study, fully three-dimensional hard rock pillars were simulated using numerical modelling to understand the effect of the discontinuity dip direction on square and rectangular hard rock pillars. Based upon the results, recommendations to assess pillars strength in the presence of a discontinuity are discussed.

5.1. Introduction:

Discontinuities are an integral part of rock strata and create potential support and stability problems during, and after, mine development. These discontinuities exist as discrete planes in a rock-mass where sliding movement may or may not occur. The strength of a rock sample with the presence of a discontinuity is significantly less than the strength of the intact rock sample depending on its orientation relative to the stress direction (Jaeger and Cook, 1979). Pillars have been shown to behave similarly to that of a rock sample suggesting that the strength of the pillar also depends on the discontinuity present in the pillar (Esterhuizen, 2006). To illustrate this concept of pillars with discontinuities, an example of a limestone pillar intersected by a major structural feature is shown in Figure 5.1.

Empirical equations for designing pillars are all based on examining the stable, unstable and failed pillars without giving much emphasis on the mode of failure. Therefore, in the presence of a major discontinuity, if the pillar is designed using empirical approaches, the pillar strength can be overestimated. Abrupt pillar failure due to the presence of discontinuity will increase the amount of load on the adjacent pillars and can lead to chain pillar failures especially if the system has low factor of safety.

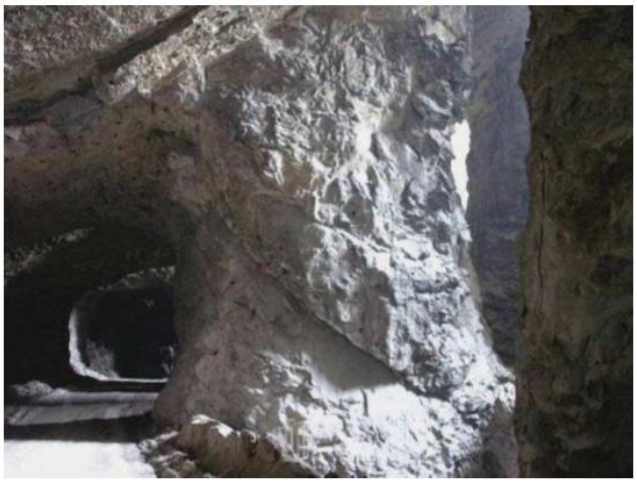

Figure 5.1: Example of the pillar with major structural feature (Esterhuizen, 2006)

Early studies, mainly by Madden et al., (1995) in the South African Coal Fields, showed that discontinuities had a significant effect on the strength of the pillars. As a result, a pillar condition rating system was introduced to better estimate the pillar strength. This system cannot be adopted as a "universal" design since the rating system is based mainly on visual inspection of fracturing, scaling of the pillars, and other visual tell-tales of the pillar condition, and its empirical database is limited to coal pillars observed in South Africa.

Later studies by Iannacchoine (1999) of limestone pillars showed a relationship between the dip angles of discontinuities relative to the pillar strength and concluded that pillar strength is most significantly affected by discontinuity dip angle at 60°. Two studies which incorporate numerical modelling to study pillars intersected by discontinuities were undertaken by Esterhuizen (1998 & 2006). One such study focused on the relationship between pillar strength relative to changes in the dip angle of a discontinuity and varying pillar width-to-height ratios in the limestone mines. The other study focused on slender and squat coal pillars in the presence of a discontinuity.

This chapter will present the numerical analysis of a discontinuity oriented at 45° to the pillar face at different dip angles and varying pillar width-to-height ratios. The orientation of the discontinuity to that of the rectangular pillars is also investigated.

5.1.1. Dip Direction/Strike:

In all the previous studies, the numerical models were evaluated with the dip directions (strike) parallel to that of the face of the pillar as shown in Figure 5.2a. For example, Esterhuizen et al. (2008) accounted for the effect of discontinuities on pillar strength in limestone mines as follows:

$$S = 0.65 * UCS * LDF * \frac{w^{0.30}}{h^{0.59}} \tag{5.1}$$

Where UCS is the uniaxial compressive strength of the intact rock, w and h are the width and height of the pillars and LDF is the large discontinuity factor which is derived from the numerical models and given as:

$$LDF = 1 - DDF * FF \tag{5.2}$$

Where DDF is the discontinuity dip factor depends on both the discontinuity dip and the pillar width-to-height ratio, and FF is the frequency factor i.e. number of large discontinuities per pillar. The DDF was developed with the numerical models only based on the discontinuity dip direction of 0° as shown in the Figure 5.2a.

Obviously, different discontinuity dip directions (strike) can be encountered in the mine to that of the pillar face. A limited study conducted by Esterhuizen (1998) with multiple discontinuities having a dip of 60° and dip direction of 45° to that of the pillar face concluded that the strength obtained was 10% less than that to the multiple discontinuities parallel (i.e. dip direction = 0°) to pillar face. This approach can be used with a single discontinuity to understand the strength of the pillars at different dip directions and different dip angles as shown in the Figure 5.2.

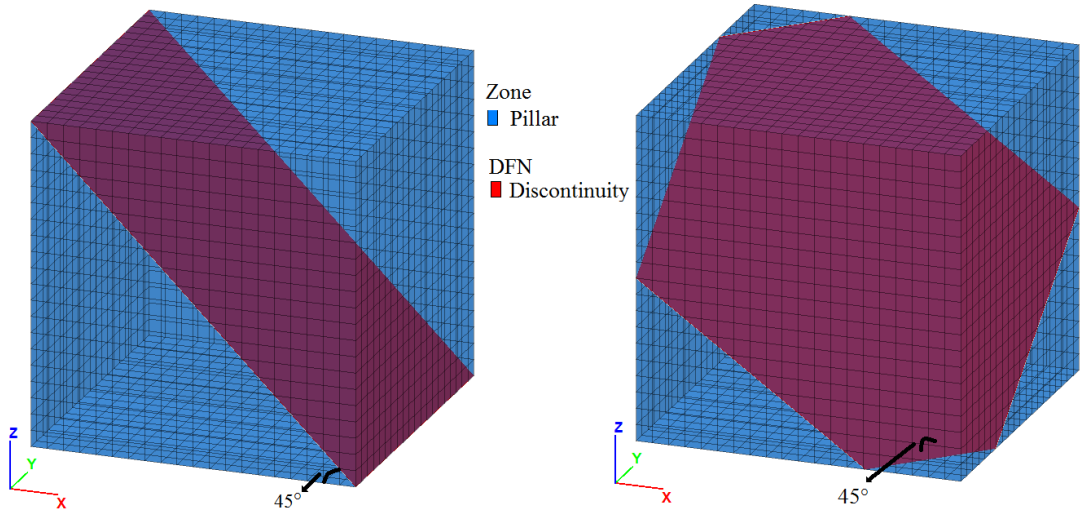

a) b)

Figure 5.2: Discontinuity with 45° dip with a) 0° dip direction and b) 45° dip direction

Rectangular pillars:

Rectangular pillars can be effective in increasing the strength of the pillars and have been suggested by several researchers (Wagner, 1992; Mark and Chase, 1997; Galvin et al., 1999; Dolinar and Esterhuizen, 2007). An equivalent width method which was introduced by Wagner (1992) which was further modified by Esterhuizen (2008) taking into consideration the confinement effect and is given as:

$$w_e = w + \left(\frac{4A}{C} - w\right) * LBR \tag{5.3}$$

Where w is the width of the pillar, A is the area of the pillar, C is the circumference of the pillar and LBR is the length benefit ratio which increases from 0 to 1 with increasing width-to-height ratios. This equation however doesn't take into account the structural features and which direction should the pillar length be larger relative to discontinuity such that the pillar strength increases.

5.2. Model Configuration for this Study

FLAC^{3D} (Itasca, 2016), a finite difference geotechnical software, was used to investigate the strength of the pillars in the presence of the discontinuity as it has a capability to model the realistic failure process of hard rock pillars (Esterhuizen, 2006). The coordinate system in the horizontal plane is represented by x- and y-directions and the z-axis as the vertical plane as shown in the Figure 5.3. The model consists of the main roof, main floor and pillar with width (W) and height (H). The height of the pillar and the extraction ratio of 75% were kept constant while the pillar and the entry width were varied to simulate different width-to-height ratios.

5.2.1. Boundary and Loading Conditions:

The bottom of the floor was fixed such that the displacements and the velocities are restricted in the normal and parallel directions. The roller boundaries were incorporated in the x- and y-plane such that the displacements and the velocities are restricted in the normal direction. The simulation of the pillar under compression was carried out by subjecting the top of the main roof to the applied velocity.

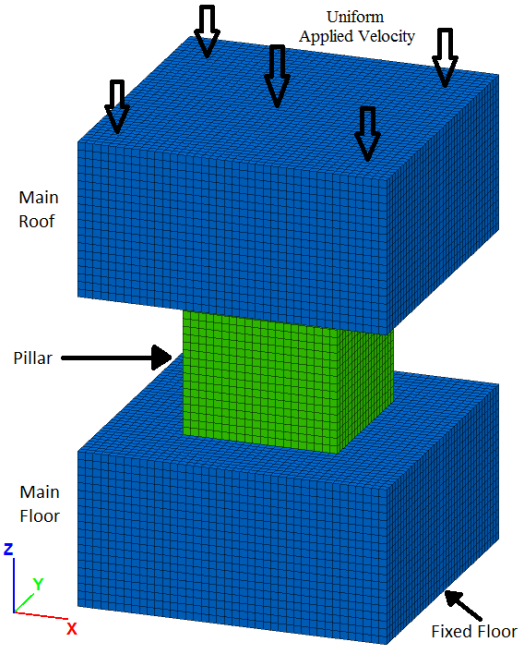

Figure 5.3: FLAC^{3D} pillar model.

The model was subjected to a vertical stress of 2.7MPa which simulates a mine of depth 100m with vertical to horizontal stress ratio of 1:1 and was run to equilibrium under the elastic conditions. After reaching equilibrium, the pillar material was then transformed from elastic to the subiquitious (bilinear). This shows that the rock mass behaves as elastic before excavation and after the excavation, the rock mass obtains the properties of brittle and plastic deformation. The model was then subjected to increasing vertical load until the pillar had completely failed and reached the residual strength of about half the peak strength (Esterhuizen, 2006). A FISH function was generated to observe the stress-strain curve from which the average stress at failure could be observed. FISH is a language used within FLAC^{3D} mainly to implement user defined functions and variables beyond the traditional code in FLAC^{3D}.

5.2.2. Model Properties

Brittle rock failure has evolved into an important and better understood phenomena in rock mechanics. As the stress state in the pillar reaches of about 0.3 to 0.5 times the uniaxial compressive strength, brittle cracks develop parallel to the major principal stress. It was necessary to simulate this phenomena before the shear failure of the rocks. Therefore, bilinear strength envelope was used in which the strength is independent of friction and is equal to 0.3 to 0.5 times the uniaxial compressive strength at low confinement then followed by friction hardening at higher confinement (Kaiser et al., 2000).

The subiquitious model, FLAC^{3D} code is capable of simulating the bilinear rock strength based on the Mohr-Coulomb strength criterion and strain softening as a function of the deviatoric plastic strain (Itasca, 2005). The properties for the model with rock mass having Rock Mass Rating (RMR) of 70 were taken from Dolinar and Esterhuizen (2007) and are shown in the Tables 5.1 and 5.2 (Esterhuizen, 2006). This model can also incorporate the joints in the model which is used to evaluate the strength of the pillar in the presence of the discontinuities.

Table 5.1: Model Properties (Dolinar and Esterhuizen, 2007)

Rock Mass Properties	Numerical Value
Bulk Modulus	40,000 MPa
Shear Modulus	24,000 MPa
Intact Rock Strength (UCS)	150 MPa
Cohesion (Brittle)	25 MPa
Friction (Brittle)	0°
Cohesion (Mohr-Coulomb)	8.1 MPa
Friction (Mohr-Coulomb)	47.6°
Tension	2.7 MPa
Dilation	30 °

Table 5.2. Joint Properties (Dolinar and Esterhuizen, 2007)

Joint Properties	Numerical Value
Joint Cohesion	1 MPa
Joint Friction	42°
Joint Tension	0.4 MPa
Joint Dilation	0°

The model element size affects the strain-softening parameters which should be determined by calibrating the numerical results to that of the theoretical results (Itasca, 2005). All the models were run using identical element sizes. The element size of 0.25 m * 0.25 m * 0.25 m was generated throughout the model and the cohesion softening was carried out to calibrate the results to that of the Lunder and Pakalnis (1997).

5.2.3. Model Calibration

Intact rock pillar models with width-to-height ratios of 0.5, 0.8, 1.0, 1.2 and 1.5 (most commonly found W/H ratio in hard rock mines) were generated to validate the numerical models to that of the theoretical results of Lunder and Pakalnis (1997) as shown in the Figure 5.4.

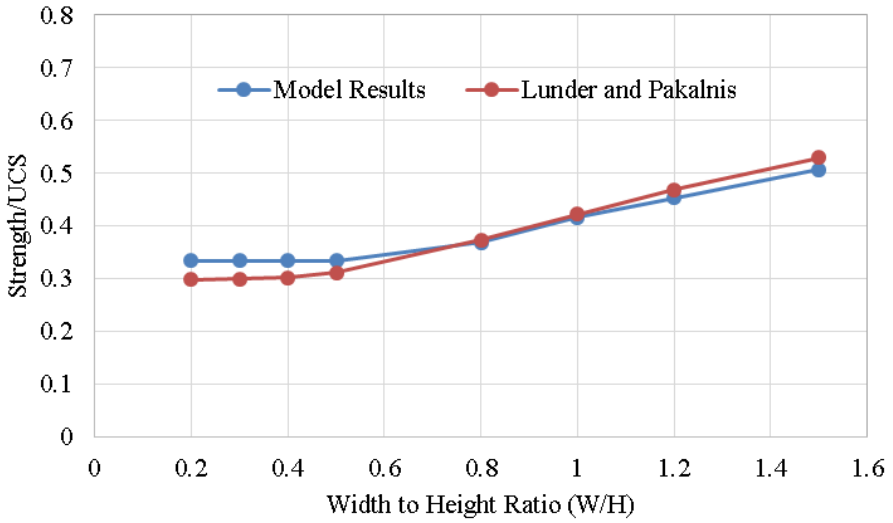

Figure 5.4: The numerical models calibrated to that of the theoretical results of intact rock pillars.

The discontinuities dipping at 50°, 60° and 70° with dip direction parallel to pillar face (i.e. Strike = 0°) and intersects the center of the pillar were introduced in the model and simulated with varying width-to-height ratios which is similar to Esterhuizen's results (2006) as shown in the Figure 5.5.

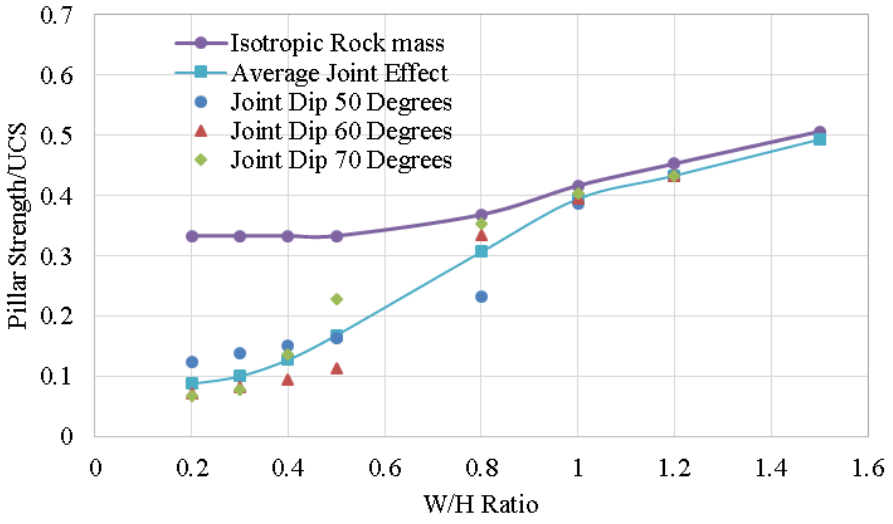

Figure 5.5: Results of the numerical models showing the effect of discontinuities dipping at 50, 60 and 70 degrees to the pillar face

Figure 5.5 also shows that the at higher W/H ratios the discontinuity dip angle has less effect on the strength of the pillars. At W/H ratio of about 1, the strength of the pillar increases with increasing discontinuity dip angle such as 70° > 60° > 50°. The strength changes to 70° > 50° > 60° dip angle in the range of W/H ratio of 0.5 to 0.8 and again changes to 50° > 70° > 60° at W/H ratio of 0.4. Finally, below W/H ratio of 0.4, the strength of the pillar decreases with increasing discontinuity dip angle i.e. 50° > 60° > 70°. This shows that the shearing along the discontinuity is the prominent failure to significantly lower the strength of the pillar.

A key parameter is that while simulating continuum models is that the pillar strength is not affected by discontinuity dip angle when oriented at angles less than the joint friction angle or at angles near perpendicular to the pillar (Jaeger and Cook, 1979). Therefore, in the results at the higher angles (i.e. higher than 80°) and at very low angles (i.e. lower than 30°) will be near equal to that of the intact pillar strength which is independent of the discontinuities.

5.3. Results and Discussions

5.3.1. Evaluating the effect of Dip Direction/ Strike:

The effect of discontinuity strike non-parallel to the pillar edges was evaluated by simulating two different dip directions i.e. 0° and 45° (Figure 5.2) at varying width-to-height ratios and varying dip angles and the results are shown in the Figure 5.6. At W/H ratio of 0.5, the dip direction has little effect on the strength of the pillar. At W/H ratios above 0.5, when the encountered discontinuity dip angles are below 45°, the pillar strength is higher when the discontinuity is oriented at 45° to the pillar face. While when the encountered discontinuity dip angles are high, the orientation of the discontinuity parallel to the pillar face lead to higher pillar strength. Therefore, it can be concluded that the dip direction can have a significant effect on the strength of the pillars.

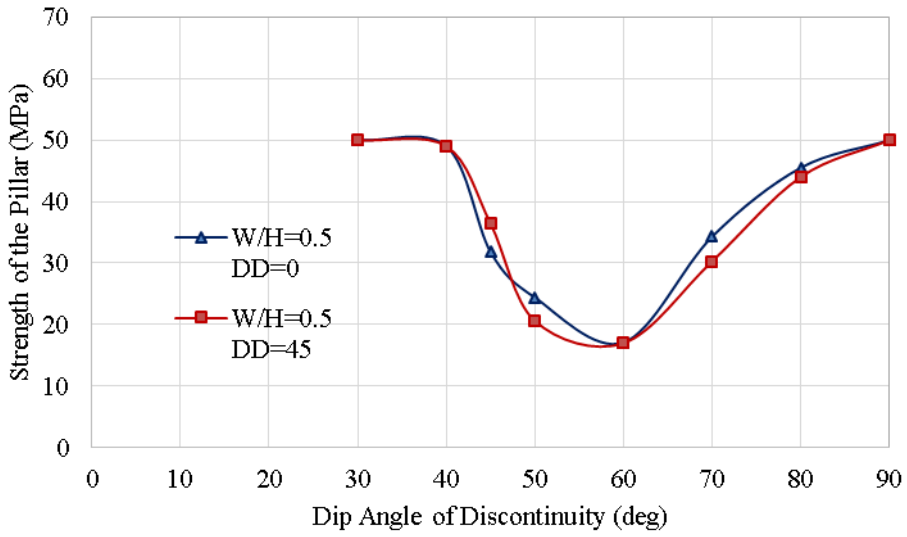
Strength of the Pillar (MPa)
Dip Angle of Discontinuity (deg)
W/H=0.5
DD=0
W/H=0.5
DD=45
0
10
20
30
40
50
60
70
80
90

a)

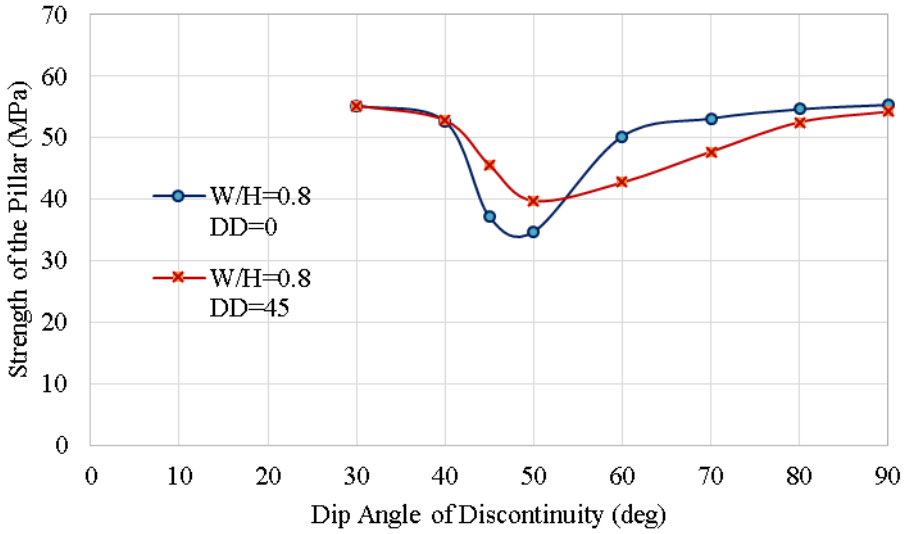
Strength of the Pillar (MPa)
Dip Angle of Discontinuity (deg)
W/H=0.8
DD=0
W/H=0.8
DD=45
0
10
20
30
40
50
60
70
80
90

b)

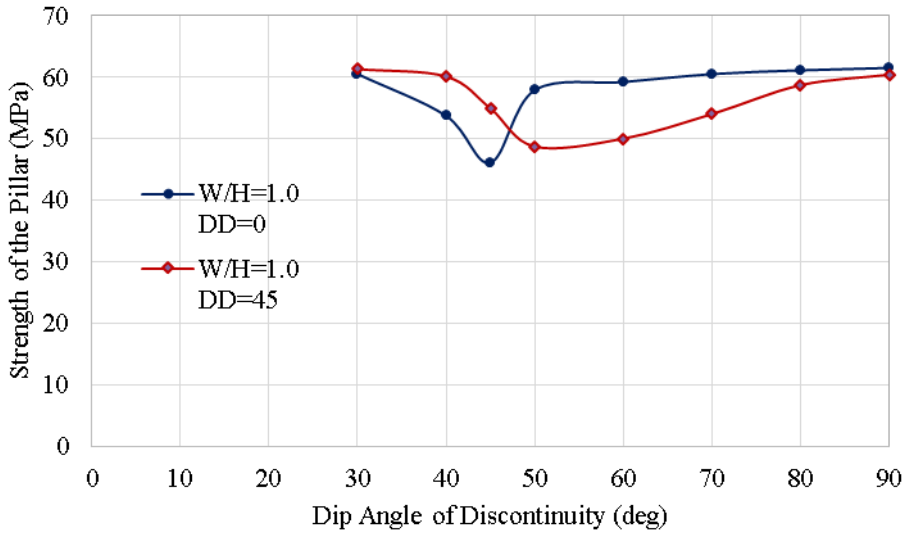

c)

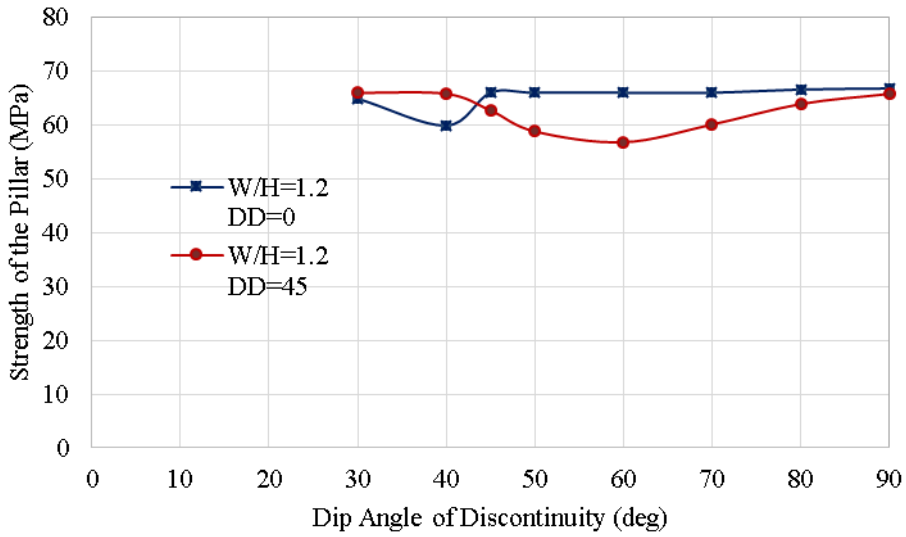

d)

Figure 5.6: Effect of the strike of the discontinuity at a) W/H ratio of 0.5 b) W/H ratio of 0.8 c) W/H ratio of 1.0 d) W/H ratio of 1.2 (Note: DD = Dip Direction (Strike))

Figure 5.7 was developed showing the effects of dip angle on the W/H ratio of the pillars with strike as 0° and 45°. In Figure 5.7a, at strike of 0°, the most critical discontinuity dip angle continues to decrease the strength as the W/H ratio increases. In Figure 5.7b, at strike of 45°, the most critical discontinuity dip angle falls in the range of 50°-60° for all

W/H ratios considered. It can be thus concluded that when the pillars are designed at the strike angle of 45°, a common strength adjustment factor for all dip angles can be developed to determine the strength of the hard rock pillars.

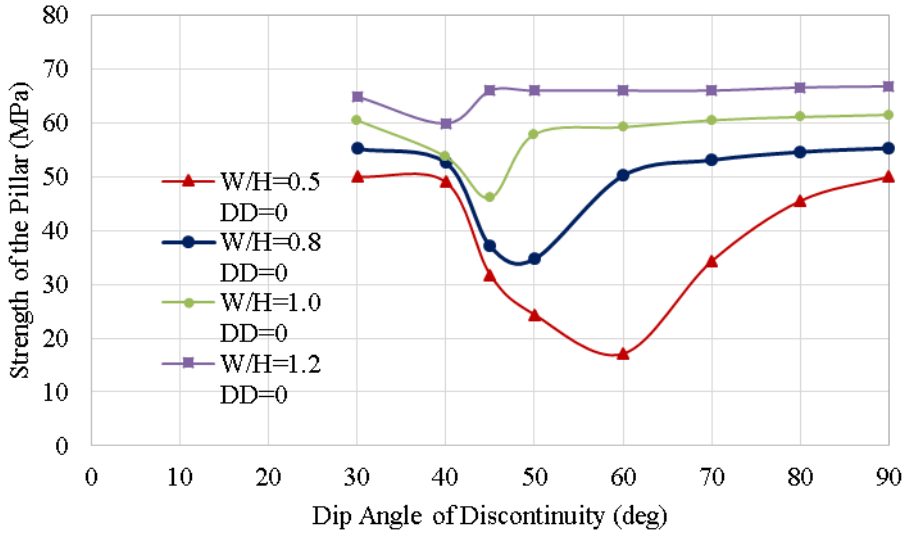

a)

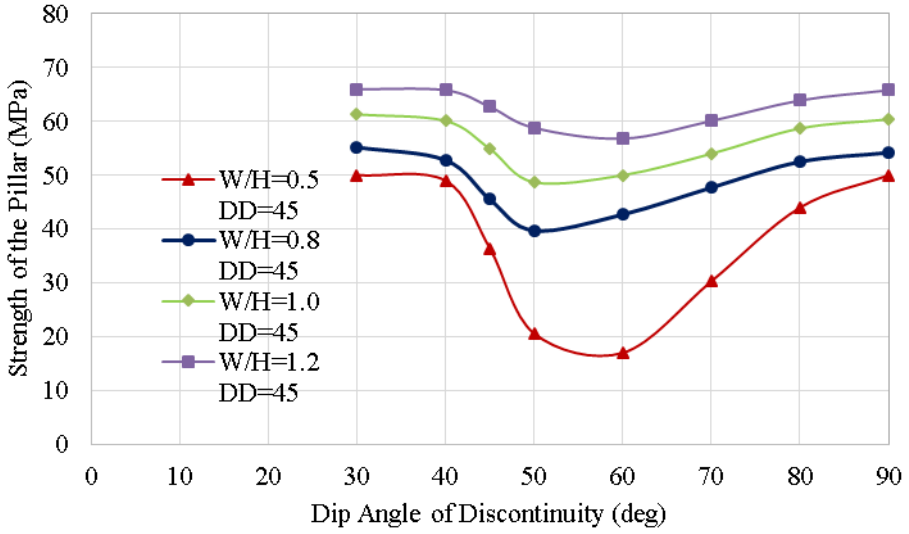

b)

Figure 5.7: Effect of discontinuities on pillar strength for a) strike = 0° b) strike = 45° (Note: DD = Dip Direction (Strike))

5.3.2. Rectangular Pillars:

The rectangular pillars were simulated to investigate the influence of dip direction of the discontinuity. For rectangular pillars, half of the pillar width was added to both the sides of the pillar as shown in the Figure 5.8 such that the discontinuity passes through the center of the pillar. The pillar length to width (L/W) ratio was kept as 2. The lowest strength obtained with the discontinuity dip angle was taken in the rectangle pillars at that W/H ratio i.e. 60° dip angle was used with W/H ratio of 0.5, 50° dip angle was used with W/H ratio of 0.8 and 45° dip angle with W/H ratio of 1.0. The dip directions of the discontinuity were varied from 0°, 22.5°, 45°, 67.5°, and 90° as shown in the Figure 5.9.

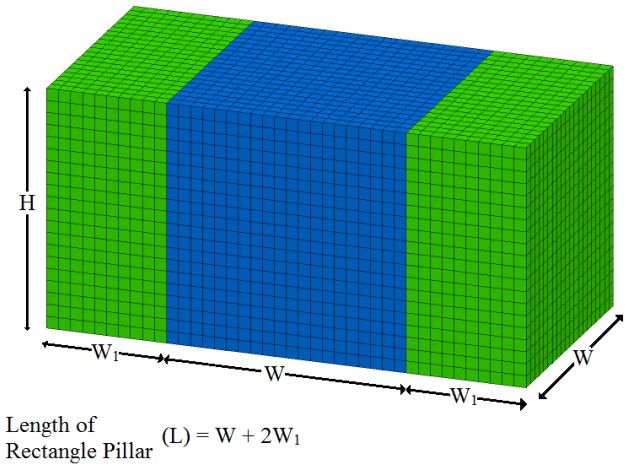

Figure 5.8: Formation of the rectangular pillar with L/W ratio of 2

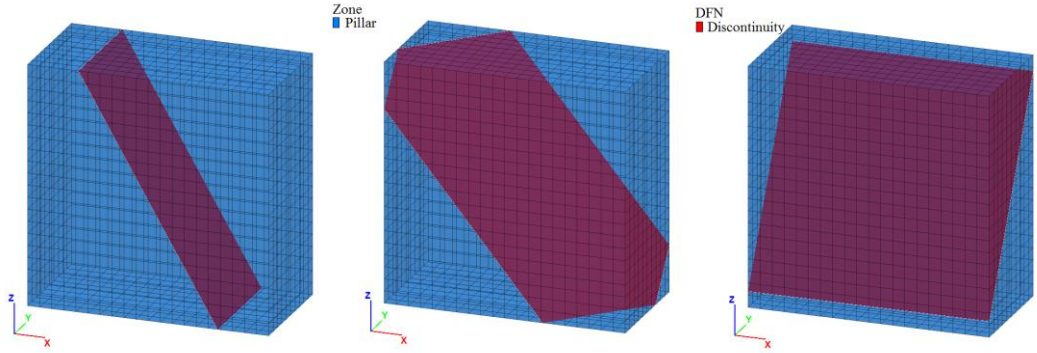

a) b) c)

Figure 5.9: Rectangular pillar with discontinuity dip angle 60° and dip direction of a) 0° b) 45° c) 90°

Figure 5.10 shows the effect of dip direction on the rectangular pillars. It can be concluded that the pillar strength is significantly lower when the discontinuity is parallel to the short axis of the pillar as shown in Figure 5.10c. It can be seen that the effect of the discontinuity on pillar strength is limited at dip directions from 0° to 45°. As the discontinuity dip direction is increased above 45° its effect increases significantly. It can also be seen that the effect of the discontinuity decreases as the W/H ratio increases.

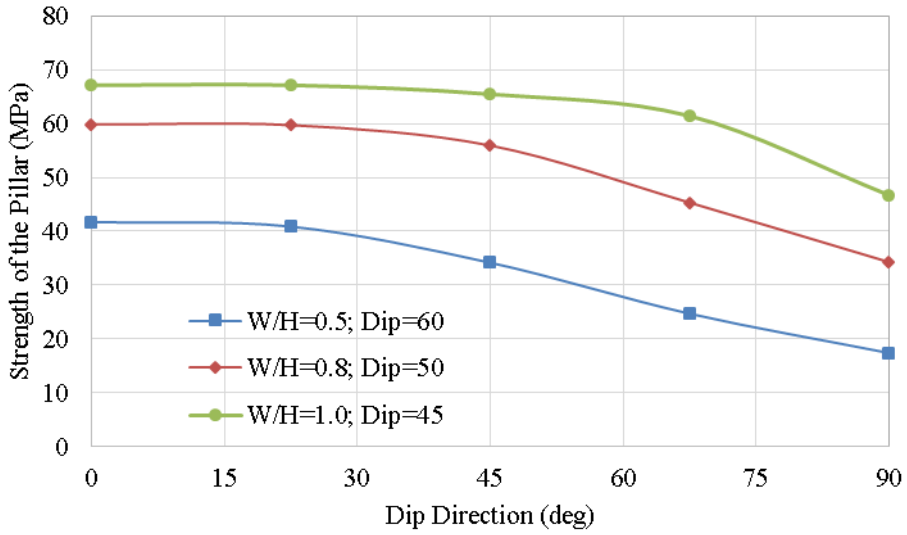

Figure 5.10: Effect of dip direction on the rectangular pillars with varying W/H ratios

5.4. Conclusions:

The effect of discontinuity dip direction has been simulated in square and rectangular hard rock pillars and the following conclusions can be made:

- If discontinuity dip angles below 45° are encountered, the advance of the excavation can be adjusted in a way such that the discontinuity dip direction is 45° to the pillar face. This will result in improved pillar strength compared to having the discontinuity parallel to the pillar faces. Conversely, the study shows that for steeper dip angles, the pillar strength may be compromised when the pillar faces are aligned at 45° to the discontinuity dip direction.

- The Discontinuity Dip factor (DDF) determined by Esterhuizen (2006) is based on discontinuities with dip directions that are parallel to the pillar faces. The results of this study can be used to modify the DDF for a dip direction of 45° relative to the pillar faces.
- The stability of rectangular pillars in the presence of discontinuities can be improved by aligning the long axis of the pillars at 0°-45° with the discontinuity dip direction.

This work demonstrates that further research through numerical modeling and field verification is needed to better quantify the strength of the pillars in the presence of discontinuities with different dip directions. The studies should include an assessment of the difference in strength of the pillars with increasing frequency of the discontinuities.

References:

Dolinar, D. R. and Esterhuizen, G. S. (2007). Evaluation of the effects of length on strength of slender pillars in limestone mines using numerical modeling. Proceedings of the 26th International Conference on Ground Control in Mining. Morgantown, WV: West Virginia University, pp. 304–313.

Esterhuizen, G. S. (1998). Effect of structural discontinuities on coal pillar strength as a basis for improving safety in the design of coal pillar systems. Safety in Mines Research Advisory Committee, COL 005a, December 1998, pp 1-104

Esterhuizen, G. S. (2006). An evaluation of the strength of slender pillars. Transactions of Society for Mining, Metallurgy, and Exploration, Inc. Vol. 320. Littleton, CO: Society for Mining, Metallurgy, and Exploration, Inc., pp. 69–76.

Esterhuizen, G. S. and Dolinar, D. R. and Ellenberger, J. L. (2008). Pillar strength and design methodology for stone mines. Proceedings of the 27th International Conference on Ground Control in Mining. Morgantown, WV: West Virginia University, pp. 241–253.

Galvin, J. M., Hebblewhite, B. K. and Salamon M. D. G. (1999). University of New South Wales coal pillar strength determinations for Australian and South African mining

conditions. Proceedings of the Second International Workshop on Coal Pillar Mechanics and Design. Pittsburgh, PA: U.S. Publication No. 99-114, IC 9448, pp. 63– 71.

Itasca Consulting Group, (2016). Fast Lagrangian Analysis of Continua in 3Dimensions, Minneapolis, Minnesota, USA.

Itasca, (2005). FLAC 3D, Fast Lagrangian Analysis of Continua, User's Manual Version 2.1, Itasca Consulting Group, Minneapolis, Minnesota.

Iannacchione, A. T. (1999). Analysis of Pillar Design Practices and Techniques for U.S. Limestone Mines, Transactions of the Institution of Mining and Metallurgy (sect. A: Mining Industry), 108, September-December pp. A152-A160.

Jaeger, J. C. and Cook N. G. W. (1979). Fundamentals of Rock Mechanics, 3rd Ed. NewYork: Chapman and Hall.

Kaiser, P. K., Diederichs, M. S., Martin, D. C. and Steiner, W. (2000). Underground works in hard rock tunneling and mining," Keynote lecture, *Geoeng2000*, Melbourne, Australia, Technomic Publishing Co., pp. 841-926.

Lunder, P. J. and Pakalnis, R. (1997). Determining the Strength of Hard Rock Mine Pillars, Bulletin of Canadian Institute of Mining and Metallurgy, V.90, pp. 51-55.

Madden, B. J., Canbulat, I., Jack, B. W. and Prohaska, G. D. (1995). A reassessment of Coal Pillar Design Procedures. Safety in Mines Research Advisory Committee, COL 021, December 1995, pp 1-148

Mark, C. and Chase, F. E. (1997). Analysis of retreat mining pillar stability (ARMPS). Paper presented at the seminar on new technology for ground control in retreat mining, Pittsburgh, US Bureau of Mines. Pp. 17-34

Wagner, H. (1974). Determination of the Complete Load-Deformation Characteristics of Coal Pillars, Proceedings of 3rd Congress of International Society of Rock Mechanics, Denver, CO, VII, Part B, pp. 1067-1081.

Every reasonable effort has been made to acknowledge the owners of copyright material. I would be pleased to hear from any copyright owner who has been omitted or incorrectly acknowledged.

Chapter 6

Performance of Inclined Pillars with a Major Discontinuity

This chapter has been published in SME Transactions as:

Jessu, K.V., Spearing, A.J.S. (2019) Performance of Inclined Pillar with a major discontinuity. *International Journal of Mining Science and Technology*. Vol. 29(3), pp. 437-443

Abstract

Discontinuities are an inherent part of the rock mass and mainly affect the stability of the excavation skin and pillars. The dip of the discontinuities and their properties also have a significant effect on the strength of the pillars. Empirical approaches are commonly used to determine the pillar strength but can overestimate the strength and don't consider the inclination of the pillars and the strength reduction caused by discontinuities. Numerical modeling is a powerful tool and if calibrated can be used to evaluate the strength of the pillars with discontinuities having a range of properties. The effect of a discontinuity on inclined pillars was conducted which has been seldom considered in evaluating the pillar strength. Three-dimensional vertical pillars were simulated, and the pillar strength was calibrated to accepted theoretical results and then the discontinuities were introduced in different pillar inclinations with distinct width to height ratios to gain an insight into the effective pillar strength reduction. Based upon the results, it was found that the discontinuities have a significant effect with the increase in the inclination of the pillars even at a higher width to height ratios.

6.1. Introduction

Pillars are frequently left in the underground mines to stabilize the relatively large openings. It is necessary to efficiently design the pillars. Under-designed pillars can lead to abrupt failure and can lead to catastrophic pillar failure such as in a room and pillar metal mine, failure of four pillars at the center of the section resulted in a failure of almost 100 pillars (Dismuke et al., 1994; Zipf, 2001). Over-designed pillars can lead to an economic loss due to the excess ore left in the mines. The design of the pillars is also dependent on the properties of the ore deposit and surrounding rockmass and the adopted mining method to extract the ore. The flat or shallow dipping ore deposits are generally extracted by employing the room and pillar mining method where the pillars act as the primary roof support in the excavations and often barrier pillars are used as the regional support for the panels. If the ore bodies are steeply dipping, the rib pillars are used as the primary support in the stopes while the sill pillars are used to distinguish the two mining

horizons. The crown pillars are the pillars left behind to establish the stability of the mine to the surface. This study deals with the pillars which are used as the primary support.

Depending on the orientation of the ore body, the pillars left in the vertical direction will lead to compression loading and the pillars in the inclined direction will undergo combined compression as well as shear loading as shown in Figure 6.1. The loading on the pillars lead to brittle failure in slender pillars and in larger pillars can lead to spalling and shear failure which is the common pillar failure mechanism. Other pillar failure mechanisms include axial splitting (Brady and Brown, 2007; Fakhimi and Hemami, 2015; Fakhimi et al., 2016) and in the presence of the discontinuities, sliding along the shear plane (Brady and Brown, 2007).

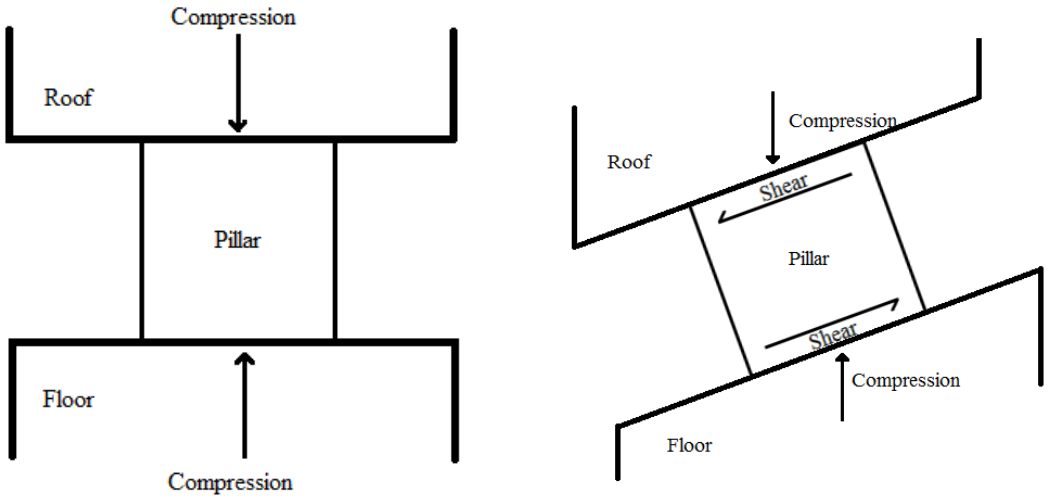

a) b)

Figure 6.1: a) Vertical pillars undergoing compression b) Inclined pillars undergoing oblique loading

Empirical approaches are mainly relevant on vertical pillars and one of the earliest studies was conducted by Hedley and Grant (1972) on the Quartzite pillars in Canada by classifying them into stable, unstable and failed categories and derived a relationship between the pillar strength, and width-to-height ratio. Lunder and Pakalnis (1997) introduced the confinement parameter in developing the strength of hard rock pillars and

it is the most commonly used empirical approach in the underground mines. The design of the pillars is given as:

$$\sigma_p = K * UCS * (C1 + C2 * \kappa) \tag{6.1}$$

Where σ_p is the ultimate strength of the pillar (MPa), K is the pillar size factor given as 0.44, UCS is the uniaxial compressive strength of the intact rock (MPa), C1 and C2 are the empirical rock mass constants given as 0.68 and 0.52 respectively and κ is the friction term which is calculated as:

$$\kappa = \tan\left[cos^{-1}\left(\frac{1 - C_{pav}}{1 + C_{pav}}\right)\right] \tag{6.2}$$

$$C_{pav} = Coeff * \left[Log\left(\frac{W}{H} + 0.75\right)\right]^{1.4(W/H)} \tag{6.3}$$

Where C_{pav}, the average pillar confinement and the Coeff is the coefficient of pillar confinement.

Research conducted on the inclined pillars concluded that the pillars dipping at angle undergo oblique loading which is a combination of compressive and shear stress and therefore have lower strength when compared to the vertical pillars (Martin and Maybee, 2000; Suorineni et al, 2014). However, the empirical designs are only developed based on stable and failed pillars without taking into consideration the failure behavior of the pillars and the effect of discontinuities in the pillars.

Rock mass consists of fractures and discontinuities that affect the stability of the excavations especially when significant discontinuities traverse the pillars. Discontinuities are discrete plane structures in the rock mass which may or may not lead to slippage along the plane as shown in Figure 6.2a. Jaeger and Cook (1994) evaluated that the strength of the rock sample reduces significantly in the presence of the discontinuities with respect to its orientation to the stress direction as shown in Figure 6.2b. Similar behavior has been observed in the pillars in the presence of the discontinuities such that the strength of the

pillar is significantly influenced by the orientation of the discontinuity and the size of the pillar (Esterhuizen, 2006).

One of the earliest studies on the influence of the discontinuities has been conducted in the South African Coal fields by estimating the failure of the pillars and classifying the pillars by pillar condition rating system (Madden, 1995). It was simply based on the visual inspections and scaling of the fractures and limited to the coal pillars in the South African Coal mines database. Iannacchoine (1999) conducted studies on determining the dip of the discontinuities effecting the pillars strength and derived that the pillar strength is significantly affected at 60° discontinuity dip angle. Esterhuizen (1998 and 2006) conducted numerical modelling studies on vertical pillars with discontinuities and developed a relationship between the strength of the pillars, discontinuity dip direction and size of the pillars in the coal and limestone mines. It was concluded that the smaller pillars are highly affected by the discontinuities and derived strength for every 10° angle of discontinuity.

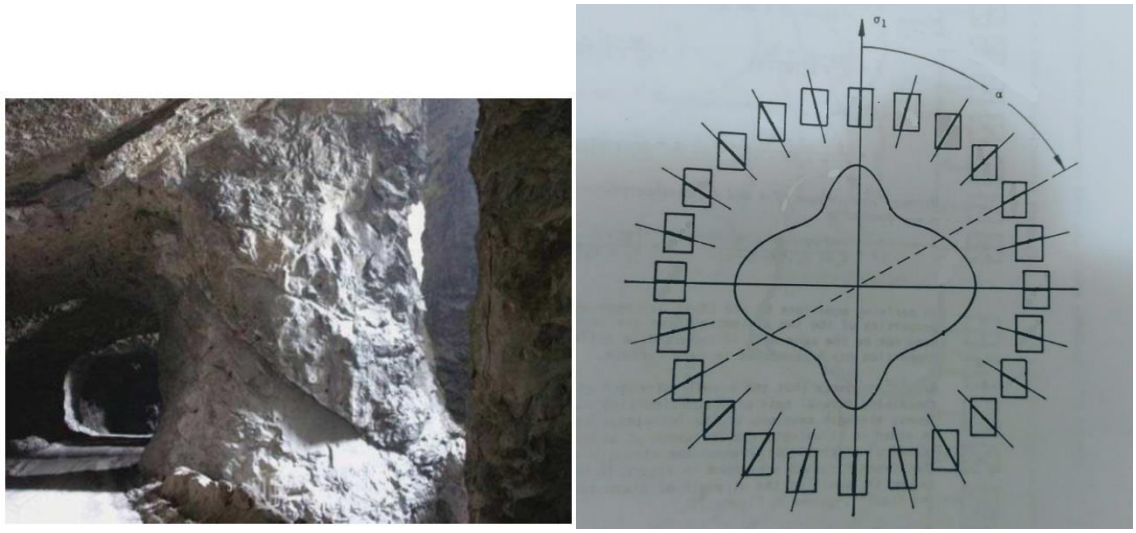

a) b)

Figure 6.2: a) Example of discontinuity in a pillar (Esterhuizen, 2006) b) Sample strength along the discontinuity dip angle (Jaeger and Cook, 1994)

This chapter will present the numerical analysis of inclined pillars with discontinuities. The inclined pillars with varying width to height ratios will be investigated against different orientations of the discontinuities to develop an understanding of the pillar strength reduction.

6.2. Model Configuration:

Numerical modeling is a very powerful tool due to its ability to model complex geometries and incorporate varied material behavior to provide a valuable insight into the failure modes of the pillars if calibrated correctly. FLAC^{3D} (Itasca, 2018), a three-dimensional finite difference numerical modeling package was used to simulate the vertical pillars and inclined pillars and to analyze the pillar strength reduction in the presence of the discontinuities. This package was selected as it has the capability to realistically simulate the failure process of the pillars (Esterhuizen, 2006). Vertical pillars and inclined pillars were simulated as shown in Figure 6.3.

The x, y, and z coordinate space was used to simulate the pillars in the model. The horizontal plane is represented in the x and y-direction while the vertical plane is presented in z-direction. The inclination of the pillars is towards the x-direction as shown in Figure 6.3b. The model consists of main floor, pillar and main roof with height being constant in all the three sections. The height of the pillar was 4m which was adopted from the Lunder and Pakalnis (1997) database. The pillar width in x and y-direction is varied to achieve different width to height ratios in the model. The extraction ratio of the vertical pillars is kept constant at 75 % and for the inclined pillars, the boundaries were established far enough from the pillar when compared to vertical pillars to avoid its influence on the pillar failure behavior. The height of the roof and floor have been kept three times that of the pillar height to avoid boundary effects on the pillars.

Boundary conditions were established by placing fixed supports at the bottom of the floor with which the displacement and velocity are restricted in normal and parallel directions. Roller supports were introduced on the sides to restrict the displacement and velocities in the normal direction. Models were subjected to uniform velocity on the top of the roof to

simulate the loading as recommended by Lorig and Cabrera (2013) with which vertical pillars undergo compression and the inclined pillars undergo oblique loading.

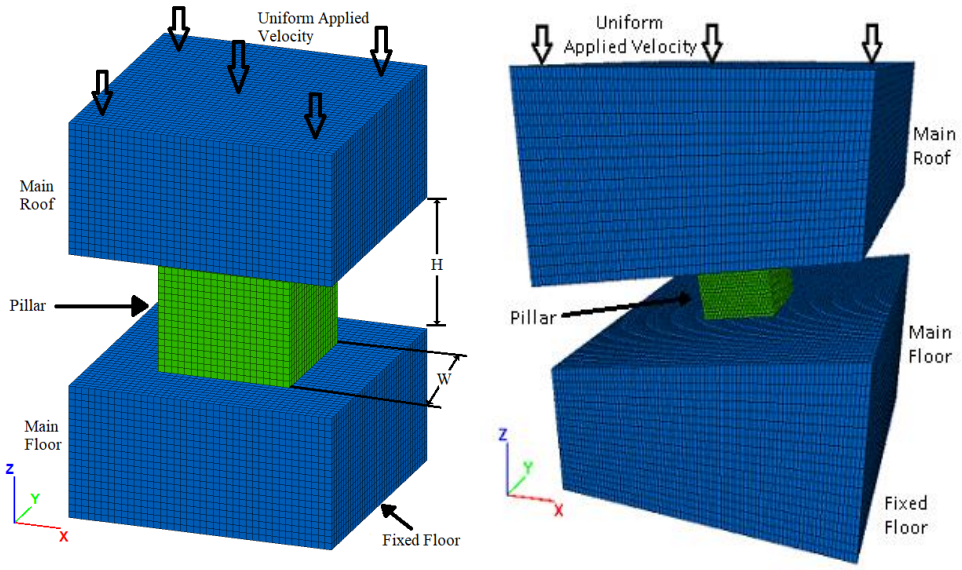

Figure 3: Numerical Models a) Vertical Pillar b) 10° Angled Pillar

Stresses were applied to the models to simulate 100m mining depth with horizontal to vertical stress of about 1:1 and the models were run to equilibrium under elastic conditions. The material properties of the pillar were transformed to bilinear material from the elastic condition after reaching the equilibrium. This was undertaken to reproduce the rock mass behavior before the excavation as elastic; and after the excavation as brittle and plastic. Then the uniform velocity was applied to the model until the pillar had completely failed and reached the residual strength equal to 50% of the peak strength. FISH code, an inbuilt language to implement user-defined functions and variables, was used to develop stress-strain relationship to determine the peak strength of the pillar. The roof and the floor rock mass were modelled using an elastic criterion which is stronger than the pillar to ensure that the failure is induced in the pillar.

The most important part of the numerical modeling is the constitutive model and the input properties to ensure the simulation produces realistic results. Pillars are best simulated by

implementing brittle Hoek-Brown criterion (Martin et al., 1999; Kaiser et al., 2000; Esterhuizen et al, 2006). This criterion basically refers to the brittle nature of the pillars at 0.3 to 0.5 times of the uniaxial compressive strength which develops brittle cracks in the pillars followed by the shear failure. Therefore, a bilinear strength envelope was introduced in which the strength is equated to one-third of the uniaxial compressive strength and independent of the friction at low confinement subsequently followed by friction hardening at the higher confinement (Kaiser et al., 2000).

A constitutive model best representing the bilinear strength envelope can be simulated by bilinear strain hardening/ softening ubiquitous joint model which is based on the Mohr Coulomb strength criterion and strain hardening/ softening as a function of the deviatoric plastic strain (Itasca, 2018). The input properties for the model are as shown in Tables 6.1 and 6.2 (Dolinar and Esterhuizen, 2007). The discontinuities in the pillar (Figure 6.4) were introduced in the form of Discrete Fracture Network (DFN) with the properties as shown in Table 6.2.

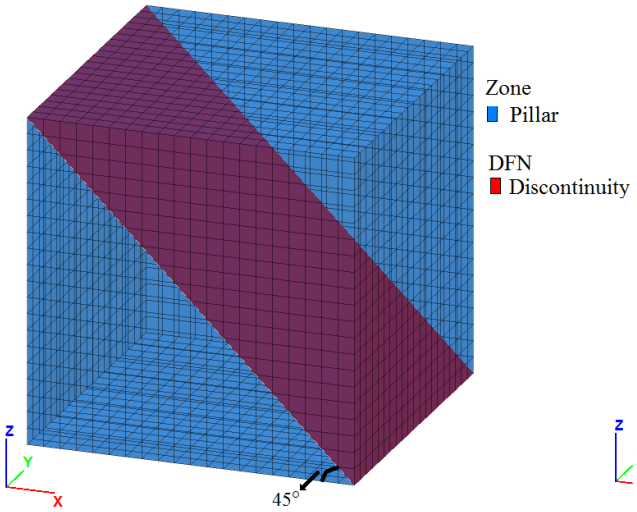

Figure 6.4: Discontinuity in the pillar

Table 6.1: Model Properties (Dolinar and Esterhuizen, 2007)

Rock Mass Properties	Numerical Value
Bulk Modulus	40,000 MPa
Shear Modulus	24,000 MPa
Intact Rock Strength (UCS)	150 MPa
Cohesion (Brittle)	25 MPa
Friction (Brittle)	0°
Cohesion (Mohr-Coulomb)	8.1 MPa
Friction (Mohr-Coulomb)	47.6°
Tensile strength	2.7 MPa
Dilation angle	30 °

Table 6.2. Joint Properties (Dolinar and Esterhuizen, 2007)

Joint Properties	Numerical Value
Joint Cohesion	1 MPa
Joint Friction	42°
Joint Tension	0.4 MPa
Joint Dilation	0°

The model element size is a critical parameter for the strain softening properties which can be determined by simulating all the models with same element size and calibrating the numerical model to the theoretical results (Itasca, 2018). All the models were run at same element size of 0.5m*0.5m*0.5m throughout the model and the cohesion softening was carried out to calibrate the vertical pillar results to that of the Lunder and Pakalnis (1997).

6.2.1. Model Calibration:

6.2.1.1.Numerical model Validation:

The model was simulated with four different width to height (W/H) ratios of 0.5, 1.0, 1.5 and 2.0 to calibrate numerical model results to that of the theoretical results of Lunder and Pakalnis (1997) as shown in Figure 6.5. The results obtained from the numerical models are similar to that of the theoretical results.

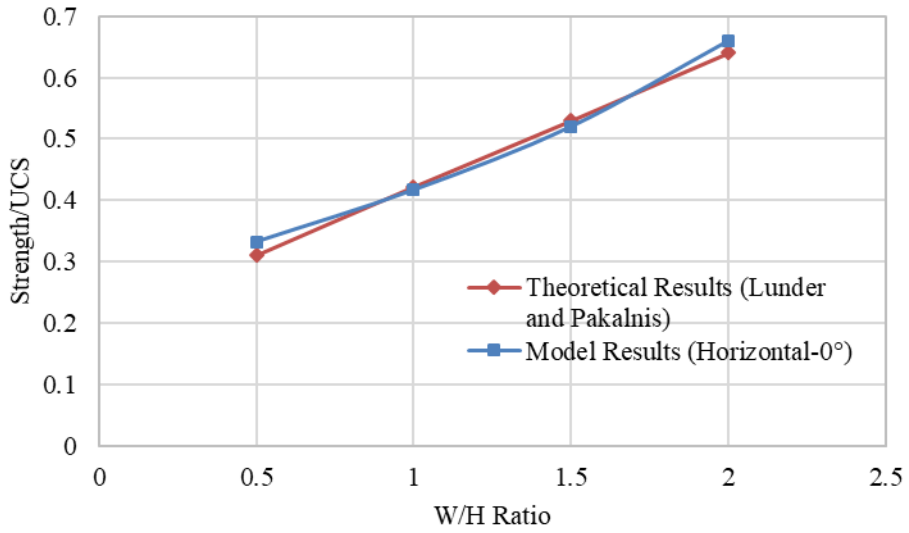

Figure 6.5: Validation plot of numerical models to that of the theoretical results

6.2.1.2.Inclined pillar strength validation:

The inclined pillars were simulated next with different inclinations from the horizontal of 0°, 10°, 20°, 30° and 40°. These simulations were carried out with different width to height ratios of 0.5, 1.0, 1.5 and 2.0 and the results are shown in Figure 6.6. These results are similar to that of the results presented by Suroineni et al., (2014) and Ma et al., (2016).

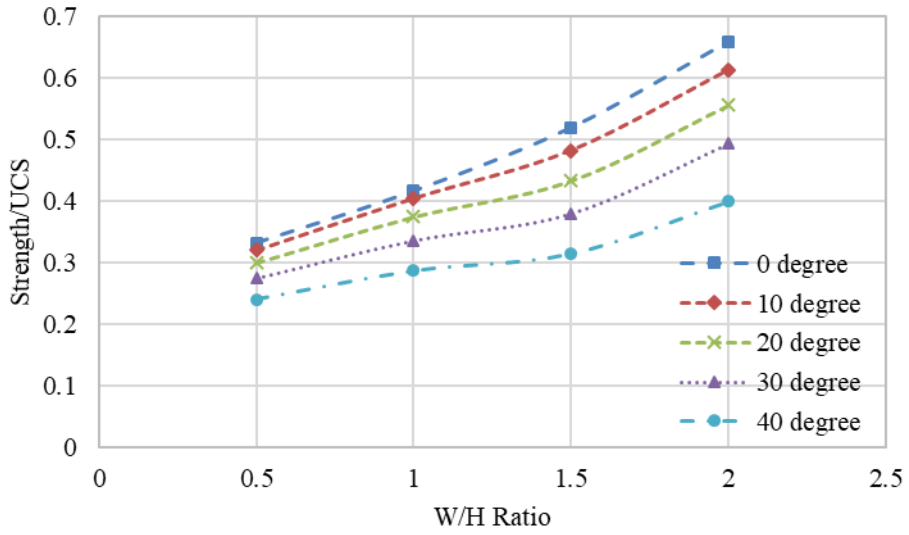

Figure 6.6: Strength variation of the inclined pillars at a varied width to height ratios

Figure 6.6 shows that the pillar strength decreases with the increase in the inclination of the pillars at any width to height ratio. It was also observed that at lower W/H ratio, there is only slight decrease in the strength of the pillars while at higher W/H ratio, there is a drastic reduction in the pillar strength at higher inclinations when compared to the pillar under pure compression. For example, at W/H ratio of 2.0, the strength of the 40° inclined pillar is 43% less than the vertical pillar. It is because the pillars in vertical direction undergo brittle failure in pillars with W/H ratio of 0.5 and the transition from the brittle to shear failure occurs in between the pillars with W/H ratio of 0.5 to 1.0. While in the inclined pillars, the brittle to shear transition occurs in pillars with higher W/H ratios as the inclination increases. The brittle failure is the dominant failure mechanism with the increase in the inclination of the pillars, and thus cause the reduction in the strength of the inclined pillars (Jessu and Spearing, 2018).

6.2.1.3.Validation of Discontinuity effects on Vertical Pillars:

To evaluate the strength of the vertical pillars with a major discontinuity, a single large DFN was included in the pillars passing through the center of the pillar extending to the sides of the pillar. The discontinuity dip angle was kept parallel to the pillar face (i.e. Strike = 0°) as shown in Figure 6.4. The models were simulated at every 10° inclination increase of the discontinuity from 0° to 90° inclination at W/H ratios of 0.5, 1.0, 1.5 and 2.0. Therefore, in total 36 models were simulated to understand the effect of discontinuity on the strength of the pillars. The results are shown in Figure 6.7 in which the graph is shown in the form of polar co-ordinates (r, θ) where r is represented as the pillar strength and the θ is the angle of inclination of the discontinuity. Figure 6.7 also shows the results beyond 90° discontinuity inclination which are represented as the mirror image of the results from the first quadrant. For example, the discontinuity dip angle of 45° would bear the same strength as the discontinuity dip angle of 135° as they are both intersecting the pillar at 45°. Therefore, the second, third and fourth quadrants are the mirror images of the first quadrant.

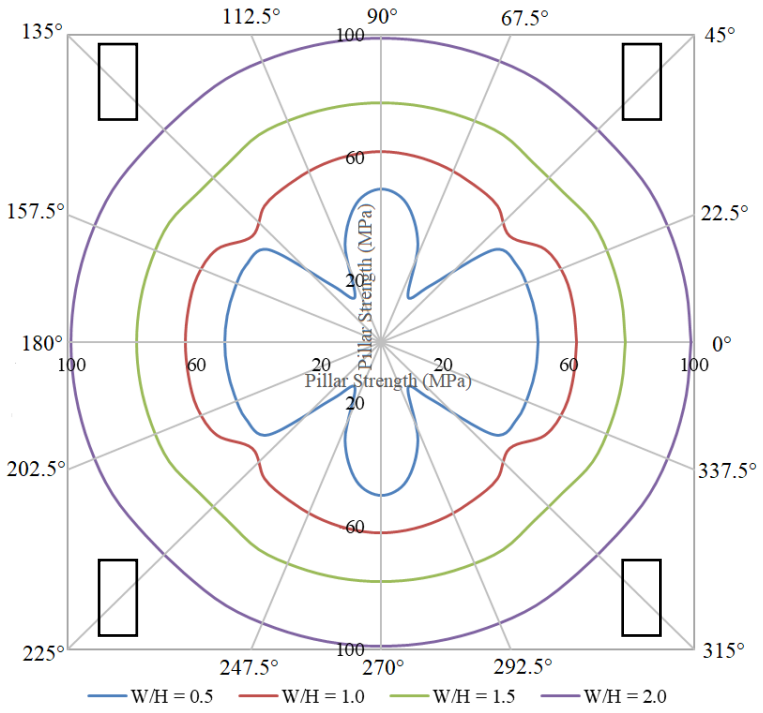

Figure 6.7: Effect of discontinuity dip angle on strength of vertical pillars

It is observed from Figure 6.7 that in pillars with W/H ratio of 0.5, the discontinuity dip angle of 60° results in significant reduction of the pillar strength which resembles the results from Esterhuizen (2006). It can also be observed that at higher W/H ratios, the discontinuity dip angle has a little to no effect on the strength of the pillars. Therefore, it can be noted that the in vertical pillars, the pillars with lower W/H ratio are significantly affected by the discontinuity dip angle parallel to the pillar face while the effect of discontinuity on the pillar strength diminishes with increase in W/H ratio.

6.3. Results and Discussions:

6.3.1. Evaluating the effect of discontinuity on inclined pillar strength:

To understand the effect of discontinuity on the strength of the inclined pillars, four different inclination (10°, 20°, 30° and 40°) of the pillars were simulated. The discontinuity dip angles were always measured from the horizontal axis (positive x-axis) of the pillar. As the 45° discontinuity intersecting an inclined pillar is not similar to that of the 135° discontinuity dip angle, therefore, the pillar strength was analyzed at every

10° discontinuity dip angle from 0° to 180°. The discontinuity effect on pillars was measured on four different width to height ratios of 0.5, 1.0, 1.5 and 2.0. Therefore, in total 288 models were simulated to understand inclined pillar strength reduction in the presence of discontinuity.

In inclined pillars, the discontinuity angle can be classified into two categories, where the discontinuity inclined towards the dip of the pillar and the discontinuity inclined against the dip of the pillar. For example, in 20° inclined pillar, the 45° discontinuity dip angle is inclined along the pillar inclination, therefore, this angle can be treated as discontinuity towards the dip of the pillar. While the 135° discontinuity dip angle is inclined opposite to the inclination of the pillar, therefore, this discontinuity can be treated as discontinuity against the dip of the pillar.

It can be observed from Figure 6.8a that in 10° inclined pillars with W/H ratio of 0.5, the 70° and 130° discontinuity dip angles significantly affect the strength of the pillar. In 20° inclined pillar with W/H ratio of 0.5 (Figure 6.8b), pillar strength is mainly affected at 80° and 140° discontinuity dip angle. Similarly, in 30° inclined pillars with W/H ratio of 0.5 (Figure 6.8c), the discontinuities effecting the pillars strength are 90° and 150° while in 40° inclined pillars (Figure 6.8d), they are 100° and 160°. This can be attributed to the largest discontinuity angle for sliding in the W/H ratio of 0.5 at any pillar inclination is 60° as shown in the Figure 6.9. Therefore, it can be concluded that when the discontinuity dip angle is measured relative to pillar inclination, the discontinuity dip angle of 60° and 120° relative to pillar inclination significantly effects the pillar strength irrespective of any inclination.

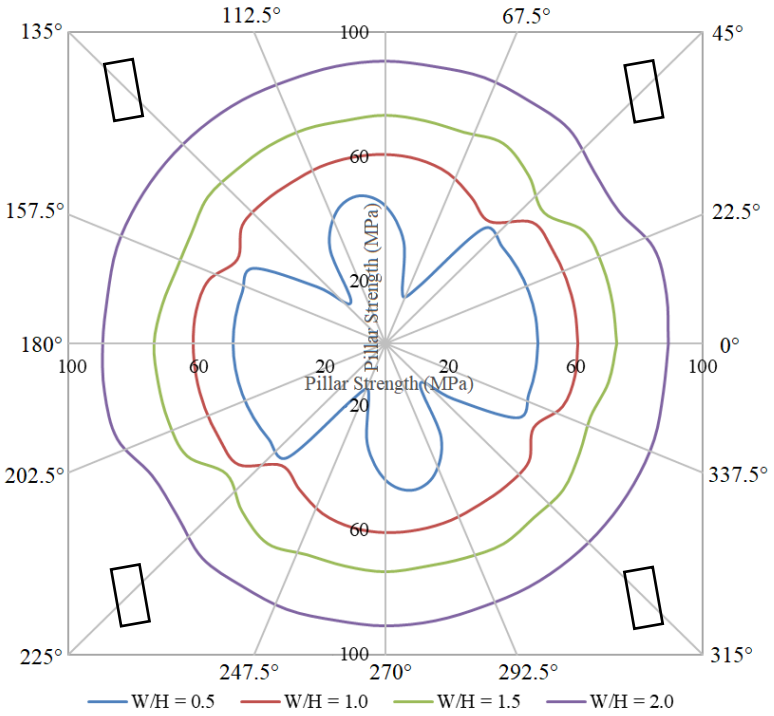
112.5°
67.5°
135°
45°
157.5°
22.5°
180°
0°
202.5°
337.5°
225°
315°
247.5°
270°
292.5°
100
60
20
Pillar Strength (MPa)
W/H = 0.5
W/H = 1.0
W/H = 1.5
W/H = 2.0

a)

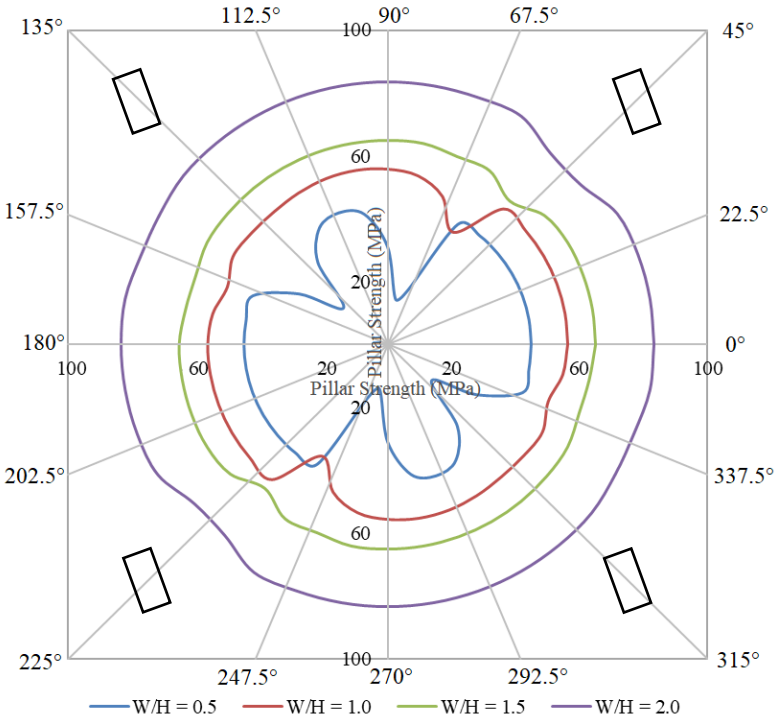
112.5°
90°
67.5°
135°
45°
157.5°
22.5°
180°
0°
202.5°
337.5°
225°
315°
247.5°
270°
292.5°
100
60
20
Pillar Strength (MPa)
W/H = 0.5
W/H = 1.0
W/H = 1.5
W/H = 2.0

b)

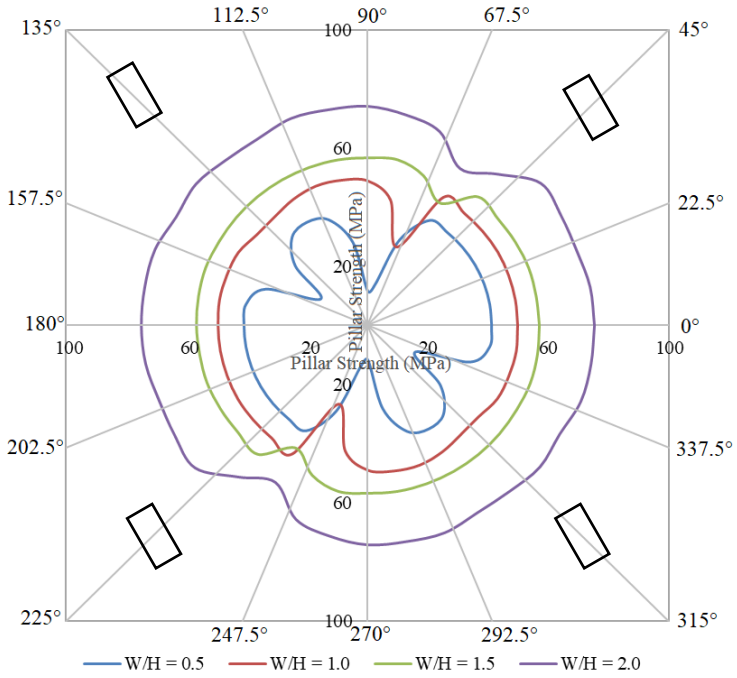

c)

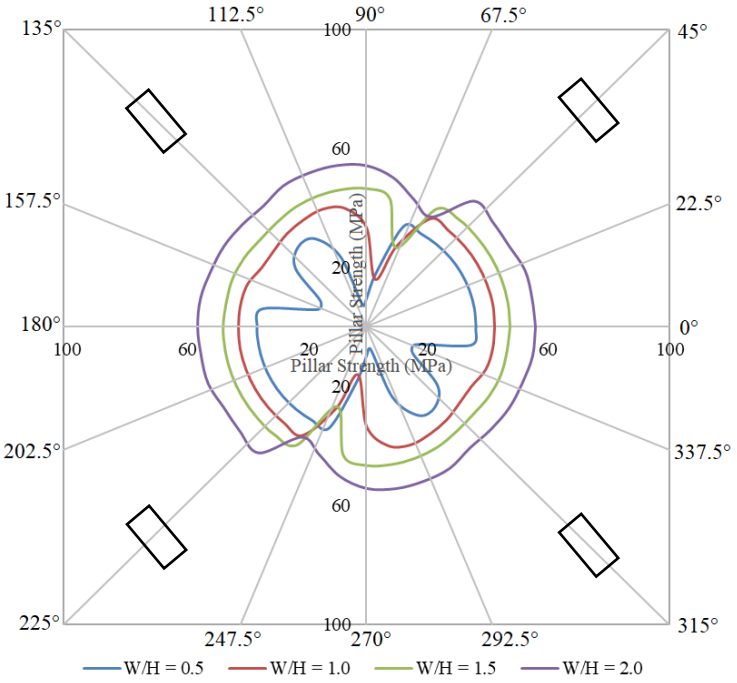

d)

Figure 6.8: Discontinuity effects on the pillars of inclination a) 10° b) 20° c) 30° d) 40°

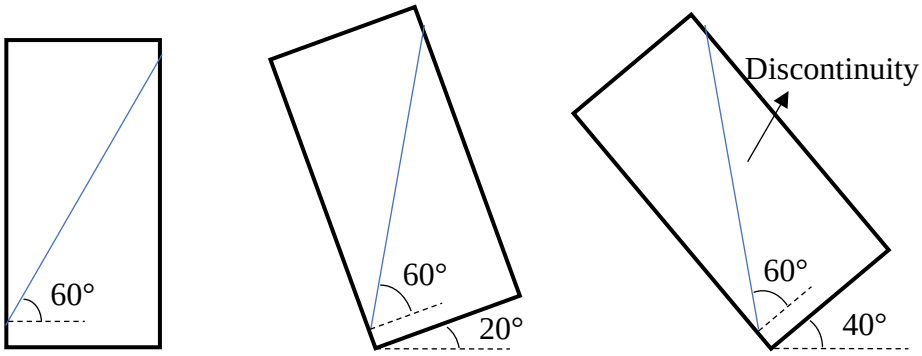

Figure 6.9: Discontinuity dip angle of 60° in pillars with Inclinations a) 0° b) 20° c) 40°

In Figure 6.8a, it can be observed that the pillar of W/H ratio 0.5 with a 70° discontinuity dip angle has similar strength (33% of the actual pillar strength) to that of the 130° discontinuity dip angle. While in the 30° inclined pillar with W/H ratio of 0.5 (Figure 6.8c), 90° discontinuity dip angle (Figure 6.10a) reduces the pillar strength to 30% while the 150° discontinuity dip angle (Figure 6.10b) reduces the pillar strength to 45%. This is due to the oblique loading on the pillars aiding the slippage for the discontinuity inclining towards the pillar dip. While for the discontinuity inclining against the dip, the oblique loading aided the closure of the discontinuity which resulted in lower strength reduction. Similar results are seen in pillars with higher W/H ratios and higher inclination pillars. Therefore, it can be concluded that in inclined pillars at any W/H ratio, the discontinuity inclining towards the pillar dip show a significant reduction in strength than the discontinuity inclining against the pillar dip.

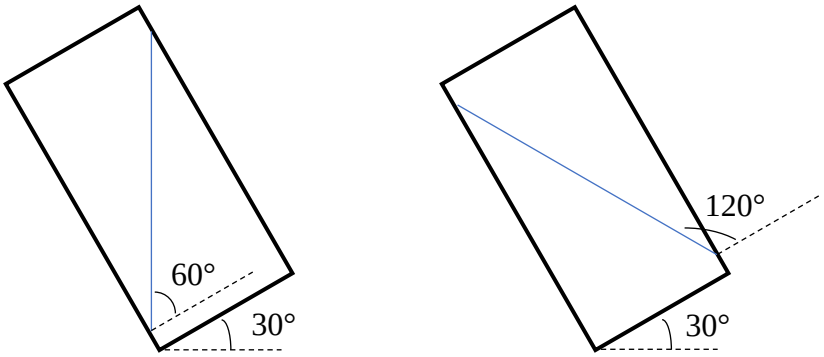

Figure 6.10: Discontinuity dipping a) towards the pillar inclination b) against the pillar inclination

In vertical pillars, at higher W/H ratios, the discontinuity has little effect on the strength of the pillars. It was observed that in highly inclined pillars even at high W/H ratios, the discontinuity reduces the strength of the pillars. For example, in 40° inclined pillar (Figure 6.8d) with W/H ratio of 1.0, with discontinuity of 90°, the strength reduces to 40% while with W/H ratio of 1.5, the discontinuity dip angle of 80° lead to strength reduction to 60%. Therefore, it can be concluded that discontinuities play a major role in defining the strength of the inclined pillars when dipping along the pillars even at higher W/H ratios.

In 40° inclined pillars (Figure 6.8d), it is interesting to note that the pillar with W/H ratio of 0.5 has higher strength than the pillar with W/H ratio of 1.0 when intersected by a discontinuity of angle 80°. When discontinuity dip angle is 70°, the pillar strength is higher for pillars with W/H ratio of 0.5 than the pillars with W/H ratio of 1.0 and 1.5. Pillars with W/H ratio of 1.5 and 2.0 had equal pillar strength when intersected with discontinuity dip angle of 60°. This is due to the failure mechanism of the 40° inclined where the brittle initiation occurs at the two corners of the pillars which coincides with the discontinuity dip angle and thus reducing the strength of the pillars with higher W/H ratio far less than the strength of lower W/H ratios. For example, the failure mechanism of the 40° inclined pillar with W/H ratio of 1.0 is shown in the Figure 6.11 (Jessu and Spearing, 2018). The discontinuity dip angle of 70° and 80° lie in that failure region, therefore, at those angles, there is a sharp reduction in strength of the pillar.

Similarly, in 30° inclined pillars (Figure 6.8c), the pillar with W/H ratio of 1.0 intersected with discontinuity dip angle of 60° has higher strength than the pillar with W/H ratio of 1.5. Therefore, the critical discontinuity angles lie in between the 60° and 90° for all the inclined pillars, where the smaller pillars can have higher strength than the larger pillars. This can lead to higher economic yield in the mines if properly executed.

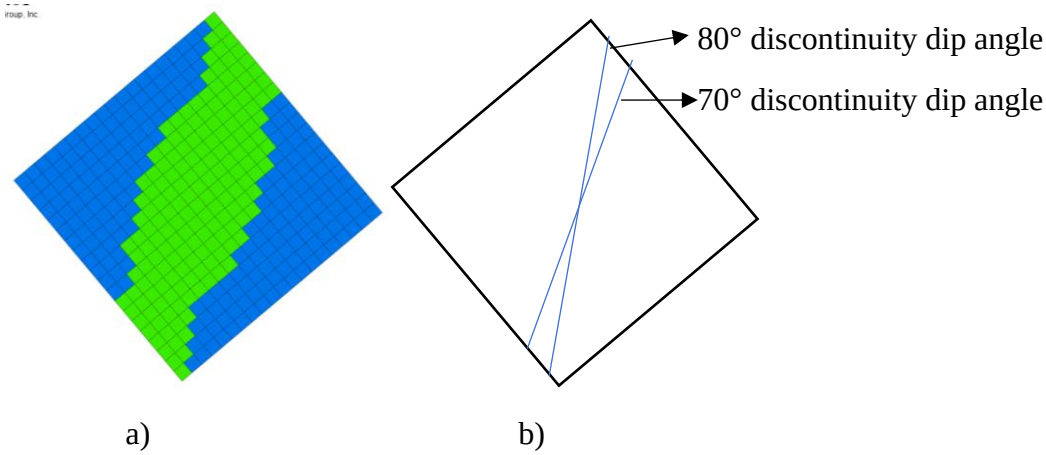

a) b)

Figure 6.11: a) Failure mechanism of the 40° inclined pillar without discontinuity (Jessu and Spearing, 2018) b) The discontinuity angles that can lie in the failure region

Note: Blue shows elastic elements and Green shows yielded elements

6.3.2. Influence of Discontinuity Dip Direction on Inclined Pillars:

To understand the influence of discontinuity dip direction on the inclined pillar strength, models were simulated as vertical pillars and 40° inclined pillars at W/H ratio of 0.5 and 1.0. Three different dip directions were simulated which are 0°, 45°, and 90°. An example of discontinuity dip direction of 0° and 45° is shown in Figure 6.12. In vertical pillars, the discontinuity dip direction at 0° and 90° represent the similar discontinuity because these are parallel to the pillar face. In inclined pillars, the discontinuity dip direction of 0° represents the discontinuity parallel to the pillar face and towards the pillar inclination, dip direction of 90° also indicates the discontinuity perpendicular to pillar inclination and dip direction of 45° refer to an intermediate of the two mentioned above. Strike and Dip Direction would be used interchangeably from this point.

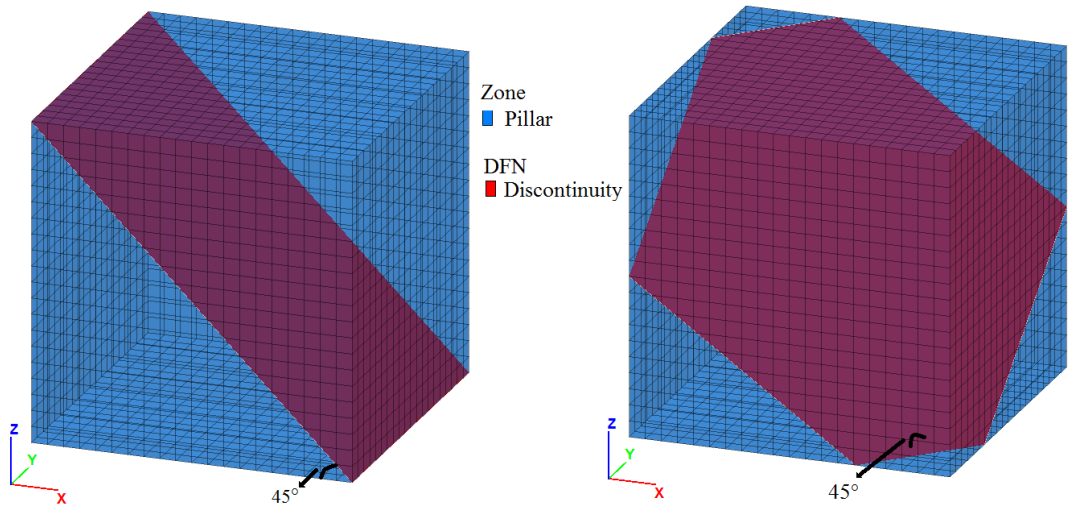

Figure 6.12: Discontinuity with 45° dip and a) 0° dip direction b) 45° dip direction

The results show that in vertical pillars with W/H ratio of 0.5 (Figure 6.13a), the strike of the discontinuity has little effect on the strength of the pillars. While in inclined pillars (Figure 6.13b), the strike of the discontinuity has a significant influence on the pillar performance. When the discontinuity is orientated towards the pillar inclination (Strike = 0°), the discontinuity angle of 100° and 160° significantly effects the pillar strength while when the strike is 45°, the discontinuity angle which is affecting the pillar strength the most is 80° and 150° and when the discontinuity orientation is perpendicular to pillar inclination, 50° and 130° dip angles reduce the strength considerably. It can be observed that when the discontinuity orientation is perpendicular to pillar inclination (Strike = 90°), the plot looks like that of the vertical pillars. The maximum strength reduction was observed when the orientation was towards the pillar inclination and discontinuity angle was 100°.

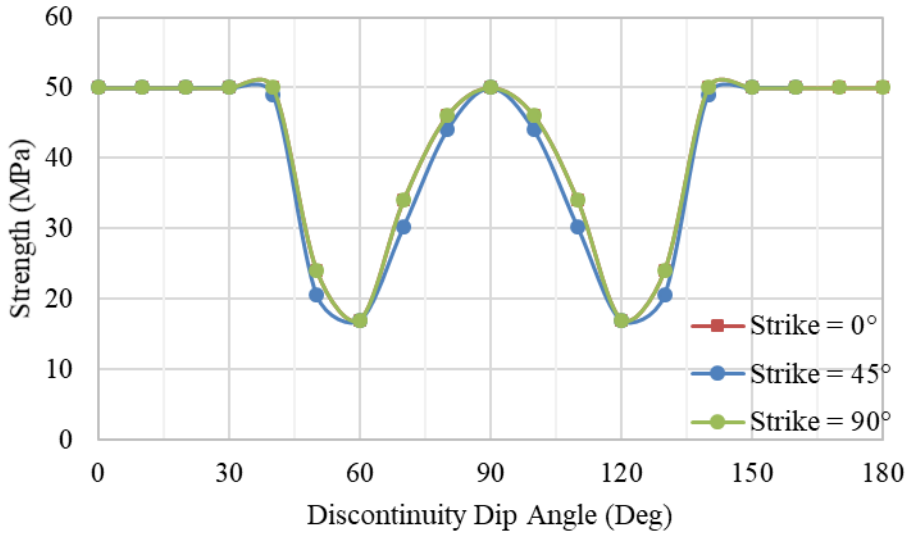
60
50
40
30
20
10
0
Strength (MPa)
0
30
60
90
120
150
180
Discontinuity Dip Angle (Deg)
Strike = 0°
Strike = 45°
Strike = 90°

a)

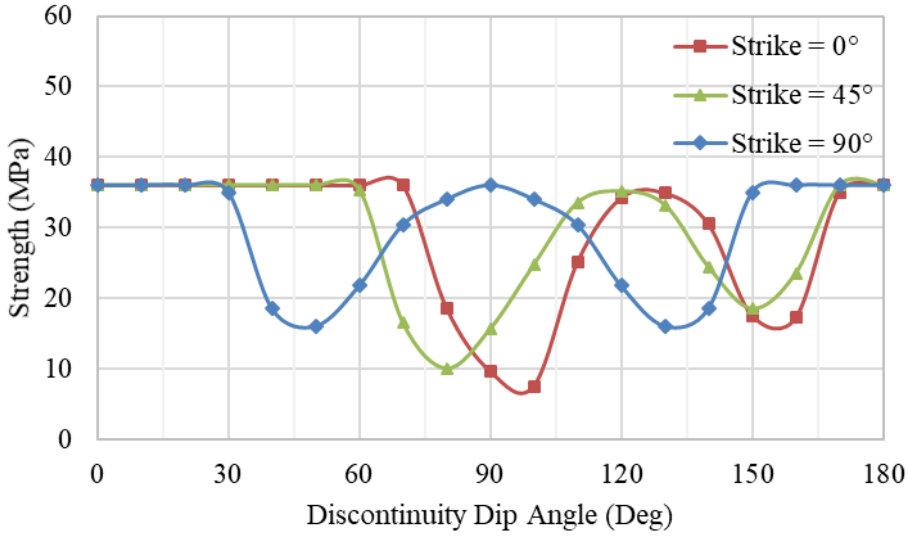
60
50
40
30
20
10
0
Strength (MPa)
0
30
60
90
120
150
180
Discontinuity Dip Angle (Deg)
Strike = 0°
Strike = 45°
Strike = 90°

b)

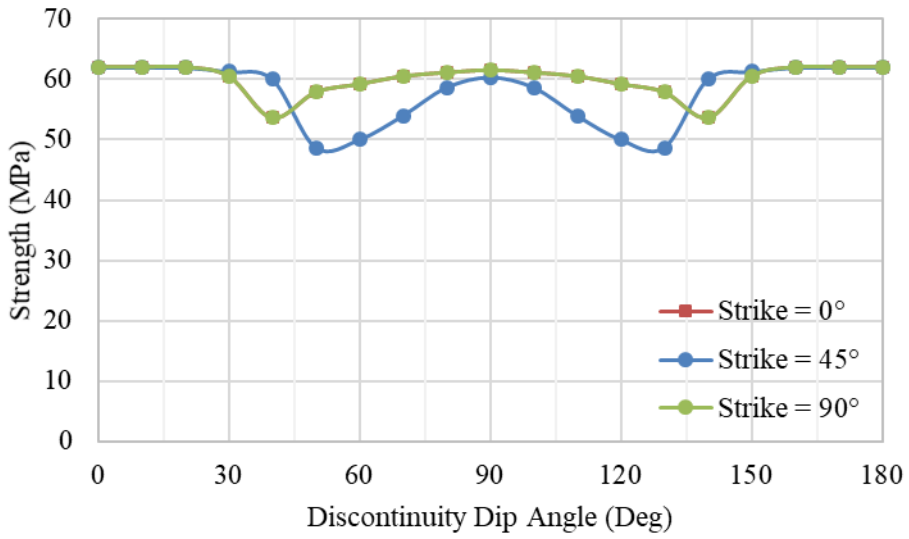

c)

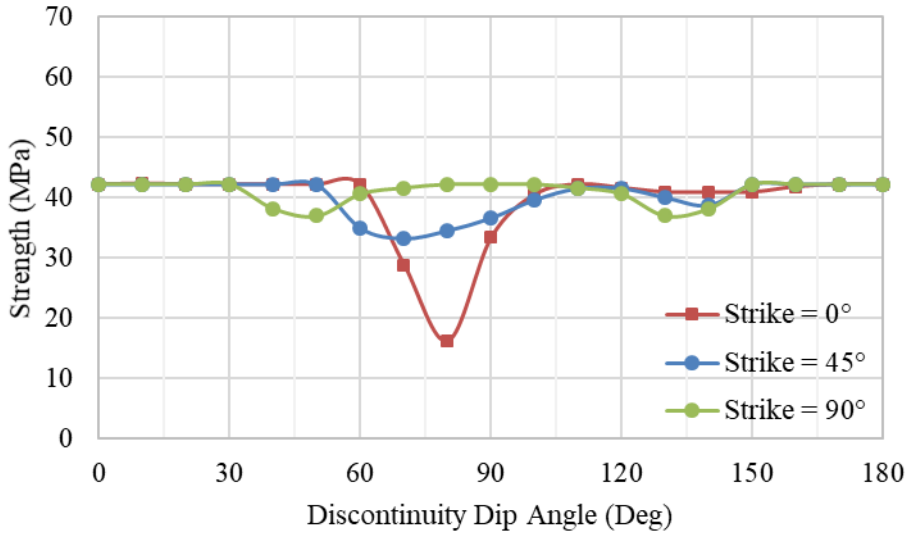

d)

Figure 6.13: Influence of discontinuity dip direction on a) vertical pillars (W/H = 0.5) b) 40° inclined pillars (W/H = 0.5) c) vertical pillars (W/H = 1.0) d) 40° inclined pillars (W/H = 1.0)

In vertical pillars with W/H ratio of 1.0 (Figure 6.13c), the strike direction of 45° has a higher influence on the pillar strength at 50° discontinuity dip. In 40° inclined pillars with W/H ratio of 1.0 (Figure 6.13d), it can be observed that the discontinuity orientated toward the pillar inclination (Strike = 0°), has the largest influence on the pillar strength at 80°. As the strike direction is oriented away from the pillar inclination such as strike of 45° and 90°, the pillar strength was reduced by 20% and 10% respectively. This shows that the strike needs to be considered along the discontinuity dip to evaluate the strength of the pillars in vertical as well as inclined pillars.

6.4. Conclusions:

The effect of discontinuity on inclined pillars was simulated and the following conclusions can be made:

- In pillars with W/H ratio of 0.5, it can be concluded that the 60° discontinuity dip angle (Towards pillar inclination) with respect to the pillar inclination has a significant drop in pillar strength irrespective to the pillar dip. Therefore, it can also be projected that for pillars with W/H ratio less than 0.5, the largest angle for sliding in the vertical pillars will be the same for the inclined pillars.

- Higher safety factors should be employed when the slender pillars of 0.5 (vertical or inclined) are encountered with discontinuities within the range of an angle higher than the friction angle and the largest angle bisecting the pillar. It is best proposed to avoid the slender pillars of W/H ratio less than 0.5 due to its high sensitivity towards the discontinuity dip angle.

- In inclined pillars with higher W/H ratios, the largest discontinuity (i.e. discontinuity from one corner to another corner) in the pillar dip direction has a significant influence on the strength of the pillar.

- The discontinuity dip towards the pillar inclination coincides with the failure mechanism of the inclined pillars thus making these discontinuities much vulnerable than the discontinuities dipping against the pillar inclination.

- In highly inclined pillars with higher W/H ratio, the discontinuities lead to very low strength due to the combination of the failure mechanism and the slippage in the discontinuity. Therefore, design of the inclined pillars should avoid the discontinuities that coincide with the failure mechanism of the inclined pillars. For example, 50° discontinuity angle with respect to pillar inclination for W/H ratio of 1.0 in vertical as well as inclined pillars.

- Alternatively, the results from highly inclined pillars show that the strength of pillar with W/H ratio of 1.5 and discontinuity dip angle of 70° has strength lower than the pillar with W/H ratio of 0.5 with the same discontinuity dip angle. As the discontinuity dip angle of 70° is largely affecting the higher W/H ratios, the excavations can be slightly reduced to accommodate the pillars with W/H ratio of 0.5. This will potentially reduce the problem of pillar failure and increase the productivity.

- The strike direction of the discontinuity is very important aspect in the inclined pillars. Pillar strength reduction due to discontinuity dip angle depends on the strike of the discontinuity.

References:

Brady, BHG; Brown, ET; 2007. Rock mechanics for underground mining. Chapman & Hall, UK.

Dismuke, S. R., Forsyth, W. W. and Stewart, S. B. V. The Evolution of Mining Strategy Following the Collapse of the Window Area at the Magmont Mine, Missouri. Proceedings of the CIM Annual General Meeting, District 6, Metal Mining, 1994; pp 3-8.

Dolinar, D. R., Esterhuizen, G. S. (2007) Evaluation of the effects of length on strength of slender pillars in limestone mines using numerical modelling. *Proceedings of the 26th International Conference on Ground Control in Mining*. Morgantown, WV: West Virginia University, pp. 304–313.

Esterhuizen, G. S. (1998). Effect of structural discontinuities on coal pillar strength as a basis for improving safety in the design of coal pillar systems, Safety in Mines Research Advisory Committee, COL 005a, 1998; pp. 1–104.

Esterhuizen, G. S. (2006). An evaluation of the strength of slender pillars. *Transactions of Society for Mining, Metallurgy, and Exploration, Inc.* 2006; Vol. 320. Littleton, CO: Society for Mining, Metallurgy, and Exploration, Inc., pp. 69–76.

Fakhimi, A., and Hemami, B. (2015). Axial splitting of rocks under uniaxial compression. *International Journal of Rock Mechanics and Mining Sciences*, *79,* 124-134.

Fakhimi, A., Hosseini, O. and Theodore, R. (2016). Physical and numerical study of strain burst of mine pillars. *Computers and Geotechnics*, *74,* 36-44.

Hedley, D. G. F. and Grant, F. (1972). Stope and pillar design for the Elliot Lake uranium mines. *Canadian Institute of Mining and Metallurgy Bulletin.* Vol. 65, pp. 37-44.

Iannacchione, A. T. (1999). Analysis of Pillar Design Practices and Techniques for U.S. Limestone Mines, *Transactions of the Institution of Mining and Metallurgy (sect. A: Mining Industry)*, 108, September-December pp. A152–A160.

Itasca Consulting Group, (2018). Fast Lagrangian Analysis of Continua in 3Dimensions, 2018, Minneapolis, Minnesota, USA.

Jaeger, J. C. and Cook, N. G. W. (1994). Fundamentals of Rock Mechanics, 3rd Edition, New York: Chapman and Hall.

Jessu, K. V. and Spearing, A. J. S. (2018) Effect of Dip on Hard Rock Pillars. South African Institute of Mining and Metallurgy. Volume 118, 765-776.

Kaiser, P. K., Diederichs, M. S., Martin, C. D., Sharp, J. and Steiner, W. (2000) Underground works in hard rock tunnelling and mining. *Proceedings of GeoEng2000*, 2000; 841–926, Melbourne, ICMS.

Lorig, L. J., and Cabrera, A. (2013). Pillar Strength Estimates for Foliated and Inclined Pillars in Schistose Material. *Proceedings of 3rd International FLAC/DEM Symposium*, Hangzhou, China, October 2013. Paper: 01-01, H. Zhu et al., Eds. Minneapolis: Itasca International Inc.

Lunder, P. J. and Pakalnis R. (1997). Determining the strength of hard rock mine pillars. *Bulletin of Canadian Institute of Mining and Metallurgy.* Vol. 90, pp. 51-55.

Ma, T., Wang, L., Suroineni, F.T. and Tang, C. (2016) Numerical Analysis on Failure Modes and Mechanisms of Mine Pillars under Shear Loading. Hindawi Publishing Corporation, Shock and Vibration 2016, Volume 2016, 1-14.

Madden, B. J., Canbulat, I., Jack, B. W. and Prohaska, G. D. (1995) A reassessment of Coal Pillar Design Procedures, Safety in Mines Research Advisory Committee, COL 021, pp. 1–148.

Martin, C. D. and Maybee W. G. (2000). The strength of hard rock pillars. *International Journal of Rock Mechanics and Mining Sciences.* Vol. 37, pp. 1239-1246.

Martin, C. D., Kaiser, P. K. and McCreath, D.R. (1999). Hoek–Brown parameters for predicting the depth of brittle failure around tunnels. *Canadian Geotechnical Journal*. 36(1), 136–151.

Suorineni, F. T., Mgumbwa, J. J., Kaiser, P. K. and Thibodeau, D. (2014). Mining of orebodies under shear loading Part 2 – failure modes and mechanisms, *Mining Technology* (Trans. Inst. Min. Metall. A), 2014; 123(4),240–249.

Zipf RK. Toward pillar design to prevent collapse in room-and-pillar mines. 108th Annual Exhibit and Meeting, Society for Mining, Metallurgy and Exploration, Denver. 2001

Chapter 7

A Parametric Study of Blast Damage on Hard Rock Pillar Strength

This chapter has been published in Energies as:

Jessu, K.V., Spearing, A.J.S., Sharifzadeh M. (2018) A Parametric Study of Blast Damage on Hard Rock Pillars. *Energies*, 11(7), 1901.

Abstract:

Pillar stability is an important factor for safe working and from an economic standpoint in the underground mines. This chapter discusses the effect of blast damage on the strength of hard rock pillars using numerical models through parametric study. Based upon the results, blast damage has a significant impact on the strength of pillars with larger width to height ratios. The blast damage causes softening of the rock at the pillar boundaries leading to the yielding of the pillars in brittle fashion beyond the blast damage zones. The models show that the decrease in pillar strength as a consequence of blasting is inversely correlated with increasing pillar height at constant width-to-height ratio. Inclined pillars are less susceptible to blast damage and the damage on the inclined sides has a greater impact on pillar strength than on the normal sides. A methodology to analyze the blast damage on hard rock pillars using FLAC^{3D} has been presented herein.

Keywords: Blast Damage, Damage Factor, Hard Rock Pillars, Numerical Modelling

7.1. Introduction:

The most common methods employed in hard rock mines is drilling and blasting. An inherent problem that exists with this method is the damage to the periphery of excavation induced by the blast. Perimeter control and smooth wall blasting have been implemented into the mines to reduce blast induced damage where it is considered an issue and is common in underground civil construction. However, some level of blast damage is inevitable, and this leads to adverse consequences in the form of stability issues in the rock excavations.

Some of the earliest research (Oriard, 1982; Forsyth and Moss, 1991; Yu and Vongpaisal, 1996) stated over-break as the only major consequence of the blast damage. It was defined as the unwanted loosening, dislocation and disturbance of the rock mass beyond the limits of the intended excavation design. Warneke et al. (2007) illustrated a clear distinction between the over-break and the blast damage which is illustrated in Figure 7.1. This chapter considers blast induced damage as the region beyond the final excavation

boundary where the rock has been damaged by blasting to employ into the numerical models.

Numerous studies have been undertaken to determine the extent of the blast damage on the rock excavations (Kutter and Fairhust, 1971; Wilson and Holloway, 1987; Djordjevic, 1999; Olsson and Ouchterlony, 2003; Fleetwood, 2010). General theories were developed to determine the extent of damage zone from small scale and field scale investigations based on explosive properties, borehole radius and material properties. Kutter and Fairhurst (1971) also found that the stress waves and the gas generated fractures propagate along the maximum principal stress direction. Ouchterlony et al. (2001) have done field studies to determine the blast damaged zone based on explosive type, charge concentration and charge diameter. It was concluded that the damaged zone can range from 0.2 m to 2.0 m, depending on the properties of the rock such as intact rock mass, jointed rock mass and heavily jointed rock mass.

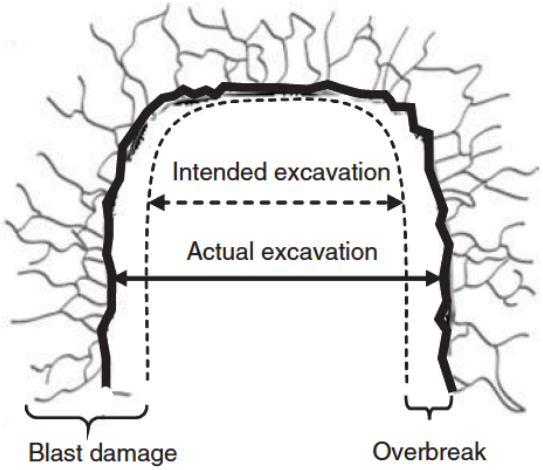

Figure 7.1: Distinction between the over-break and blast damage

Numerous studies have been undertaken to determine the extent of the blast damage on the rock excavations (Kutter and Fairhust, 1971; Wilson and Holloway, 1987; Djordjevic, 1999; Olsson and Ouchterlony, 2003; Fleetwood, 2010). General theories were developed to determine the extent of damage zone from small scale and field scale investigations based on explosive properties, borehole radius and material properties. Kutter and

Fairhurst (1971) also found that the stress waves and the gas generated fractures propagate along the maximum principal stress direction. Ouchterlony et al. (2001) have done field studies to determine the blast damaged zone based on explosive type, charge concentration and charge diameter. It was concluded that the damaged zone can range from 0.2 m to 2.0 m, depending on the properties of the rock such as intact rock mass, jointed rock mass and heavily jointed rock mass.

Hoek et al., 2002 classified the rock damage from blasting by introducing a blast damage factor (D). A qualitative classification was presented as good blasting representing D = 0 and the poor blasting representing D = 0.8. Sharifzadeh and Pal (2014) attempted to quantify the blast damage factor by deducing a relationship between deformation modulus and intact rock modulus by taking blasting effect into consideration. Torbica and Lapcevic (2015) quantified the blast damage by reducing Geological Strength Index (GSI) by 10 units in the damaged rock zone. It was concluded that the results of the reduced GSI method were equivalent to that of the D factor, showing that reduced GSI can be used as an alternative for determining the properties of the degraded rock mass.

There are no theoretical methods to account for excavation stability in the tunnels and pillars considering blast damage. Therefore, numerical modelling is one of the most appropriate method to observe the effect of blast damage on the excavations when the model parameters, rock properties and constitutive models are employed properly. Shen and Barton (1997) described the damaged zone with increased jointing and evaluated the stress distribution around the tunnels with the help of discontinuum modelling UDEC. Saiang (2008) evaluated the properties of the rock in the blast damaged zone with the discrete element modelling PFC^{2D}. These properties were used in FLAC to perform the parametric study on the properties affecting the stress distribution of the tunnels. Blast damage thickness had a moderate effect and deformation modulus had a high effect on the stress distribution in the tunnels. Mitelman and Elmo (2014) developed a hybrid element discrete modelling approach to study the induced damage in tunnels. Torbica and Lapcevic (2015) used Phase2 to demonstrate the blast effect on the tunnels where the

degraded rock properties were used for only the specified thickness of the blast zone. In these studies, the periphery of the tunnels was simulated by reducing the intact rock properties of the blast effected zone.

Baharani et al., 2010 conducted finite element analysis on pillars considering the blasting effect where a hypothetical case study was performed. It was concluded that the slender pillars are prone to strain bursting and the strength of the wider pillars is affected due to drill and blast methods. It was also shown that the yielding of the pillar side walls is higher due to blast damage. Limited study has been conducted on pillars with blast damage. Therefore, in this chapter, a parametric study of damage factor and damage thickness over different pillar dimensions was conducted to understand the blast damage effect on the strength of the pillars.

7.2. Theoretical Background:

Pillar design theories are predominantly concerned with the factor of safety which is the ratio of pillar strength to the maximum pillar stress. This approach ignores aspects such as:

- The presence of geology and water
- A weak roof or floor
- The effects of blasting
- The dip

To overcome these other often ignored parameters a higher factor of safety is adopted; such as 1.4 for a hard rock pillars (Lunder, 1994).

To date many studies have been done to develop the empirical approaches on hard rock pillar strength (Hedley and Grant, 1972; Potvin et al., 1989) in different rock types. Lunder (1994) is considered as one of the most prominent empirical approaches that have been used in the mines. It is given as:

$$\sigma_p = K * UCS * (C_1 + C_2 * \kappa) \tag{7.1}$$

Where σ_p is the ultimate strength of the pillar (MPa), K is the pillar size factor, and UCS is the uniaxial compressive strength of the intact rock (MPa), C_1 and C_2 are the empirical rock mass constants and κ is the friction term which is calculated as:

$$\kappa = \tan\left[cos^{-1}\left(\frac{1 - C_{pav}}{1 + (C_{pav})}\right)\right] \tag{7.2}$$

$$C_{pav} = Coeff * \left[Log\left(\frac{W}{H} + 0.75\right)\right]^{1.4\left(\frac{W}{H}\right)} \tag{7.3}$$

Where C_{pav} is the average pillar confinement and Coeff is the coefficient of the pillar confinement.

The empirical studies are based on a specific database which does not consider the rock mass properties. To improve upon these empirical equations, studies were conducted with numerical models considering the fracture sets (Esterhuizen et al., 2008; Elmo and Stead, 2010), but blast damage has yet to be considered.

7.2.1. Blast Damage Zone Properties:

Rock properties play an important role in describing the damage in the blast damage zone. Blasting creates fractures in the blast damage zone which reduces the strength of the rock mass. The most important rock properties regarding blast damage are massive rock modulus, cohesion and friction (Hoek et al., 2002).

The rock modulus in the blast damage zone is expressed as the degraded rock modulus (E_{rm}), which depends on the intact rock modulus (E_i), damage factor (D) and GSI, published by Hoek and Diederichs (2006):

$$E_{rm} = E_i\left(0.02 + \frac{1 - D/2}{1 + e^{((60+15D-GSI)/11)}}\right) \tag{7.4}$$

As the most popular forms of numerical modelling are developed in terms of Mohr Coulomb or Bilinear failure criterion, the cohesion (C`) and friction (Ø`) were evaluated by Hoek et al., 2002 and are given as:

$$\emptyset' = sin^{-1}\left[\frac{6am_b(s+m_b\sigma'_{3n})^{a-1}}{2(1+a)(2+a)+6am_b(s+m_b\sigma'_{3n})^{a-1}}\right] \quad (7.5)$$

$$C' = \frac{\sigma_{ci}[(1+2a)s+(1-a)m_b\sigma'_{3n}](s+m_b\sigma'_{3n})^{a-1}}{(1+a)(2+a)\sqrt{1+(6am_b(s+m_b\sigma'_{3n})^{a-1})/((1+a)(2+a))}} \quad (7.6)$$

$$\sigma'_{3n} = \sigma'_{3max}/\sigma_{ci} \quad (7.7)$$

Where m_b is the reduced value of the rock mass material constant, a and s are the rock structure constants, σ_{ci} is the uniaxial compressive strength of the intact rock sample, and σ'_{3max} is the upper limit of the confining stress.

The degraded rock modulus, cohesion and friction would be the key parameters employed in numerical models for blast damage zone which will be derived by the Equations (7.5-7.7), and the massive rock properties will be employed for the zone beyond the blast damaged zone.

7.2.2. Effect of Pillar Height:

The pillar height has a considerable effect on determining strength of the hard rock pillars. Kaiser (2010) described that the strength of the pillar decreases with the increase in pillar height at a constant pillar width to height ratio (W/H). Many studies have been done on understanding the size effect which shows that at constant width to height ratio, as the sample size increases the strength of the sample decreases (Ayres da Silva, 2013). Alternatively, the blast thickness would encompass a larger amount of the smaller pillar and conversely, a smaller amount of the larger pillar. For example, a 0.25m blast thickness on the pillar height of 1 m with W/H ratio of 1 would lead to 44% pillar damage while on the pillar height of 2 m with W/H ratio of 1 would lead to 23%. Therefore, it is important

to understand the influence of blast damage at different pillar heights at constant pillar width to height ratios.

7.2.3. Effect of Pillar Inclinations:

The pillar inclinations lead to inclined loading conditions which reduce the pillar strength with increasing pillar inclination and larger width to height ratios (Suorineni et al., 2011; Suorineni et al., 2016). In the inclined pillars, the pillar sides towards the dip lead to the pillar failure. While blasting affects all the sides of the pillar similarly, for inclined pillars it would be interesting to understand the pillars sides with blast damage that are more susceptible to pillar strength reduction. Therefore, the effect on strength of the inclined pillars due to the blast damage on all the pillar sides, dip sides and strike sides are also studied in this chapter.

The scope of this chapter is to understand the effects of blast damage on the hard rock pillars in vertical as well as inclined direction with use of numerical modelling. The parametric study has been conducted with pillar parameters such as width to height ratio, pillar height and pillar inclination and with blast parameters such as blast damage factor and blast damage thickness.

7.3. Numerical Modelling:

To develop an understanding of the pillar behavior with blast damage, FLAC^{3D} 5.0 (Itasca, 2017), a finite difference element software, was employed throughout the body of the work. Majority of the studies on the ground control and especially on the pillar stability have employed FLAC^{3D} for its inbuilt well developed constitutive models. The problem deals with blast damage in the pillar which depends on blast factor (D) and Blast Zone thickness (T). Therefore, these two parameters were varied to understand the response of the models. The results were presented in either normalized fashion or the actual results depending on the factor analyzed. Normalized result is the ratio of the pillar strength considering blast damage to that of the actual pillar strength.

7.3.1. Grid Generation:

The model was created in a three-dimensional framework with the origin at the center of the pillar, as shown in Figure 7.2. The horizontal plane of the coordinate system is denoted by x and y axes and the vertical plane in the z axis. The model consists of pillar, main roof and main floor. The model's extent in the vertical plane was three times the pillar width to ensure no interaction effects of model boundaries on the pillar. The excavation surrounding the pillar was set at seventy five percent extraction ratio, therefore the excavation width is equal to that of the pillar width.

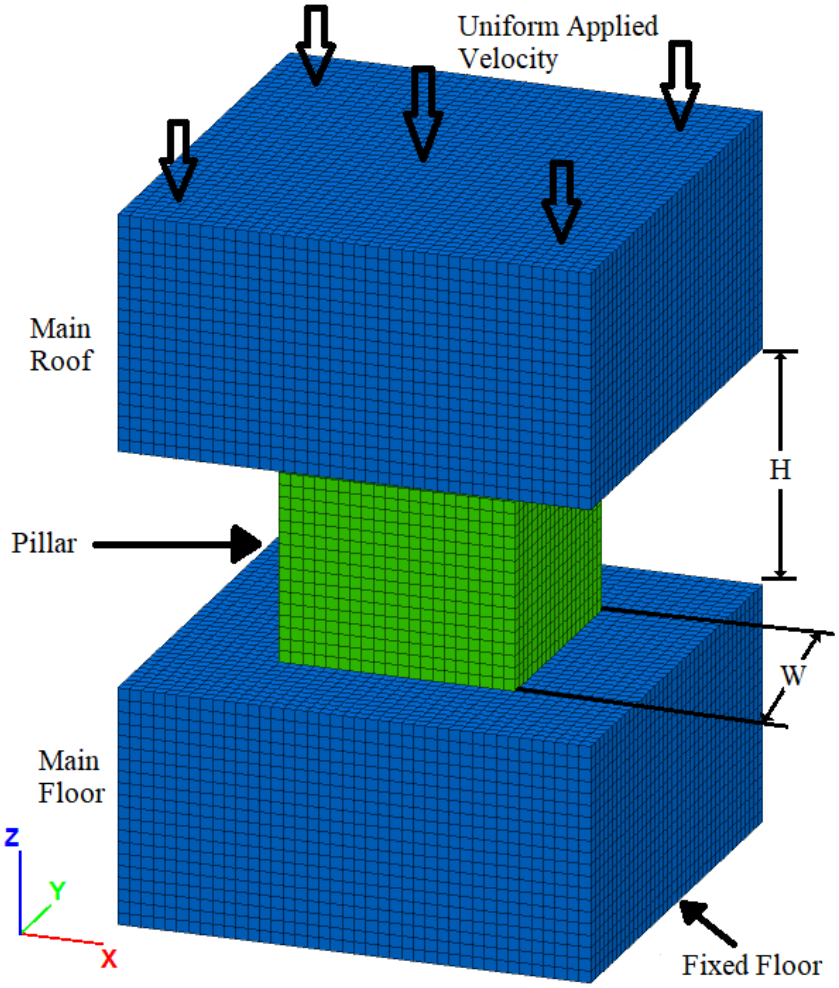

Figure 7.2: FLAC^{3D} pillar model

7.3.2. Mesh Generation and Loading rate:

The mesh size and the loading rates play a critical role in developing the numerical models effectively and are dependent on each other. Mesh size depends on the area of concentration on the pillar that will be helpful in understanding the impact of blast damage on pillar behavior. The blast damage reported in the excavation ranges from 0.25m to 2m (Ouchterlony et al., 2001). Therefore, the minimum mesh size should be about 0.25m*0.25m*0.25m or less such that the blast zone thickness of 0.2m can be analyzed on the pillars.

Loading rate can be either stress-controlled or strain controlled. It is recommended to use strain-controlled loading rates to obtain reliable stress strain graphs (Itasca, 2017). The model run time and the stress strain curve is dependent on the loading rate. To understand the effect of loading rate, a pillar with W/H ratio of 1.0 was applied with three different loading rates. Table 7.1 shows that the model run time increases exponentially with decreasing loading rates. Figure 7.3a shows that with low loading rates, the models obtained good and reliable stress strain graphs.

The loading rate is largely depended on the mesh size. Past numerical studies on pillars have adopted large meshes (Esterhuizen et al., 2006; Lu et al., 2008; Perry et al., 2013) and therefore employed higher loading rates. The relationship between the mesh size and loading rate was defined with the help of stress strain graphs. It was found that smaller mesh sizes needed very low loading rates, and as the mesh size increases, higher loading rates can be employed. Three mesh sizes were varied to understand the stress strain behavior at 1.0E-6 m/step loading rate. It serves well for 0.5 and 0.25 meshes, showing smooth curves nevertheless for 0.125 mesh, the loading rate seems to be higher resulting in bumps in the stress strain curve (Figure 7.3b). Smaller mesh size also results in higher model run times. Optimization of the loading rate, mesh size and model running time is required to obtain a good stress strain graph. Therefore, a 1.0E-6 m/ step loading rate is suitable for a mesh size of 0.25*0.25*0.25 and has been used throughout this chapter.

Table 7.1. Model run times at different loading rates

Loading Rate (m/step)	Model Run time (min.)
1.0E-5	1
1.0E-6	4
1.0E-7	34

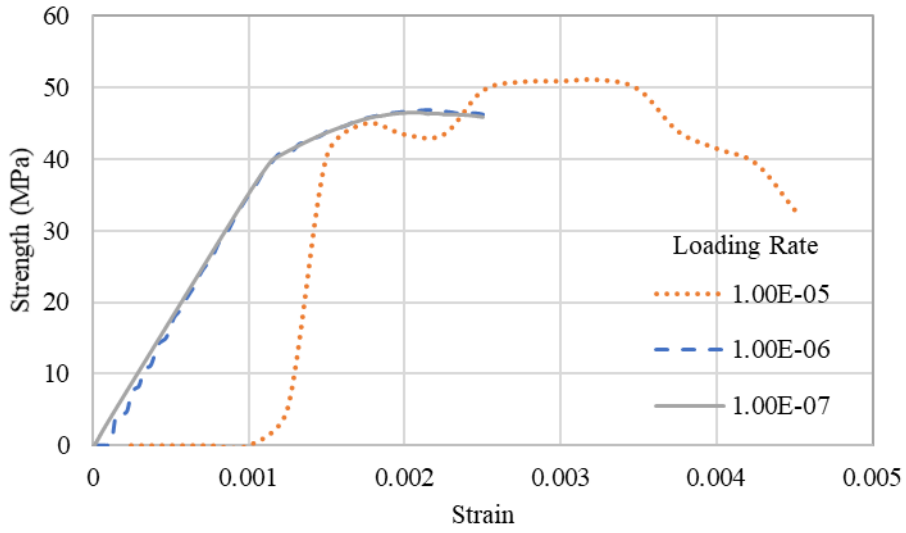

a)

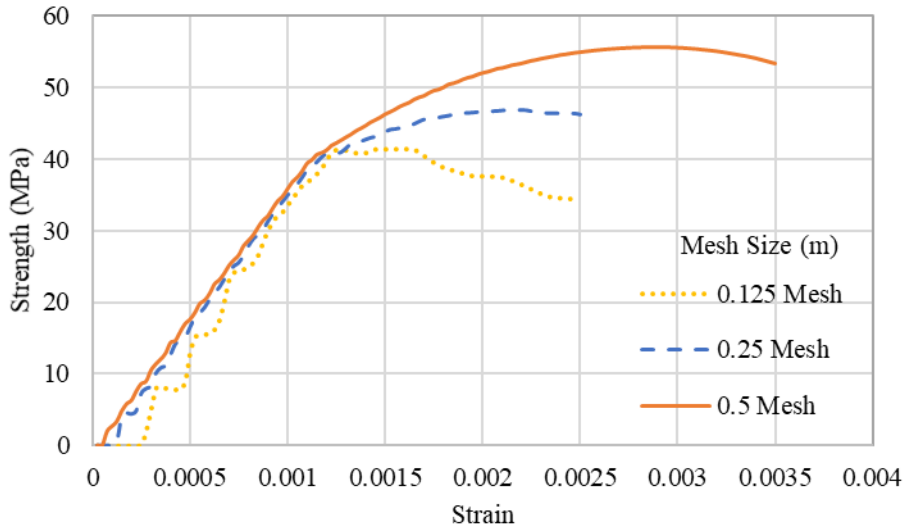

b)

Figure 7.3: Stress strain graphs a) at different loading rates b) at different mesh sizes

7.3.3. Boundary Conditions:

Roller boundaries were applied on the x and y boundaries, which restricted displacement and velocity normal to the planes. These boundaries simulate the chain of pillars around the model. The main floor was pinned, restricting the displacements and the velocities both normal and parallel to the plane. The load was applied as uniform velocity on the top of the main roof to simulate the compressive loading on the pillars. The model was subjected to a vertical stress of 2.7 MPa with vertical to horizontal stress ratio of 1:1 which simulates a mine of depth 100m.

7.3.4. Material Properties:

The material properties and failure criteria prove to be critical in developing realistic numerical models. Model constitute of main roof, main floor and pillars and as the focus of the thesis is on the pillars; the main roof and the main floor are simulated as elastic materials. The pillars are best represented with brittle Hoek Brown criterion (Martin et al., 1999; Kaiser et al., 2000; Esterhuizen et al., 2006), which is established on the formation of brittle cracks at 0.3 to 0.5 times the uniaxial compressive strength, followed by shear failure in the pillars. Therefore, a bilinear strength envelope was used in which strength is equal to one third of the uniaxial compressive strength and is independent of friction at lower confinement followed by friction hardening at higher confinement (Kaiser et al., 2000)

Bilinear Strain-Hardening/Softening Ubiquitous Joint model, an inbuilt FLAC^{3D} constitutive model, was used to simulate the bilinear rock strength behavior based on Mohr Coulomb failure criterion and strain softening as a function of deviatoric plastic strain (Itasca, 2017). The rock and joint properties for the constitutive model are obtained from Esterhuizen (2006), using Uniaxial Compressive Strength and Rock Mass Rating of 120 MPa and 70, respectively, and are shown in Tables 7.2 and 7.3.

Table 7.2: Model Properties (Dolinar and Esterhuizen, 2007)

Rock Mass Properties	Numerical Value
Bulk Modulus	40,000 MPa
Shear Modulus	24,000 MPa
Intact Rock Strength (UCS)	150 MPa
Cohesion (Brittle)	25 MPa
Friction (Brittle)	0°
Cohesion (Mohr-Coulomb)	8.1 MPa
Friction (Mohr-Coulomb)	47.6°
Tension	2.7 MPa
Dilation	30 °

Table 7.3: Joint Properties (Dolinar and Esterhuizen, 2007)

Joint Properties	Numerical Value
Joint Cohesion	1 MPa
Joint Friction	42°
Joint Tension	0.4 MPa
Joint Dilation	0°

Strain softening parameters are dependent on the model mesh size. These parameters are established by calibrating all the numerical models to that of the theoretical results using the same element size throughout all the models (Itasca, 2017). It was determined that while using a large mesh size, the softening should occur at very low plastic strain and when the small mesh size is adopted, the softening occurs over a large plastic strain. Therefore, the mesh size was kept at 0.25m*0.25m*0.25m with a loading rate of 1.0E-6 for all the models, and cohesion softening was performed to calibrate the numerical model results to that of the Lunder (1994) results.

To simulate the blast damage in the model, rock properties were changed to degraded rock properties in the blast damaged zones with the help of FISH code (an inbuilt function in $FLAC^{3D}$ for developing user defined variables and functions), as shown in Figure 7.4. That shows the blast damage zone of thickness was 0.5 m, where the Young's modulus, Mohr-Coulomb cohesion and Mohr-Coulomb friction were altered in the blast damaged zones using equations for blast damage factor (D) of 0.25, 0.5, 0.75 and 1.0, and are

presented in Table 7.4. A flowchart has been developed representing step by step procedure for numerical modelling of pillars in FLAC^{3D} as shown in the Figure 5.

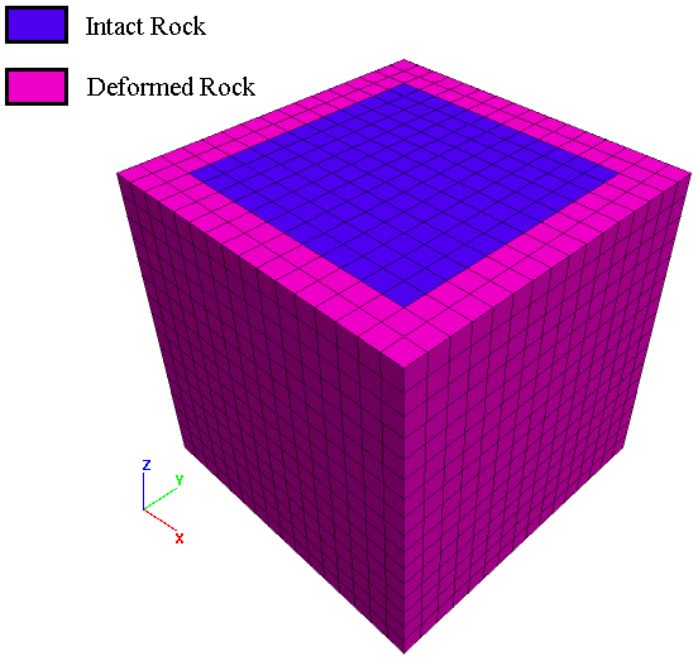

Figure 7.4: Pillar model with massive rock in the core and degraded rock on the sides

Table 7.4: Degraded rock properties

Damage Factor (D)	D = 0.25	D = 0.50	D = 0.75	D = 1.00
Degraded Modulus	54 GPa	39 GPa	27 GPa	18 GPa
Degraded Cohesion	6.1 MPa	5.5 MPa	4.9 MPa	4.1 MPa
Degraded Friction	41.1°	39.1°	36.3°	32.0°

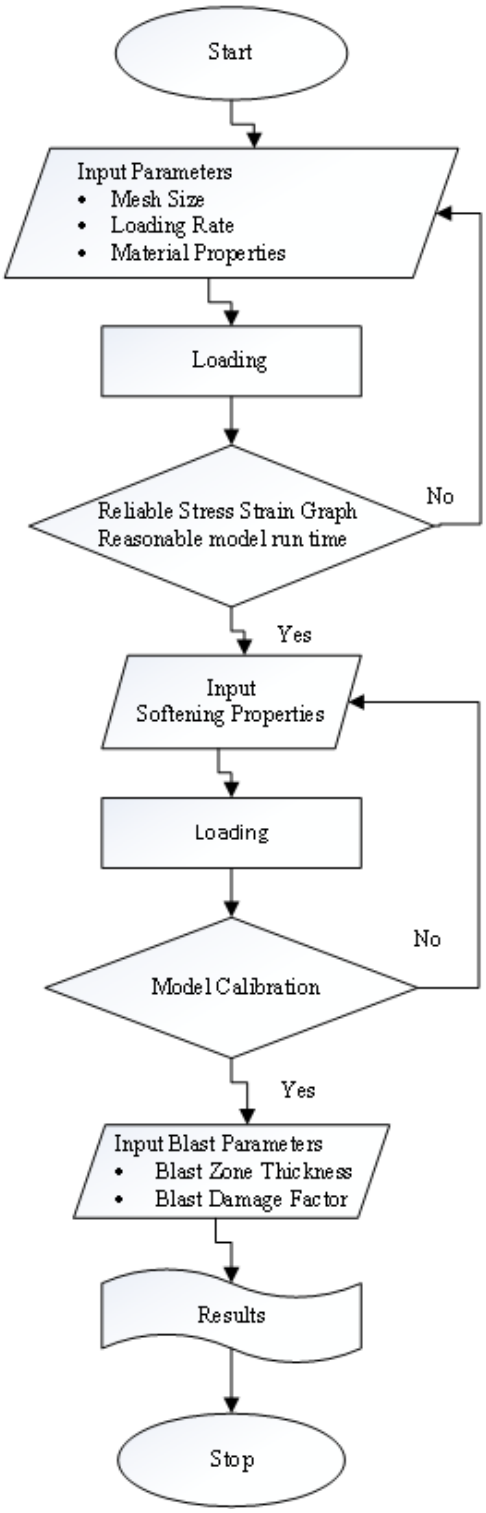

Figure 7.5. Flowchart indicating numerical modelling procedure in FLAC^{3D} to simulate pillars

7.3.5. Model Calibration:

The models were created at pillar width to height ratios of 0.5, 1.0, 1.5 and 2.0. The pillar height adopted in these models was about 4 m, which is similar to that of the pillar height in Lunder's Database (1994). The strength results were obtained through the stress strain curves developed by FISH code. The model strength of the pillars was then calibrated to that of the theoretical results as shown in Figure 7.6. It was observed that the difference between the model results and the theoretical results was less than 5%.

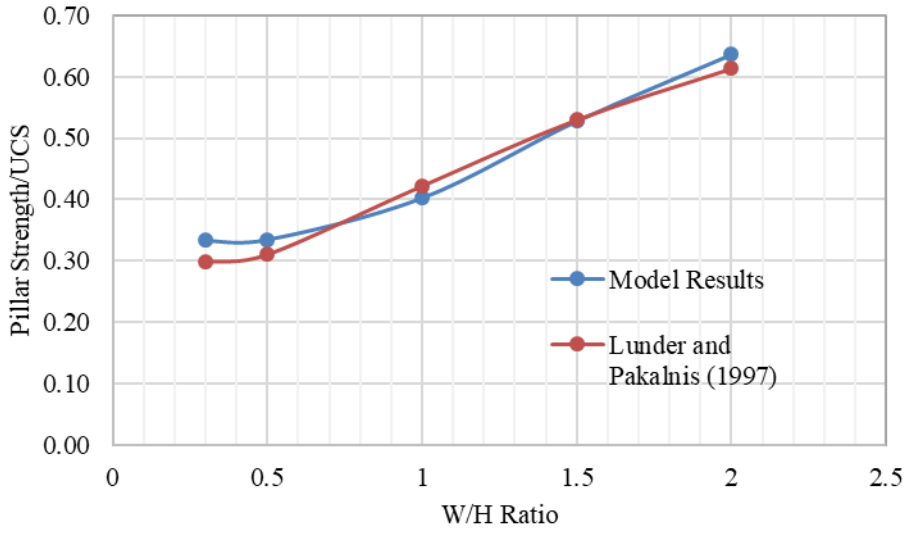

Figure 7.6: Model calibration results

7.4. Results and Discussion:

7.4.1. Effect of Blast Damage on Pillar width to Height Ratio:

Five width-to-height (W/H) ratios were simulated: 0.5, 1.0, 1.5, 2.0 and 2.5. These models used four different blast factors (D): 0.25, 0.50, 0.75 and 1.00, and four different blast thickness (T): 0.25 m, 0.50 m, 0.75 m, and 1.0 m. For a width to height ratio of 1.0, sixteen models were simulated to understand the blast effect on the pillar strength. Therefore, a total of eighty models were simulated to understand the blast effect on varying width to height ratio.

Assuming the blast damage on the pillars would decrease pillar strength, the results are presented in a normalized fashion, mainly for qualitative purposes, to understand the percentage decrease in pillar strength due to blasting when compared to the pillar strength with no damage effect. Pillar with no blast effect (disturbance factor of zero and damage thickness of 0) represents the baseline value. For example, if the pillar strength with no blast effect was 50 MPa and the pillar strength with 0.5 disturbance factor and 0.5m damage thickness was 35, then the normalized pillar strength ratio would be 1.0 for no blast effect and 0.7 for pillar with 0.5 disturbance factor and 0.5m damage thickness.

Assuming aforementioned methodology, the results are shown in Table 7.5. From the results, the blast effect on the slender pillars (W/H < 0.8), the damage has a little effect on the strength. It is due to the fact that the slender pillars fail in a brittle fashion which starts from the center of the pillar (Esterhuizen, 2006). The models show that the blasting had a more considerable effect on pillars with higher width to height ratios. With blast damage of 1m and disturbance factor of 0.75, the decrease in strength of pillar was observed to be about 7% for W/H ratio of 1, 16% for W/H ratio of 1.5, 22% for W/H ratio of 2.0 and 27% for W/H ratio of 2.5.

It was analyzed that the decrease in pillar strength with W/H ratio of 1.5 by 16% makes it equivalent to the pillar strength with W/H ratio of 1.0 with no blast effect. Similarly, 22% decrease in the pillar strength with W/H ratio of 2.0 has the pillar strength with W/H ratio of 1.5 with no blast effect. To take into account the blasting with disturbance factor of 0.75 and damage thickness of 1m, it can be recommended to add 1m along all the sides of the pillar. Therefore, the normalized strength of the pillars can be used to derive the thickness of the sides to be left on the pillars to account for blasting.

Table 7.5. Normalized pillar strength results at varying disturbance factor and blast damage thickness

W/H ratio	Disturbance Factor	Damage Thickness	Normalized Strength
1.0	0	0	1.00
1.0	0.25	0.25	0.98
1.0	0.25	0.50	0.97
1.0	0.25	0.75	0.96
1.0	0.25	1.00	0.94
1.0	0.50	0.25	0.98
1.0	0.50	0.50	0.97
1.0	0.50	0.75	0.97
1.0	0.50	1.00	0.94
1.0	0.75	0.25	0.99
1.0	0.75	0.50	0.97
1.0	0.75	0.75	0.96
1.0	0.75	1.00	0.94
1.0	1.00	0.25	0.99
1.0	1.00	0.50	0.96
1.0	1.00	0.75	0.95
1.0	1.00	1.00	0.93
1.5	0	0	1.00
1.5	0.25	0.25	0.98
1.5	0.25	0.50	0.96
1.5	0.25	0.75	0.94
1.5	0.25	1.00	0.93
1.5	0.50	0.25	0.96
1.5	0.50	0.50	0.91
1.5	0.50	0.75	0.88
1.5	0.50	1.00	0.86
1.5	0.75	0.25	0.92
1.5	0.75	0.50	0.85
1.5	0.75	0.75	0.85
1.5	0.75	1.00	0.84
1.5	1.00	0.25	0.91
1.5	1.00	0.50	0.86
1.5	1.00	0.75	0.84
1.5	1.00	1.00	0.84

2.0	0	0	1.00
2.0	0.25	0.25	0.98
2.0	0.25	0.50	0.96
2.0	0.25	0.75	0.93
2.0	0.25	1.00	0.94
2.0	0.50	0.25	0.96
2.0	0.50	0.50	0.92
2.0	0.50	0.75	0.88
2.0	0.50	1.00	0.87
2.0	0.75	0.25	0.93
2.0	0.75	0.50	0.86
2.0	0.75	0.75	0.82
2.0	0.75	1.00	0.80
2.0	1.00	0.25	0.89
2.0	1.00	0.50	0.81
2.0	1.00	0.75	0.77
2.0	1.00	1.00	0.78
2.5	0	0	1.00
2.5	0.25	0.25	1.00
2.5	0.25	0.50	0.99
2.5	0.25	0.75	0.95
2.5	0.25	1.00	0.97
2.5	0.50	0.25	0.98
2.5	0.50	0.50	0.95
2.5	0.50	0.75	0.89
2.5	0.50	1.00	0.88
2.5	0.75	0.25	0.95
2.5	0.75	0.50	0.89
2.5	0.75	0.75	0.86
2.5	0.75	1.00	0.83
2.5	1.00	0.25	0.92
2.5	1.00	0.50	0.83
2.5	1.00	0.75	0.79
2.5	1.00	1.00	0.73

Damage caused by blasting on the excavation has been considered as a technique to combat excessive stress accumulated near underground excavations in highly stressed

rock masses (Roux et al., 1957; Salamon, 1983; Andrieux et al., 2003; Sainag, 2008). Krauland and Soder, 1988 suggested that destressing and preconditioning practices strategically create fractures in the rock mass near excavation to soften the rock locally to transfer the stress away from the excavation boundaries. The models with blast damage show a similar effect on the pillars.

For this, five models were analyzed with a width to height ratio of 1.5 and five different blast damage combinations: D = 0 and T = 0 m, D = 0.5 and T = 0.5 m, D = 0.5 and T = 1.0 m, D = 1.0 and T = 0.5 m, and D = 1.0 and T = 1.0 m. The stress strain curve of these models is shown in Figure 7.7. It can be observed that the modulus of the pillars decreases with increase in disturbance factor and damage thickness. The stress strain curve of the pillar with no damage shows a point (40MPa) where the modulus changes which can be denoted as the pillar transitioning from brittle failure to shear failure. This transition happens in the pillar with blast damage of disturbance factor 0.5 at 48MPa and in the pillar with blast damage of disturbance factor 1.0 at 54MPa. It can be deduced that with the increase in blast damage, the tendency of the brittle failure increases in the pillars. Finally, it can be observed that the pillar with W/H ratio of 1.5 and disturbance factor of 1.0 and damage thickness of 1m is undergoing complete brittle failure.

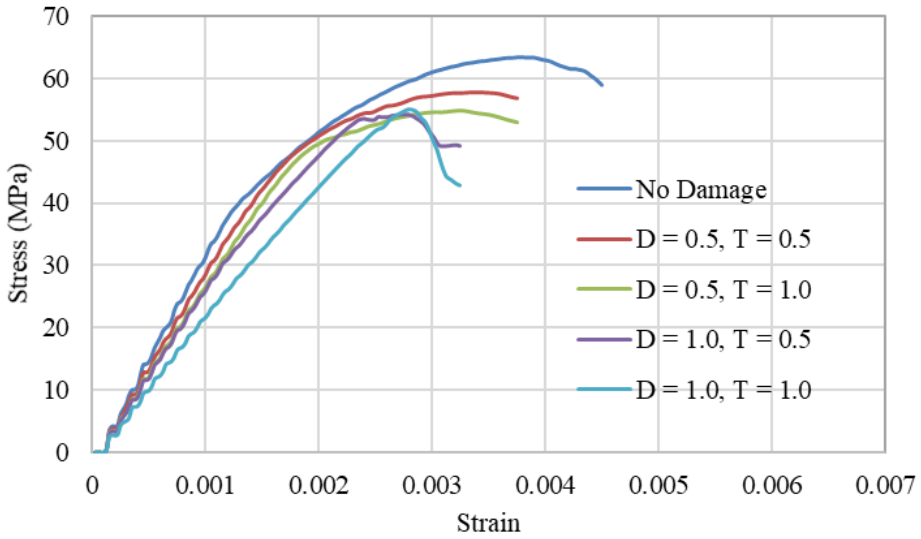

Figure 7.7: Stress-strain graphs of the pillars with blast damage

To understand the failure behavior of the pillars with blast damage, failure regions were observed from the plastic state plot to better describe the regions undergoing plastic flow. These plots can be used to determine which regions have or are undergoing shear and tensile failure. The plots show the failure regions at the central section of the pillar as shown in Figure 7.8. Three points on the stress strain curve in Figure 7.7 were selected which correspond to the plastic state plots in Figure 7.8. The points were selected in the following manner: before loading began, at the pillar failure initiation and at the transition point between brittle and shear failure. Before loading point shows the pillar with massive rock and degraded rock in the model, while the failure initiation point shows the crack initiation in the pillar and the transition point shows the total brittle failure in the pillar.

Based upon the plots in Figure 7.8b-d the following observations were made. In Figure 7.8b, the model plots have been extrapolated showing massive rock mass and degraded rock mass at the central section of the pillar. Initially, failure regions were analyzed in pillar with no damage. In the pillar without damage, the failure starts at the sides of the pillars (Figure 7.8c) and propagates the whole side into brittle failure (Figure 7.8d). In Esterhuizen (2006), similar brittle failure has been described in the pillars at higher width to height ratios.

Next the failure regions were analyzed in pillars with disturbance factor of 0.5 and blast damage thickness of 0.5m. Figure 7.8b shows the central section of the pillar with two zones on each side as the degraded rock in 0.5m damage thickness model. In Figure 7.8c, it can be observed that the failure initializes in the massive rock which can be ascribed to softening of the degraded rock due to blasting and the stresses getting transferred to the massive rock. In Figure 7.8d, it can be observed that the total brittle failure in the pillar has been increased when compared to that of the pillar without damage which can be attributed to increase in the transition point from brittle failure to shear failure to 48MPa. This can therefore, decrease the region for shear failure which ultimately decreases the strength of the pillar with blast damage.

For pillar with disturbance factor of 0.5 and damage thickness of 1.0m, Figure 7.8b shows the four zones on each side with degraded rock mass which account for one meter of blast damage thickness. In Figure 7.8c, it can be observed that the failure initiation occurs in massive rock as well as in the degraded rock which can be attributed to the higher stress causing fracture initiation in both the rock mass. The softening effect on the degraded rock due to blasting is evident while as the massive rock is far away from the boundary extents that the stresses required to initiate the fracture in the pillar affect both the massive rock mass as well as the degraded rock mass. In Figure 7.8d, at the transition point of brittle to shear failure in the pillar, it can be observed that the total brittle failure is more than that in the pillar without damage and pillar with disturbance factor of 0.5 and damage thickness of 0.5m. As the brittle failure in the pillar increases, the region undergoing shear failure decrease which in turn decreases the overall strength of the pillars.

Next the failure regions were analyzed in the pillars with disturbance factor of 1.0 and damage thickness of 0.5m which is shown in Figure 7.8b. In Figure 7.8c, it can be observed that the failure initiates in the massive rock mass due to the softening effect in the degraded rock mass caused due to blasting where stresses get transferred to the massive rock. In Figure 7.8d, it is observed that the degraded rock mass is so weak that it does not provide any confinement to the core which increases the brittle failure of the pillar and decreases the region for shear failure. Therefore, the overall strength of the pillar decreases significantly.

The pillar model with disturbance factor of 1.0 and damage thickness of 1.0 is shown in Figure 7.8b. It can be observed that the fracture initiation is evident in the massive rock mass which is beyond the very weak degraded rock mass. Figure 7.8c shows that the total brittle failure in the pillar which is more than any of the pillars analyzed above. Due to the very low confinement, this pillar with W/H ratio of 1.5, disturbance factor of 1.0 and damage thickness of 1.0 has a lower strength than that of the pillar with W/H ratio of 1.0.

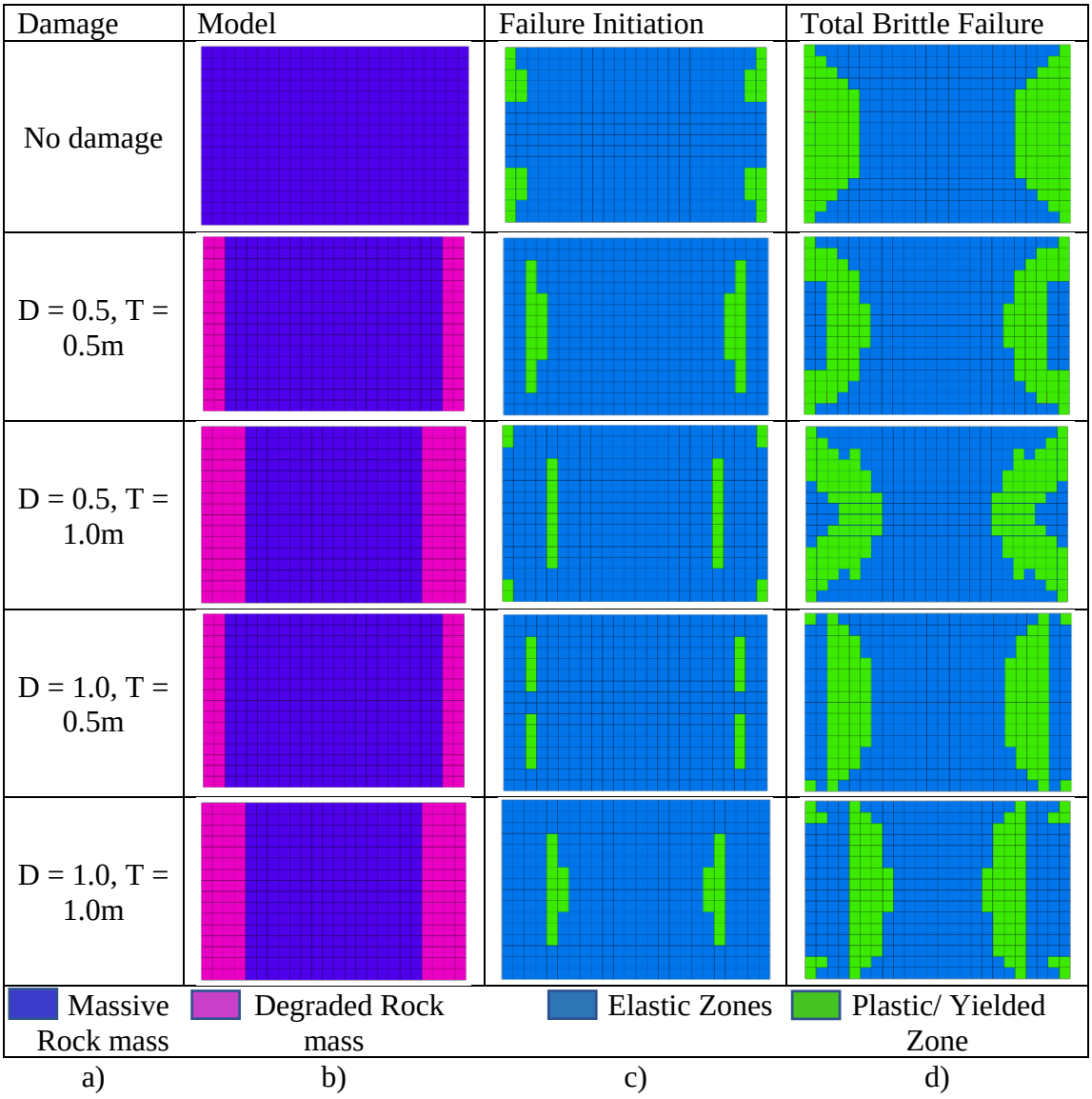

Figure 7.8: Plasticity state plots of pillar with W/H ratio of 1.5 with different damage characteristics a) model type b) model plots (point before loading) c) failure initiation point d) transition point (total brittle failure)

7.4.2. Effect of Blast damage on Pillar Height:

All the previous models to this point were modeled with a pillar height of 4m. Therefore, the effect of blast damage on a pillar width to height ratio of 1.5 at different pillar heights was also analyzed. Figure 7.9 shows three pillar sizes with pillar height of 2m, 4m and 6m and a damage thickness of 0.5m. Since this now incorporates different pillar heights, the

strength of the normal pillars was analyzed at different pillar width to height ratios. Figure 7.10 shows that shorter pillar heights represent higher strength while larger pillar heights lead to lower strength, in accordance with Kaiser (2010).

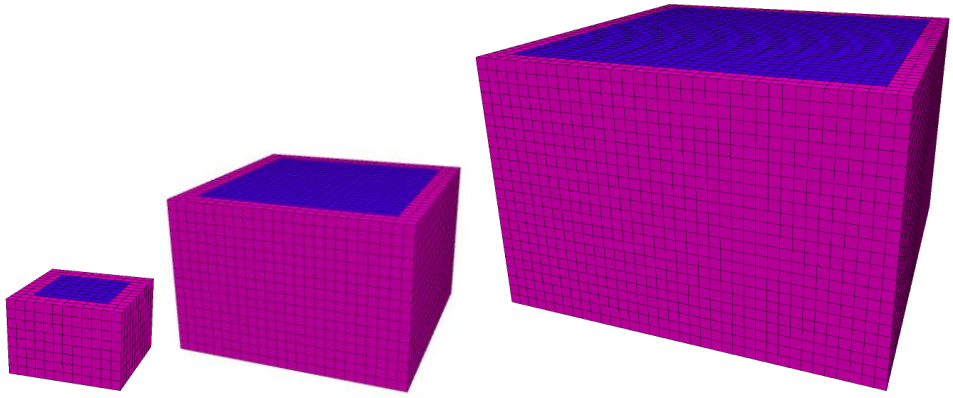

a) b) c)

Figure 7.9: Pillars with width to height ratio of 1.5 and pillar height of a) 2m b) 4m c) 6m

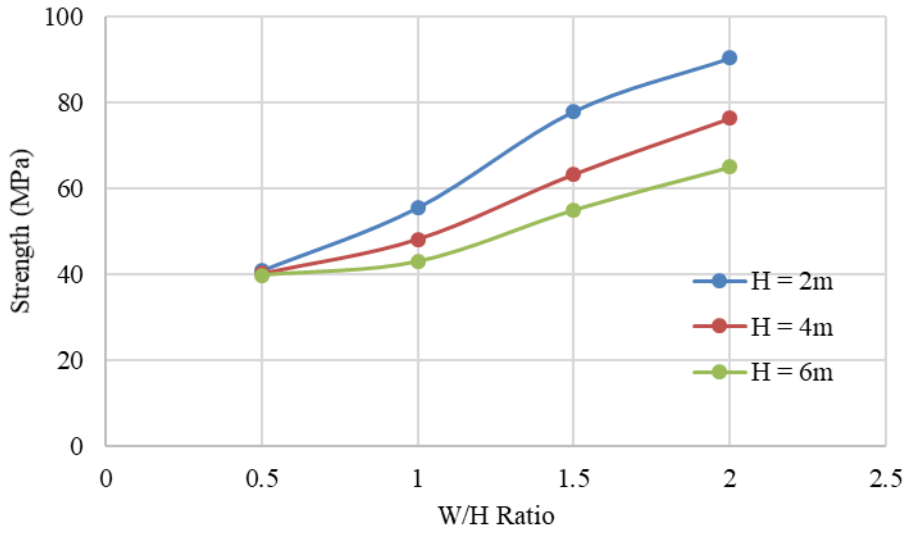

Figure 7.10: Pillar strength at different pillar heights

The pillars with a W/H ratio of 1.5 and damage factor (D) of 0.5 were analyzed at different blast thickness (T) of 0.25m, 0.5m, 0.75m and 1m. Figure 7.11 shows that the blast

damage has a significant effect on pillars with lower pillar height. It was also observed that at a blast thickness of 1.0m, the strength of the pillars with different heights converges to a single point with 10% deviation.

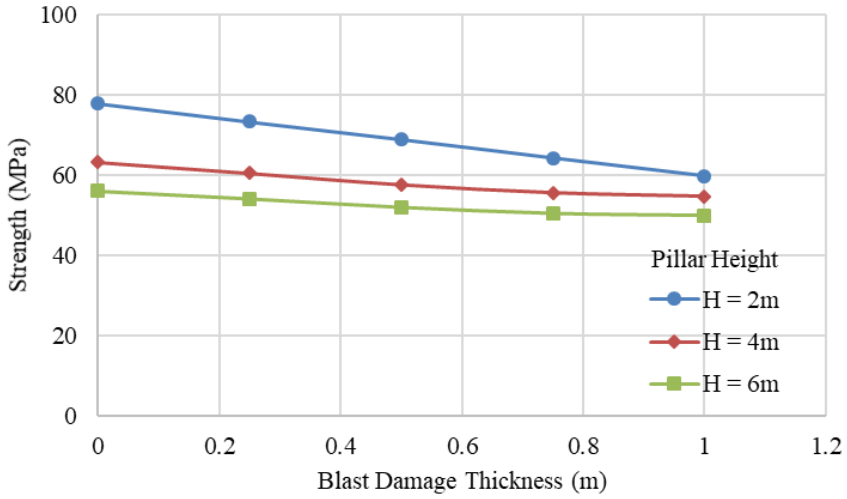

Figure 7.11: Pillar strength at different pillar heights with a blast damage of 0.5 at varying blast thickness with W/H ratio of 1.5

7.4.3. Effect of Blast Damage on Inclined Pillars:

The effect of blast damage on inclined pillars (Figure 7.12) was evaluated next. The strength of the inclined pillars with height of 4m with a W/H ratio of 1.5 were evaluated with a blast damage factor of 0.5 at different blast thickness. It was determined that the strength of the inclined pillars is less susceptible to blast damage. Figure 7.13 shows the decrease in strength of the pillars at 0°, 20° and 40° inclination with a W/H ratio of 1.5 and damage factor of 0.5 at varying blast thicknesses. Considering that the inclined pillars have less strength than that of the vertical pillars, the decrease in 10% of the pillar strength because of blasting in inclined pillars would lead to significant strength reduction.

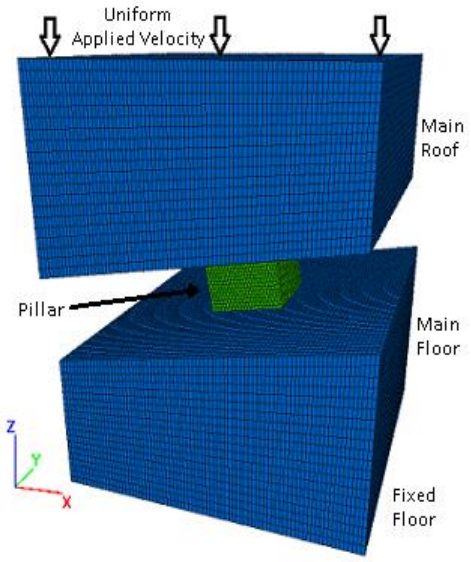

Figure 7.12: Inclined pillar model

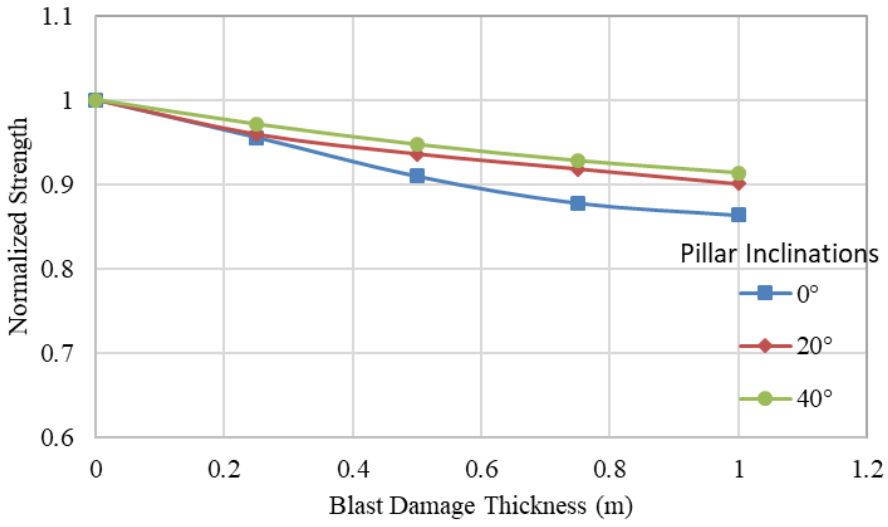

Figure 7.13: Effect of blast damage on inclined pillars at varying assumed blast damage thickness

7.5. Conclusions:

Based on the investigation of blast damage on hard rock pillars, the following conclusions can be drawn:

- Damage factor and damage thickness are important features that need to be considered when evaluating pillar strength. The decrease in pillar strength is considerable in pillars with W/H ratio higher than 1.0. The pillar strength can decrease upto 7% for W/H ratio of 1.0, 16% for W/H ratio of 1.5, 22% for W/H ratio of 2.0 and 27% for W/H ratio of 2.5.
- Considering a constant blast damage in the region, the hard rock mine pillars with larger W/H ratios would have more strength than that of the pillars with smaller W/H ratios.
- The numerical models with W/H ratio of 0.5 show that the pillar failure starts at the center of the pillar which is also evident with the pillars with damage and W/H ratio 0.5. Therefore, the slender pillars are prone to strain bursting with or without the damage due to blasting. As the pillar failure occurs from the center of the pillar, the strength of the pillar remains similar.
- Numerical models revealed that the brittle failure plays an important role in defining the strength of the pillars with blast damage zone. Initiation of the brittle failure beyond the damaged zone resulting in reduction of core causes failure at a relatively low brittle failure in the pillar resulting in loss of pillar strength.
- Numerical model results show that the degraded rock modulus in the blast damage zone is a significant parameter in softening the rock resulting in transfer of the stresses inside the pillar. Blast damage zone which is itself a critical factor leads to increase of the brittle failure in the pillar resulting in loss of pillar strength.
- Pillar height is an essential dimension in determining the strength of the pillars. Blast thickness on pillars with different heights at constant W/H ratios has a distinct impact on reduction of pillar strength. Blast damage causes substantial

reduction of the pillar strength with smaller heights and insignificant reduction with larger pillar heights.

- Inclined pillar strength is less susceptible to blast damage. The blast damage on the dip sides of the inclined pillar is more significant on the pillar strength reduction than on the normal sides. When compared to the vertical pillars, the inclined pillars have lower strength at a constant width to height ratio.
- A methodology has been presented for analyzing the strength and failure characteristics of hard rock pillars. This methodology can help engineers generate models to analyze the failure mechanisms in these pillars due to blasting damage.
- Considering blast damage when designing pillars could enhance mine safety and improve stability and possibly profitability.

References:

Andersson, P. (1992). Excavation disturbed zone in tunneling. SveBeFo Report No. 8 Swedish Rock Engineering Research, Stockholm.

Andrieux, P. P., Brummer, R. K., Liu, Q., Simser, B. P. and Mortazavi, A. (2003). Large scale panel destress blast at Brunswick mine. Journal Canadian Institute of Mining, Metallurgy and Petroleum. 78–87.

Ayres da Silva, L. A., Ayres da Silva, A. L. M. and Sansone, E. C. (2013). The shape effect and rock mass structural control for mine pillar design Rock Mechanics for Resources, Energy and Environment. 563–567

Djordjevic, N. (1999). Two-Component Model of Blast Fragmentation. Proceeding of the International Symposium on Rock Fragmentation by Blasting, Fragblast 6, Johannesburg, South Africa, SAIMM, pp. 213-219.

Elmo, D., and Stead, D. (2010). An integrated numerical modelling–discrete fracture network approach applied to the characterisation of rock mass strength of naturally fractured pillars. Rock Mechanics and Rock Engineering 43(1):3–19

Esterhuizen, G. S., Dolinar, D. R. and Ellenberger, J. L. (2008). Pillar strength and design methodology for stone mines. Proceedings of the 27th International Conference on Ground Control in Mining. Morgantown, WV: West Virginia University, pp. 241–253.

Esterhuizen, G. S. (2006). An evaluation of the strength of slender pillars. Transactions of Society for Mining, Metallurgy, and Exploration, Inc. 320: 69–76.

Forsyth, W. W. and Moss, A. E., Editors. (1991). Investigation of development blasting practices. CANMET MRL, 91 143 pp.

Fleetwood, K. G. (2010). Near-field blast vibration monitoring and analysis for prediction of blast damage in sublevel open stoping. (Dissertation). Kalgoorlie (WA): Curtin University.

Hedley, D. G. F. and Grant, F., (1972). Stope and pillar design for the Elliot lake uranium mines. Can. Inst. Min. Metall. Bull. 65: 37–44.

Hoek, E. and Diederichs, M. S. (2006). Empirical estimation of rock mass modulus. International Journal of Rock Mechanics and Mining Sciences. 43:203–215.

Hoek, E., Carranza Toress, C. and Corkum, B. (2002). Hoek-Brown failure criterion – 2002 edition, Proc. 5th. North American Rock Mechanics Symposium and 17th Tunneling Association of Canada Conference. ATM TAC 2002. University of Toronto, University of Toronto, pp. 267-271.

Itasca Consulting Group, (2016). Fast Lagrangian Analysis of Continua in 3Dimensions, Minneapolis, Minnesota, USA

Kaiser, P. K., Kim, B., Bewick, R. P. and Valley, B. (2010). Rock strength and depth and implications for pillar design. 5th International Seminar on Deep and High Stress Mining, Santiago, Chile, 463-476.

Kaiser, P. K, Diederichs, M. S., Martin, C. D., Sharp, J. and Steiner, W. (2000). Underground works in hard rock tunnelling and mining. Proceedings of GeoEng2000, Melbourne, ICMS. p. 841–926

Kutter, H. K., Fairhurst, C. (1971). On the Fracture Process in Blasting. Int. J. Rock Mech. Min. Sci. 8:181-202.

Krauland, N. and Söder, P. E. (1988). Rock stabilisation by destress blasting experiences from Boldien mines, Rock Mechanics Meeting, BeFo, Stockholm, Sweden.

Lu, J., Ray, A., Morsey, K. and Peng, S. (2008). Effects of rock/coal interface property on coal pillar strength. In: Proceedings of the 27th International Conference on Ground Control in Mining:262-267;2008.

Lunder, P. J. (1994). Hard Rock Pillar Strength Estimation an Applied Approach. (Thesis). Vancouver (BC): University of British Columbia.

Martin, C. D., Kaiser, P. K., McCreath, D. R. (1999). Hoek–Brown parameters for predicting the depth of brittle failure around tunnels. Canadian Geotechnical Journal. 36(1):136–151.

Mitelman, A. and Elmo, D. (2014). Modelling of blast-induced damage in tunnels using a hybrid finite-discrete numerical approach. Rock Mechanics and Geotechnical Engineering. 6(6):565–573.

Olsson, M. and Ouchterlony, F. (2003). New formula for blast induced damage in the remaining rock. SveBeFo Report No. 65, Swedish Rock Engineering Research, Stockholm.

Oriad, L. L. (1982). Blasting effect and their control. In: W. Hustrulid (Editor), Underground Mining Methods Handbook. Soc. Mining Engg., AIME, New York, pp. 1590-1603.

Ouchterlony, F., Olsson, M. and Bergqvist, I. (2001). Towards new Swedish recommendations for cautious perimeter blasting, EXPLO 2001, Hunter Valley, NSW, Australia.

Perry, K. A., Unrug, K. F., Harris, K. W. and Raffaldi, M. J. (2013). Influence of Roof/Floor Interface on Coal Pillar Performance. In: Proceedings of the 32nd International Conference on Ground Control in Mining.

Potvin, Y., Hudyma, M. and Miller, H. D. S. (1989). Rib pillar de sign in open stoping. *Can. Inst. Min. Metall. Bull.* 82:31–36.

Roux, A. J. A, Leeman, E. R. and Denkhaus, H. G. (1957). Destressing: a means of ameliorating rockburst conditions. Part I: the concept of destressing and results obtained from its application. SAIMM: 101–127.

Salamon, M. G. D. (1983). Rockburst hazard and the fight for its alleviation in South African Gold Mines. Rockbursts: Prediction and Control. IMM, London: 11-36.

Saiang, D. (2008) Blast-induced damage: a summary of SveBeFo investigations. Luleå: Luleå tekniska universitet, (Technical report / Luleå University of Technology, n. 21, 2008). 42 p.

Sharifzadeh, M. and Pal, M. (2014). Quantification of rock mass disturbance using rock-mass property, rock characterization and blast characterization in underground hard-rock, in proceeding of the 8th Asian Rock Mechanics Symposium, Oct 14-16, Sapporo, Japan: ARMS. p. 518-527

Shen, B. and Barton, N. (1997). Disturbed zone around tunnels in jointed rock masses. International Journal of Rock Mechanics and Mining Sciences. 34(1): 117-125.

Suorineni, F. T., Mgumbwa, J. J., Kaiser, P. K. and Thibodeau, D. (2011). Mining of orebodies under shear loading Part 1 – case histories, Mining Technology (Trans. Inst. Min. Metall. A), 120(3):138–147.

Suorineni, F. T., Mgumbwa, J. J., Kaiser, P. K. and Thibodeau, D. (2014). Mining of orebodies under shear loading Part 2 – failure modes and mechanisms, Mining Technology (Trans. Inst. Min. Metall. A), 123(4):240–249.

Torbica, S. and Lapčević, V. (2015). Estimating extent and properties of blast-damaged zone around underground excavations. Rem: Revista Escola de Minas, 68(4):441–453

Warneke, J., Dwyer, J. G. and Orr, T. (2007). Use of a 3 D scanning laser to quantify dift geometry and overbreak due to blast damage in underground manned entries. In: E. Eberhardt, D. Stead and T. Morrison (Editors), Rock Mechanics: Meeting Society's Challenges and Demands. Taylor & Francis Group, London, Vancouver, Canada, pp. 93-100

Wilson, W. H. and Holloway, D. C. (1987). Fragmentation Studies in Instrumented Concrete Models. Proceedings of the International Congress on Rock Mechanics, Herget and Vongpaisal (eds), Montreal, Canada, International Society for Rock Mechanics, pp.735-741.

Yu, T. R. and Vongpaisal, S. (1996). New blast damage criteria for underground blasting. CIM Bulletin, 89(998): 139–145.

Chapter 8

Direct Strain Evaluation Method for Laboratory based Pillar Performance

This chapter has been accepted with minor revisions in JRMGE as:

K.V. Jessu, A.J.S. Spearing (2019) Direct Strain Evaluation method for Laboratory based Pillar Performance. Journal of Rock Mechanics and Geotechnical Engineering (Accepted. Yet to Publish)

Abstract

Pillar stability is one of the basic and important safety and economic design aspects for underground mines. Generally, the stability of the pillars is evaluated through empirical approaches which are based on case studies and rock mass conditions in the mines, so the applicability can be constrained. The numerical based approaches are potentially more useful as parametric studies can be undertaken and if calibrated can be more representative. Both empirical and numerical approaches are dependent on the strength evaluation of the pillars while the strain developed in the pillars is seldom taken into the consideration. Sakurai (1981) developed a failure strain method which can be adapted to understand the pillar stability. For this chapter, gypsum and sandstone samples were tested in the laboratory with different width to height (W/H) ratios to adapt the strain evaluation method to the laboratory-based pillars. A correlation was then developed between the strain and the width to height ratio for the pillar monitoring purposes. Based on the results, a flowchart has been created to conduct back analysis on the existing pillars to establish their stability and design new pillars taking into consideration the strain analysis of the existing pillars within the W/H ratios modelled.

Keywords: Failure strain; Critical Strain; Pillars; Width-to-height ratio; Stability

8.1. Introduction

Pillars can be defined as the insitu rock mass left in between two or more underground openings for stability and support purposes. Nordlund et al., (1995) stated that the pillar stability should be considered to be important for the stability of the walls, floor, and roof. Pillars are an essential part of most underground mining methods where instability could cause significant falls or catastrophic damage, for example, failure of 4 pillars in the central section of a room-and-pillar metal mine led to a run-on failure of almost 100 pillars (Dismike et al., 1994; Zipf, 2001).

Empirical and numerical approaches are the typical methods employed to design pillas in underground mines. Salaman and Munro (1967) introduced a pillar design method resulting from the Coalbrook colliery pillar failure disaster based on the tributary area

theory and 27 failed pillars. Hedley and Grant (1972) conducted one of the earliest research in the Canadian uranium mines based on the stable, unstable and failed pillars in the mines in order to develop a relationship between the pillar strength, width-to-height ratio, and unit strength of rock. By analyzing 178 pillars, Lunder and Pakalnis (1997) proposed a confinement parameter and developed the following relationship:

$$\sigma_p = K * UCS * (C1 + C2 * \kappa) \tag{8.1}$$

where σ_p is the ultimate strength of the pillar (MPa), K is the pillar size factor, UCS is the uniaxial compressive strength of the intact rock (MPa), C1 and C2 are the empirical rock mass constants and κ is the friction term which is calculate as:

$$\kappa = \tan\left[cos^{-1}\left(\frac{1 - C_{pav}}{1 + C_{pav}}\right)\right] \tag{8.2}$$

$$C_{pav} = Coeff * \left[Log\left(\frac{W}{H} + 0.75\right)\right]^{1.4(W/H)} \tag{8.3}$$

where C_{pav}, the average pillar confinement and the Coeff is the coefficient of pillar confinement. It can be argued that the approaches proposed by Hedley and Grant (1972) and Lunder and Pakalnis (1997) are the two most common methods that are used to design the pillars in hard rock underground mines. Few other researchers (Kimmelmann, et al, 1984; Krauland and Soder, 1987; Potvin et al., 1989; Sjoberg, 1992) developed empirical relations to evaluate the strength of the pillars.

Martin and Maybee (2000) investigated the pillar strength using both empirical and numerical modelling, and they concluded that the Hoek-Brown brittle failure criterion is suitable for predicting the strength of the pillars. Numerical approaches (Hoek and Brown, 1980; Kaiser and Tang, 1998; Esterhuizen et al., 2006, 2008; Suroineni et al., 2011, 2014) were adopted to understand the failure modes of pillars at different width-to-height ratios and to develop relationships between the strength and width-to-height ratio of pillars. All these approaches deal with the strength of the pillar while strain developed in the pillars has been basically ignored for design purposes. The strain can be measured in situ by

extenso-meters, convergence meters and strain guages on instruments, which can then be used to account for the stable, unstable and failure statuses of the pillars according to the real-time montioring.

Lane et al. (2001) and Roberts et al. (2007) conducted studies on the pillars in Doe Run Lead Mines in Missouri, USA and they calibrated the NFOLD, a Displacement-Discontinuity stress analysis method with the convergence readings of the pillars to the model and developed the progressive failure mechanism of the pillas. Estimating the strain developed in the pillars is one of the best means to back analyze the stability of the pillars. Therefore, a strain-based evaluation of the pillars would be ideal to understand the performance of the pillars.

Sakurai (1981) developed a direct strain evaluation method which was applied to the stability analysis of tunnels. The method describes the critical strain (ε_c) as the ratio of the uniaxial compressive strength (UCS) to the elastic modulus (E_{50}) of rocks, which is given as:

$$\varepsilon_c = \frac{UCS}{E_{50}} \tag{8.4}$$

The critical strain was developed from the laboratory tests, which differs from the field-scale critical strain. Therefore, a factor p was introduced to account for the rock mass behavior to calculate the critical strain from the laboratory test. The critical strain in the field scale was dependent on the rock type and the p factor, ranging from 1 to 3.5 for granite, sandstone and shale (Sakurai 1999).

Sakurai (1981) described that the failure strain (ε_f) is different from the critical strain (ε_c) as shown in Figure 8.1. It was concluded that for brittle materials, the critical strain was observed to be same as the failure strain. The soft materials showed a large difference in the critical and failure strains. Therefore, a co-relation between the failure and critical strains was established:

$$\varepsilon_f = \frac{\varepsilon_c}{1 - R_f} \tag{8.5}$$

where R_f is a parameter that defines the conversion of the failure strain to the critical strain and was found to lie in between 0.05 and 0.8. It was basically derived from the UCS of samples in the laboratory. The samples for UCS tests carried out by Sakurai (1981) have a width-to-height ratio of 0.4, while it can be adapted to different width-to-height ratios to simulate the pillars.

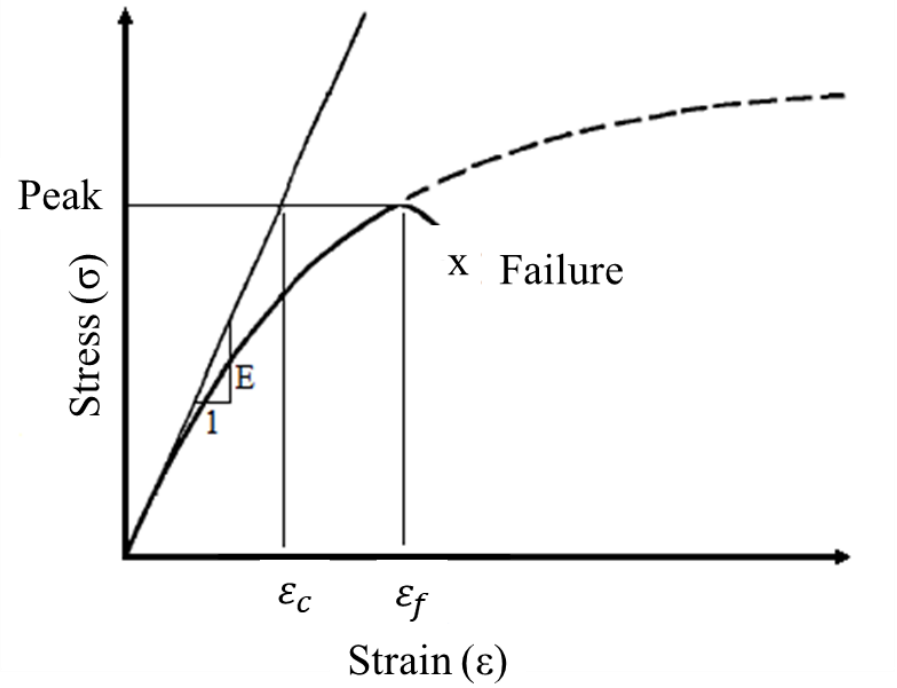

Figure 8.1: Sakurai's (1981) illustration for critical and failure strain

Based on the generalized crack initiation and propagation thresholds (Cai et al., 2004), the R_f was determined by Cai et al. (2011), which ranged in between 0.1 and 0.3 for most hard rockmasses in underground excavations. It was indicated that the damage coalesence near the peak strength is a major factor for the R_f which can also increase upto 0.4. Idris et. al, 2015 adopted the direct strain evaluation theory and defined R_f as 0.2 for understanding the performance of the pillar by numerical modelling for different rock mass properties. Napa-García and Navarro Torres (2017) conducted numerical studies

with the strain criterion theory by applying Hoek-Brown constitutive model and varying width-to-height ratios, geological strength index (GSI), m_i, and UCS. A relationship was developed between the width-to-height ratio of the pillars and R_f factor where R_f was found to be in the range of 0.5-0.95. The relationship developed had high variablility in the values of R_f factor. This can be due to the different strength of the rocks as suggested by Sakurai (1999), the critical strain varies highly with the rock types.

Esterhuizen (2006) indicated that the pillars for a lower width-to-height ratio, the peak load at the onset of brittle spalling and the ultimate strength can be small. This implies that the critical strain and the failure strain are small which shows that strain can be used as a parameter to understand the stability of the pillars.

This chapter will deal with the laboratory-based strain evaluation method adopted from Sakurai (1981) for higher width-to-height ratios for two different materials, and co-relations of critical strain, failure strain and width-to-height ratio will be expressed and used for back analysis in the mines.

8.2. Materials and Test Methods

Moulded Gypsum and Sandstone Core samples under uniaxial compression loading were tested in this study. The moulded gypsum has been extensively used as a representation of brittle rock by many researchers (Bobet and Einstein, 1998; Wong et al., 2009). It can be prepared by mixing the gypsum powder ($CaSO_4.{}^1/_2\,H_2O$) with water and then being stored in a 40°C oven to remove any excessive water after fabrication.

For the sake of consistency, all the samples were prepared at the same time in a single batch were cast from a mixture of gypsum and water with mass ratios of 100:35 was cast into gypsum moulds. PVC tubes of 50mm inner diameter (Figure 8.2a) were used to cast the samples. The molds were kept in the oven at 40 °C until the mass of the samples reached a constant value in 3 days. The surfaces of the samples were ground to be smooth and parallel according to the ISRM standards (Ulusay and Hudson, 2007). Gypsum

samples of five width-to-height ratios are shown in Figure 8.2b. For each width-to-height ratio, five samples were tested, therefore, a total of 25 samples were cast.

Sandstone samples with two different diameters were used in the study i.e. 54 mm and 42 mm. The sandstone samples were prepared with five different width-to-height ratios. The surfaces at the ends were ground to achieve the parallel faces as specified in the ISRM standards (Ulusay and Hudson, 2007). Figure 8.3 shows the sandstone samples with four different width-to-height ratios. Three samples were tested on the sandstone samples of same different width-to-height ratio, therefore, in total 15 samples of 42 mm diameter and 15 samples of 54 mm diameter were tested. For simplicity, samples of 54 mm diameter is referred to as sandstone-54 and samples of 42 mm diameter as sandstone-42 .

a) b)

Figure 8.2: a) PVC pipes used for casting b) gypsum molds

Prepared moulded gypsum and sandstone samples were subjected to uniaxial compression loading in a Uniaxial Compression Testing Machine (Figure 8.4), which was controlled by a servo computer programme GCTS CATS 1.8 software. Load and displacement data were automatically recorded by the machine at a rate of 600 samples/min. The loading rate adopted was displacement-based and fixed at 0.12 mm/min which was in accordance with the ISRM standards that the UCS samples should fail in 5-10 minutes. The parameters used in this study are givenin Table 8.1.

a) b)

Figure 8.3: Sandstone samples with a diameter of a) 42mm b) 54mm

Figure 8.4: Uniaxial compressive testing machine

Table 8.1: Sample parameters and loading conditions.

Specimen Parameters
Rock Type (Molded Gypsum, Sandstone) Specimen Width (42 mm, 50 mm, and 54 mm) Width-to-Height ratio (0.4, 0.5, 1.0, 1.5, 2.0)
Loading Condition
Uniaxial Compressive Loading (0.12 mm/min)

8.3. Results and Discussion:

8.3.1. Rock Properties of the Rock Types:

Initially, the samples with a width-to-height ratio (W/H) of 0.4 or a length-to-diameter ratio of 2.5, as per the ISRM standards, were tested for elastic modulus and UCS of rock. Three types of samples were chosen for testing, including moulded gypsum and sandstone in the diameter of 54 mm and length of 135 mm, and sandstone in the diameter of 42mm and length of 105 mm. The stress-strain graphs of the UCS samples of molded gypsum, sandstone-54, and sandstone-42 are presented in Figure 8.5a, 8.6a, and 8.7a respectively. The failure modes were found to be axially splitting in the gypsum samples and single shear plane failure in the sandstone samples, as shown in Figure 8.5b, 8.6b, and 8.7b. The properties of the samples are represented in Table 8.2.

The results show that the UCS of the samples ranges from 13MPa to 27 MPa. The standard deviation is 1–2 MPa, which is less than 10% of the strength results. The elastic modulus was determined by the slope at half of the peak strength as shown in Figure 8. It was found that the elastic modulus is in the range of 2.8-3.8 GPa for all the rock types. The deviation was about 0.03-0.20 GPa which is less than 10% of the modulus results. Despite being moulded, the strength of gypsum samples presented large variaion ((maximum - minimum)/average = 29%) and medium coefficent of variation (COV) of 12%, while the deformation modulus showed small COV of 7%. Since these materials are remoulded, small variations were to be expected to agree with the deformation results. It was also observed that, despite being natural, the sandstone exhibited smaller variation than the moulded gypsum.

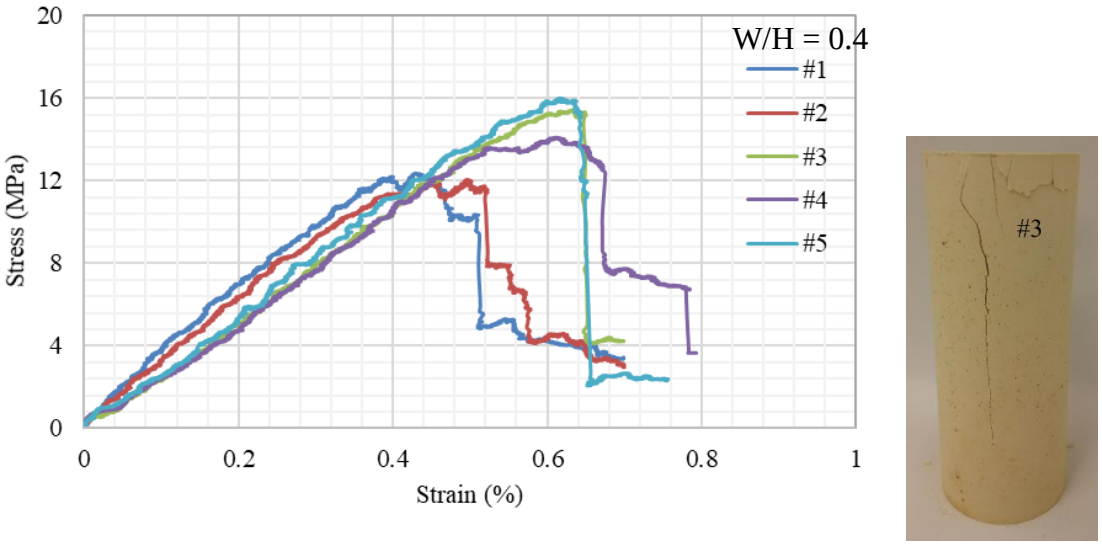

a) b)

Figure 8.5: a) Stress-strain curves and b) failure mode of moulded gypsum samples under uniaxial compression loading

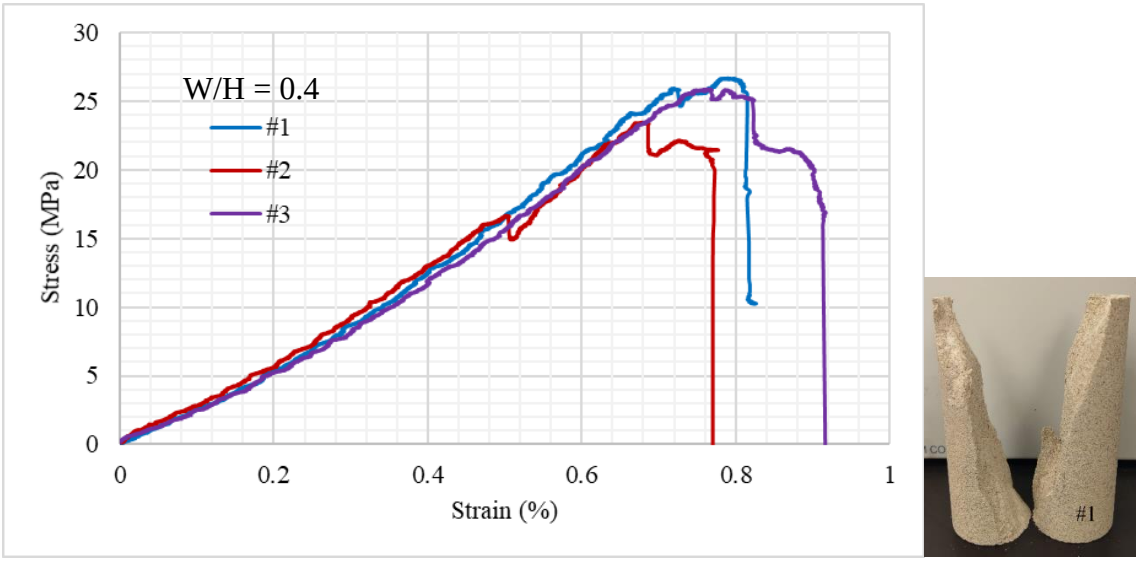

a) b)

Figure 8.6: a) Stress-strain curves and b) failure mode of sandstone-54 samples under uniaxial compression loading

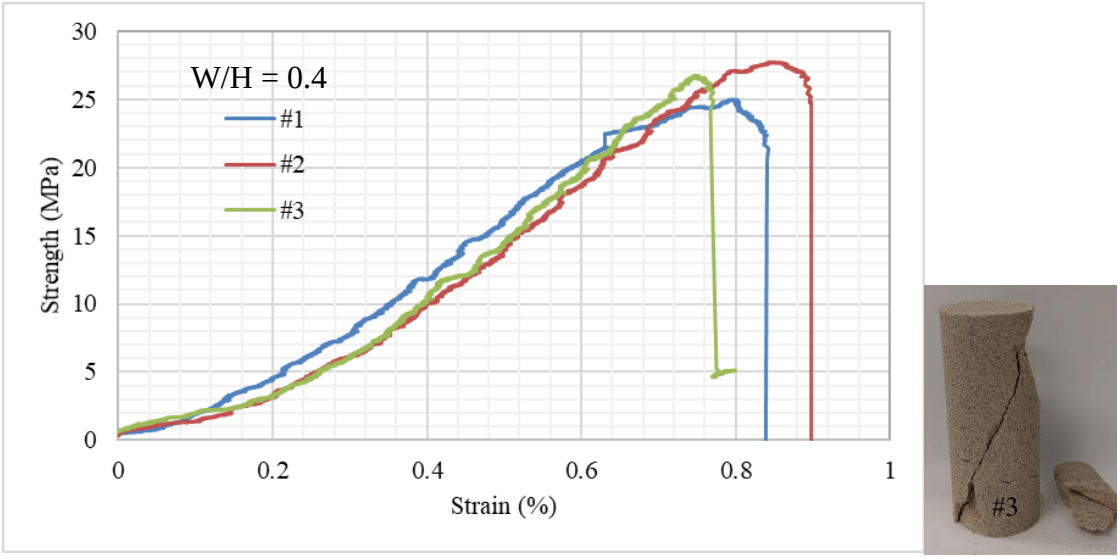

Figure 8.7: a) Stress-Strain curves and b) failure mode of sandstone-42 samples under uniaxial compression loading

Table 8.2: Results of UCS and Elastic Modulus

Properties / Sample	Average UCS (MPa)	UCS Standard Deviation (MPa)	Coefficent of Variation	Average Elastic Modulus E_{50} (GPa)	E_{50} Standard Deviation (GPa)	Coefficent of Variation
Molded Gypsum	13.9	1.8	12%	2.8	0.20	7%
Sandstone-54	25.3	1.7	7%	3.6	0.03	1%
Sandstone-42	26.9	2.2	8%	3.8	0.20	5%

Hoek and Brown (1980) developed a relationship between the diameter and the strength of intact rock samples, which is given as:

$$\sigma_{cd} = \sigma_{c50}\left(\frac{50}{d}\right)^{0.18} \tag{8.6}$$

where σ_{cd} is the UCS of the sample with the diameter d and σ_{c50} is the UCS of the sample with the diameter 50 mm.

According to Equation (8.6), as the diameter decreases, the strength of the sample increases.

From Table 8.2, it can be observed that the strength of the sandstone-54 is less than that of the sandstone-42. To compare the strengths of the sandstone samples with diameter of 42 mm and 54 mm, the UCS of 50 mm diameter was calculated by Equation (8.6). It was found that the sandstone samples follow the relationship developed by Hoek and Brown (1980), and σ_{c50} was equal to 25.7 MPa for samples of 54 mm diameter and 26.1 MPa for samples of 42 mm diameter.

Table 8.3: Comparision of UCS of samples with different diameters.

Specimen	Diameter (mm)	UCS (MPa)	σ_{c50} (MPa)
Sandstone-54	54	25.3	25.7
Sandstone-42	42	26.9	26.1

Direct Strain Evaluation method was applied to the UCS samples. The critical strain was calculated by determining the ratio of peak strength to the elastic modulus of the sample. The strain measured at the peak strength from the stress-strain curves is the failure strain. Taking one of the moulded gypsum sample for example, its peak strength, failure strain, elastic modulus and calculated crtical strain were determine, as shown in Figure 8.8. The peak strength was identified as 15.4 MPa and the failure strain was observed as 0.6346. Elastic modulus was determined by regression analysis, as shown in Figure 8.8. The critical strain was calculated using Equation (8.4).

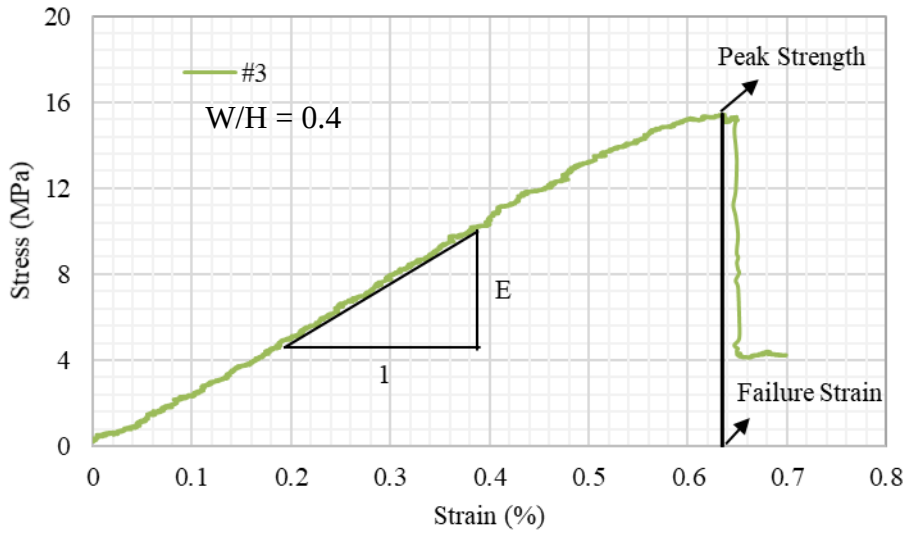

Figure 8.8: Example of measuring the failure strain, peak strength and elastic modulus of moulded gypsum sample with W/H = 0.4.

The R_f factor was then calculated by Equation (8.5) and is presented in Figure 8.9. From the Equation 8.5, it can be noted that when R_f is equal to zero, the critical strain is equal to the failure strain. It can be observed from Figure 8.9 that R_f is less than 0.1 or even close to zero, and the failure strain is slightly higher than the critical strain. This is due to the fact that in brittle materials, the failure strain is equal to the critical strain. The results observed are similar to those obtained in Sakurai (1981).

8.3.2. Strength and Strain Analysis of different W/H ratios:

The moulded Gypsum, Sandstone-54 and Sandstone-42 were tested at different width-to-height ratios of 0.5, 1.0, 1.5 and 2.0. The diameter was kept constant, i.e. 50 mm diameter for moulded gypsum, 54 mm for Sandstone-54, and 42 mm for Sandstone-42. The sample heights were varied to attain the different width-to-height ratios. The average strengths of the samples with the standard deviation are shown in Figure 8.10.

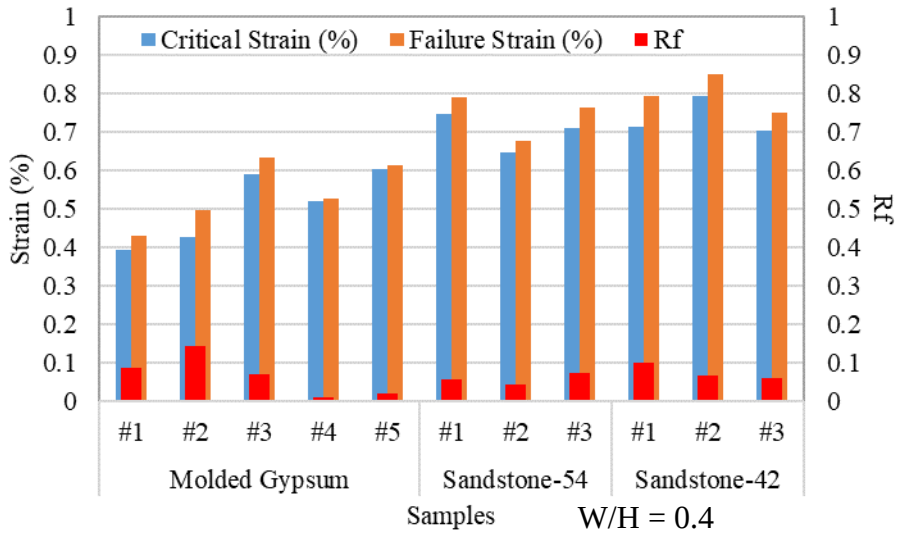

Figure 8.9: The critical strain, failure strain and R_f factor of all the UCS samples (W/H =0.4)

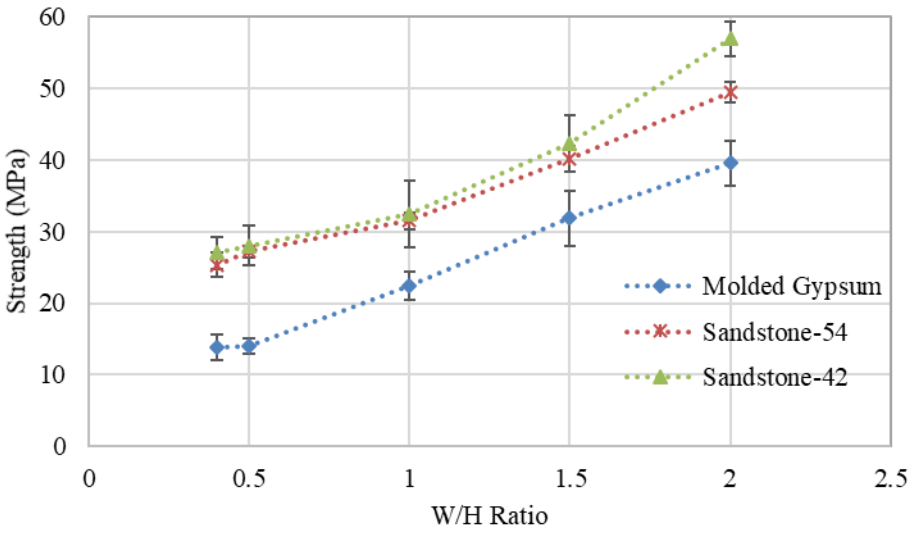

Figure 8.10: Strength of the samples at different width-to-height ratios

From Figure 8.10, it can be observed that the strength of the sandstone-42 is higher than that of the sandstone-54 samples due to the size effect. As the gypsum is softer than the sandstone, the strength of the gypsum was found to be the lowest at different W/H ratios. It is evident that the strength of the samples is positively corelated with the width-to-height

ratio due to the brittle behaviour observed in the slender samples, while in the samples with the higher width-to-height ratios, side spalling is evident, followed by the shear failure. The rate of increase in the strength is similar in both sandstone samples and the moulded gypsum.

The critical strain was obtained by the Equation (8.4) where the strength of the samples with different width-to-height ratios was divided by the average elastic modulus (Table 8.2). Figure 8.11 shows the critical strains obtained in all the rock samples. From Equation (8.4), it can be interpreted that the critical strain is dependent on the strength of the samples and it is clear that as the strength increases, the critical strain increases. The strength of the samples increases with the increase in width-to-height ratio, thus, the critical strain has a positive correlation with the width-to-height ratio. It is interesting to note that the strength varies largely for the two different rock types while the strain remains in a very small range of values. This shows that the ratio of strength to elastic modulus varies in a very a small range considering the two rock types.

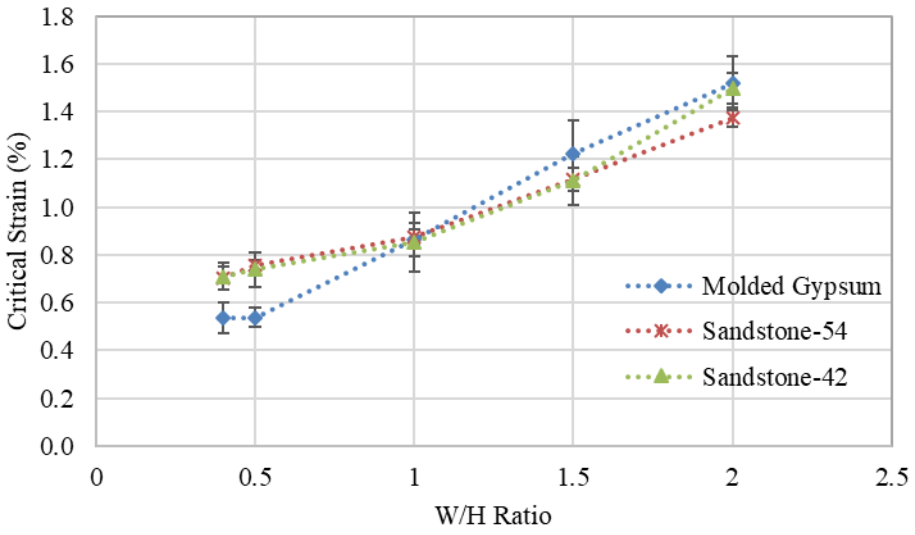

Figure 8.11: Critical strain verses width-to-height ratio

Using the help of stress-strain curves of the samples, the failure strains was obtained. Equation (8.5) was modified to create a simplified factor (SR_f) which relates the failure strain (ε_f) to critical strain (ε_c):

$$SR_f = \frac{\varepsilon_f}{\varepsilon_c} \tag{8.7}$$

Based on Equation (8.7), it can be interpreted that when the failure strain is equal to the critical strain, the factor is equal to 1 which represents the brittle failure of the samples. When the factor is higher than 1, the failure strain is much higher than the critical strain representing side spalling followed by the shear failure.

Figure 8.12 shows the simplified factor results for all the samples with different W/H ratios. It was observed that for W/H ratio of 0.5, the simplified factor is found to be 1, which indicates that the samples fail in the brittle manner. The simplified factor ranges from 1 to 3.5 and increases with the increase in W/H ratio. For all the rock types studied herein, assuming that the simplified factor has a linear relationship with W/H ratio, it can be represented as:

$$SR_f = 0.56 + 1.14 * \left(\frac{W}{H}\right) \qquad R^2 = 0.97 \tag{8.8}$$

Equation (8.8) can be better expressed as:

$$\varepsilon_f = \varepsilon_c \qquad For \frac{W}{H} < 0.5$$

$$\varepsilon_f = \left[0.56 + 1.14 * \left(\frac{W}{H}\right)\right] \varepsilon_c \qquad For\ 0.5 < \frac{W}{H} < 2.0 \tag{8.9}$$

this equation is only applicable for W/H ratios between 0.5 and 2. As Equation (8.9) is based on the laboratory experiments, the factor *p* suggested by Sakurai (1999) can be used to relate the laboratory-based critical strain to the field-based critical strain.

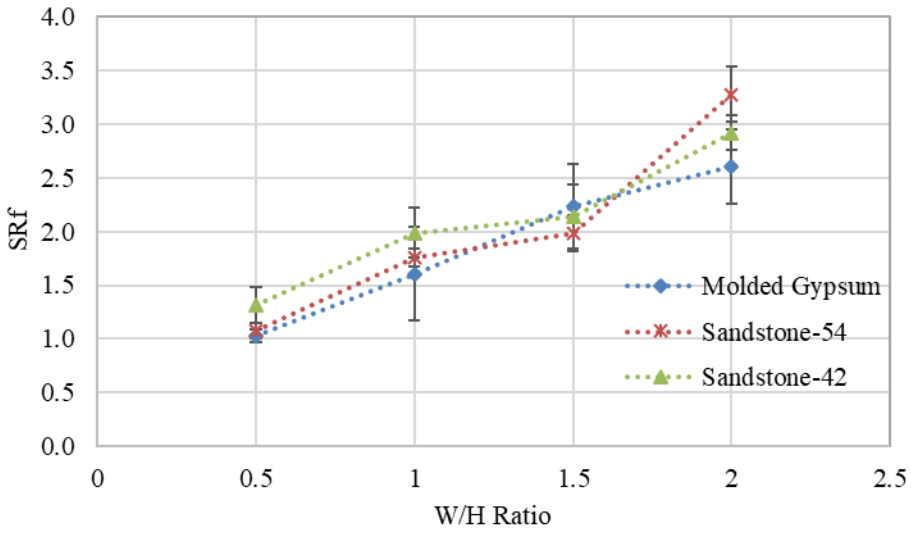

Figure 8.12: SR_f for all samples with different W/H ratios.

8.3.3. Application of the Strain Evaluation Method for Pillars

Back analysis can be adopted for monitoring and optimization of pillars. Displacements, strains and stresses measured in situ can be used as the input variables for understanding and optimizing the design. Displacements and strains can be obtained by convergence instruments, extensometers and instrumented rockbolts. In situ deformation modulus can be determined by plate bearing tests. With these input parameters and Equation (8.9), real-time stability analysis can be conducted through real time monitoring of the pillars and suggestions can be made for reinforcements and optimization of pillars.

To monitor the pillars with the strain evaluation method, the pillar stress of specific pillar should be evaluated. As pillars are developed with a factor of safety, the critical strain would be significant when it was calculated according to the pillar stress acting on the pillar rather than the pillar strength. Therefore, the pillar stress is taken into consideration to calculate the critical strain. The deformation modulus obtained from the plate bearing tests and the pillar stress would lead to the critical strain. The critical strain and the width-to-height ratio of the pillars can be used as the input parameters in Equation (8.9) to determine the failure strain. If the failure strain is higher than the strain observed by the instruments in situ, then the pillars are stable, and conversely the lower failure strain would

induce the failure of pillars. Under such circumstances, the pillars need to be redesigned with higher safety factors and extra reinforcements are required such as rockbolts, cablebolts, shotcrete etc. The flowchart of applying the strain evaluation method to pillars is shown in Figure 8.13.

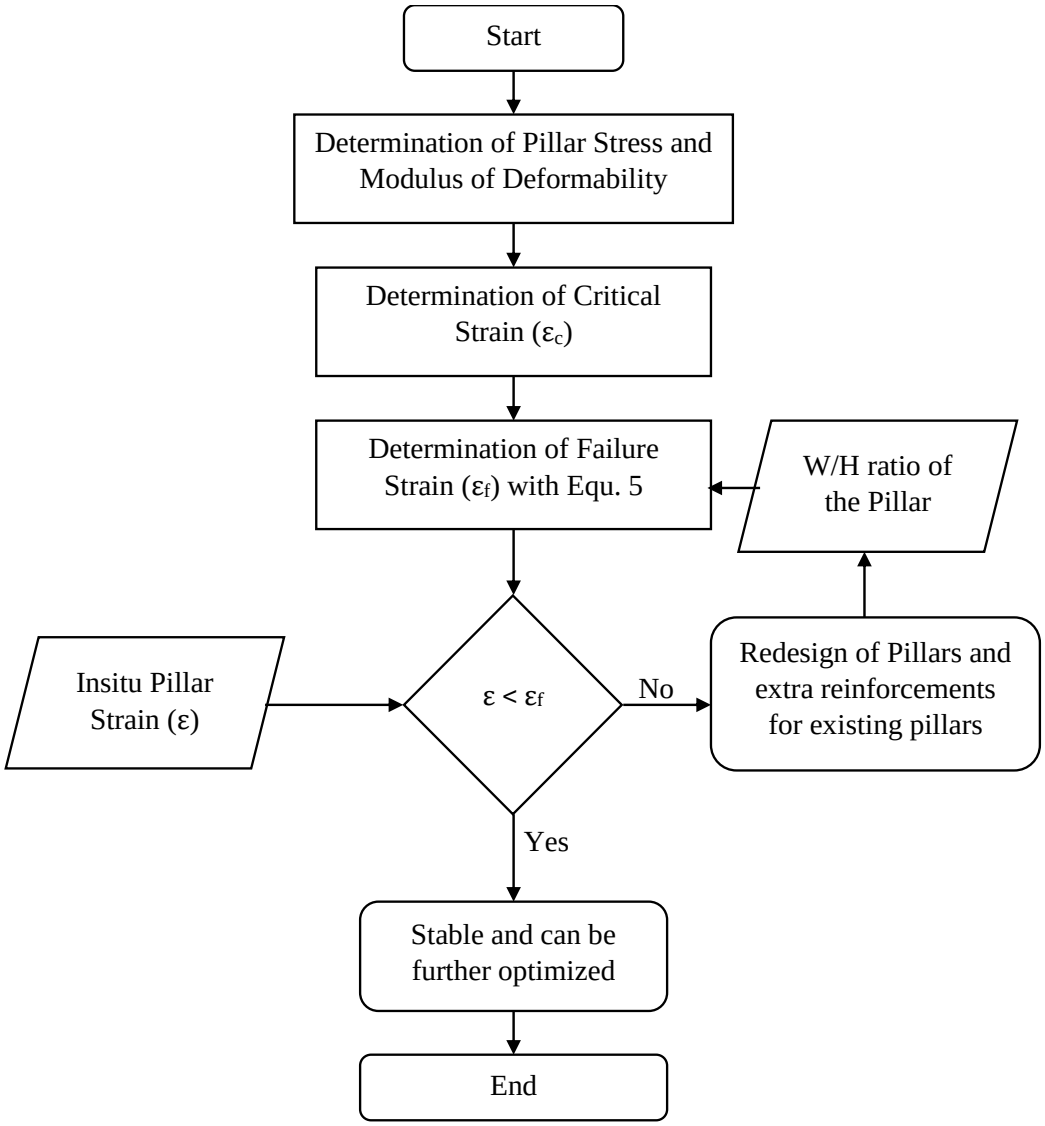

Figure 8.13: Flowchart showing the applicability of the strain evaluation method for pillars

To design the pillars, a safety factor of 1.4 is used (Lunder and Pakalnis, 1997; Maybee and Martin, 2000). If the strain observed in situ is equal to or higher than the failure strain

calculated by Equation (8.9), then that failure strain is taken as the basis to design the new pillars. To account for the uncertainties in the material properties, the safety factor should be multiplied by the failure strain to design the new pillars.

8.3.4. Limitations of the Strain Based theory

As the tests were only conducted on the laboratory scale, there are limitations that need to be understood for the applicability of the theory. These are summarized as follows:

- The strain-based theory is only applicable for the pillars with massive ground condition or highly jointed rock mass. The large discontinuities will have different failure mechanisms which cannot be predicted through the above-mentioned equations.
- As the laboratory-based pillars are associated with stiff platens on the ends, the theory does not take into consideration the roof and floor conditions at the field scale.
- Only two rock types were tested for the applicability of the strain-based theory to pillars in this chapter. In the future work, further studies should be conducted for different types of rocks to correctly implement the theory in the field.

8.4. Conclusions

Laboratory experiments on two different rock types with different width to height ratios were conducted and strain analysis was performed. The following conclusions can be made:

- The real-time monitoring which is prevalent in the mines can be used to verify the Equation (8.9) and predict the real-time stability of the pillar. This would lead to very safe monitoring procedure than the visual monitoring of the fractures on the pillars.
- The strain values of the stable pillars would also be beneficial as it can show that the pillars can still be optimized.

- The critical strain remains in a very small range of values even though the strength of the samples varies largely with the rock types. Therefore, strain values would be beneficial over all the rock types with wide range of strengths.
- The brittle failure causes the failure strain equal to or nearly equal to the critical strain which is evident in the samples with W/H ratio of 0.4 (i.e. UCS samples).
- The simplified reduction factor (SR_f) was developed to understand the relationship between the critical strain and the failure strain at different W/H ratios. The simplified reduction factor has a positive linear relationship with W/H.
- A flowchart was developed to back analyze the existing pillars. Based on this, optimization or redesigning the pillars with higher safety standards can be carried out.
- The safety factor is considered for the geotechnical structures due to the change in material properties, therefore, factor of safety is considered adopted in Equation 8.9 by multiply it to the failure strain.

Further tests on different rock types need to be conducted to improve the applicability of the strain evaluation method to pillars.

References:

Bobet, A. and Einstein, H. H. (1998). Fracture coalescence in rock-type materials under uniaxial and biaxial compression. Int. J. Rock Mech. Min. Sci., 35, pp. 863-888

Cai, M. (2011). Rock mass characterization and rock property variability considerations for tunnel and cavern design. Rock Mech. Rock Eng., 44, pp. 379-399

Cai, M., Kaiser, P. K., Tasaka, Y., Maejima, T., Morioka, H. and Minami, M. (2004) Generalized crack initiation and crack damage stress thresholds of brittle rock masses near underground excavations. Int. J. Rock Mech. Min. Sci., 41, pp. 833-847

Dismuke, S. R., Forsyth, W. W. and Stewart, S. B. V. (1994). The Evolution of Mining Strategy Following the Collapse of the Window Area at the Magmont Mine, Missouri. Proceedings of the CIM Annual General Meeting, District 6, Metal Mining, pp 3-8.

Esterhuizen, G. S. (2006). An evaluation of the strength of slender pillars. *Transactions of Society for Mining, Metallurgy, and Exploration, Inc.* Vol. 320. Littleton, CO: Society for Mining, Metallurgy, and Exploration, Inc., pp. 69–76.

Esterhuizen, G. S., Dolinar, D. R. and Ellenberger, J. L. (2008). Pillar strength and design methodology for stone mines. *Proceedings of the 27th International Conference on Ground Control in Mining*, Morgantown, WV: West Virginia University, pp. 241–253.

Hoek, E. and Brown, E. T. (1980). Underground Excavations in Rock. London: Institution of Mining and Metallurgy, 527 pages

Hedley, D. G. F and Grant, F. (1972). Stope and pillar design for the Elliot lake uranium mines. *Canadian Institute of Mining and Metallurgy Bulletin*, Vol. 65, pp. 37-44.

Idris, M. A., Saiang, D. and Nordlund, E. (2015). Stochastic assessment of pillar stability at Laisvall mine using artificial neural network, *Tunnelling and Underground Space Technology*, vol. 49, pp. 307–319.

Kaiser, P. K. and Tang, C. A. (1998). Numerical simulation of damage accumulation and seismic energy release during brittle rock failure – Part II: rib pillar collapse. International Journal of Rock Mechanics and Mining Sciences, 35, 123-134.

Kimmelmann, M. R., Hyde, B. and Madgwick, R. J. (1984). The use of computer applications at BCL Limited in planning pillar extraction and design of mining layouts. Proceedings of ISRM symposium: design and performance of underground excavations, London, 53-63.

Krauland, N. and Soder, P. E. (1987). Determining pillar strength from pillar failure observations. Eng Min J, 8, 34-40.

Lane, W. L., Yanske, T. R., Clark, L. M., Roberts, D. P. (2001). Pillar extraction and rock mechanics at the Doe Run Company in Missouri 1991 to 2000. Underground mining methods-engineering fundamentals and international case studies, Society for mining, Metallurgy, and Exploration, 95-103.

Lunder, P. J. and Pakalnis, R. (1997). Determination of the strength of hard rock mine pillars. Bulletin for Canadian Institute of Mining and Metallurgy, 90(1013):51–55

Martin, C. D. and Maybee, W. G. (2000). The strength of hard-rock pillars. International Journal of Rock Mechanics and Mining Sciences, 37:1239–1246

Napa-García, G. F. and Navarro Torres, V. F. (2017). Applicability of failure strain for the stability evaluation of square pillars in room and pillar mining, in M Hudyma & Y Potvin (eds), *Proceedings of the First International Conference on Underground Mining Technology*, Australian Centre for Geomechanics, Perth, pp. 557-565.

Nordlund, E., Radberg, G. and Jing, L. (1995). Determination of failure modes in jointed pillars by numerical modelling. Fractured and jointed rock masses, Balkema, 345-350.

Zipf, R K. (2001). Toward pillar design to prevent collapse in room-and-pillar mines. 108th Annual Exhibit and Meeting, Society for Mining, Metallurgy and Exploration, Denver.

Potvin, Y., Hudyma, M., Miller, H. D. S. (1989). Rib pillar design in open stope mining. Bulletin for Canadian Institute of Mining and Metallurgy, 82(927):31–36

Roberts, D. P., Tolfree, D. and McIntire, H. (2007). Using confinement as a means to estimate pillar strength in a room and pillar mine. 1st Canada-US Rock Mechanics Symposium, Vancouver, 2007, 1455-1462.

Sakurai, S. (1981). Direct strain evaluation technique in construction of underground opening. *Proceedings of the 22nd US Symposium on Rock Mechanics*, American Rock Mechanics Association, Alexandria, 1981, pp. 278–282.

Sakurai, S. (1999). Interpretation of field measurements in tunneling practice. *Proceedings of the 9th ISRM Congress*, International Society for Rock Mechanics, Lisbon, pp. 1517–1523.

Salamon, M. D. G. and Munro, A. H. (1967). A study of the strength of coal pillars. *J. S. Afr. Inst. Min. Metall.* September 1967.

Sjoberg, J. S. (1992). Failure modes and pillar behaviour in the Zinkgruvan mine. In: Tillerson JA, Wawersik WR (eds) Proceedings of the 33rd U.S. rock mechanics symposium. A.A. Balkema, Sante Fe. Rotterdam, pp 491–500

Suorineni, F. T., Mgumbwa, J. J., Kaiser, P. K., Thibodeau, D. (2011). Mining of orebodies under shear loading Part 1 – case histories, *Mining Technology (Trans. Inst. Min. Metall. A)*, 120(3), 138–147.

Suorineni, F. T., Mgumbwa, J. J., Kaiser, P. K., Thibodeau, D. (2014). Mining of orebodies under shear loading Part 2 – failure modes and mechanisms, *Mining Technology* (Trans. Inst. Min. Metall. A), 123(4),240–249.

Wong, L. and Einstein, H. (2009). Crack Coalescence in Moulded Gypsum and Carrara Marble: Part 2—Microscopic Observations and Interpretation. Rock Mechanics and Rock Engineering. 42. 513-545. 10.1007/s00603-008-0003-3.

Ulusay R, Hudson JA. The complete ISRM suggested methods for Rock Characterization, Testing and Monitoring: 1974-2006. International Society of Rock Mechanics, 2007

Chapter 9:

Discussion and Conclusions

9.1. Introduction

The major geotechnical design concerns in an underground mine are dependent on the parameters such as pillar dimensions, stope dimensions and the direction of the mining sequence relevant to the stress tensor. Pillar design is generally done by using empirical approaches that do not consider all the parameters that can influence the design. Some of the factors effecting the failure mechanism of the pillars are the inclination of the orebody with respect to the stress tensor, presence of geological discontinuities and blasting effect on the skin of the pillars.

9.2. Discussion

The inclination of the pillars causes the loading regime to change from normal loading condition to that of the oblique loading condition which creates a combination of compression and shear loads as shown in Figure 9.1. While the empirical approaches are based on normal loading conditions, designing the inclined pillars that are undergoing oblique loading with the same empirical approach can be misleading.

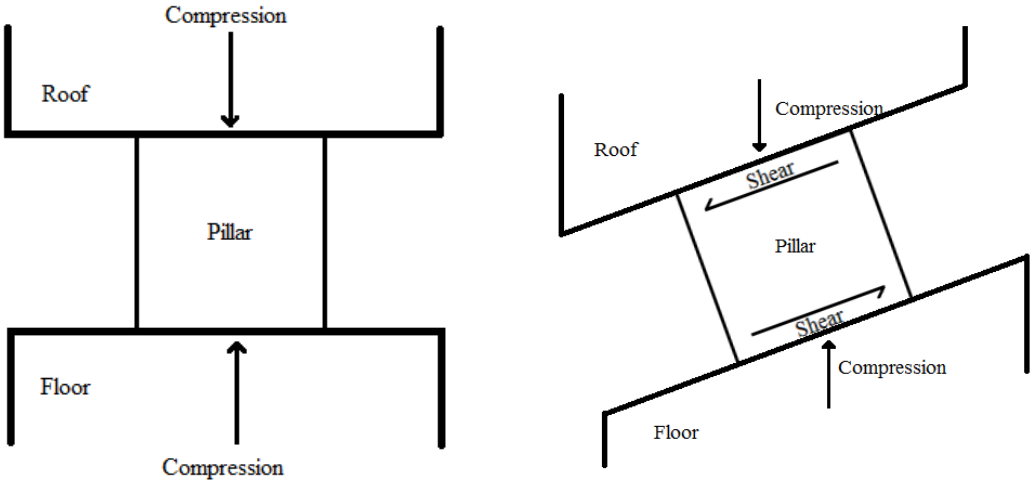

a) b)

Figure 9.1: a) Normal loading b) Inclined loading on the pillars

The geological discontinuities are a fundamental part of the rock mass system and hence can be present in the pillars that may cause a sliding or toppling failure in the pillars. In the literature, the discontinuities have only been considered in the pillars parallel to the pillar face. While the discontinuities can exist at any direction to the pillar face, relying on the factors developed for discontinuities facing the pillar face would be unreliable.

Presence of discontinuity in an inclined pillar would also lead to the sliding failure along the discontinuity plane. While the failure mechanism of the inclined pillars is dependent on the oblique loading, the sliding along the discontinuity in an inclined pillar would also be dependent on the oblique loading. Therefore, the role of a discontinuity in a pillar under normal loading would therefore not be a representative of the discontinuity in an inclined pillar undergoing oblique loading.

Drill and blast methods lead to damage of the skin of the pillars that has not been addressed adequately in the past. The stress redistribution would be mainly through the intact rock pillar unaffected by the blast damage, therefore, the failure mechanism of the pillar effected by the blasting could be different when compared to the failure mechanism of the pillars with no blast damage. Blasting damages, the pillar skin and this is not considered for strength evaluation of the pillars.

The condition of the pillars is generally monitored in a qualitative manner; such as visual inspection, the fracture development on the pillar face and by using a borehole with say a borehole camera. A quantitative measure can be rather used to monitor the condition of pillars that would provide with more useful information about the current state of the pillars as well as the potential to further optimize the pillars.

This thesis was undertaken to improve pillar design by investigating the failure mechanisms of the pillars and evaluate the strength of the pillars with respect to the pillar

failure mechanism. Specifically, the main objectives were to compare the failure of horizontal pillars, with no discontinuities and no blast damage to:

- The failure mechanisms of the inclined pillars under oblique loading and to derive a strength reduction factor to account for the inclination of the pillars
- The normal and inclined pillars in the presence of a single discontinuity in any orientation and to evaluate the major discontinuity angles effecting the pillar strength. One single discontinuity was considered as it is important to understand the failure mechanism about that orientation. While the effect of multiple discontinuities can be evaluated with the frequency factor developed by Esterhuizen (2008).
- A parametric study of the blast damage factors to study the influence of the factors on the pillars to evaluate the failure mechanism and the strength of the pillars.

In addition, a quantitative measure such as strain is used to evaluate the condition of the pillars.

Laboratory testing was used to investigate the behaviour of the samples under oblique loading conditions. Axial strain at peak strength was used to develop a quantitative measure for determining the condition of the pillars. Three-dimensional numerical modelling tool was used to investigate the failure mechanisms of the pillars under oblique loading, in the presence of discontinuity and the blast damage and evaluate the strength accordingly. The numerical models were calibrated with the Lunder and Pakalnis (1997) empirical approach that is widely used in the industry for the horizontal pillars with normal loading conditions. Following are the major conclusion from this analysis.

9.3. Conclusions

9.3.1. Failure mechanisms and strength of the inclined pillars

The following conclusions can be made from this investigation:

- Laboratory based studies on the sandstone and moulded gypsum indicated that the loss of strength at an inclination is consistent throughout all the width-to-height ratios. Therefore, a strength reduction factor can be proposed to account for pillar inclination. For Gypsum specimens, strength reduction factors were 0.78 and 0.56 for 10° and 20° inclinations and for sandstone samples, strength reduction factors were 0.71 and 0.43 for 10° and 20° inclinations.
- The strength loss can be directly related to the failure mechanism of the samples. In the inclined samples, the additional spalling at the corners of the inclined pillars lead to the strength loss when compared to the horizontal samples.
- The dominant failure mechanism in the inclined pillars is the brittle failure mechanism where the difference between the brittle spalling of the pillars and the ultimate pillar strength is small due to the failure of the pillar through the core as shown in Figure 9.2.

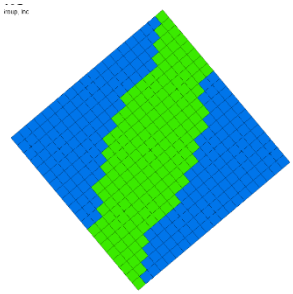

Figure 9.2: Brittle failure of the 40° inclined pillar.

Note: Blue shows elastic elements and Green shows yielded elements

- The failure mechanism of the inclined pillars with W/H ratio of less than 1 was found to be starting from the two diagonally opposite edges of the pillar along the direction of the dip which pass through the centre of the pillar causing violent outburst. While the failure mechanism of the large pillars was found to also start form the two diagonally opposite edges of the pillar along the direction of the pillar which causes a major part of brittle spalling which reduces the confinement for the core of the pillar leading to lower pillar strength.
- Strength reduction factors were evaluated at four different inclinations, so an equation could be derived to give the strength of the inclined pillar at any specific inclination and this can be incorporated into the empirical approach to account for inclination. The linear relationship was developed between the average strength reduction factors (RF) and inclination of the pillar (θ). The equation can be written as:

$$RF = 1 - 0.0077(\theta) \qquad R^2 = 0.9785 \qquad (9.1)$$

9.3.2. Failure mechanism and the strength of the pillars in the presence of discontinuity

- The largest angle of discontinuity that passes through the two corners of the pillars significant effects the strength of the pillar as the failure is through the sliding along the discontinuity. Therefore, if the discontinuity orientations are known, it would be helpful in orientating the pillar according to the discontinuity to improve the performance of the pillar.
- The orientation of the discontinuity (strike direction) with respect to pillar face is important in evaluating the strength of the pillars. If the orientation of the discontinuity is known, the pillars can be orientated in such a manner to obtain a pillar with an effective higher strength.

- In two circumstances, the pillars have higher strength despite the presence of a discontinuity are: a) If the inclination of the discontinuity is lower than the internal angle of friction and b) If the inclination of the discontinuity is such that its end points are in the floor and roof.
- In inclined pillars less than W/H ratio of 1.0, a discontinuity towards and against the pillar dip causes significant decrease in pillar strength due to the sliding failure. While in the larger inclined pillars, substantial decrease in the pillars strength occurs when a discontinuity is inclined towards the pillar dip as shown in Figure 9.3. This is due to the discontinuity inclination coinciding the failure mechanism of the inclined pillars that aids the slippage along the discontinuity.
- In pillars with W/H ratio of less than 1.0, the largest angle for sliding would remain same for the normal and inclined pillars. For examples, in W/H ratio of 0.5, the 60° discontinuity angle with respect to the pillar inclination has a significant effect on pillar strength.
- The pillar designs with discontinuity inclinations between the discontinuity friction angle (typically 30°) and 70° with respect to pillar inclination should be done with the help of the charts developed.

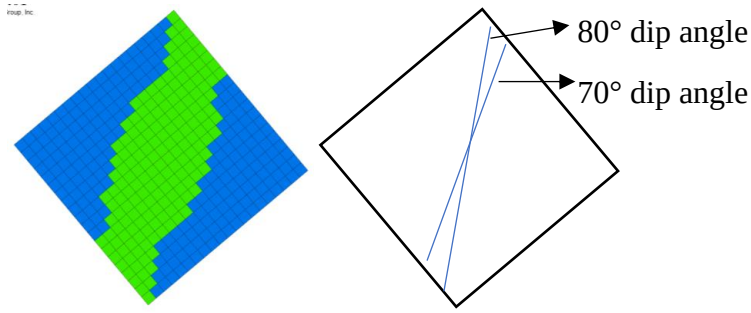

a) b)

Figure 9.3: a) Failure mechanism of the 40° inclined pillar without discontinuity b) The discontinuity angles that can lie in the failure region

Note: Blue shows elastic elements and Green shows yielded elements

9.3.3. Failure mechanism and strength evaluation for blast effect on pillars

- Parametric study revealed that the blast damage factor and the blast thickness with respect to the pillar width-to-height ratio are important parameters in defining the pillar strength and the failure mechanisms of the pillars with blast damage.
- Deformation modulus of the damaged rock plays an important role in the defining the failure mechanisms of the pillar. Lower deformation modulus in the skin of the pillars leads to the softening of the rock that transfers stress redistribution into the intact part of the pillars. This leads to the higher brittle spalling of the pillar sides and reduces the confinement of the core leading to the lower pillar strength.
- To account for the blast damage on pillars in normal pillar and inclined pillars, charts and tables are generated, which presents an estimate for a pillar strength.
- Damage factor and damage thickness can be estimated from the excavations. The factors in the table can provide additional thickness around the pillar to counteract the blast damage for an appropriate width-to height ratio.

9.3.4. Monitoring the condition of the pillars

- The Direct Strain Evaluation method developed by Sakurai (1981, 1999) to understand the stability of the tunnels has been extended in this thesis to monitor the stability of the pillars.
- Laboratory based tests showed that the ultimate compressive strength of samples has a relatively large standard deviation in rock types while the critical strain remains in a much small range of values. This shows that monitoring of the pillars in any rock type would be very beneficial with the help of strain analysis.

- A simplified reduction factor was developed with the help of laboratory tests which is a ratio of failure strain (ε_f) to the critical strain (ε_c) for different geometries of the samples. A positive linear relationship was determined between the simplified reduction factor and the width-to-height (W/H) ratio of the pillars which is given as

$$\varepsilon_f = \varepsilon_c \qquad For \frac{W}{H} < 0.5 \qquad (2)$$

$$\varepsilon_f = \left[0.56 + 1.14 * \left(\frac{W}{H}\right)\right] \varepsilon_c \quad R^2 = 0.97 \quad For\ 0.5 < \frac{W}{H} < 2.0 \qquad (3)$$

- A back-analysis flow chart was developed to monitor the existing pillars and analyse the strain developed on the pillars to design the new set of pillars in a better and optimized manner. If the monitoring showed that the strain developed on the pillar is lower than the failure strain from the equations developed, then the pillar would be classified as stable and then the strain developed on the pillar can be used as basis for the next set of pillars.

9.3.5. Step by step utilization of the theories presented in this thesis

Pillar design needs a step by step by procedure (Figure 9.4) to consider all the factors that will influence the strength performance of the pillar. The data required for designing the pillar is the rock strength (Uniaxial Compressive Strength), the depth of pillar and the required extraction ratio to determine the stress on the pillars. Then the factors come into play such as the orientation of the orebody, the presence of discontinuities and the blast damage to design an appropriate size of the pillar that can withstand the stress on the pillar. The pillars need to be continuously monitored to understand the pillars stability and then classify the pillars as stable, unstable and failed. In addition, monitoring would help in indicating the pillar stability such as stable, unstable and failed. According to the stability of the pillar, additional support or optimization of the pillar can be carried out. Therefore, the step by step procedure for pillar design and the monitoring is shown in Figure 9.4.

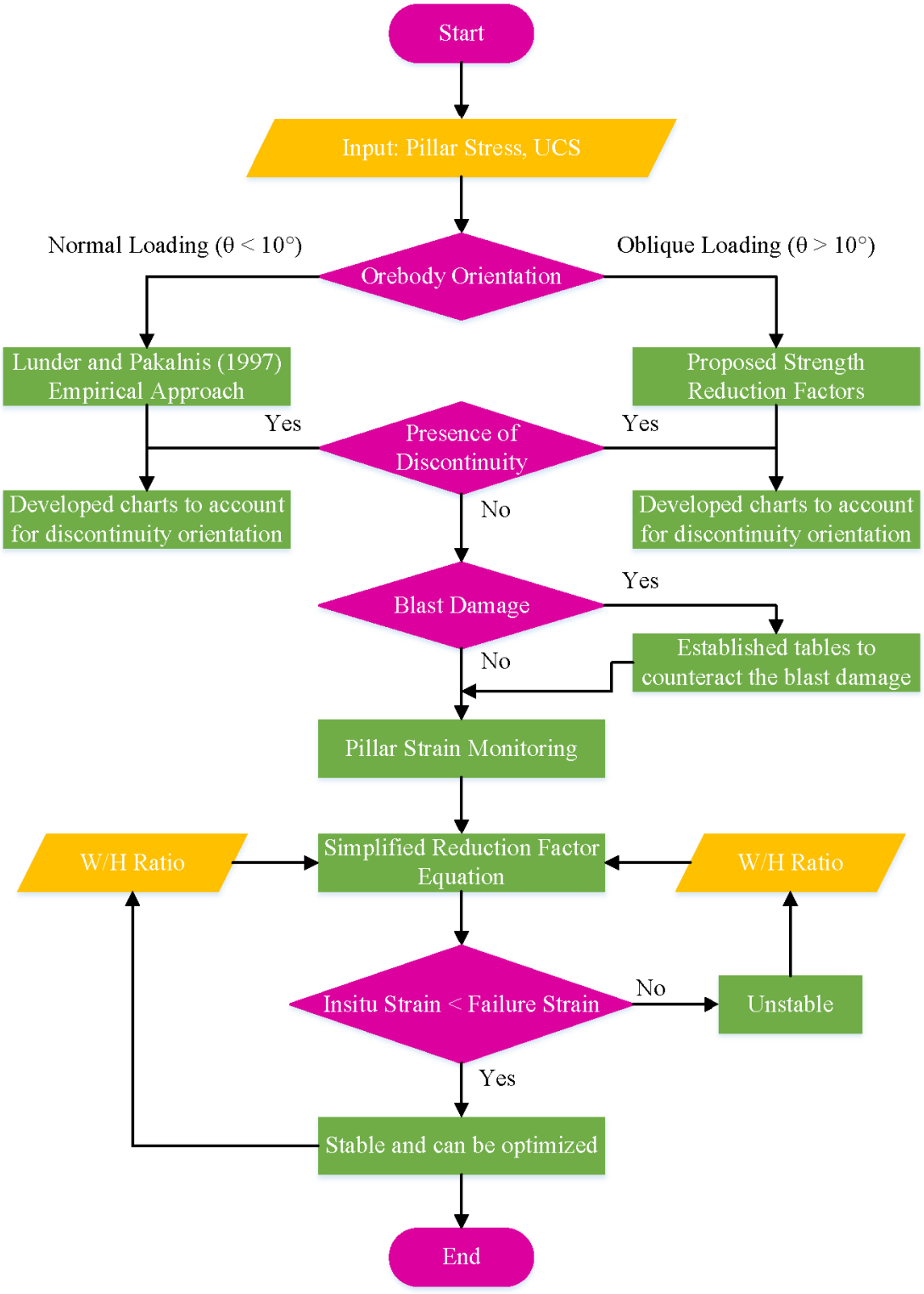

Figure 9.4: Step by step procedure for pillar design and monitoring

First phase in designing the pillars is to determine the orebody orientation as shown in Figure 9.5. If the orebody orientation is below 10°, the pillars will undergo normal loading or near normal loading, therefore, the Lunder and Pakalnis (1997) could be used to design the pillars. At higher orientation above 10°, the pillars undergo incline loading which leads to additional spalling on the sides of the pillars leading to lower strength than the normal loading pillars, therefore, strength reduction factors should be applied that are determined in Chapter 3.

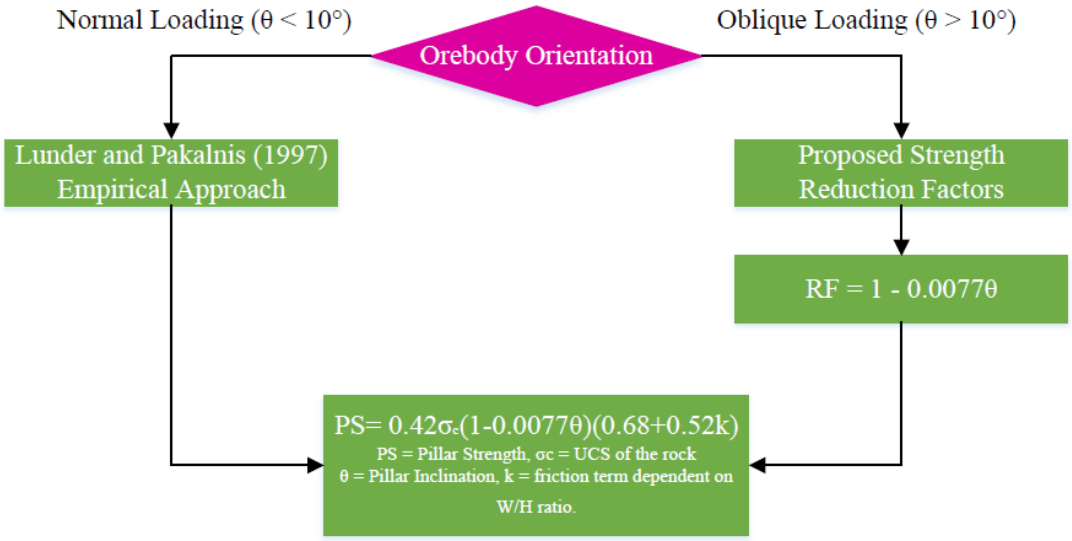

Figure 9.5: Chart showing decision process for considering orebody orientation

Second phase involves in determining the presence of discontinuity in the pillar as shown in Figure 9.6. If the pillar is intersected by a discontinuity, the strike and the dip of the discontinuity with respect to the pillar should be considered in determining the strength of the pillar. If the discontinuity inclination lies in the range of discontinuity friction angle and 70°, then the factors from the charts developed in Chapter 5 and 6 need to be considered for designing the pillars.

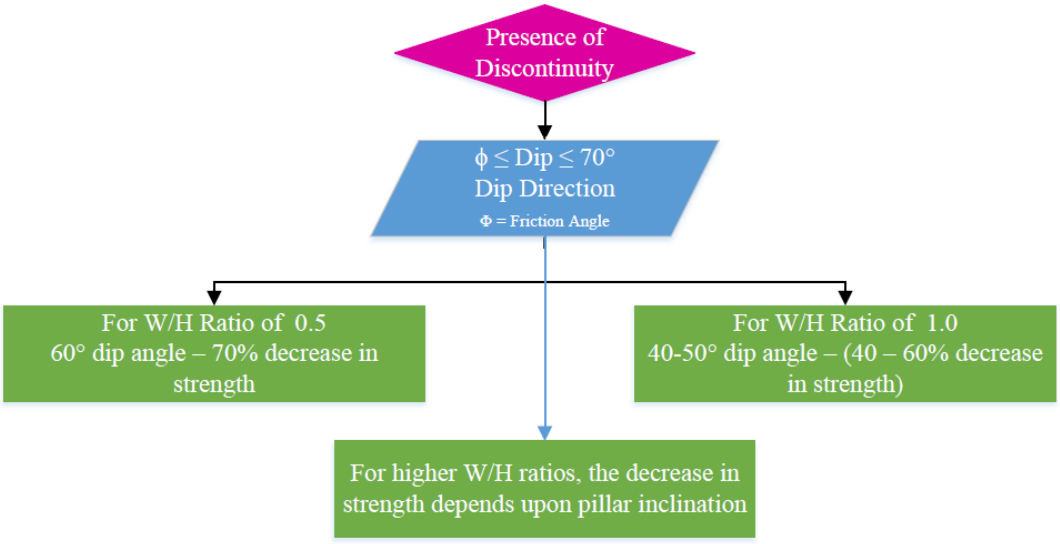

Figure 9.6: Chart showing decision process for considering presence of discontinuities.

The third phase involves defining the blast damage on the pillars as shown in Figure 9.7. The blast damage and blast thickness are the two important parameters that effect the strength performance of the pillars. If the blast damage factor was found to be less than 0.5, then the effective reduction in pillar strength can be taken as 10%. While if the blast damage factor is more than 0.5, then the tables developed in Chapter 7 should be used to account for different blast thickness and design a pillar which would provide adequate strength.

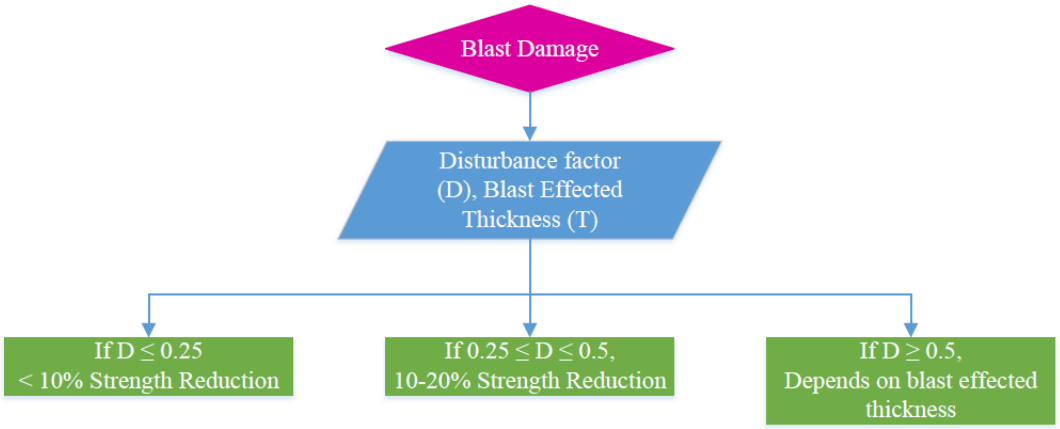

Figure 9.7: Third Decision process to account for blast damage

After the pillars are developed, monitoring the pillar is essential to understand the condition of the pillar that can be classified as stable, unstable and failed as shown in Figure 9.8. Strain analysis from the laboratory testing provides a medium for monitoring the pillars. The strain developed on the pillars can be checked against the equation derived in Chapter 8 to establish the condition of the pillar. Accordingly, the next set of pillars can be developed based on the strain data provided by these pillars.

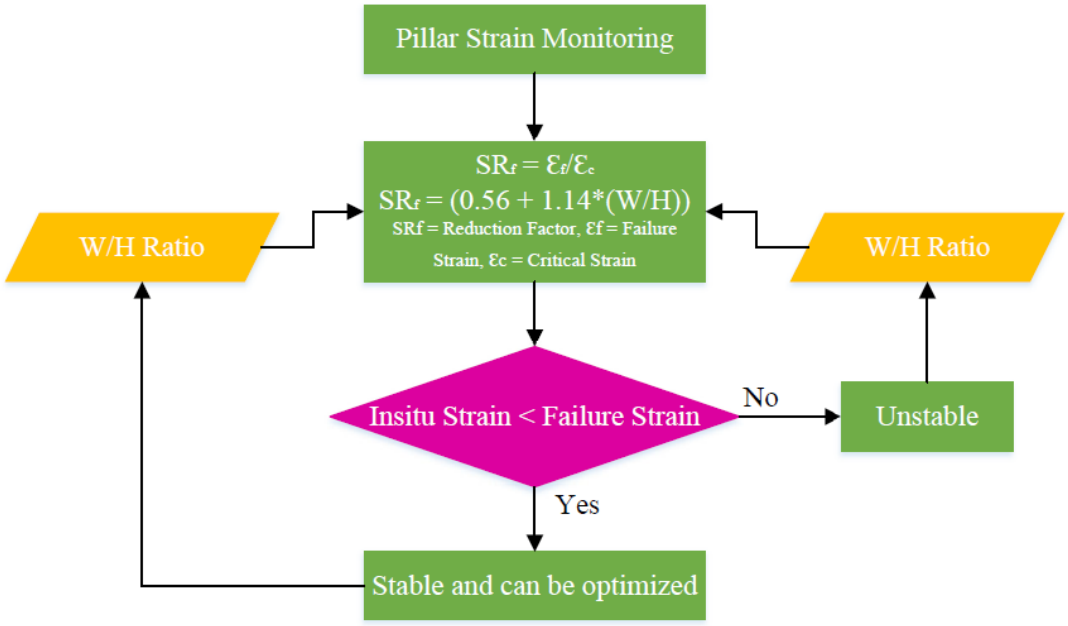

Figure 9.8: Monitoring process of the pillars

The step-by-step procedure would lead to improved pillar design and the continuous monitoring of the pillars would increase the productivity and safety of the workings.

9.4. Limitations and Future Work

Laboratory and numerical modelling in this thesis has created a database of the results that can be used as a basis to conduct more work in the areas of inclined loading conditions, in the presence of discontinuity, blast damage and monitoring of the pillars such as:

- In the laboratory tests, due to constraints, only two inclinations were tested to determine the strength of the inclined samples. More rock types should be tested under inclined loading condition to understand the failure mechanism of each rock type and determine the reduction factors.
- Discontinuities have been studied in the normal and inclined pillars in this thesis. The joint sets having different fracture lengths and fracture spacing should be studied in inclined pillars to account for different fracture lengths, orientations and spacing.
- A parametric study has been conducted for determining the blast damage effects on the pillars while in-situ calibration of these tables would lead to better establishment of pillar designs.
- For the strain analysis only two different rock types were tested due to the shortage of the samples. Increase in database of the strain analysis of the laboratory samples would lead to better and optimized equation for monitoring of the pillars in the underground.

Appendix A

Failure Mechanisms of Sandstone samples in Horizontal and Inclined loading

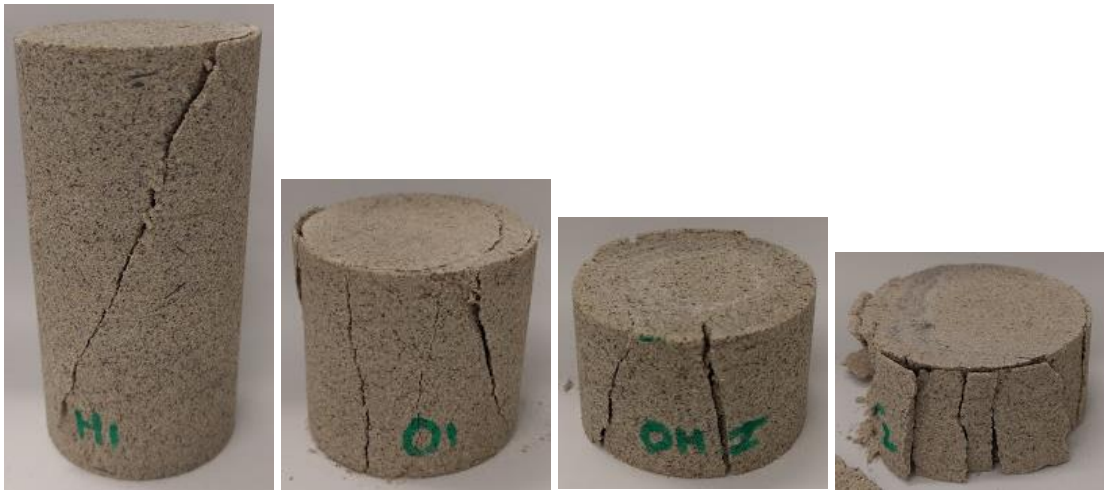

a) b) c) d)

Figure A.1: Failure mechanisms of the sandstone specimen in normal loading condition with W/H ratio of a) 0.5 b)1.0 c) 1.5 d) 2.0

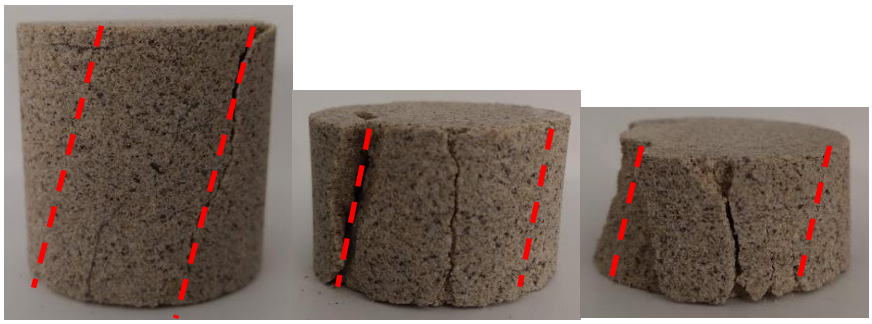

a) b) c)

Figure A.2: Failure mechanisms of the sandstone specimen in 10° inclined loading condition with W/H ratio of a)1.0 b) 1.5 c) 2.0

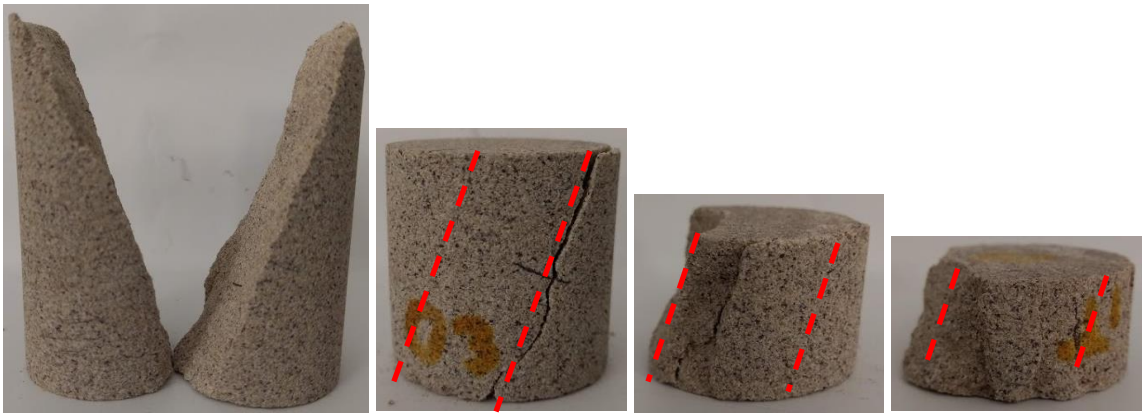

a) b) c) d)

Figure A.3: Failure mechanisms of the sandstone specimen in 20° inclined loading condition with W/H ratio of a) 0.5 b) 1.0 c) 1.5 d) 2.0

Appendix B

Effect of 22.5° Discontinuity Dip Direction on Pillar Strength

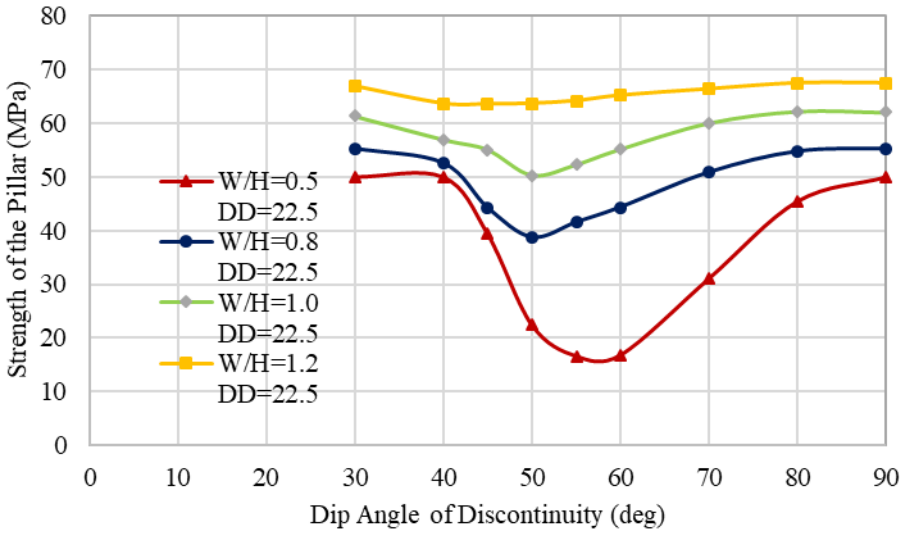

Figure B.1: Effect of discontinuity dip direction of 22.5° on different pillar width to height ratios.

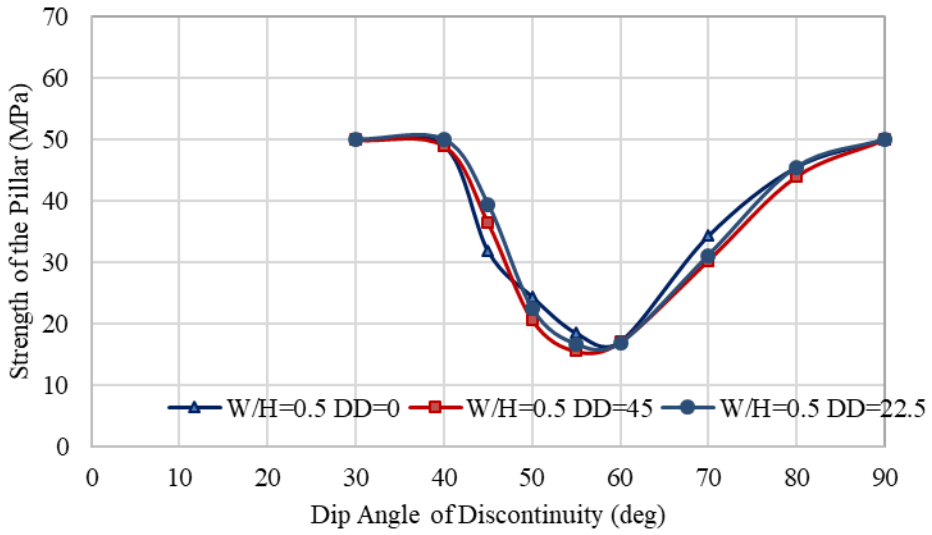

a)

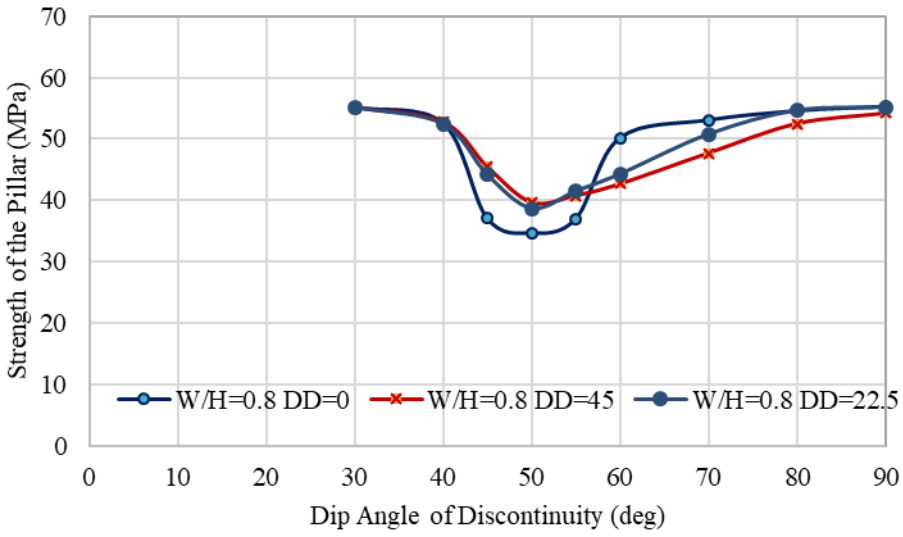
Strength of the Pillar (MPa)
70
60
50
40
30
20
10
0
0
10
20
30
40
50
60
70
80
90
Dip Angle of Discontinuity (deg)
W/H=0.8 DD=0
W/H=0.8 DD=45
W/H=0.8 DD=22.5

b)

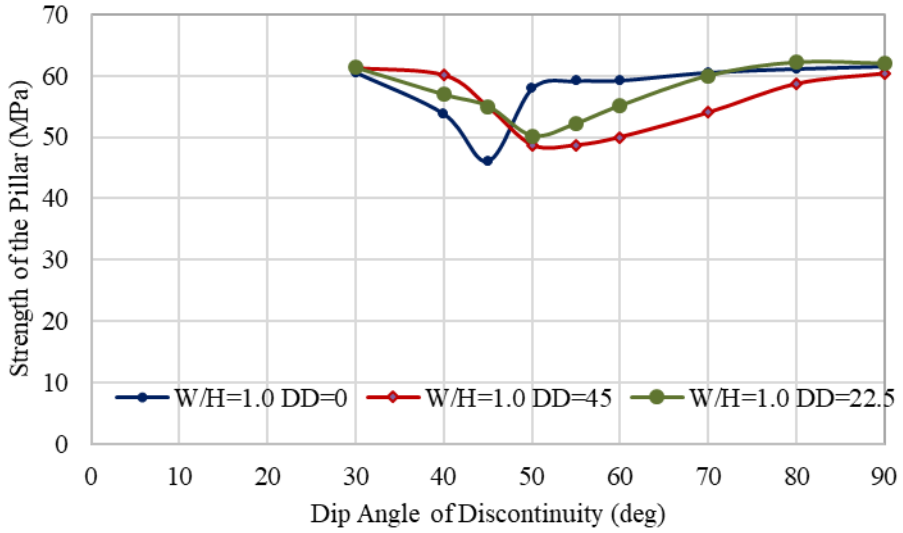
Strength of the Pillar (MPa)
70
60
50
40
30
20
10
0
0
10
20
30
40
50
60
70
80
90
Dip Angle of Discontinuity (deg)
W/H=1.0 DD=0
W/H=1.0 DD=45
W/H=1.0 DD=22.5

c)

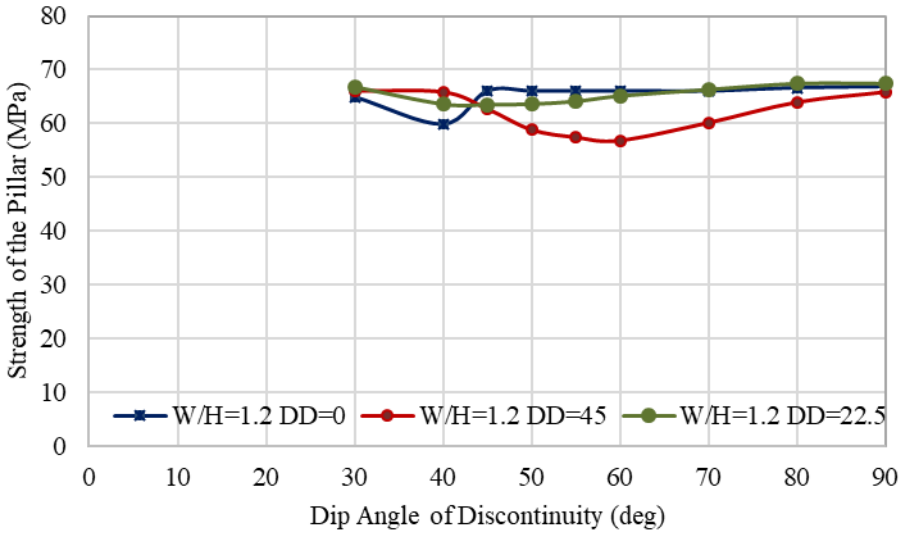

d)

Figure B.2: Effect of three different discontinuity dip directions at a) W/H ratio of 0.5 b) W/H ratio of 0.8 c) W/H ratio of 1.0 d) W/H ratio of 1.2

Appendix C

Declaration of Authorship

DECLARATION OF AUTHORSHIP

I Kashi Vishwanath Jessu, contributed:

- 85% of the design and analysis of the research study and authoring the paper entitled "A Parametric Study of Blast Damage on Hard Rock Pillar Strength". Anthony J.S. Spearing assisted with the design, analysis and supervision of the study and reviewed the paper. Mostafa Sharifzadeh assisted with the format and review of the paper.
- 85% of the design and analysis of the research study and authoring the paper entitled "Laboratory and Numerical Investigation on Strength of Inclined Pillars". Anthony Spearing assisted with the design, analysis and supervision of the study and reviewed the paper. Mostafa Sharifzadeh assisted with the format and review of the paper.

Kashi Vishwanath Jessu

Date: 02/11/18

I endorse that this level of contribution by the candidate indicated above is appropriate.

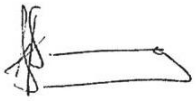

Prof. A.J.S. (Sam) Spearing

Supervisor and Co-author

Dr. Mostafa Sharifzadeh

Co-supervisor and Co-author

DECLARATION OF AUTHORSHIP

I Kashi Vishwanath Jessu, contributed:

- 85% of the design and analysis of the research study and authoring the paper entitled "Effect of Dip on Pillar Strength". Anthony Spearing assisted with the design, analysis and supervision of the study and reviewed the paper.
- 85% of the design and analysis of the research study and authoring the paper entitled "Influence on Inclined Pillars with Major Discontinuity". Anthony Spearing assisted with the design, analysis and supervision of the study and reviewed the paper.

Kashi Vishwanath Jessu

Date: 02/11/18

I endorse that this level of contribution by the candidate indicated above is appropriate.

Prof. A.J.S. (Sam) Spearing

Supervisor and Co-author

DECLARATION OF AUTHORSHIP

I Kashi Vishwanath Jessu, contributed:

- 75% of the design and analysis of the research study and authoring the paper entitled "Effect of Discontinuity Dip Direction on Hard Rock Pillar Strength". Anthony J.S. Spearing assisted with the design, analysis and supervision of the study and reviewed the paper. Gabriel Esterhuizen assisted with the supervision and review of the study. Todd Kostecki assisted with the review of the study.

Kashi Vishwanath Jessu

Date: 02/11/18

I endorse that this level of contribution by the candidate indicated above is appropriate.

Prof. A.J.S. (Sam) Spearing

Supervisor and Co-author

Date: November 2nd, 2018

Todd Kostecki

Co-author

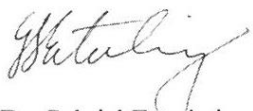

Dr. Gabriel Esterhuizen

Co-author

DECLARATION OF AUTHORSHIP

I Kashi Vishwanath Jessu, contributed:

- 85% of the design and analysis of the research study and authoring the paper entitled "Direct Strain Evaluation for Laboratory based Pillar Performance". Anthony Spearing assisted with the design, analysis and supervision of the study and reviewed the paper.

Kashi Vishwanath Jessu

Date: 14/12/2018

I endorse that this level of contribution by the candidate indicated above is appropriate.

Prof. A.J.S. (Sam) Spearing

Supervisor and Co-author

Appendix D

Copyright Licenses

Gmail

Kashi Vishwanath Jessu <kashijessu@gmail.com>

RE: Society for Mining, Metallurgy, and Exploration, Inc.

Georgene Renner <renner@smenet.org> Fri, Dec 14, 2018 at 3:01 AM
To: Kashi Vishwanath Jessu <kashijessu@gmail.com>

Dear Mr. Vishwanath

You have permission from SME to use the information in TP-17-015.R1 - Effect of Discontinuity Dip Direction on Hard Rock Pillar Strength in your thesis.

Please acknowledge that this information was in the 2018 SME Transactions, published by SME, Englewood, Colorado, USA.

Sincerely

Georgene Renner

Georgene Renner

Senior Editor, Mining Engineering magazine

renner@smenet.org

Society for Mining, Metallurgy & Exploration

12999 E Adam Aircraft Circle

Englewood CO 80112

303-948-4254

800-763-3132 x254

From: Kashi Vishwanath Jessu [mailto:kashijessu@gmail.com]
Sent: Wednesday, November 28, 2018 4:24 AM
To: Georgene Renner <renner@smenet.org>
Subject: Re: Society for Mining, Metallurgy, and Exploration, Inc.

[Quoted text hidden]